

NASA Contractor Report 174759

Mass Transfer From a Circular Cylinder - Effects of Flow Unsteadiness and
"Slight Nonuniformities"

M. L. Marziale and R. E. Mayle

Rensselaer Polytechnic Institute
Troy, New York

September 1984

Prepared for

NATIONAL AERONAUTICS AND SPACE ADMINISTRATION
Lewis Research Center
Under Grant NSG-3262

CONTENTS

Page

LIST OF SYMBOLS	iii
1. INTRODUCTION	1
2. HISTORICAL REVIEW	9
3. THEORETICAL CONSIDERATIONS	13
3.1 Constituent Equations and Significant Parameters	13
3.2 The Analogy Between Heat and Mass Transfer	18
4. EXPERIMENTAL APPARATUS AND PROCEDURE	22
4.1 Wind Tunnel Apparatus	22
4.2 Casting of Naphthalene Surfaces	29
4.3 Naphthalene Surface Profiles	35
4.4 Mass Transfer Data Reduction	48
4.5 Turbulence Measurement	49
5. RESULTS	62
5.1 Flow Measurements	62
5.2 Mass Transfer Measurements - Stationary Cylinder	71
5.3 Mass Transfer Measurements - Oscillating Cylinder	90
5.4 Investigation into Spanwise Variations in Mass Transfer	108
6. CONCLUSIONS	143
6.1 Steady-State Experiments	143
6.2 Oscillation Experiments	144
6.3 Investigation into the Observed Spanwise Variation of Mass Transfer	146
7. LITERATURE CITED	148
APPENDICES	152
A Procedure for the Setup of the Measuring Table	152
B Measurement of Length Scales Using the Correlation Function	156
C Theoretical Considerations of the Amplification of Flow Nonuniformities in a Stagnation Zone	161
D Tabular Listing of Mass Transfer Data	173

Page intentionally left blank

Page intentionally left blank

LIST OF SYMBOLS

C	-	mass concentration
D	-	diameter of test cylinder
\mathcal{D}	-	diffusion coefficient
e	-	AC voltage component
E	-	DC voltage component
f	-	frequency of oscillation in cycles per second
h_m	-	mass transfer coefficient
\dot{m}''	-	mass transfer rate per unit area per unit time
M	-	mesh size of a turbulence generating screen, measured from the center of one wire to the center of an adjacent wire
n	-	frequency of turbulence in cycles per second
Nu	-	Nusselt number
P	-	pressure
Pr	-	Prandtl number
Pr_t	-	turbulent Prandtl number = ϵ/ϵ_H
R	-	radius of the test cylinder
Re	-	Reynolds number
Sc	-	Schmidt number
Sc_t	-	turbulent Schmidt number = ϵ/ϵ_M
Sh	-	Sherwood number
St	-	Strouhal number
t	-	time
T	-	temperature
Tu	-	turbulence level = $\sqrt{\overline{u'^2}}/U$

u'	-	streamwise turbulent velocity
U	-	local mean velocity
U_{∞}	-	mean velocity far upstream of test cylinder
ΔU	-	perturbation velocity
V	-	cross-stream, cross-span mean velocity component
w'	-	spanwise turbulent velocity
W	-	spanwise mean velocity
x	-	streamwise coordinate measured from the cylinder's axis in the upstream direction
X	-	streamwise coordinate measured from the screen position in the downstream direction.
z	-	spanwise coordinate measured from the center of the naphthalene strip
Δ	-	naphthalene sublimation depth
ϵ	-	eddy diffusivity of momentum
ϵ_h	-	eddy diffusivity of heat
ϵ_m	-	eddy diffusivity of mass
ρ	-	density
ρ_{NS}	-	density of solid naphthalene
$\rho_{N,V}$	-	density of naphthalene vapor at the surface
ν	-	kinematic viscosity
ν_T	-	eddy viscosity
ϕ	-	angular coordinate measured along the surface of the cylinder from the stagnation line
ϕ_o	-	maximum angular displacement of oscillation

PART 1

INTRODUCTION

The design practices utilized by the modern gas turbine industry are at a critical stage of development. Currently designs are based upon steady two-dimensional modeling of the gas flow around blades or vanes. Quasi-steady and quasi-two-dimensional design systems are also in use to account for "slow" transients and certain three-dimensional effects. The recent advances in finite-difference, steady flow boundary layer programs allow the designer to account for such important effects as strong favorable pressure gradients, free stream turbulence, low Reynolds number, and surface curvature. These highly sophisticated treatments have led the designer quite far in predicting the aerodynamic losses and heat loads in a turbine and, accordingly, any design system advances of a steady, two-dimensional nature will be of only secondary importance. (The single exception to this is the problem of predicting boundary layer transition from laminar to turbulent flow.)

Significant advances in turbine technology will require exact knowledge of the manner in which the flow proceeds through a turbine. In reality, this flow is three dimensional in nature and contains, in addition to the random fluctuations of turbulence, a regular periodic unsteadiness. The necessity of including three-dimensional effects in a next generation design system has been recognized and research in this regard has already begun; however, only a few in the turbine field recognize the equal importance of unsteady flows. Practically no relevant information on unsteady flows is currently available to the designer.

Of particular importance is the effect of these unsteady flows upon the local heat transfer rate in the leading edge region of turbine blades. Since the effectiveness of cooling schemes in this region is limited by geometrical considerations and since the maximum heat load per unit area is on the leading edge of a blade, blade life critically depends upon leading edge design. Currently the uncertainty on leading edge design schemes is on the order of 70%, and the degree of inaccuracy in leading edge heat transfer predictions due to the effects of unsteady flows remains, as of yet, unknown. The initial intent of the reported research effort was to partly fill this void.

Examining the flow through a turbine, it is obvious that, in order for work to be extracted, the streamlines of the flow must be unsteady. Present design systems account for this unsteadiness by assuming that the flow leaves a blade row in a steady uniform manner and at a constant exit angle; therefore, relative to the following blade row, which is moving with respect to the preceding row, the inlet velocity is steady. The analysis on the following blade row is then performed by examining the flow relative to the individual blades. The flow leaving a blade row is in reality, however, nonuniform and highly unsteady.

A number of factors contribute to the unsteadiness of the exiting flow. These include the effects of wakes formed by the passage vortex and leakage flows, the secondary flows caused by the inlet velocity and temperature profiles, and the flow fluctuations originating in the burner; however, probably the most significant type of unsteadiness in the flow through a turbine is that created by the wakes behind the individual airfoils. Due to the variations of velocity and temperature

in these wakes, the flow relative to the following row fluctuates in a regular periodic manner.

To illustrate this point, the wake behind a row of airfoils is depicted two dimensionally in Fig. 1. Using a turbulent wake calculation for a typical turbine situation, the maximum deficits of velocity and total temperature at the leading edge position of the following row will be approximately

$$\frac{U_{\infty} - U}{U_{\infty}} = .17 \qquad \frac{T_{\infty} - T}{T_{\infty} - T_c} = .13$$

respectively, where U and T are the wake centerline values and T_c is the coolant inlet temperature. (For highly loaded and cooled blades these values are even higher.) The wake width, $2b$, at this position may also be estimated and is found to be on the order of the gap width, τ . There is hence a slight interference between adjacent wakes, although they are not fully mixed.

In relation to a position fixed with respect to the next blade row, the individual wakes of the airfoils in the preceding row pass at a period equal to the pitch, P , of the preceding row divided by the wheel speed, ωr . Since the fluid in the wakes is moving slower than the main-stream fluid, it drifts upstream. The magnitude of this velocity deficit varies as the wake passes, and hence the flow incident to the second blade row varies both in direction and magnitude with time; that is, the incident flow is unsteady. To illustrate this effect, the velocity triangles at an interrow position are depicted in Fig. 2. Here velocities relative to the rotating row are depicted by the subscript R and the wake vectors by dashed lines. All vectors are assumed to be parallel at the first row

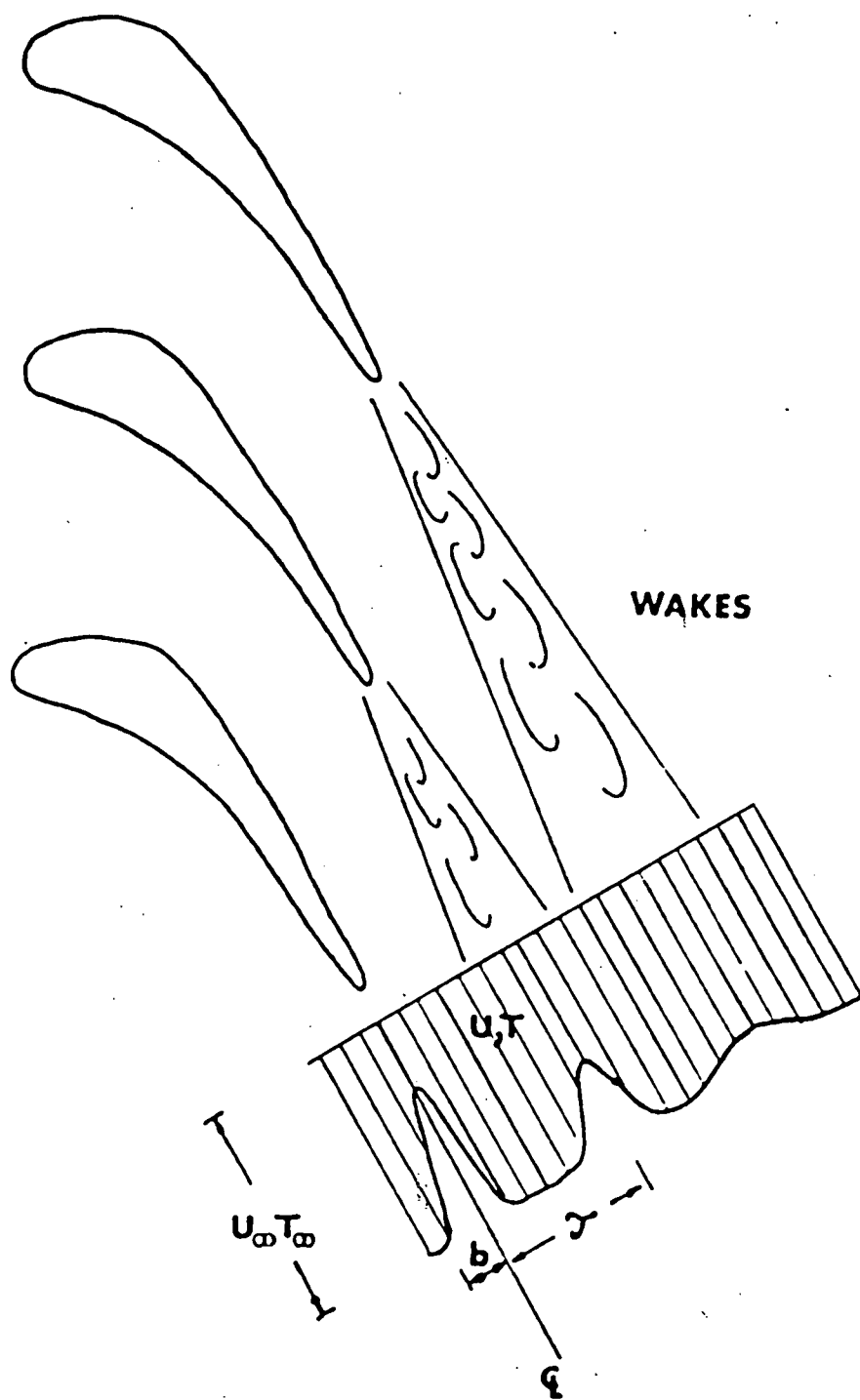


Figure 1. Airfoil wakes

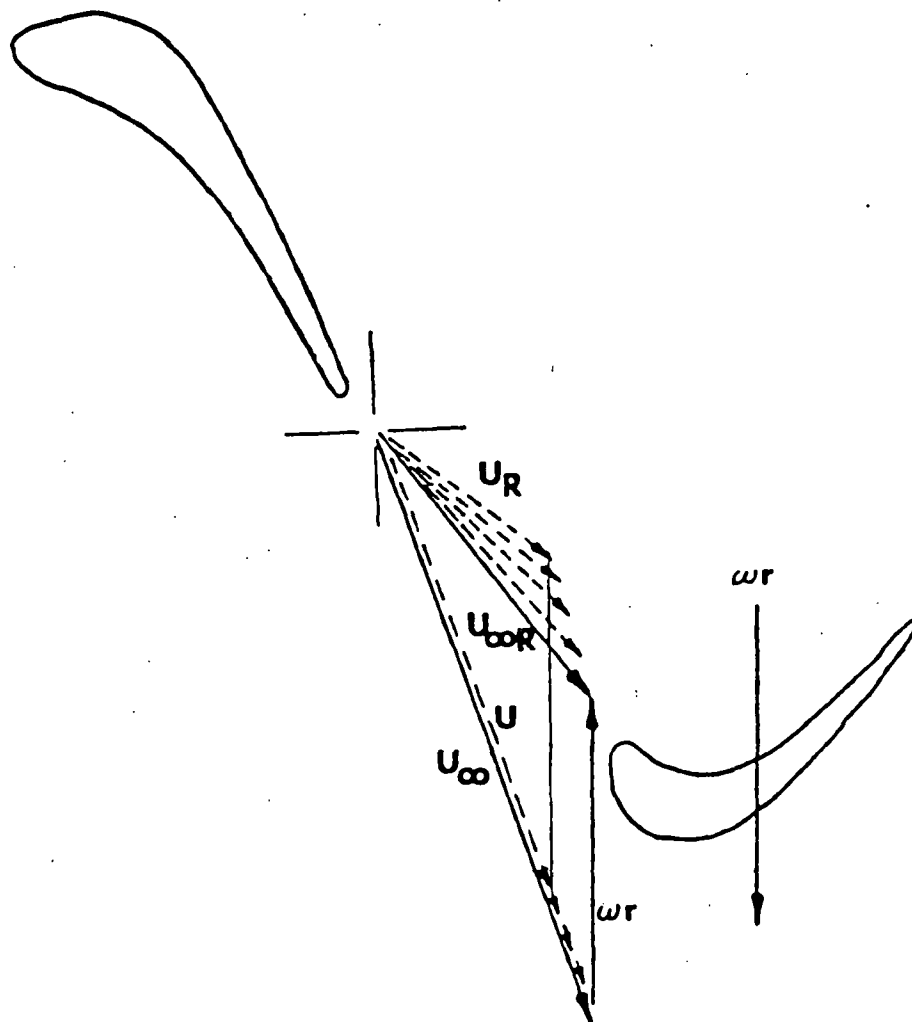
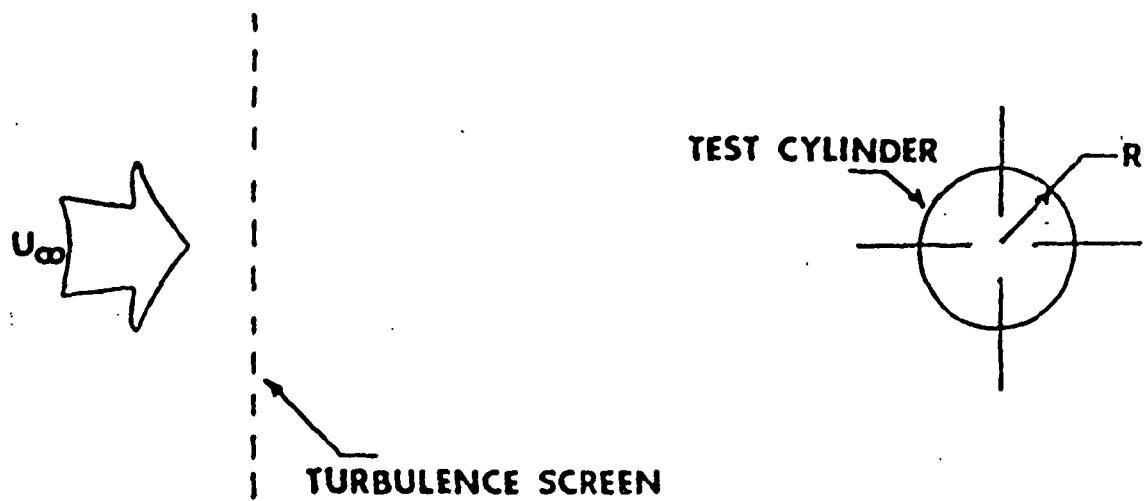


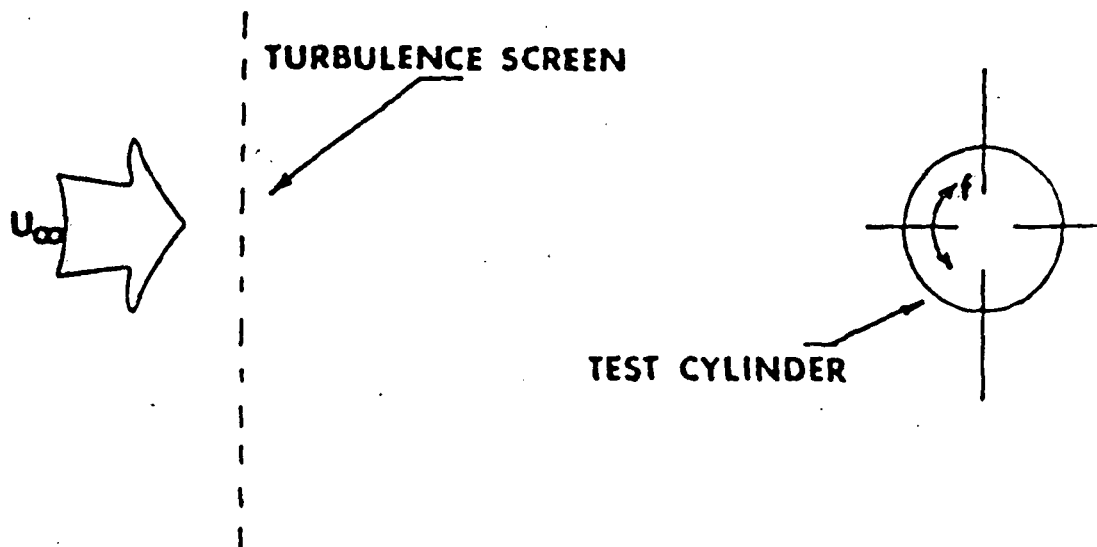
Figure 2. Velocity triangles at an interrow position

exit. In addition to the velocity deficit there is also a temperature deficit in the wake fluid as a result of both the decreased velocities and the injection of coolant along the surface of the upstream blade. This deficit is also a function of time when examined from a reference frame fixed with respect to the next blade row. Consequently, the flow incident on this second blade row is unsteady with fluctuations in: 1) its angle of attack, 2) its magnitude, and 3) the freestream temperature. Incidentally, since the turbulence characteristic of the wake is different than that of the mainstream, it also varies.

As a part of an ongoing investigation into these unsteady effects, the current research effort examined the effect of a periodic variation in the angle of attack upon the local heat transfer rate in the leading edge region of a turbine blade. To model this effect, a simple and rather basic experiment was used. The flow arrangements of the experiment performed are schematically shown in Fig. 3. Since the leading edge region in most blade designs is formed by a cylindrical surface, a circular cylinder was used as a large scale model of the leading edge region. In all of the experiments a nominally uniform steady flow with a superimposed level of turbulence was used. To establish a basis of comparison for later tests, the initial series of experiments, illustrated in Fig. 3a, were performed on a stationary cylinder. The results of these tests can also be compared with the large volume of currently available measurements of the transfer rate from a circular cylinder in a uniform flow. For the unsteady phase of the investigation, the cylinder was oscillated rotationally about its axis. This flow configuration, illustrated in Fig. 3b, simulates the fluctuation in the angle of attack



3a. Stationary cylinder



3b. Oscillating cylinder

Figure 3. Experimental configurations

of the flow incident to the turbine blade, since the incident flow angle fluctuates relative to the test cylinder. The parameters relevant to the experiment were chosen to model the actual turbine situation.

The oscillation of the test cylinder made the use of a heat transfer measurement technique unrealistic, since a heat transfer test body requires hundreds of electrical heating and thermocouple connections. These would fare poorly through the literally half-million cycles necessary to complete a single test. For this reason, a mass transfer measurement technique was utilized in the experiments. As will be discussed later, heat transfer information can be inferred from the mass transfer results using the well-known heat-mass transfer analogy.

During the investigation, a remarkable three-dimensional effect was observed. Although the flow field incident to the test cylinder was "nominally" uniform with a mean velocity constant to within $\pm .2\%$, large variations in the local transfer rate along the stagnation line were observed. A separate investigation into the nature and causes of this phenomena became a significant portion of the final research effort. To the author's knowledge, the reported measurements of spanwise variations in the local transfer rate and their connection to the incident flow field are the first of their kind. The results suggest that the well studied stagnation flow situation is, as of yet, not fully understood. As will be discussed later, this flow is, in a respect, unstable with significantly large deviations from the typical two-dimensional models. The results of the current research suggest that the full characterization of realistic stagnation flow fields, such as those found in a turbine, should consider this type of effect.

PART 2

HISTORICAL REVIEW

Numerous investigations, both theoretical and experimental, have been conducted to determine the heat transfer rate from a cylinder in a high Reynolds number crossflow. For the most part, these studies have assumed the incident flow field to be nominally steady and uniform, and that the effects of turbulence are also two dimensional in the average sense. For the case without turbulence, the usual theoretical treatment, first utilized by Frossling [1] and later by Merk [2] is to use a laminar boundary layer analysis together with an experimentally determined free-stream velocity distribution to yield the local transfer rate over the forward portion of the cylinder up to separation. An analysis valid for the turbulent wake found after separation has yet to be presented. The laminar analyses demonstrate that the local nondimensional heat transfer coefficient, Nu , is dependent only on the incident Reynolds number, Re , and the Prandtl number, Pr , a ratio of the diffusivity of vorticity, ν , to the diffusivity of heat, α . In the leading edge region, the dependence of the local heat transfer coefficient on these parameters is well represented by the relation

$$Nu \propto Re^{1/2} Pr^n$$

where the selected value for the coefficient n depends upon the Prandtl number range of interest.

Early experiments to determine the rate of heat and mass transfer from cylinders in crossflow, such as those of Drew and Ryan [3], Small [4], and Schmidt and Wenner [5], were for the most part incompatible with each

other and with the developed laminar theory. This discord was somewhat clarified by subsequent investigations which quantitatively demonstrated the substantial effect of incident turbulence on the local transfer rate. The first results of this type were reported by Comings, Clap and Taylor [6]. The additional intensive investigations of Bollen [7] and Zapp [8] indicated that heat transfer distributions characteristic of Reynolds numbers higher than the incident Reynolds number were obtained when the incident turbulence level was elevated and increases in the local heat transfer as large as 40% were observed. More recent studies [9 - 17] provide additional proof of the significant increase in the local transfer rate with an increase in turbulence level. Additionally a number of recent investigations, notably those of Yardi and Sukhatme [18] and Traci and Wilcox [19], suggest that not only is the turbulence level important but also its scale. In particular, it appears that the maximum effect of incident turbulence occurs when its integral length scale is on the order of ten times the boundary layer thickness. Unfortunately, the data from measurements of the transfer rate in turbulent fields is too widely scattered to provide a precise empirical relation and the comparison of the data from different investigators is limited by the rather widespread variation in the methods utilized to measure and report turbulence. Generally, the data suggests that, when the turbulent length scale is kept constant, the dependence of the local heat transfer coefficient on the turbulent intensity, Tu , is of the form

$$Nu/\sqrt{Re} = fnc(Tu\sqrt{Re})$$

In addition to the nominally two-dimensional work, theoretical and experimental investigations have been conducted for spanwise periodic

incident flows. Treating only the region near stagnation, Suter, Maeder and Kestin [20] and Suter [21] obtained solutions to the laminar boundary layer equations which exhibit a regular spanwise pattern of streamwise vortices lying within the boundary layer. The theoretical work of Sadeh, Suter and Maeder [22] suggests that spanwise periodic disturbances in the incident flow can be unstable insofar as they are greatly amplified as the flow approaches stagnation. This conclusion, although derived in a questionable manner, is confirmed by a number of flow visualization studies performed in the wakes of cylinders and turbulence grids. A quasisteady vortical behavior is remarkably evident in the results of Colak-Antic [23] obtained using a hydrogen bubble technique and in the smoke injection visualization work of Nagib and Hodson [24]. The hot-wire studies performed by Hassler [25] quantitatively demonstrate the development of the wake field behind a row of cylinders into a quasiregular unsteady flow on the stagnation zone. As pointed out in the extensive review of the subject presented by Morkovin [26], the experimental work to date strongly suggests the existence of an inherent instability in stagnation flows which give rise to a quasisteady vortex cell structure. As discussed by Morkovin, a full physical understanding of the phenomena has yet to be presented, and it is not yet known whether the observed three dimensionality can exist without being driven by slight irregularities in the incident flow field. The current research effort shows that the magnitude of the effect of the phenomena on the local transfer rate, even when driven by very small irregularities in the oncoming flow, necessitates a substantial alteration in the current physical conception and modeling of realistic stagnation flows.

A number of theoretical investigations have also been performed in an attempt to evaluate the effects of periodic unsteadiness in the flow incident to the stagnation zone. Lighthill [27] has presented a general theory to model the response of a laminar boundary layer to periodic fluctuations in the magnitude of the external flow field, and has applied the theory to stagnation flows. Rott [28] and Glauert [29] have derived exact solutions for the case of a flow stagnation on a plate which oscillates in its own plane. In this case the flow fluctuates not only in magnitude but also in direction. Recently, Childs [30] theoretically considered the problem of a circular cylinder oscillating rotationally in a steady incident stream, bringing into consideration the additional effects of curvature. In this case, the flow relative to the cylinder fluctuates in direction only. Expressions for the unsteady laminar skin friction and the local heat transfer coefficient were derived by extension of the methods of Lighthill, Rott and Glauert. The results suggest that the time-averaged, local transfer rate is slightly decreased but differs by less than 4% from the steady case. To date, the importance of incident turbulence to the effects of periodic unsteadiness in the flow field has not been theoretically or experimentally investigated. The reported research includes a study of this aspect of the problem.

PART 3

THEORETICAL CONSIDERATIONS

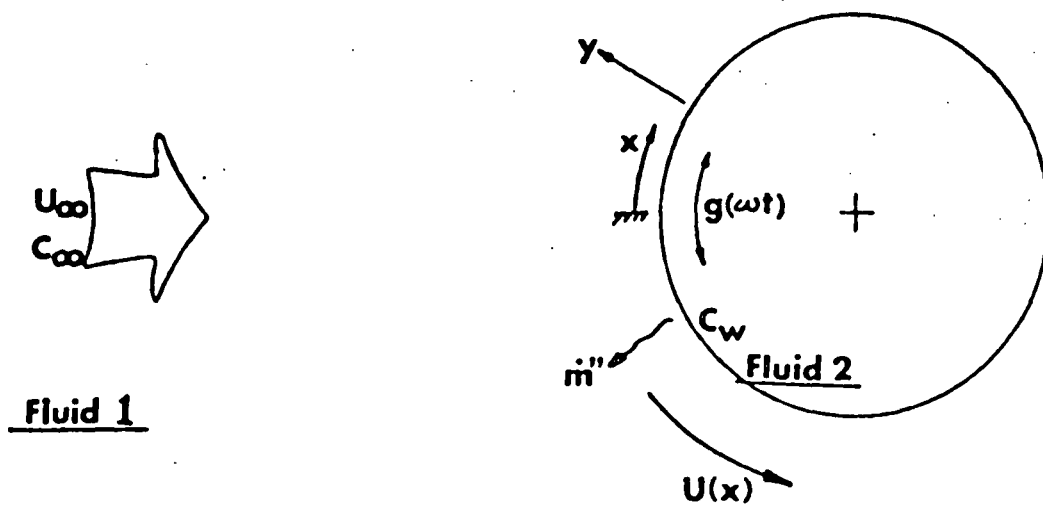
3.1 Constituent Equations and Significant Parameters

Consider a cylinder oscillating rotationally in an incompressible laminar flow as depicted in Fig. 4a. The flow is assumed to be steady, uniform and two dimensional. A fluid (Fluid 2), different than that of the mainstream flow (Fluid 1), is transported from the cylinder into the flow by a mass transfer process. At the surface of the cylinder the mass concentration of Fluid 2 is kept constant at a value C_w . The concentration of Fluid 2 in the undisturbed flow is C_∞ . By virtue of the heat-mass analogy, discussed in Sec. 3.2, this problem is analogous to that depicted in Fig. 4b, where heat is transported from cylinder whose surface is kept at a constant temperature, T_w into a fluid whose temperature far upstream of the cylinder is T_∞ .

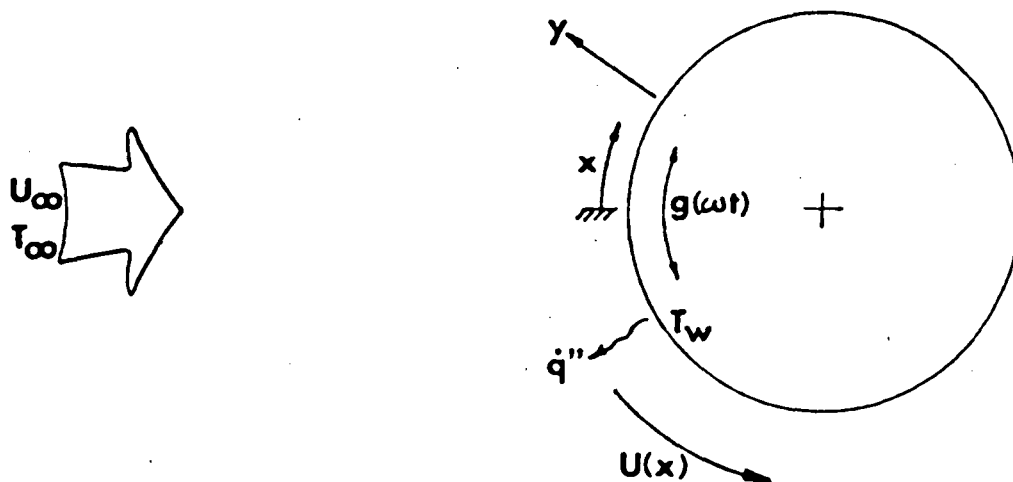
For this discussion, a boundary layer coordinate system, depicted in Fig. 4a, will be used. This reference frame is fixed in space. The coordinate x indicates the distance along the surface of the rotating cylinder from a line which passes through the cylinder's axis. The coordinate y is measured from the surface of the cylinder. The corresponding velocities are denoted by u and v , and the pressure by p . The local mass concentration of Fluid 2 is denoted by C . The position of a point P on the surface of the cylinder is described, with respect to this coordinate system, by

$$x(P) = x_0(P) + Ag(2\pi ft)$$

where $x_0(P)$ denotes its time-averaged position, A is the maximum displacement,



4a. Mass transfer - constant surface concentration



4b. Heat transfer - constant surface temperature

Figure 4. Illustration of transfer processes from an oscillating cylinder

g is a periodic function, f is the frequency of oscillation and t denotes time. The surface velocity is then given by $A \frac{dg}{dt}$.

The appropriate boundary layer equations are

$$\frac{\partial u}{\partial x} + \frac{\partial v}{\partial y} = 0 \quad (\text{Continuity})$$

$$\frac{\partial u}{\partial t} + u \frac{\partial u}{\partial x} + v \frac{\partial u}{\partial y} = U \frac{\partial U}{\partial x} + \nu \frac{\partial^2 u}{\partial y^2} \quad (\text{Conservation of momentum})$$

$$\frac{\partial C}{\partial t} + u \frac{\partial C}{\partial x} + v \frac{\partial C}{\partial y} = \mathcal{D} \frac{\partial^2 C}{\partial y^2} \quad (\text{Mass diffusion equation})$$

where $U(x)$ is the free stream velocity external to the boundary layer, and ν denotes the kinematic viscosity and is assumed to be constant. The diffusion coefficient for the diffusion of Fluid 2 into Fluid 1 is \mathcal{D} .

The boundary conditions are

$$C = C_w, u = A \frac{dg}{dt}, v = 0^\dagger \text{ at } y = 0$$

$$C \rightarrow C_\infty, u \rightarrow U(x) \text{ as } y \rightarrow \infty$$

It is appropriate to put the governing equations into a dimensionless form. For this purpose, the dimensionless quantities

$$u^* = u/U_\infty \quad x^* = x/R$$

$$v^* = v/U_\infty \quad y^* = y/R$$

$$U^* = U/U_\infty \quad t^* = ft$$

$$C^* = \frac{C - C_w}{C_\infty - C_w}$$

[†]As will be discussed in the analogy section, the boundary condition $v = 0$ is an approximation.

are defined, where R denotes the cylinder's radius and U_∞ the magnitude of the flow velocity far upstream of the cylinder. Using these quantities, the governing equations can be written in a nondimensional form as

$$\frac{\partial u^*}{\partial x^*} + \frac{\partial v^*}{\partial y^*} = 0$$

$$\left(\frac{fD}{U_\infty}\right) \frac{\partial u^*}{\partial t^*} + u^* \frac{\partial u^*}{\partial x^*} + v^* \frac{\partial u^*}{\partial y^*} = U^* \frac{\partial U^*}{\partial x^*} + \left(\frac{v}{U_\infty D}\right) \frac{\partial^2 u^*}{\partial y^{*2}}$$

$$\left(\frac{fD}{U_\infty}\right) \frac{\partial C^*}{\partial t^*} + u^* \frac{\partial C^*}{\partial x^*} + v^* \frac{\partial C^*}{\partial y^*} = \left(\frac{\mathcal{D}}{v}\right) \frac{\partial^2 C^*}{\partial y^{*2}}$$

and the boundary conditions can be written as

$$C^* = 0, \quad u^* = \left(\frac{A}{D}\right) \left(\frac{fD}{U_\infty}\right) \frac{dg(t^*)}{dt^*} \quad \text{at } y^* = 0$$

$$C^* = 1, \quad u^* = U^*(x^*) \quad \text{as } y^* \rightarrow \infty$$

By inspection of these dimensionless equations, it is obvious that the laminar problem is governed by four nondimensional groupings:

$\left(\frac{U_\infty D}{v}\right)$, (v/\mathcal{D}) , $\left(\frac{fD}{U_\infty}\right)$ and (A/D) . The first three are the Reynolds number,

Re , a ratio of inertial to viscous forces; the Schmidt number, Sc , a ratio of the diffusivity of vorticity to the diffusivity of mass; and the Strouhal number, a nondimensional oscillation frequency. The remaining parameter, (A/D) is the characteristic amplitude of oscillation which will be denoted by ϕ_0 . To model the actual turbine situation, the Reynolds number in the reported investigation was varied between 75,000 and 125,000, and Strouhal numbers from 0.0071 to 0.1406 were used.

An oscillation amplitude of $\phi_0 = 0.105$, which is also characteristic of that in a turbine, was used for the majority of the experiments. The effect of a larger amplitude, $\phi_0 = 0.210$, was also investigated. In the experiments, naphthalene vapor was utilized as the mass transfer substance. The Schmidt number for the diffusion of naphthalene in air is approximately 2.5.

Since the flow in a turbine contains a degree of superimposed turbulence, the experiments were performed for a number of incident turbulent conditions. Experimentally, turbulence in an incident flow field is typically characterized by a turbulence level, Tu , a ratio of the root mean square turbulent velocity fluctuation to the free stream velocity, and an integral length scale parameter, L , an average eddy size, which is typically nondimensionalized by the diameter of the cylinder, D . Turbulence levels up to 4.9% were used and L/D varied between 0.012 and 0.188.

3.2 The Analogy Between Heat and Mass Transfer

The existence of a direct analogy between the heat transfer rate from an isothermal surface and the rate of mass transfer from a surface of constant mass concentration is readily demonstrated by an examination of the governing physical equations.

The flow of a constant property fluid is governed by the continuity and Navier-Stokes equations and their appropriate boundary conditions. These equations, and hence the character of the flow, are unaltered by the presence of heat or mass transfer, provided that the properties of the fluid, i.e. its density and viscosity can be assumed to remain constant. In the reported experiments the maximum local mass concentration, that is the ratio of the local density of naphthalene to the density of the air flow, was on the order of 2.9% hence, this constant property assumption is valid. Additionally, in order for an analogy to exist, the boundary conditions on the equations of motion for the heat and mass transfer situations must be identical. For the heat transfer case, the velocities both normal and perpendicular to the surface are zero; however, for the mass transfer case there is a finite velocity, V_w , at the boundary due to the transport of vapor from the surface. This velocity is equal to the mass flow rate, \dot{m} , of the diffusing vapor divided by its density. For the present case the velocity is on the order of $2(10^{-5})$ ft/sec. Since the velocity of the mainstream is on the order of 30 ft/sec, only very small errors are incurred by assuming $V_w = 0$.

Having shown that the flow fields in the mass and heat transfer situations are essentially identical, the analogy between the two processes can be demonstrated by an examination of the relevant transfer equations

and boundary conditions. To maintain generality, the turbulent form of the equations will be used.

Mass transfer in a two-component, nonreactive system is characterized by the equation

$$\frac{DC^*}{Dt^*} = \frac{1}{Re \cdot Sc} \frac{\partial}{\partial x_i^*} \left[\left(1 + \frac{\epsilon}{\nu} \frac{Sc}{Sc_t} \right) \frac{\partial C^*}{\partial x_i^*} \right]$$

where $\frac{D}{Dt}$ denotes the material derivative and an indicial notation has been employed for convenience. The quantity C^* denotes a ratio of mass concentrations:

$$C^* = \frac{C - C_w}{C_\infty - C_w}$$

where C_w is the concentration of the diffusing substance at the wall and C_∞ is the concentration of the unaffected flow. Sc_t is the turbulent Schmidt number, defined as the ratio of the turbulent diffusivity of momentum to the turbulent diffusivity of mass; and is in general a function of position, Reynolds number and Schmidt number. The relevant boundary conditions are

$$C^* = 0 \text{ at the surface}$$

$$C^* \rightarrow 1 \text{ at a distance far from the surface}$$

The heat transfer process is described by the dimensionless turbulent energy equation:

$$\frac{DT^*}{Dt^*} = \frac{1}{Re \cdot Pr} \frac{\partial}{\partial x_i^*} \left[\left(1 + \frac{\epsilon}{\nu} \frac{Pr}{Pr_t} \right) \frac{\partial T^*}{\partial x_i^*} \right]$$

where the coordinates and velocities are nondimensionalized by characteristic parameters T^* is the ratio

$$T^* = \frac{T - T_w}{T_\infty - T_w}$$

where T_w is the temperature of the isothermal surface, T_∞ is the temperature of the fluid far from the wall, and T is the local fluid temperature. Pr_t denotes the turbulent Prandtl number defined as the ratio of the turbulent diffusivity of momentum, ϵ , to the turbulent diffusivity of heat. In general, Pr_t varies with position, Reynolds number, and Prandtl number. The appropriate boundary conditions for the energy equation are

$$T^* = 0 \quad \text{on the surface}$$

$$T^* \rightarrow 1 \quad \text{at a distance far from the surface}$$

The two descriptive transfer equations are seen to be of identical form provided that $Pr_t = Sc_t$, an assumption which is well supported by experimental evidence. Therefore, since the imposed boundary conditions are identical, the two equations have the same solution when T^* and Pr are replaced by C^* and Sc , respectively.

A solution to the equations would provide the local transfer rates on the surface. Typically, these are given in nondimensional form by the Sherwood number, Sh , and the Nusselt number, Nu , which are defined as

$$Sh = (\partial C^* / \partial n^*)_w$$

$$Nu = (\partial T^* / \partial n^*)_w$$

where n is a nondimensional coordinate normal to the surface and the subscript w indicates that the values at the surface are used. Since the definitions of these quantities are also similar, it is obvious that for a specific point on the surface

$$Sh = \text{fnc} (Re, Sc)$$

$$Nu = \text{fnc} (Re, Pr)$$

where the functions in the two equations are identical. It is then obvious that distributions of the local heat transfer rate can be inferred from the measured mass transfer distributions by simply replacing Sh and Sc by Nu and Pr , respectively. The mass transfer results may be considered as heat transfer results at a Prandtl number equal to the appropriate Schmidt number.

For the case at hand, flow over a circular cylinder, the dependence of the Nusselt number on the Prandtl number may be determined from a laminar boundary layer series solution of the type used by Frossling [1]. This dependence is well represented by

$$Nu \propto Pr^n$$

where the value of n depends upon the Prandtl number range of interest. Naphthalene, which was used in the experiments as the mass transfer substance, has a Schmidt number of approximately 2.5. Utilizing an experimentally determined velocity distribution and the calculation procedures of Childs [30], the results of laminar analyses for Prandtl numbers of 2.5 and .7 were compared, and a value of $n = .38$ was determined. Hence, the heat transfer coefficients on a circular cylinder in a cross stream may be calculated from the experimental mass transfer results by the equation

$$Nu = Sh \left(\frac{Sc}{Pr} \right)^{.38}$$

$$Sc \approx 2.5 \quad Pr \approx .7$$

PART 4

EXPERIMENTAL APPARATUS AND PROCEDURE

4.1 Wind Tunnel Apparatus

The experiments were performed in a low speed, open circuit wind tunnel built specifically for the study of turbine blade leading edge problems. This facility is schematically illustrated in Fig. 5. The air supply is provided by a centrifugal blower with variable angle inlet control vanes for adjusting the tunnel flowrate. The blower rotates at 1820 rpm producing a maximum flowrate of 13500 cfm. From the blower the air passes through a plenum, which is schematically illustrated in Fig. 6a, containing a series of screens and baffles and a honeycomb flow straightener and is then accelerated through a two-to-one contraction nozzle into a turbulence generating section. The flow passes from the turbulence section into the working section of the tunnel in which the test cylinder is located. The flow then exits the tunnel and circulates back into the room. As will be explained later, it became necessary to reduce the operating temperature of the tunnel during the mass transfer tests. For this purpose, a large central air-conditioning unit was installed in the tunnel room. Air from this unit mixes with that exiting the tunnel and, in this manner, the operating temperature for experiments can be held constant to within 2°F. Temperatures on the order of 65° to 70°F were typically chosen. Through the course of each test, the temperature of the incident flow was monitored using a thermocouple placed in the flow. The velocity of the incident flow was monitored with a pitot static tube. The thermocouple and pitot static tube

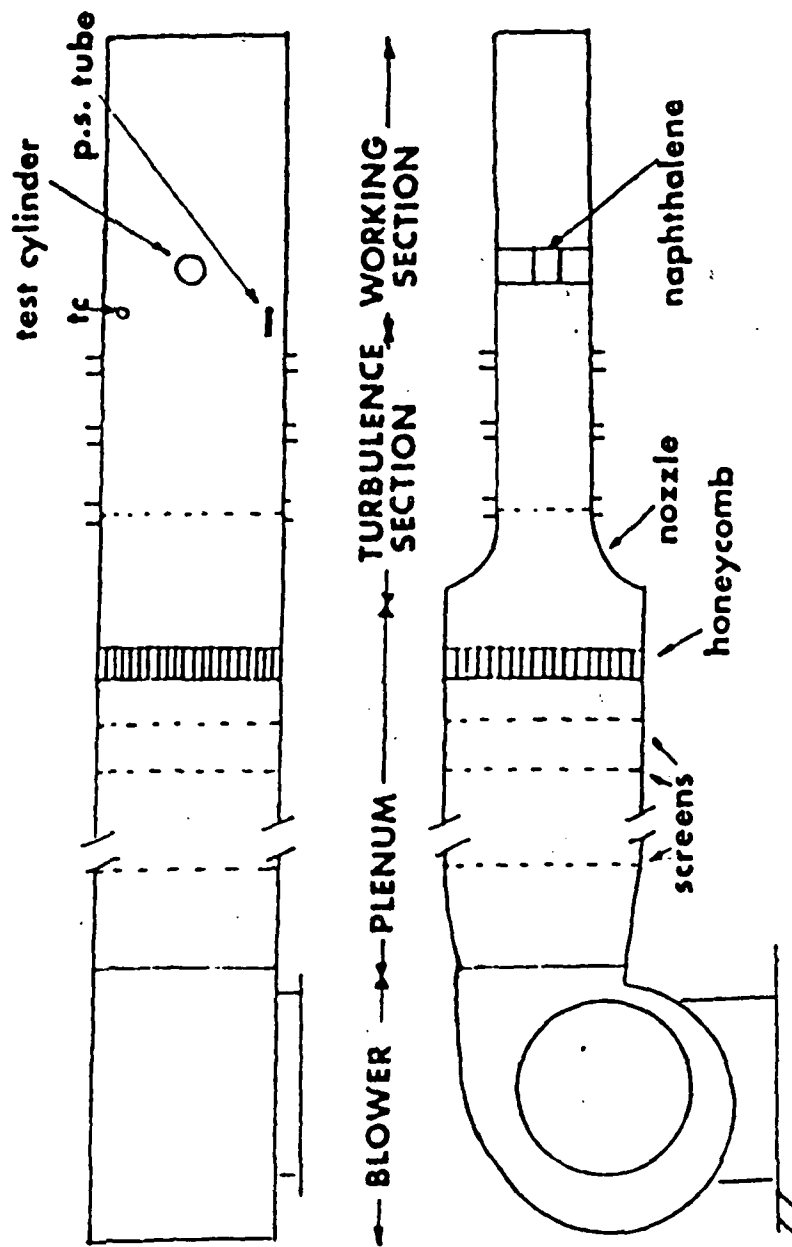
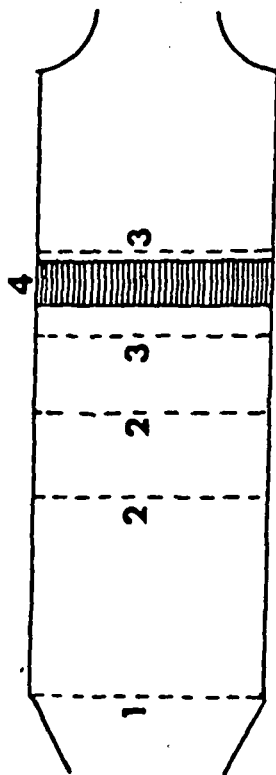


Figure 5. Schematic of wind tunnel facility

20"



6a. Normal configuration

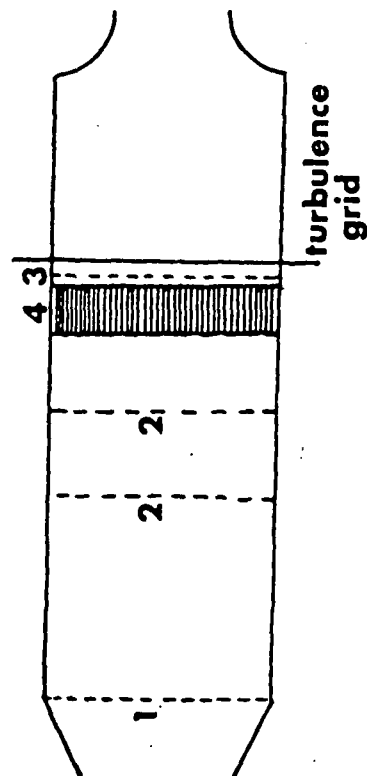
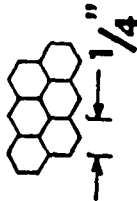
1 woven wire screen 32M

2 baffle



3 woven wire screen 16M

4 honeycomb flow straightener



6b. Configuration for turbulence screen installer

Figure 6. Plenum chamber configurations

were installed in the working section of the tunnel ahead of and to either side of the test cylinder as shown in Fig. 5. The positions were chosen to be external to the flow region affected by the presence of the cylinder.

The special requirements of the experiments necessitated the construction of a working section specifically designed for the program. The section measures 18" high by 30" wide and is 70" long. The available flow velocities through the section are such that the Reynolds number of the flow incident to the 6" diameter test cylinder can be varied between 50,000 and 130,000; modeling those typical of incidents flows on the leading edges of turbine blades. For rigidity, the working section was constructed mainly from aluminum channels and plate. A 25" plexiglass panel on the side of the working section provided access to the test cylinder.

The turbulence generating section was also constructed specifically for this series of experiments. For the generation of turbulence, two types of screens were used; hand manufactured round-bar biplane-grids and commercially produced woven wire meshes. The dimensions of the screens used are given in Table 1. To provide greater variability of turbulence level and length scale, three positions are available in the generating section for installation of the screens, allowing the screens to be positioned 15", 30.5", 53.0" upstream of the cylinder's leading edge. The highest intensity available from the section was 2.7%. In an attempt to attain higher incident turbulence levels, a large grid was also constructed for installation in the plenum chamber. The utilized plenum chamber configuration is illustrated in Fig. 6b. This screen provided an intensity of 4.9%. The practical lower limit on the turbulence intensity is the

residual intensity of the tunnel which was determined to be approximately 0.6%.

The configuration of the test cylinder in the tunnel is shown in Fig. 7. The cylinder is composed of three sections held together by an axial tension rod. With the rod in place, the upper and lower cans fit into and hold the central test section, which contains a cast insert of naphthalene - a substance that sublimates at room temperatures. With the tension rod removed, the upper can is free to lift vertically through its bearing allowing the test section to be removed for measurement. The naphthalene surface was measured before and after each test, as described in section 4.3, to determine the amount of local sublimation during the test. The test cylinder was constructed in the manner described to facilitate fast insertion and removal of the test section. As the naphthalene sublimates continually, this was of primary importance to the measurement accuracy. For practical considerations, naphthalene surfaces were cast and measured at a location separate from the wind tunnel laboratory. The measurement and casting procedures will be discussed later.

For the unsteady experiments, the test cylinder with its cast naphthalene surface was oscillated rotationally using a simple direct link driving mechanism mounted to the bottom of the test section. This mechanism is schematically illustrated in Fig. 8. It can be shown analytically that for a sufficiently large value of L/R^2 the oscillation is approximately sinusoidal. This was desirable for easy comparison with theoretical models. A value of $L/R^2 \approx 5$ was used, and the actual oscillation was within 2% of a true sinusoid. The mechanism is powered by a 1/2 hp rotor which drives the smaller disk in the system through a timing

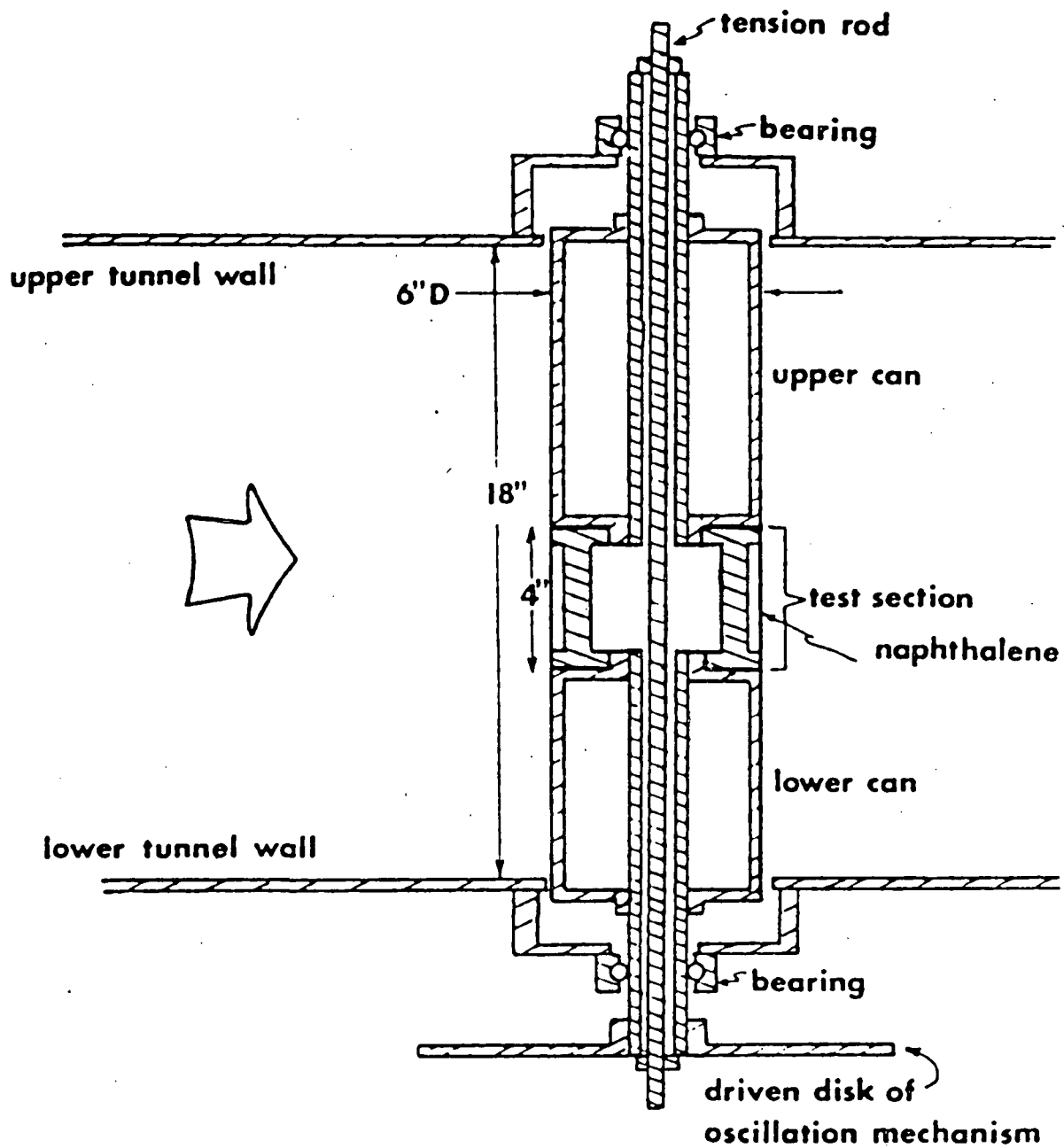


Figure 7. Configuration of test cylinder

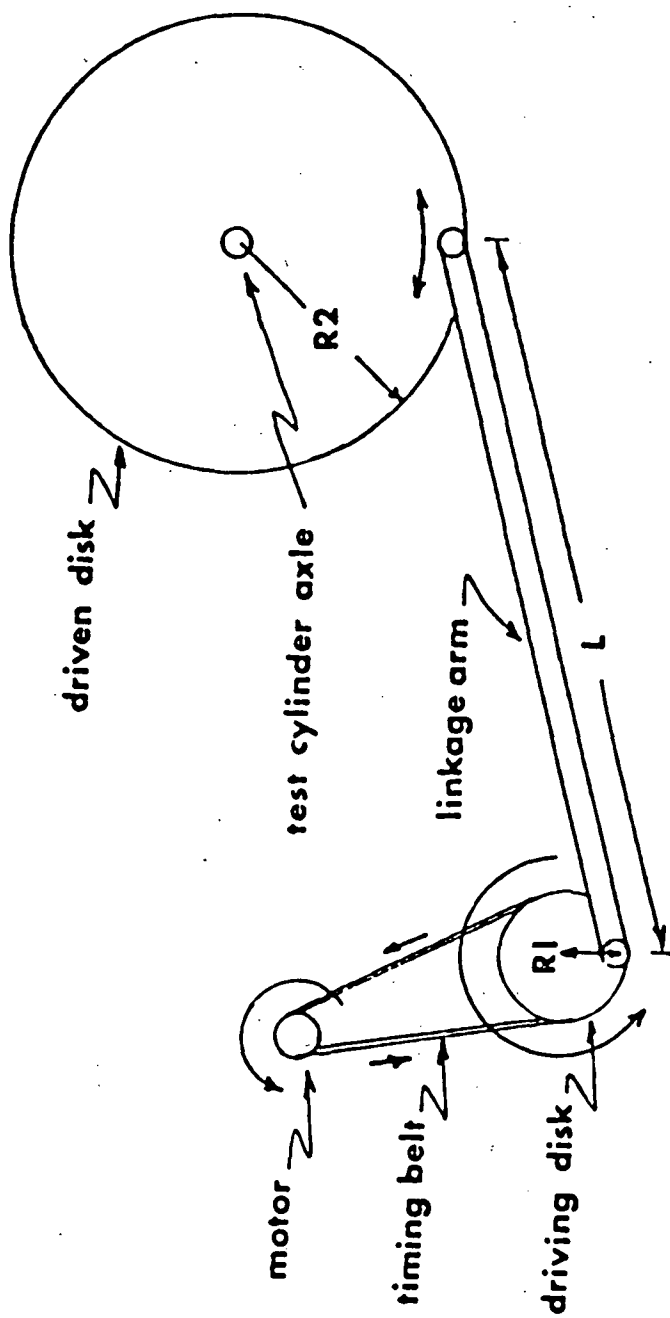


Figure 8. Oscillation mechanism

belt and pulley system. Oscillation amplitudes of $\pm 6^\circ$ were utilized for the majority of the unsteady experiments, and the frequency was varied up to 5.5 Hz. At higher frequencies, vibrations of the test section generated by the oscillatory motion became significant.

4.2 Casting of Naphthalene Surfaces

For the mass transfer tests, naphthalene was cast into the insertable steel test section. The apparatus used for forming the insert is shown in Fig. 9 and a drawing of the test section is shown in Fig. 10. To cast a naphthalene insert into the test section, the cylindrical stainless steel sleeve shown in the figure is slip fit over the rims of the test section to form a mold cavity. This sleeve was machined with a 1/2"-thick wall both to avoid distortion of its shape and to provide a substantial heat sink for the molten naphthalene. In use, this heat sink allowed the freeze front formed by the radial solidification of the naphthalene from both the inner and outer walls of the cavity to be a substantial distance away from the outer surface, providing greater strength and uniformity of the cast surface. To obtain very smooth surfaces, the inner surface of the steel sleeve was honed to a mirror finish when manufactured. To maintain this finish, the sleeve surface was periodically polished with 600 grit wet sandpaper, removing scratches and marks resulting from use.

Before the naphthalene was cast, both the sleeve and the test section were cleaned and degreased by immersion in a bath of clean acetone. After cleaning the mold was assembled with care taken to avoid hand contact with the inner surfaces. Before casting the surface, sufficient time was allowed for the room and casting apparatus to reach a steady temperature

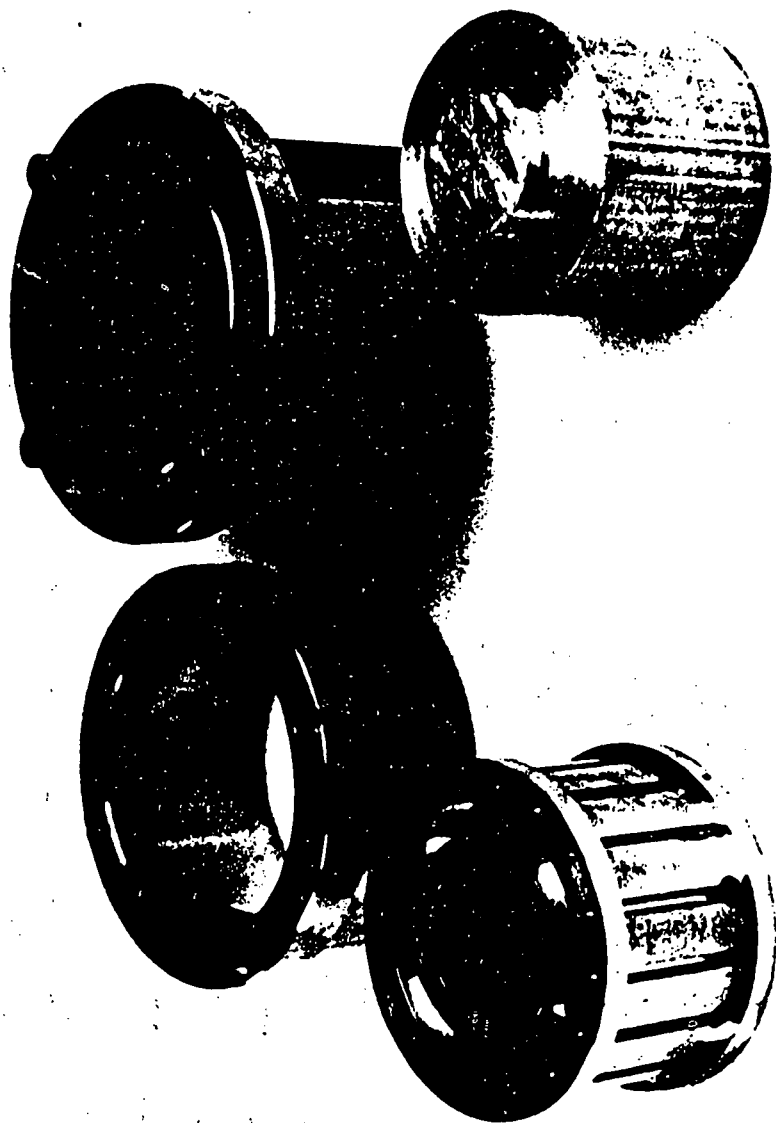


Figure 9. Casting apparatus

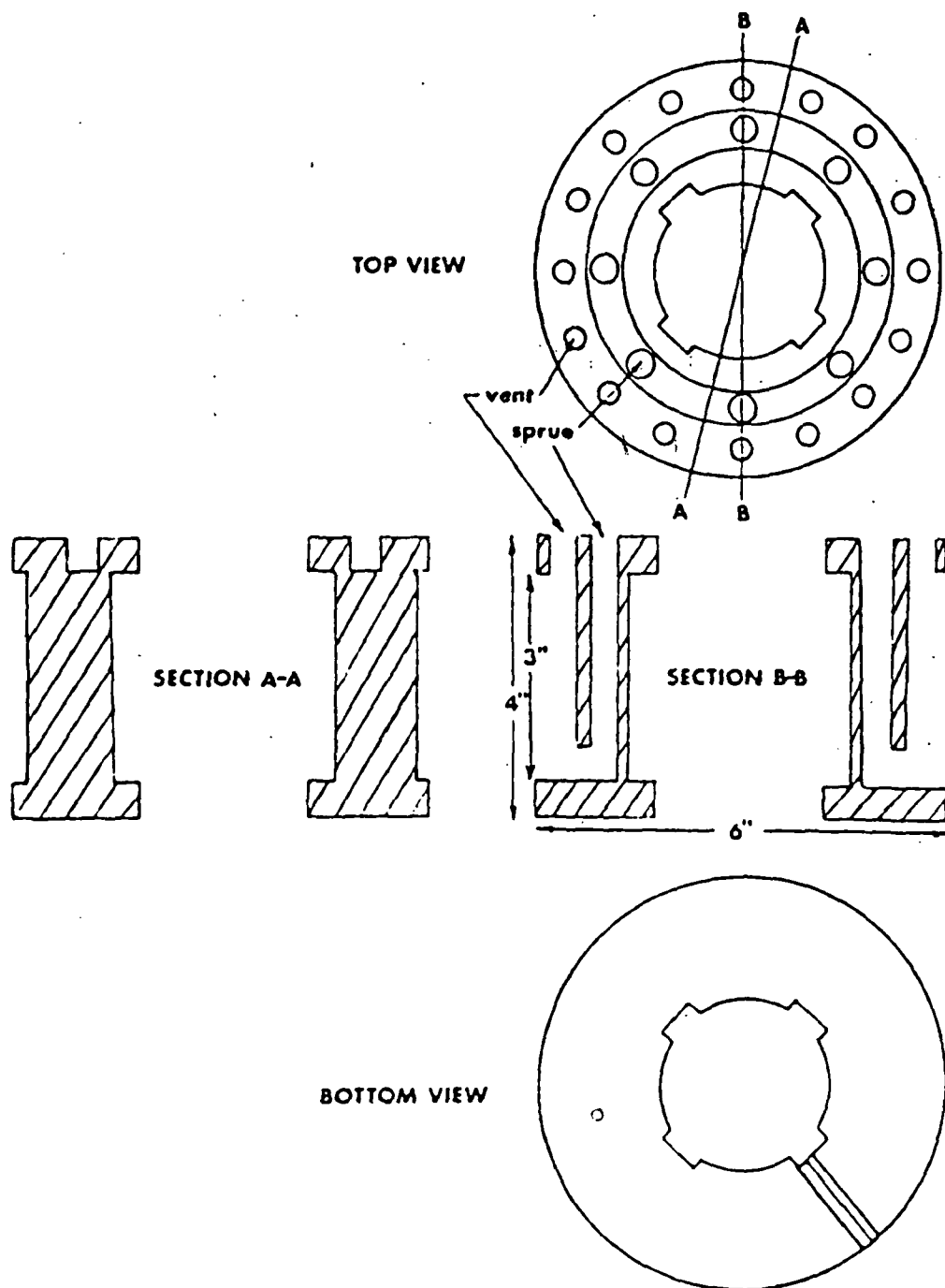


Figure 10. Schematic of test section

of approximately 75°F. Certified grade naphthalene crystals (residue after ignition of .002%) supplied by Fischer Chemical were then melted down in a clean glass flask. The liquid naphthalene was heated to 160°C. Before pouring, local boiling in the flask was allowed to settle. The liquid naphthalene was poured into the mold through the inner ring of holes visible in Fig. 11. The naphthalene traveled down these sprues and entered the mold cavity from the bottom. The outer ring of holes served as vents for the cavity, allowing entrapped air to escape. While the naphthalene in the cavity solidified, it was necessary to periodically unclog the vent holes by pouring hot naphthalene over the top of the mold. This also served to provide additional naphthalene to fill shrink cavities which formed on the surface near the vent holes. This process was continued until molten naphthalene was no longer visible through either the vent holes or the sprues.

The pouring having been completed, the ambient room temperature was lowered to the experimental operating temperature of approximately 65°F, and sufficient time was allowed for the mold to reach steady state (typically 8 hours). This decrease in temperature from the ambient pouring temperature was found to be vital in order to obtain high quality surfaces. Surfaces cast without this decrease were regionally covered with loose naphthalene dust. Attempts to remove this dust resulted in local dips in the naphthalene surface, which were found to cause significant experimental errors. Efforts to further improve surface quality by using larger temperature changes and quenching of the mold, resulted in cracking of the cast.

When the mold had sufficiently cooled, the outer steel ring was removed. To simplify its removal, the entire mold was placed on the

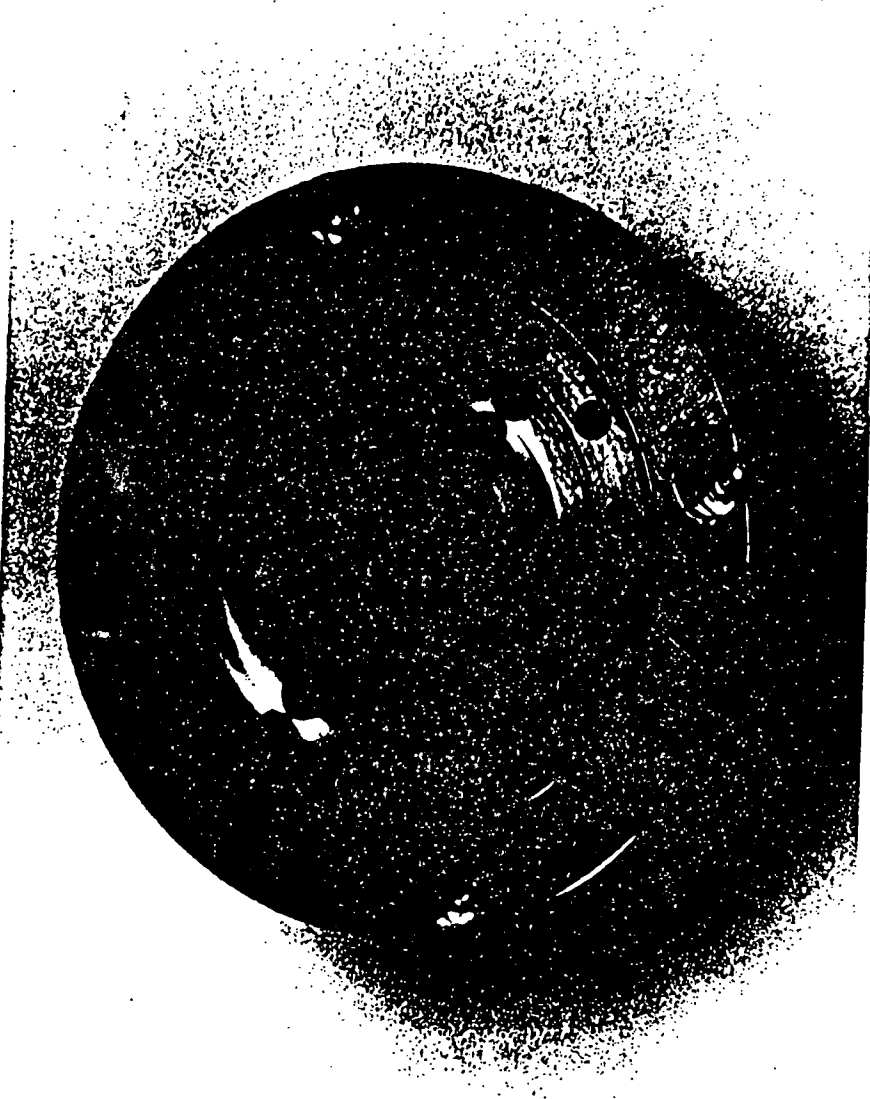


Figure 11. Assembled mold

aluminum pin shown in Fig. 9. (Aluminum was used to avoid damage to the mold.) The specially made drift block also shown in the figure was then positioned onto the steel sleeve, its four pins fitting corresponding holes on the top surface of the sleeve. At this point the sleeve was driven downward with a single, sharp hammer blow to the top of the drift, thus separating the sleeve from the naphthalene case with a shearing motion. To aid in this separation the sleeve was machined with a very slight taper on the order of a tenth of a degree. The substantial blow required to open the mold, necessitated the use of steel for the mold components to avoid impact damage. (A prototype aluminum mold was damaged beyond use after only a few castings.) When removed from the sleeve, the surface of the test section was visually inspected for flaws. A successfully cast surface had a uniform glass-like finish. Significantly flawed surfaces were discarded. (Surfaces with very slight single flaws were occasionally used. In these instances the orientation of the test section in the tunnel was chosen to place the flaw in a region near the rear stagnation point.)

As a final step in the preparation of the test section, the steel rims were dusted with clean towel paper to remove any loose naphthalene particles which could interfere with the profile measurements. Care was taken to minimize contact with the naphthalene surface. Mounting holes and keyways on the top and bottom of the section were also cleaned up at this time to insure a smooth fit onto the measuring table and into the wind tunnel. The prepared test section was then ready to be measured.

It should be pointed out at this time that the procedure described above was arrived at through a detailed trial-and-error process,

and is somewhat different than that used by other authors. Evacuating the mold cavity as described by Sogin and Subramanian [31] was found to be unnecessary. Other authors utilized a parting dust on the inside of the mold cavity to ease in opening of the mold. This technique was avoided as it would cause contamination of the naphthalene surface and probably give rise to substantial experimental errors. Also to guarantee the utmost surface quality, an insert was cast for each test using new naphthalene. Old surfaces were removed in an acetone bath.

Experience with the mass transfer technique has demonstrated a direct connection between the local smoothness and repeatability of the resultant data. Surface casting procedures should be executed with the utmost care and attention to detail. Flawed surfaces should be discarded. The mass transfer technique can yield very repeatable data, but only if carefully performed.

4.3 Naphthalene Surface Measurements

The distribution of the local mass transfer rate on the surface of the test cylinder was determined by differencing profile measurements taken before and after each test. These profile measurements were made using the apparatus shown in Figs. 12 thru 15. When the test cylinder was mounted to the rotary table, four electronic displacement gauges (Federal products type EHE 1048) contacted its surface; one on each steel rim to establish a reference line, and two measuring gauges on the naphthalene surface. The surface could be rotated with respect to the four gauges by means of the rotary table and the two measuring gauges could traverse the naphthalene surface in the spanwise (vertical) direction using the cross slide.

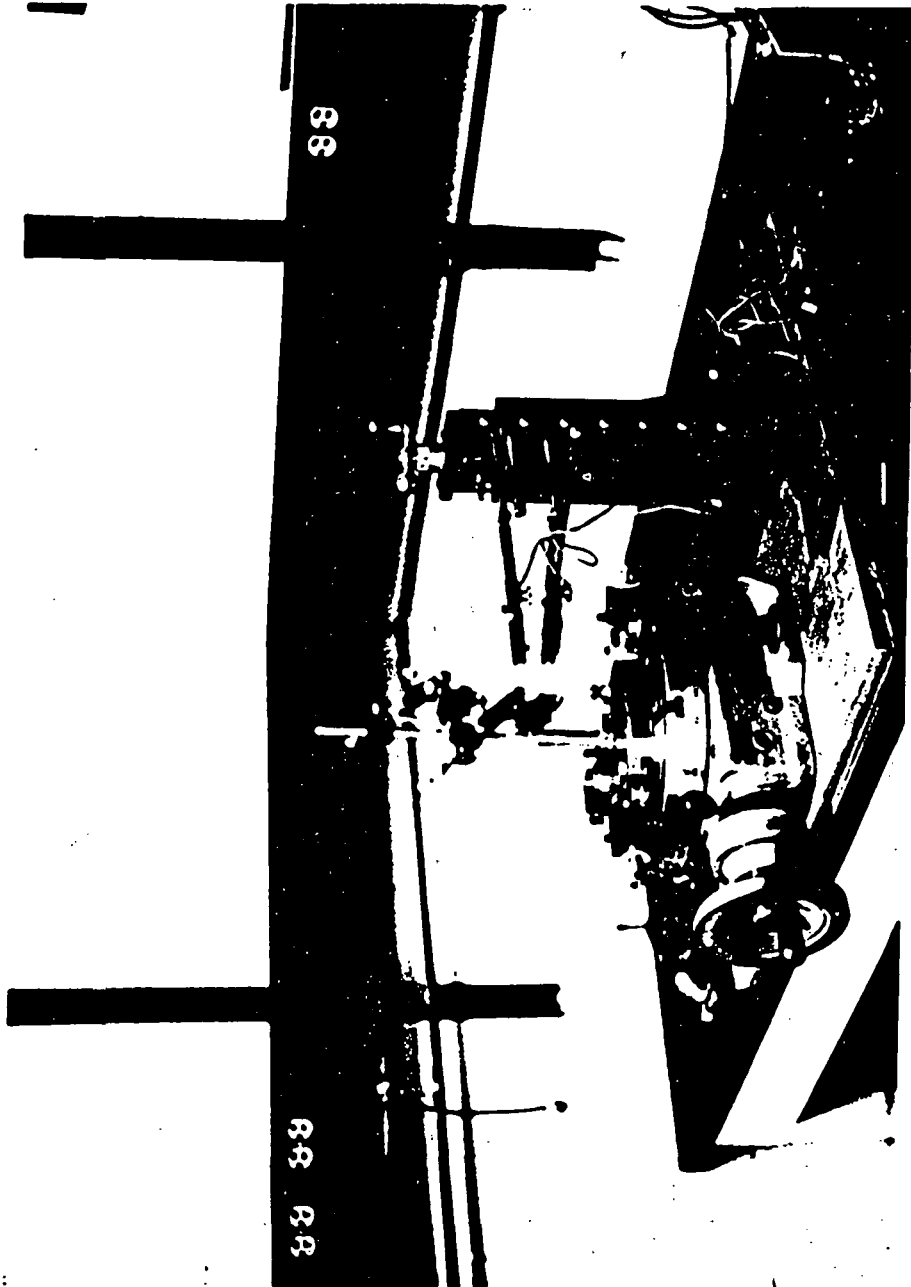


Figure 12. Measuring table

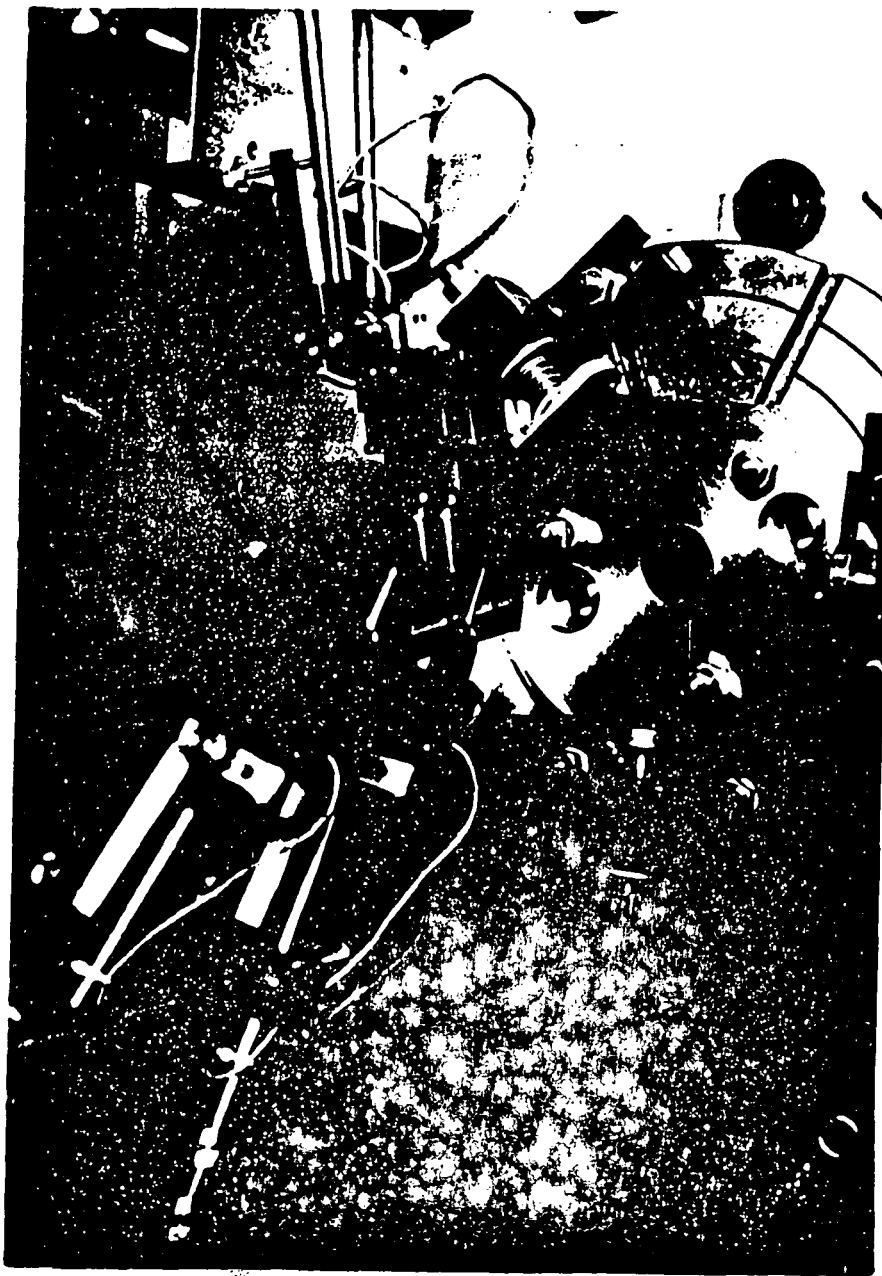


Figure 13. Surface of measuring table

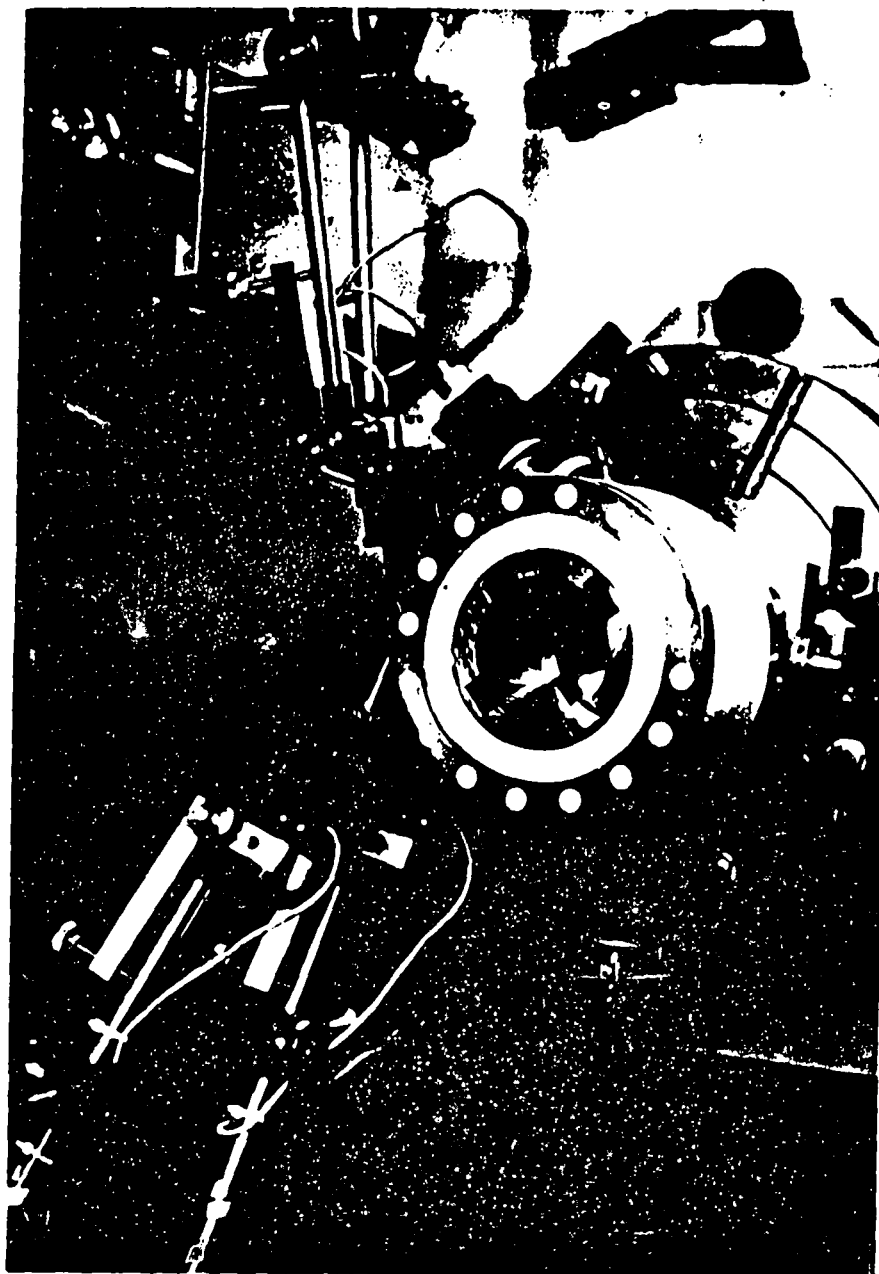


Figure 14. Measuring table with cylinder installed



Figure 15. Contact line of measuring gauges

The test section with its naphthalene surface was positioned on the table by the alignment fixture plate visible in Fig. 12, and shown in greater detail in Fig. 16. This fixture was designed to provide the minimum amount of support necessary to constrain the section against movement, thus optimizing mounting accuracy. It consists of a steel plate holding three support pins which fit into corresponding locations on the base of the test section, as illustrated in Fig. 15. The conically tipped pin fits the small diameter hole in the section, one spherical pin fits the vee-groove and the other simply rests against the flat face of the section's base. The three support pins combined with the rather substantial weight of the test section provide full support. The height of the pins was adjustable to insure that the naphthalene surface was approximately parallel to the axis of rotation of the table.

The alignment fixture was positioned on the rotary table by two adjustable clamp heads bolted to the surface of the table. A third spring loaded head, mounted 135° from each of the other two, held the plate firmly against the adjustable screws. This apparatus, illustrated in Fig. 13, allowed the test section to be accurately centered on the table and, in addition, eased removal and placement of the section onto the alignment fixture. To remove the section, the table was rotated to place one of the adjustable pins 180° from the contact line of the measuring gauges, and the reading of the bottom reference gauge contacting the lower steel rim was recorded. The section was then carefully backed away from the gauges using the adjustable head. To install the section the procedure was reversed, the section being slowly moved inward until the previously recorded position was reached. This technique successfully avoided movement

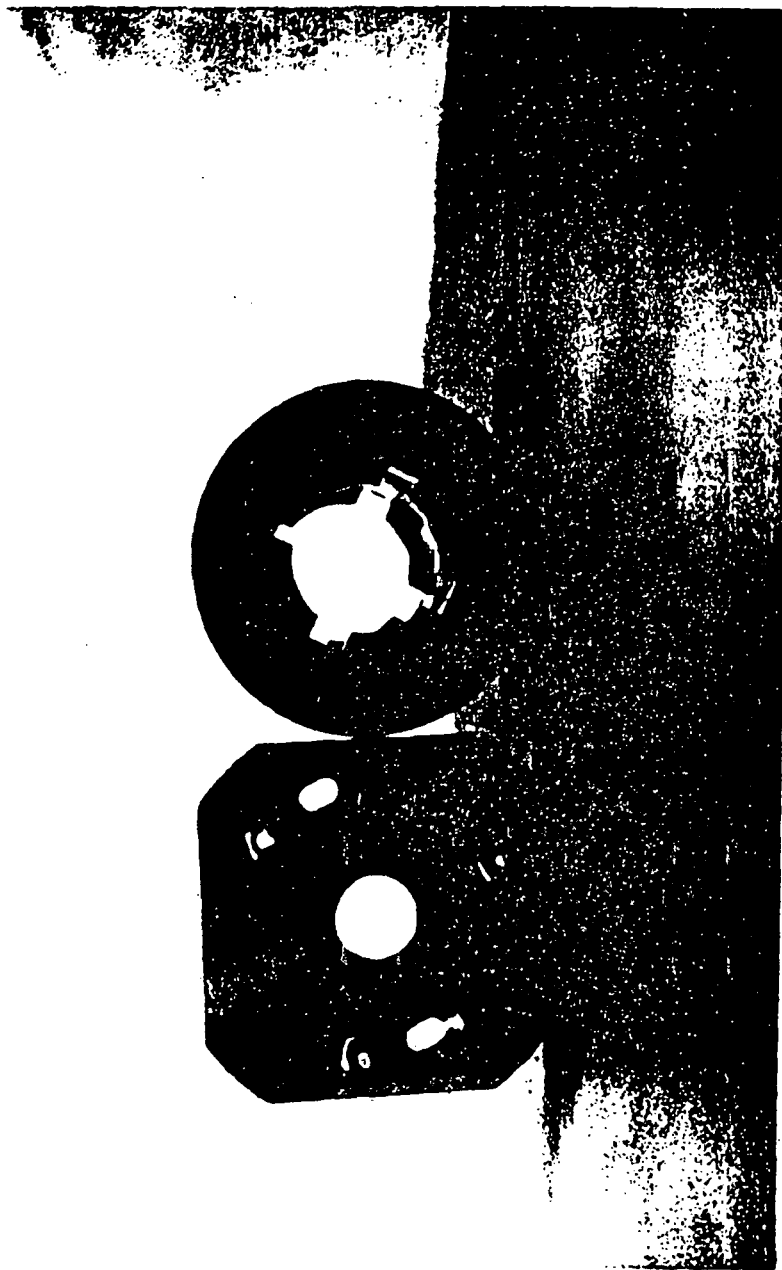


Figure 16. Alignment plate and bottom face
of test section

of the gauges relative to one another, which is inherent to the accuracy of the measurements, while sacrificing to a small degree the repeatability of the actual mounting position of the cylinder. However, as will be pointed out below, neither the position of the cylinder on the table nor its repeatability had an effect on the measurement accuracy. The rather small 20 mil measuring range of the gauges did necessitate fairly accurate centering and leveling of the section on the table to avoid over-ranging the gauges during the measurement traverses. Typically the positioning adjustments were realigned every 5 or 6 tests to avoid exceeding the range limitations during experimental measurements. (The procedure is discussed in Appendix A.)

Errors due to inaccuracies in the cylinder's position were avoided by using the steel rims on either side of the naphthalene insert to establish a reference surface. As this surface remained fixed with respect to the insert, the actual position of the cylinder during the measurement intervals was unimportant. The position of the reference surface was determined by the readings of the two gauges contacting the steel rims. The two gauges contacting the naphthalene insert provided simultaneous measurement of two points on its surface.

Profile measurements were made before and after each experiment and, by differencing these tare and final profiles, a profile of the local sublimation depth was determined. The procedure used is illustrated in Fig. 17 where the off-horizontal tilt of the section, the gauging range and the sublimation depth have been greatly exaggerated for illucidation. Also, for simplicity, only one measuring gauge is shown on the naphthalene surface. The reading from each transducer is the distance from its zero

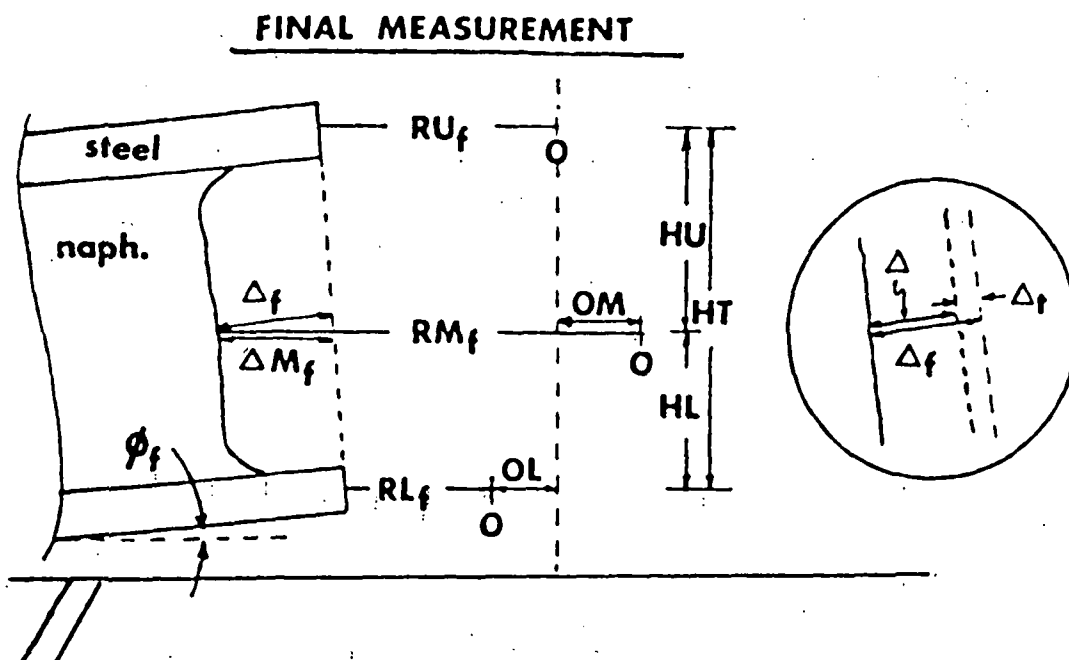
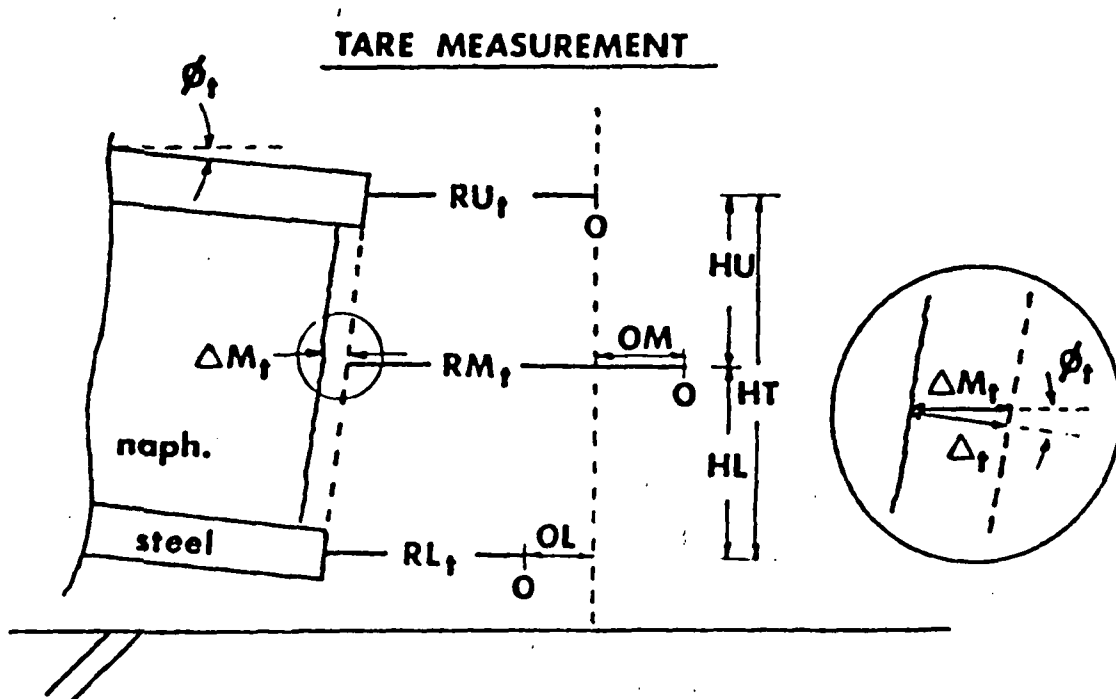


Figure 17. Schematic of measurement procedure

position to its contact point. These are the distances RU_T , RM_T and RL_T for the tare measurement; and RU_F , RM_F and RL_F for the final measurement. The distances from the zero position of the measuring and lower gauges to an arbitrary vertical line, which for convenience is chosen to pass through the zero position of the upper gauge, are OM and OL , respectively. (It should be noted that the zero positions of the gauges need not lie along a common line and no effort was made in this regard.) The vertical distances from the line of action of the measuring gauge to the lines of action of the upper and lower gauges are HU and HL respectively. Using simple geometry

$$\Delta M_T = RM_T - \frac{HU}{HT} RL_T - \frac{HL}{HT} RU_T + (OM + OL \frac{HU}{HT})$$

$$\Delta M_F = RM_F - \frac{HU}{HT} RL_F - \frac{HL}{HT} RU_F + (OM + OL \frac{HU}{HT})$$

$$\Delta_T = \Delta M_T \cos \phi_T$$

$$\Delta_F = \Delta M_F \cos \phi_F$$

$$\Delta = \Delta_F - \Delta_T$$

where Δ is the sublimation depth to be determined. The angles ϕ_T and ϕ_F are limited by the gauging range; that is

$$\phi_T, \phi_F < \sin^{-1} (\text{gauging range/section height}) = .020"/3" = 0.38^\circ$$

hence

$$(\cos \phi_T, \cos \phi_F) > 0.9999.$$

Thus, only very small errors are incurred by assuming

$$\Delta_T = \Delta M_T, \quad \Delta_F = \Delta M_F$$

and the full equation for the sublimation depth is

$$\Delta = (RM_F - RM_T) + \frac{HU}{HT} (RL_T - RL_F) + \frac{HL}{HT} (RU_T - RU_F)$$

It should be noted that the described measurement calculation assumes that the line of action of each transducer is along a true horizontal, and that the contact points of the transducers on the section lie along a common vertical line. Careful set-up of the transducers was required to avoid substantial deviations from these assumptions. The procedure used is described in Appendix A.

As the output of the gauges is in the form of a voltage, ΔM_T and ΔM_F could be obtained directly by electronic combination of the outputs. An op-amp system was constructed for this purpose; however, due to calibration shifts in the circuit, it was found to be faster and more accurate to read the gauges directly.

Tare or Final profiles of the naphthalene surface consisted of a series of measurements of the type described. The surface can be traversed circumferentially in increments as small as 15 seconds, and vertically in increments as small as 1 mil using the rotary table and the cross slide, respectively. Generally, two types of profiles were utilized in the experiments. In one type, a purely circumferential traverse in increments of 4° was used, providing a circumferential distribution of the local mass loss at the spanwise positions of the two measuring gauges. In tests where spanwise distributions were of interest,

the test section was profiled with spanwise traverses, typically in .05-inch increments at a number of degree positions. Typical measuring intervals for either type of profile were on the order of 40 minutes.

Due to the rather large time required to perform the measurements, it was necessary to perform the experiments in a manner which insured that the naphthalene loss due to free sublimation during the measurement intervals was an insignificant percentage of the total sublimation depth. As the total depth was limited to that measurable with the transducers, this was achieved by performing the experiments at relatively low operating temperatures. Temperatures on the order of 65°F were used. The tunnel room temperature is controlled with a central air conditioning unit, and can be kept constant to within 2°F. The ambient temperature of the measuring room was matched to the operating temperature of the tunnel using a room air conditioner. In this manner the vapor pressure of the naphthalene was kept low, limiting free sublimation losses to approximately .1 mils for each test. The duration of a test in the wind tunnel was typically on the order of 9 hrs giving maximum sublimation depths on the order of 10 mils. The use of these rather large run times combined with the low operating temperatures greatly enhanced the experimental repeatability by reducing the importance of free sublimation. Typically, the experimental results obtained were repeatable to within about 2%.

Although the free sublimation rate was substantially reduced by this procedure, the measured sublimation depth was compensated for losses during the measurement intervals. To determine the proper compensation, points measured at the beginning of each profile were repeated after its completion. Combining the two sets of readings in the same manner

described above yielded a direct measure of the naphthalene lost during the interval. Tare and final traverses were made in the same order, such that the elapsed time between the two measurements at specific points on the surface was uniform; hence the free sublimation losses around the cylinder were also approximately uniform and equal to those measured. The direct measurement provided fairly accurate determination of the proper compensation for losses during the measurement intervals and, indeed, was found to be far more reliable than calculation attempts. To account for the additional losses during installation of the cylinder, the measured loss depth was increased by a percentage determined from the ratio of the installation time to the measurement time. Typically, the elapsed time from complete installation of the section in the tunnel to complete installation on the measuring table was on the order of 8 minutes, requiring the measured loss to be increased by about 20%.

The techniques that were utilized in the mass transfer measurements were developed in large part by experience and, in general, the quality of the data obtained improved with time. The initial design conceptions and aspects of the techniques were extensions of procedures used by a number of other authors, such as Sogin and Subramanian [31], Kestin and Wood [14], and, most notably, Taylor [32]; however, the evolved procedure has been found to give a much higher degree of repeatability than those previously reported.

4.4 Mass Transfer Data Reduction

Distributions of the local Sherwood number, Sh , a nondimensional mass transfer coefficient, were calculated from the previously discussed profile measurements. Using the measured local depth of naphthalene sublimation, Δ , the time averaged mass transfer rate is

$$\dot{m}'' = \frac{\rho_{NS}(\Delta - \delta)}{\tau}$$

where ρ_{NS} is the density of solid naphthalene and τ is the time duration of the test and δ is the loss correction. The mass transfer coefficient, h_m , is defined as

$$h_m = \dot{m}'' / \overline{\rho_{N,V}}$$

where $\overline{\rho_{N,V}}$ is the average density of naphthalene vapor at the surface of the cylinder during the test interval. This was determined by numerical integration of the instantaneous vapor density relation, i.e.

$$\overline{\rho_{N,V}} = \frac{1}{\tau} \int_0^{\tau} \rho_{N,V} dt$$

where the values of ρ_{NV} were calculated from temperature measurements taken at 1 minute intervals throughout the test. To evaluate the instantaneous density from the measured temperature, the vapor pressure relationship

$$\log_{10} P_V \left[\frac{\text{lbf}}{\text{ft}^2} \right] = 11.884 - \frac{6713}{T[^\circ\text{R}]}$$

given by Sogin [33] was utilized along with the ideal gas law. The Sherwood number is defined as

$$Sh = h_m D / \mathcal{D}$$

Although the reported Sherwood number distributions were repeatable to within $\pm 2\%$, exact knowledge of their accuracy is limited by the unknown accuracy in the utilized Schmidt number and vapor density relations. The values given by Sogin were used both to provide conformity with the measurements of previous investigators and also because they are, to the knowledge of the author, the only reliably determined values. Techniques for estimating the diffusion coefficient theoretically, as reported in [34], suggest values of the Schmidt number between 2.35 and 2.75. Other suggested vapor density relations such as those of [35] and [36] are within 1.5% of that used in the temperature range of interest.

4.5 Turbulence Measurements

Turbulence quantities were measured using the two-channel hot wire anemometer system schematically depicted in Fig. 18. The system consists of two TSI 1051 anemometers, two TSI 1047 signal conditioners which provide AC frequency filtering, a TSI 1015C correlator which provides various combinations of the output signals, and two TSI 1076 mean square voltmeters for the measurement of AC signals. The DC components of the outputs were measured with a TSI 1047 signal averaging circuit and an HP3466A voltmeter. An HP3580A spectrum analyzer was used to determine spectral distributions of the AC signals.

For the measurements, the anemometers were operated in a constant temperature mode; that is the resistance and hence the temperature of the corresponding sensing elements were kept constant via a Wheatstone bridge feedback loop. The output of each anemometer is a voltage which varies with the instantaneous cooling rate of the sensor. When the sensor is

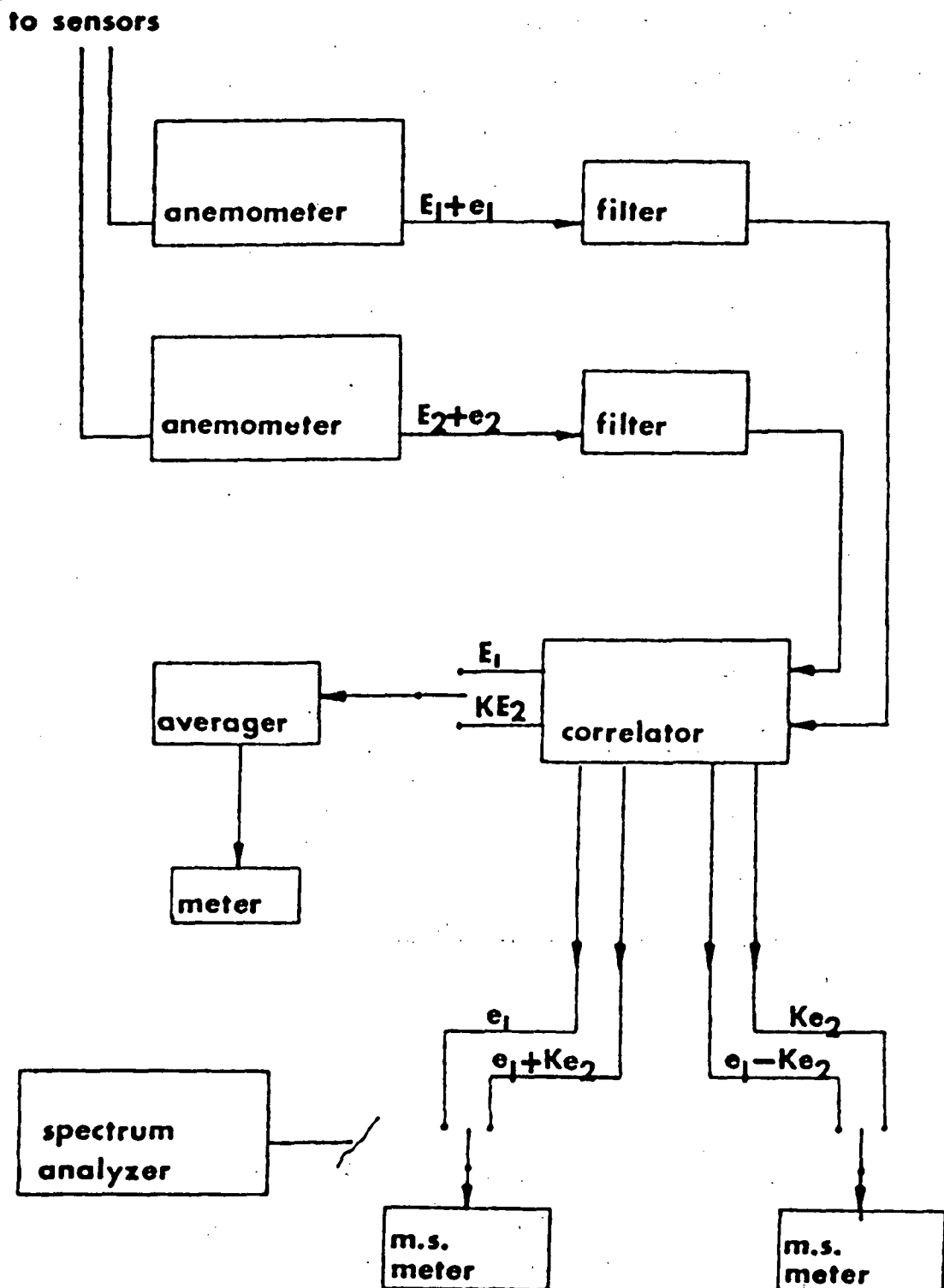


Figure 18. Schematic of hot wire anemometer system

positioned normal to an incident flow field of constant temperature, its cooling rate varies solely as a function of the incident flow rate and hence the output voltage of each anemometer can be directly correlated to the local velocity. As discussed by Bradshaw [37], the commonly utilized correlation function is

$$U^{.45} = AF(T)E^2 + B$$

where U is the mean velocity of the incident flow, E is the DC output voltage of the anemometer and A and B are constants which are adjusted to fit the curve to the response of a particular sensor. The function $F(T)$ accounts for long-term shifts in the flow temperature and is given by Bradshaw [37] as

$$F(T) = \frac{T_w - T_o}{T_w - T} \left[\frac{T_o}{T} \frac{T_w + T}{T_w + T_o} \right]^{.17}$$

where T_o is a reference temperature, T_w is the operating temperature of the wire, and T is the fluid temperature. In the reported measurements the wire temperature was 250°C. The reference temperature used was 21°C, a typically operating temperature of the tunnel.

Turbulent variations in the flow field generate an AC voltage signal, e_T . If the magnitude of the turbulent velocity fluctuations is small, the relationship can be considered to be linear, i.e.

$$e_T = \left. \frac{\partial E}{\partial U} \right|_{U=U_o} u'$$

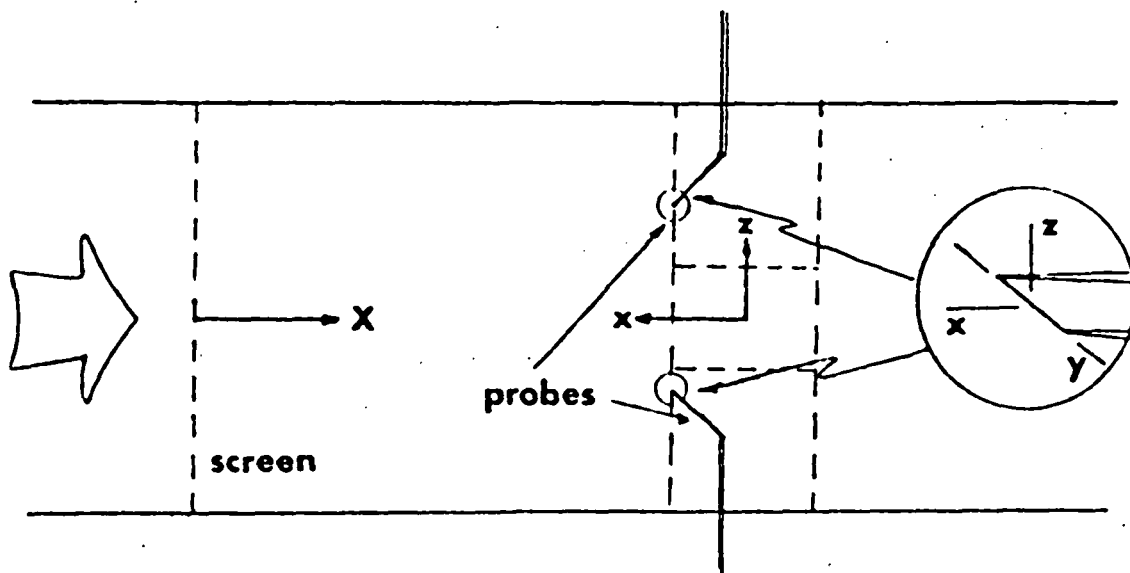
where u' is the streamwise turbulent velocity component and U_o is the measured mean velocity. In addition to the turbulence components of

interest, the AC signal of a real system contains a level of spurious noise generated by a number of sources. In the current research, the ambient noise was found to be a rather predominant portion of the output signals and methods were instituted for its elimination. In particular, pressure variations generated by the intermittent passage of blades in the wind tunnel blower and AC noise generated in the electronics of the measurement system were found to be significant.

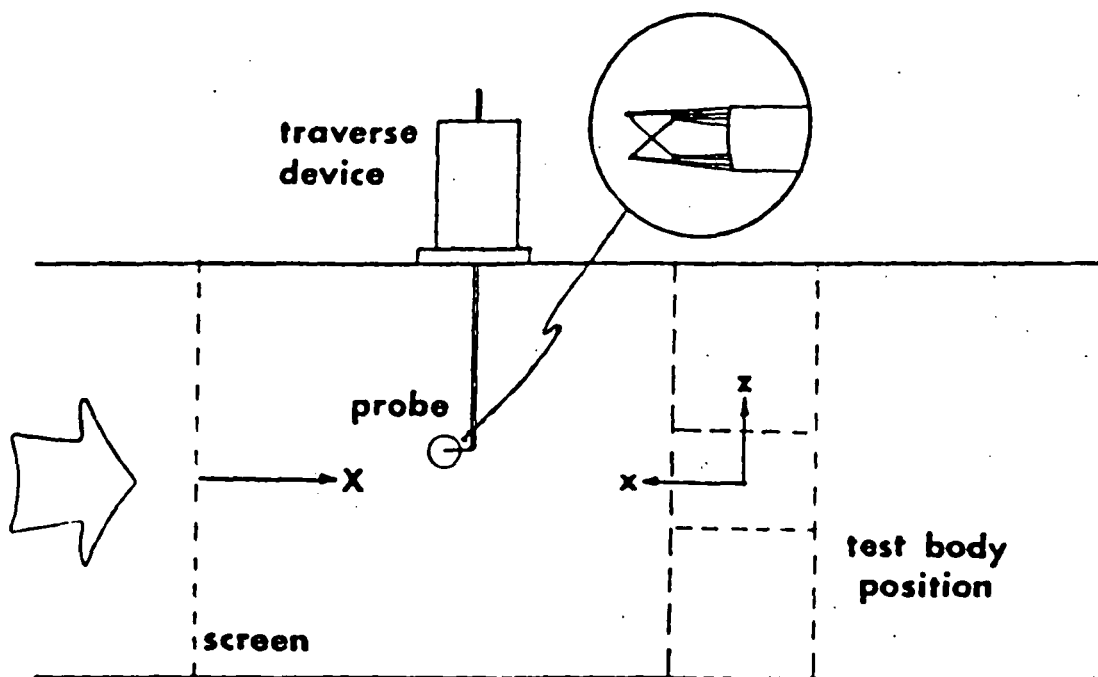
The reported turbulence levels and length scales were measured with the test cylinder removed from the tunnel. Two hot wire sensors, TSI type 1218 were used for the removal of noise from the turbulence signals. These sensors were positioned along a line corresponding to the leading edge position of the test cylinder with their wires oriented normal to the flow and normal to their common line. To minimize interference from the probe supports, the probes were held in specially constructed 45° adapters. This measurement configuration is illustrated in Fig. 19a.

The wires were calibrated in the wind tunnel through the fully connected measurement system to avoid errors due to changes in the sensor configurations and slight miscalibration of the electronics. The DC portions of the output voltages, denoted by E_1 and E_2 , were recorded along with the flow temperature at a number of incident flow rates, which were measured with a pitot static tube positioned near the wires. The correlation function was curve fit to the data by selection of the constants A and B.

The calibration equation having been determined for each wire, the tunnel flow rate was adjusted to the range of interest. At this



19a. Measurement of turbulence levels and length scales



19b. Measurement of spanwise distributions of flow quantities

Figure 19. Hot wire probe configurations

operating speed, the response of the two sensors to fluctuations in the mean velocity, $\frac{\partial E_1}{\partial U}$ and $\frac{\partial E_2}{\partial U}$, were calculated from their respective calibration equations. To match the turbulent response of the two wires, the correlator gain pot* in the channel two system was adjusted to provide a DC readout of

$$KE_2 = E_2 \frac{\partial E_1 / \partial U}{\partial E_2 / \partial U}$$

where K is the actual gain setting.

With the response of the two wires thus matched, the AC signals, e_1 and Ke_2 could be combined to eliminate ambient noise from the true turbulence signal. Each AC signal contains three primary components: that due to turbulence, e_T ; that due to pressure fluctuations, e_P ; and that due to the circuit noise, e_c .

$$e_1 = e_{T1} + e_{P1} + e_{c1}$$

$$Ke_2 = e_{T2} + e_{P2} + e_{c2}$$

The pressure noise of the two signals should be identical in time, that is

$$e_{P1}(t) = e_{P2}(t) = e_P(t)$$

Since separate electronic systems were used to monitor the wire outputs, e_{c1} and e_{c2} should be uncorrelated in time and if the wires are placed a sufficient distance apart there should also be no correlation between the turbulence signals, e_{T1} and e_{T2} . Hence, taking the mean square of the sum and difference of the outputs

* For this purpose it was necessary to replace the original single turn pot with a 10 turn pot.

$$\overline{(e_1 + Ke_2)^2} = \overline{e_{T_1}^2} + \overline{e_{T_2}^2} + 4\overline{e_p^2} + \overline{e_{c_1}^2} + \overline{e_{c_2}^2}$$

$$\overline{(e_1 - Ke_2)^2} = \overline{e_{T_1}^2} + \overline{e_{T_2}^2} + \overline{e_{c_1}^2} + \overline{e_{c_2}^2}$$

If the turbulent field is uniform, the mean square turbulence quantities should be equal, i.e.

$$\overline{e_{T_1}^2} = \overline{e_{T_2}^2} = \overline{e_T^2}$$

Then, the signals of interest are

$$\overline{e_T^2} = \frac{\overline{(e_1 - Ke_2)^2}}{2} - \frac{(\overline{e_{c_1}^2} + \overline{e_{c_2}^2})}{2}$$

and

$$\overline{e_p^2} = \frac{\overline{(e_1 + Ke_2)^2}}{4} - \frac{(\overline{e_{c_1}^2} + \overline{e_{c_2}^2})}{4} - \overline{e_T^2}$$

The electrical noise levels were determined by turning off the tunnel and measuring the two AC outputs. The true turbulence level and the apparent turbulence due to pressure noise can then be calculated using the pre-determined sensitivity, $\frac{\partial U}{\partial E_1}$,

$$Tu = \sqrt{\overline{e_T^2}} \frac{\partial U}{\partial E_1}$$

$$Tu_p = \sqrt{\overline{e_p^2}} \frac{\partial U}{\partial E_1}$$

The reported integral length scales were determined by fitting an experimentally measured spectral distribution to the theoretical spectral distribution given by Taylor [38],

$$\frac{UE(n)}{\overline{u'^2} L} = \frac{4}{1 + 4\pi^2 \left(\frac{nL}{U}\right)^2}$$

where L is the integral length scale, n is the turbulence frequency in Hz and the function $E(n)$ represents the frequency distribution of the turbulent velocity u . The relationship is typically plotted on log-log axes in the form shown in Fig. 20. The measured spectra were also plotted on log-log axes in the form

$$\frac{UE(n)}{u'^2 D} = \text{fnc}\left(\frac{nD}{U}\right)$$

The integral scale could then be determined by overlaying the theoretical curve onto the data plot and shifting the curve to a best fit position. The value of L/D was obtained from the amount of relative shift in the horizontal direction.

To obtain the frequency spectra, it was necessary to compensate the directly measured spectral distributions for the frequency response characteristics of the hot wire used. As discussed by Bradshaw [37], a hot-wire sensor behaves like a low pass filter and has a frequency response of the form

$$\frac{1}{1 + n^2 \tau^2}$$

where τ is a time constant which depends on the physical characteristics of the sensor. The time constant for the tungsten sensors used in the experiments was determined by a comparison of the slope of the approximately linear high frequency ranges of the directly measured spectra with the slope of the high frequency range of the theoretical curve. The values for M determined in this manner varied by only 8%, and were averaged to provide a value for M of $5.6(10^{-4})$ sec. This compares well with the value of $6(10^{-4})$ sec suggested by Bradshaw for a typical tungsten wire in air flow.

In addition to the measurements of turbulence levels and scales,

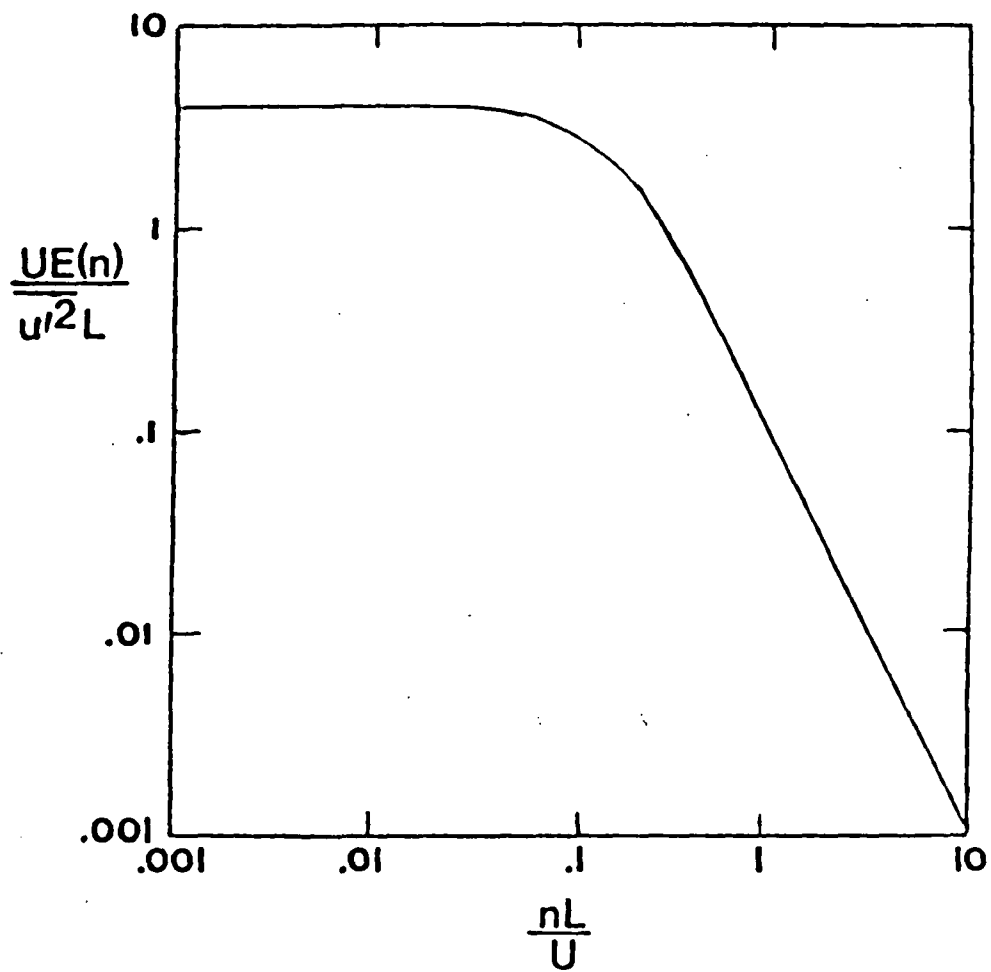


Figure 20. Theoretical energy spectrum of turbulence
(due to Taylor)

the investigation into the observed spanwise variations in mass transfer required the determination of the spanwise distribution of various flow quantities. A boundary layer cross wire probe, TSI 1243, was used with its sensors positioned in the stagnation plane and oriented at $\pm 45^\circ$ to the flow. The configuration is depicted in Fig. 19b. Distributions of the mean velocity, U , the mean square of the mainstream turbulence component, $\overline{u'^2}$, the mean square of the spanwise turbulence component, $\overline{w'^2}$, and the mean shear stress $\overline{u'w'}$ were measured. As suggested by Nagib [39], the spanwise distributions of the quantities were obtained by slowly traversing the flow and recording the appropriate outputs on a strip chart recorder. Using an automatic traverse device mounted to the top wall of the tunnel, the portion of the span ahead of the naphthalene insert was traversed at a speed of approximately $\frac{1}{2}$ mm/sec. Distributions were measured at a number of streamwise positions on the stagnation plane of the test cylinder both with and without the cylinder installed. The high frequency oscillations on the strip chart output were visually averaged to provide the reported distributions.

Since both sensors and hence both anemometer channels were required to determine the turbulence quantities of interest, the direct elimination of spurious noise was not possible. To eliminate low frequency noise from the measurements, the signals were passed through a 50 Hz high-pass filter provided in the signal conditioner units.

Methods for the determination of the turbulence quantities of interest can be obtained from an examination of the response of a sensor skewed at an angle, ϕ_0 , to the flow. If an idealized noise-free system is considered, the AC output of the sensor is

$$\begin{aligned}
e &= \left. \frac{\partial E}{\partial U} \right|_{U_0, \phi_0} u' + \left. \frac{\partial E}{\partial \phi} \right|_{U_0, \phi_0} d\phi \\
&= \left. \frac{\partial E}{\partial U} \right|_{U_0, \phi_0} u' + \frac{1}{U_0} \left. \frac{\partial E}{\partial \phi} \right|_{U_0, \phi_0} w' \\
&= s_1 u' + s_2 w'
\end{aligned}$$

where s_1 and s_2 denote the sensitivity of the output to the components u and w , respectively.

Consider now the case of two sensors with identical response characteristics positioned at $\phi = \pm 45^\circ$. The AC signals from the corresponding anemometers will be

$$\begin{aligned}
e_{+45} &= s_1 u' + s_2 w' \\
e_{-45} &= s_1 u' - s_2 w'
\end{aligned}$$

The mainstream turbulence component, u' , can be determined by addition of the signals

$$u' = \frac{e_{+45} + e_{-45}}{2s_1}$$

and the cross stream component by subtraction of the signals

$$w' = \frac{e_{+45} - e_{-45}}{2s_2}$$

The time averaged shear stress component is obtained from the difference of the mean squares of the outputs

$$\overline{u'w'} = \frac{\overline{e_{+45}^2} - \overline{e_{-45}^2}}{4s_1 s_2}$$

The two sensitivities, s_1 and s_2 , of a particular element can be determined by a calibration procedure. For a wire normal to the flow the response curve may be correlated in the manner described above. As the wire is turned away from a perpendicular position, the rate of cooling and hence the output voltage decreases. This may be considered in the correlation equation as a change in the effective velocity, i.e.

$$E^2 = \frac{U_{\text{eff}}^{.45} - B}{AF(T)}$$

where

$$U_{\text{eff}} = Uf(\phi)$$

Then the sensitivity to a cross stream turbulence component is

$$s_2 = \frac{1}{U} \frac{\partial E}{\partial U_{\text{eff}}} \frac{\partial f}{\partial \phi}$$

or by rearrangement

$$s_2 = \frac{\partial E}{\partial U} \frac{1}{f(\phi)} \frac{\partial f}{\partial \phi}$$

The sensitivity to a mainstream turbulence component is

$$s_1 = \frac{\partial E}{\partial U}$$

As discussed in Hinze [40], the functional dependence of the output on angle in a range near 45° is well represented by

$$f(\phi) = \sin \phi$$

Using the relationship the sensitivities for $\phi = 45^\circ$ are

$$s_1 = s_2 = \frac{\partial E}{\partial U}$$

Returning to the correlation equation, the effect of angle may be included in the constants A and B, i.e.

$$E^2 = \frac{U^{.45} - B_1}{A_1 F(T)}$$

to provide an equation for the output voltage of the skewed wire which depends only upon the incident velocity. The correlation constants A_1 and B_1 for each of the cross wire sensors were determined directly from a calibration of the probe in its measurement configuration, i.e. with the sensors at $\phi = +45^\circ$. In the manner previously described, the sensitivities of the individual wires were matched using the gain pot in the channel two system.

Since the variations in the local mean velocity were small, on the order of $\pm 0.2\%$, a special technique was also instituted for their measurement. Using the signal conditioners, the DC output from one of the two anemometers and its corresponding cross wire element was biased to eliminate the bulk signal and then amplified. The output was then plotted on the strip chart recorder. The variations in the mean velocity were then discernible along with high frequency turbulent fluctuations.

PART 5

RESULTS

5.1 Flow Measurements

A free-stream velocity distribution about the cylinder was obtained from the surface static pressure measurements using Bernoulli's equation. This distribution is shown in Fig. 21 where the local free-stream velocity divided by the mean incident velocity is plotted against the angle around the cylinder in radians measured from stagnation. The results are shown only for one side since the static pressure measurements were symmetric about stagnation. The velocity distribution for an unbounded potential flow around an infinitely long circular cylinder is also shown in the figure. A comparison indicates that the acceleration of fluid around the cylinder's surface is slightly less than that for potential flow. This is caused by the blockage effect of the wake. Using a fifth-order polynomial, the best fit to the actual velocity distribution is given by

$$\frac{U_\phi}{U_\infty} = 1.915\phi - 0.320\phi^3 - 0.526\phi^5 \quad (\phi < 1.2)$$

where ϕ is the angular position measured in radians.

The velocity distribution along the stagnation plane is shown in Fig. 22, where the local velocity is nondimensionalized by that far upstream and x/R denotes the upstream distance measured from the axis of the test cylinder. This velocity distribution is, to within the limits of experimental error, identical to that predicted by potential flow theory. Hot-wire anemometer measurements taken in the spanwise direction indicate

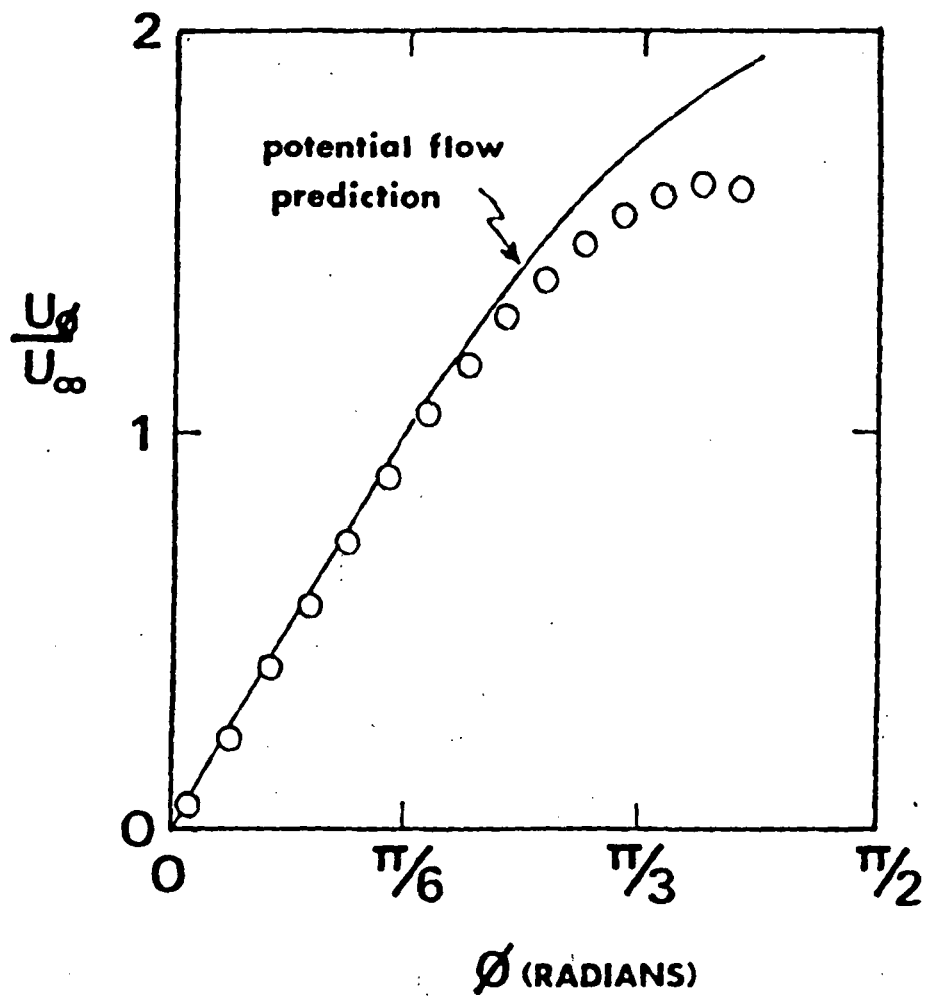


Figure 21. Velocity distribution around test cylinder

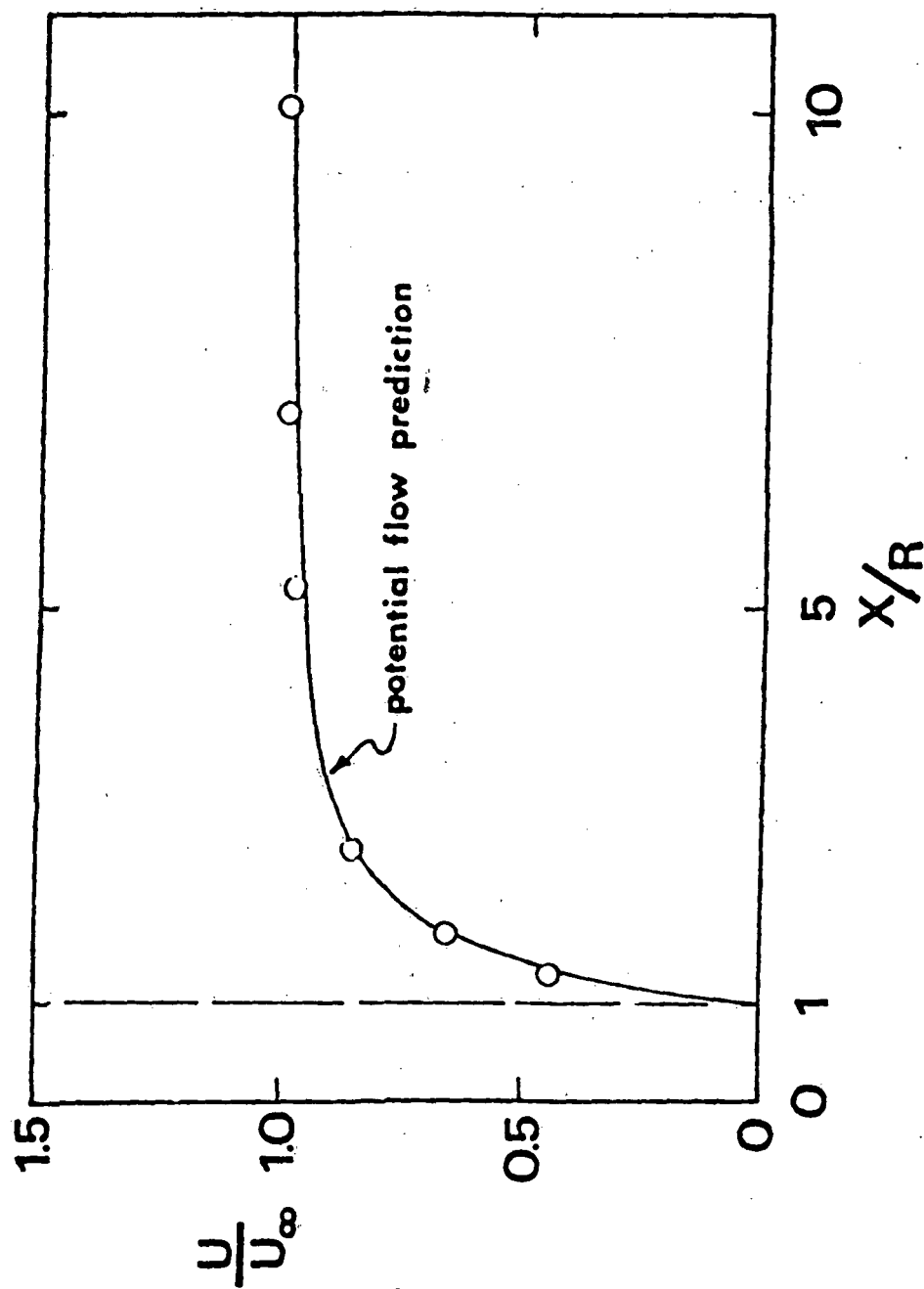


Figure 22. Velocity distribution along the stagnation plane

that the incoming flow without turbulence generating screens is uniform to within $\pm 0.2\%$.

The turbulence level and pressure noise of the tunnel flow in the absence of a turbulence generating screen are plotted in Fig. 23 as a function of the flow velocity. Although the cylinder was removed from the tunnel for the measurements, the flow velocity is given in the form of a Reynolds number based on the cylinder's diameter to establish a frame of reference. The turbulence level varies slightly with the flowrate, reaching a maximum at a Reynolds number of about 88,000. The pressure noise is seen to change drastically with flowrate and reaches magnitudes larger than the true turbulence level. The variations of both quantities is felt to be caused by the flowrate control of the tunnel, which consists of a set of variable angle inlet control vanes.

The physical characteristics of the turbulence generating screens used in the mass transfer tests are presented in Table 1. The turbulence levels behind the generating screens were measured at a Reynolds number (again based on the cylinder's diameter) of 110,000, a midrange value of the Re's used in the mass transfer tests. Turbulence levels and scales were measured for all available positions of each screen. The results are presented in Table 2.

In Fig. 24, the growth in the integral scale of turbulence behind each of the three turbulence section screens is plotted as a function of the downstream distance based on the mesh size M . A linear relationship of the form

$$\frac{L}{M} = a + b \frac{X}{M}$$

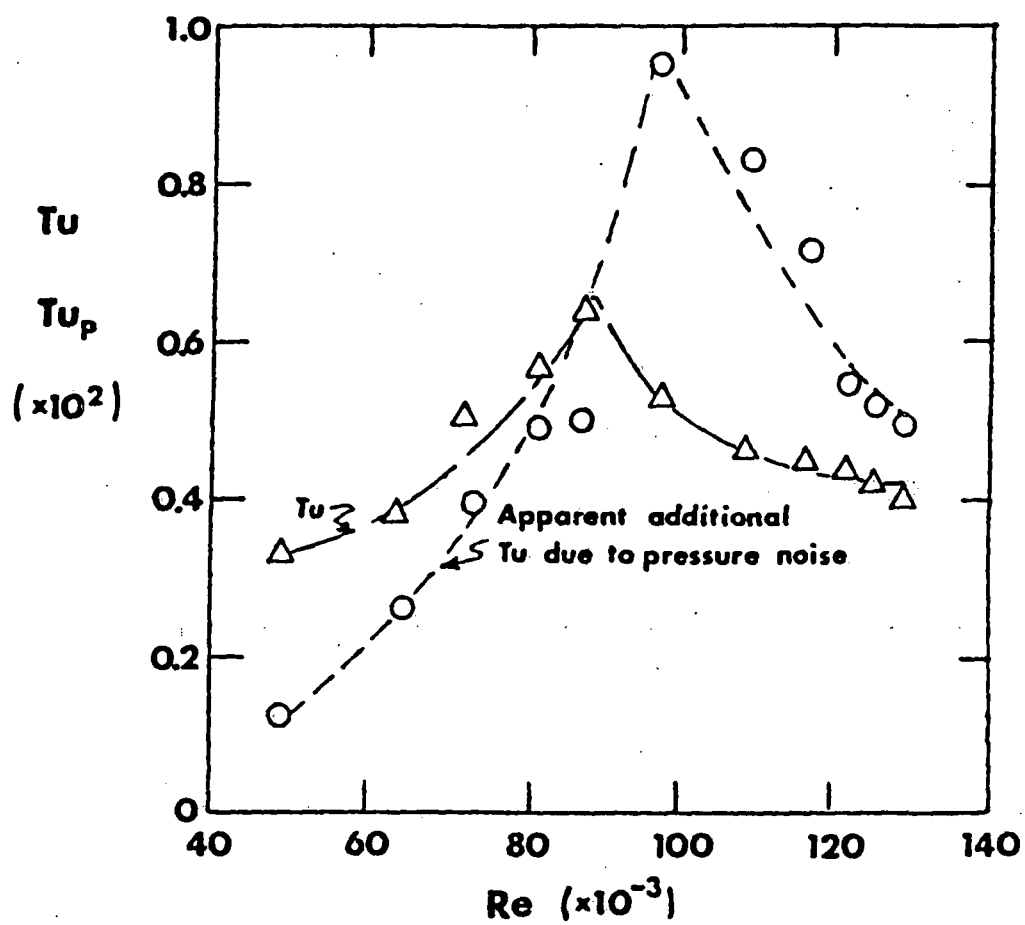
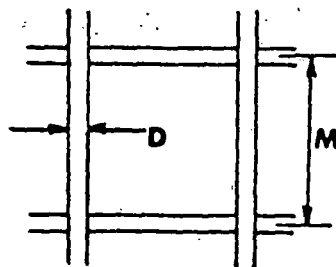


Figure 23. Ambient turbulence and noise levels without generating screens

Table 1. Physical characteristics of turbulence generating screens

Screens used in generating section

	M	D	M/D	type
1	.875"	.188"	4.65	hand manufactured round bar biplane mesh
2	.621"	.127"	4.89	hand manufactured round bar biplane mesh
3	.125"	.028"	4.46	woven wire screen
4	.063"(z dir.) .056"(y dir.)	.012" .012"	5.25 4.67	woven wire screen



Plenum chamber screen - installation configuration illustrated in Fig. 6b

5	10.0"	2.0"	5.00	biplane mesh constructed with flat boards
---	-------	------	------	---

Table 2. Turbulence levels and length scales

$M = .125''$

Position (X/M)	L/D	L/M	Tu(%)
144	.012	.560	.677
268	.017	.816	.436
448	.028	1.360	.339

$$L/M = .1496 + .00266(X/M)$$

$$(\bar{U}^2/\bar{u}^2) = 212.8 [(X/M) - 33.76]$$

$M = .621''$

29.0	.018	.177	1.869
53.9	.022	.209	1.361
90.2	.033	.338	1.086

$$L/M = .0857 + .00270(X/M)$$

$$(\bar{U}^2/\bar{u}^2) = 91.26 [(X/M) + 3.44]$$

$M = .875''$

20.6	.030	.206	2.651
38.3	.038	.263	1.801
64.0	.050	.343	1.182

$$L/M = .1415 + .00315(X/M)$$

$$(\bar{U}^2/\bar{u}^2) = 134.0 [(X/M) - 11.96]$$

Plenum chamber screen

$$M = 10'', L/D = .188, Tu = 4.9\%$$

Ambient conditions without screens

$$L/D = .087, Tu = .39\% - .68\% \text{ as shown in Fig. 23}$$

$M = .0625''$ - results discussed in Section 5.4

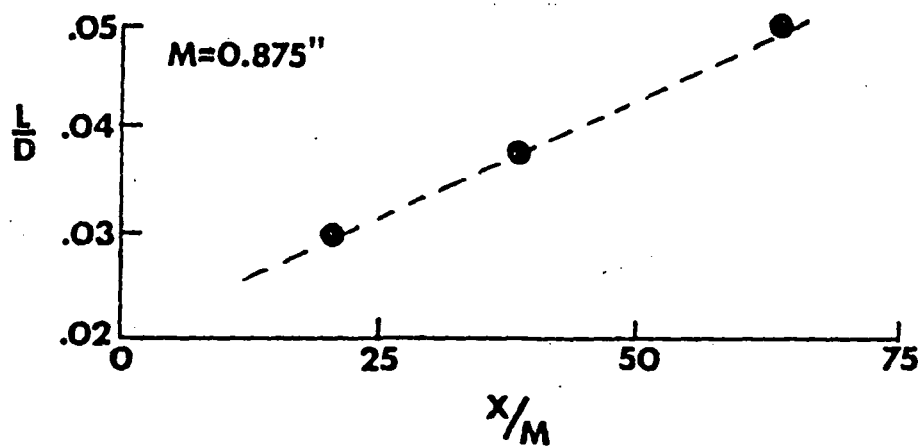
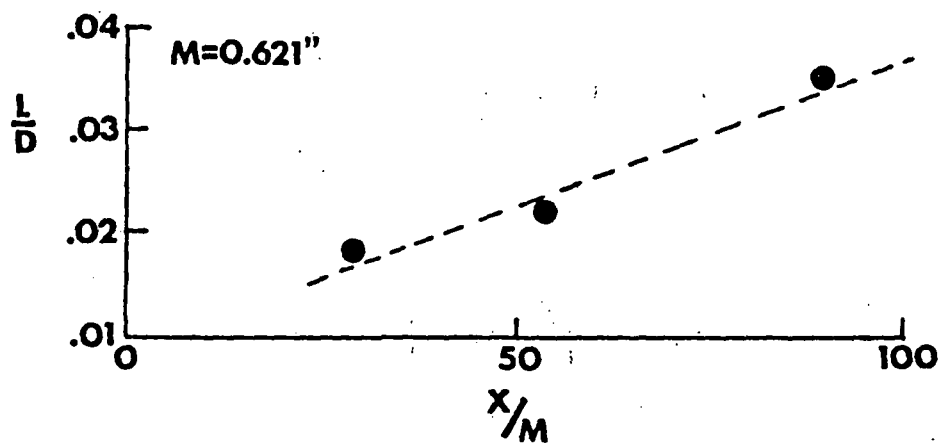
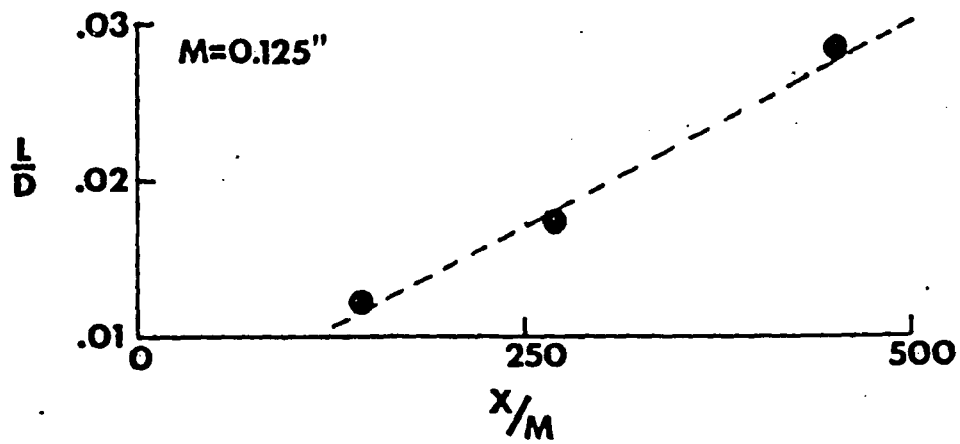


Figure 24. Growth of length scale behind generating screens

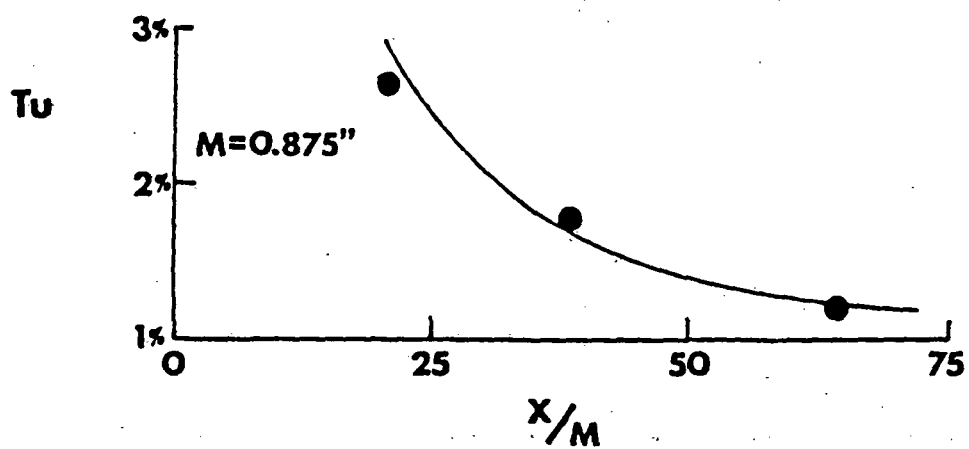
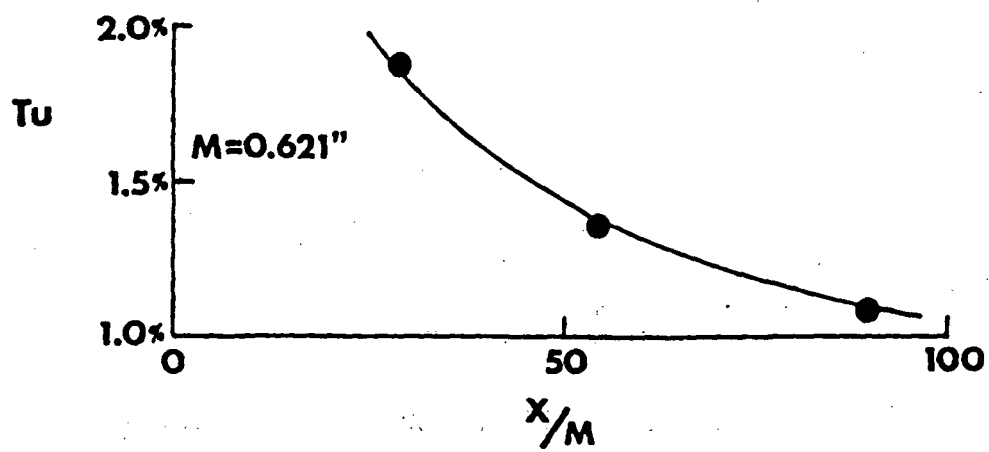
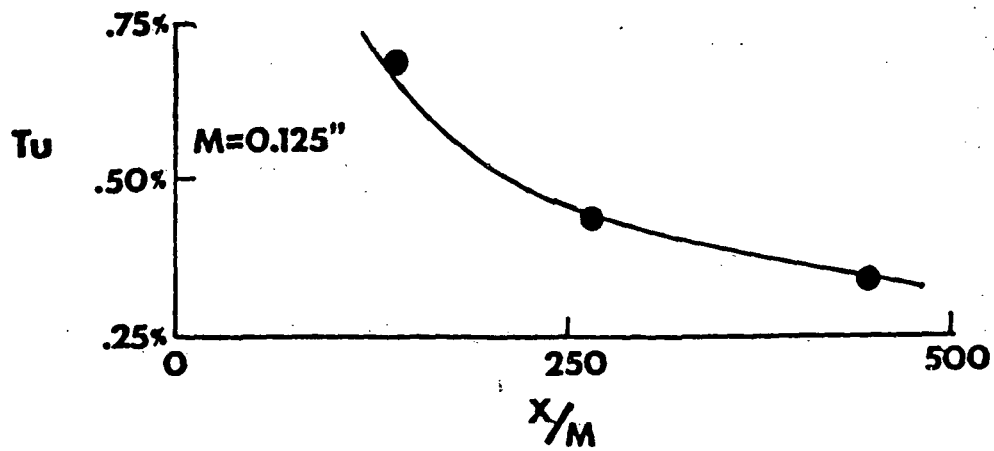


Figure 25. Decay of turbulence behind generating screens

was fit to each set of data. The determined values of the constants a, b for each screen are presented in Table 2. The values are comparable with those obtained by Dryden et al. [41] in an extensive investigation of the turbulence field behind screens.

The decay in turbulence level behind each of three turbulence section screens is presented in Fig. 25. The data for each screen was curve fit to the relationship

$$\frac{u^2}{u'^2} = A \left(\frac{x}{M} + \frac{x_0}{M} \right)$$

by adjustment of the constants A and x_0 . The determined values of constants are also given in Table 2.

5.2 Mass Transfer Measurements - Stationary Cylinder

To establish a base of comparison for the investigation into the effect of oscillation of the test cylinder on the local mass transfer rate, a set of mass transfer experiments were performed on a stationary cylinder using a variety of incident Reynolds numbers and turbulence conditions. In this phase of the investigation, a number of the turbulence conditions available in the wind tunnel were found to produce strong spanwise variations in the mass transfer rate. These results are presented and discussed later. The nominally two-dimensional mass transfer results reported in this section are compared to the measurements of other investigators to demonstrate the accuracy of the developed measurement techniques.

The first series of steady-state tests were performed in the absence of a turbulence generating screen. Circumferential distributions

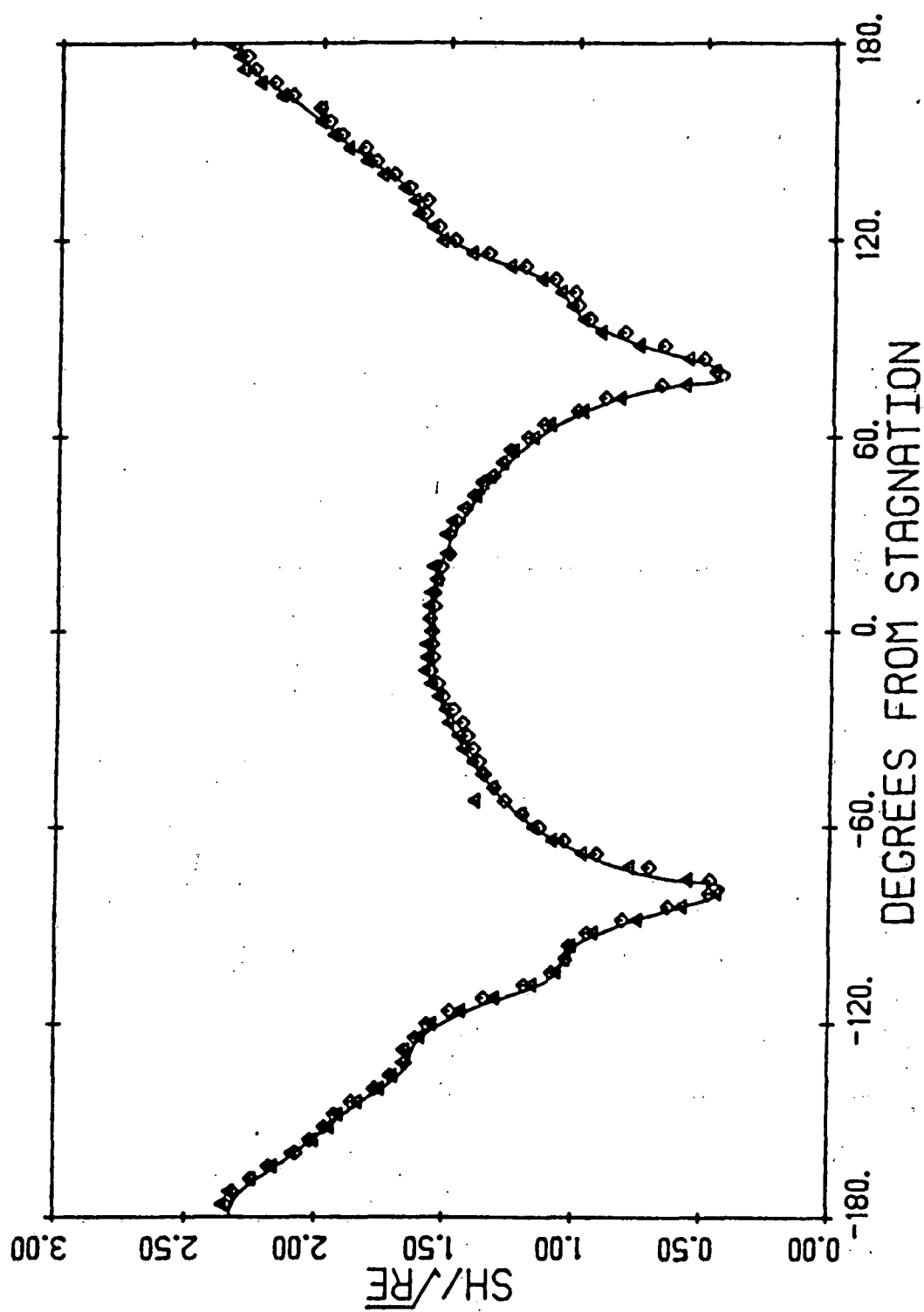


Figure 26. Mass transfer distribution ($Re = 75,000$)

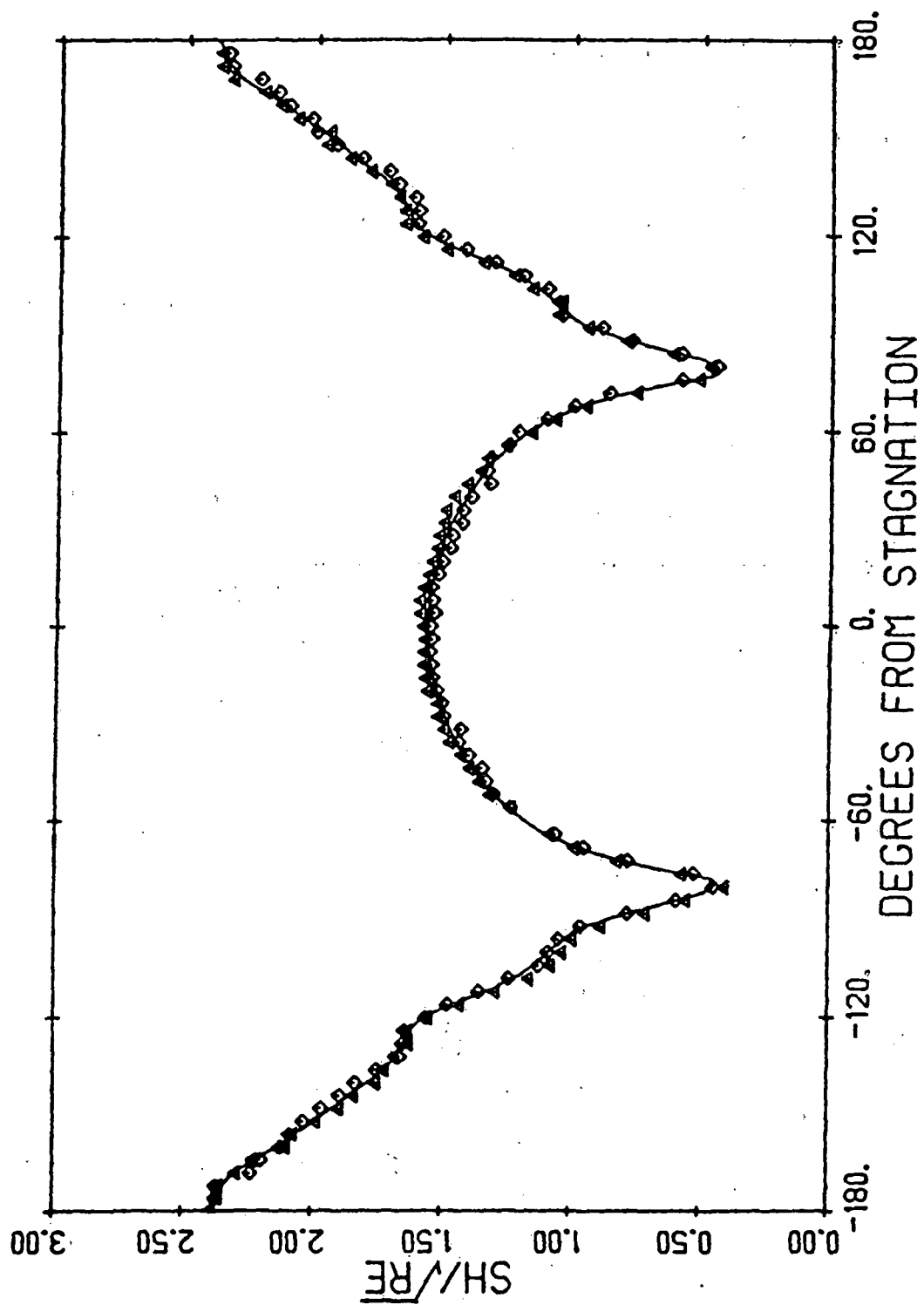


Figure 27. Mass transfer distribution ($Re = 82,500$)

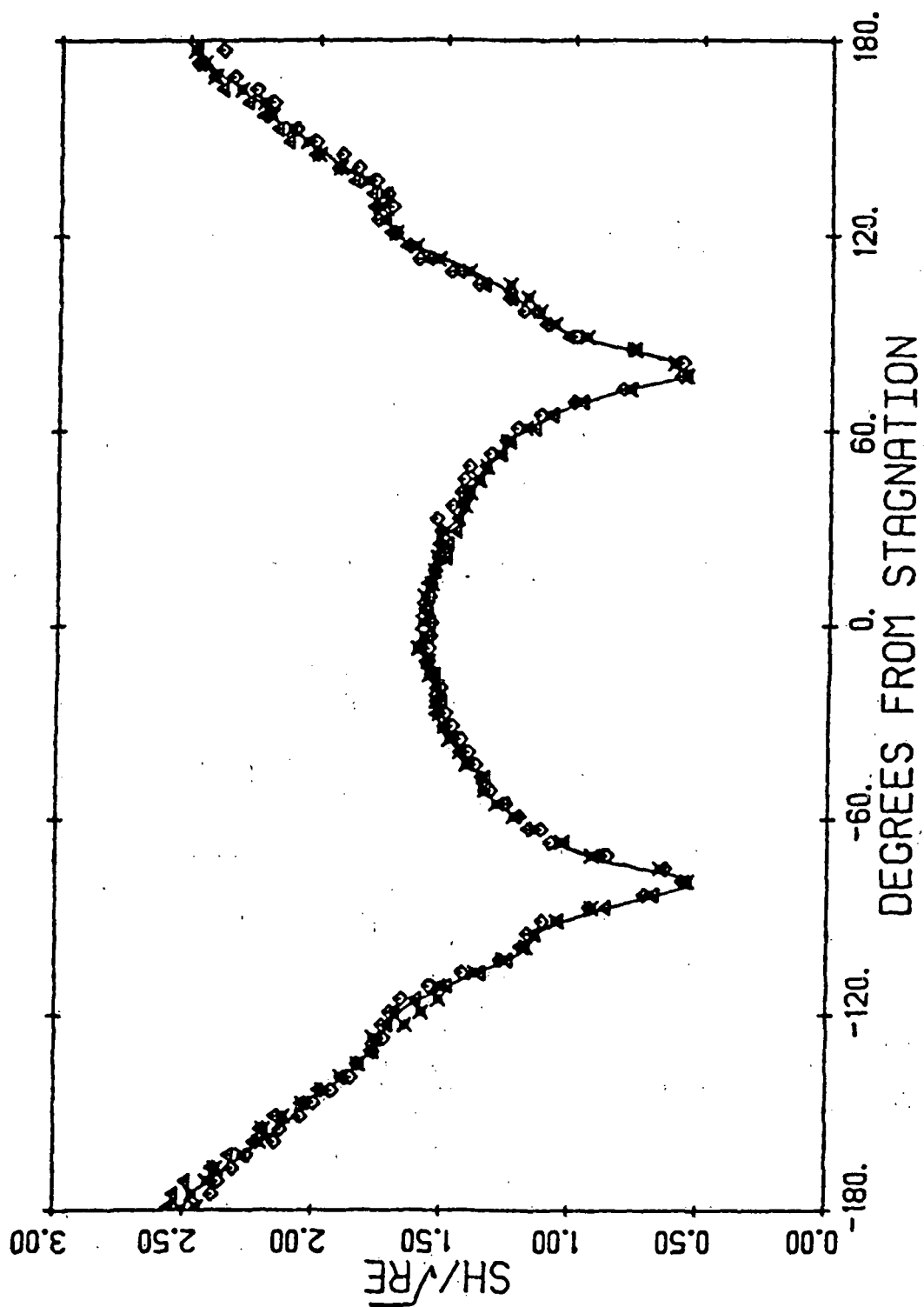


Figure 28. Mass transfer distribution ($Re = 110,000$)

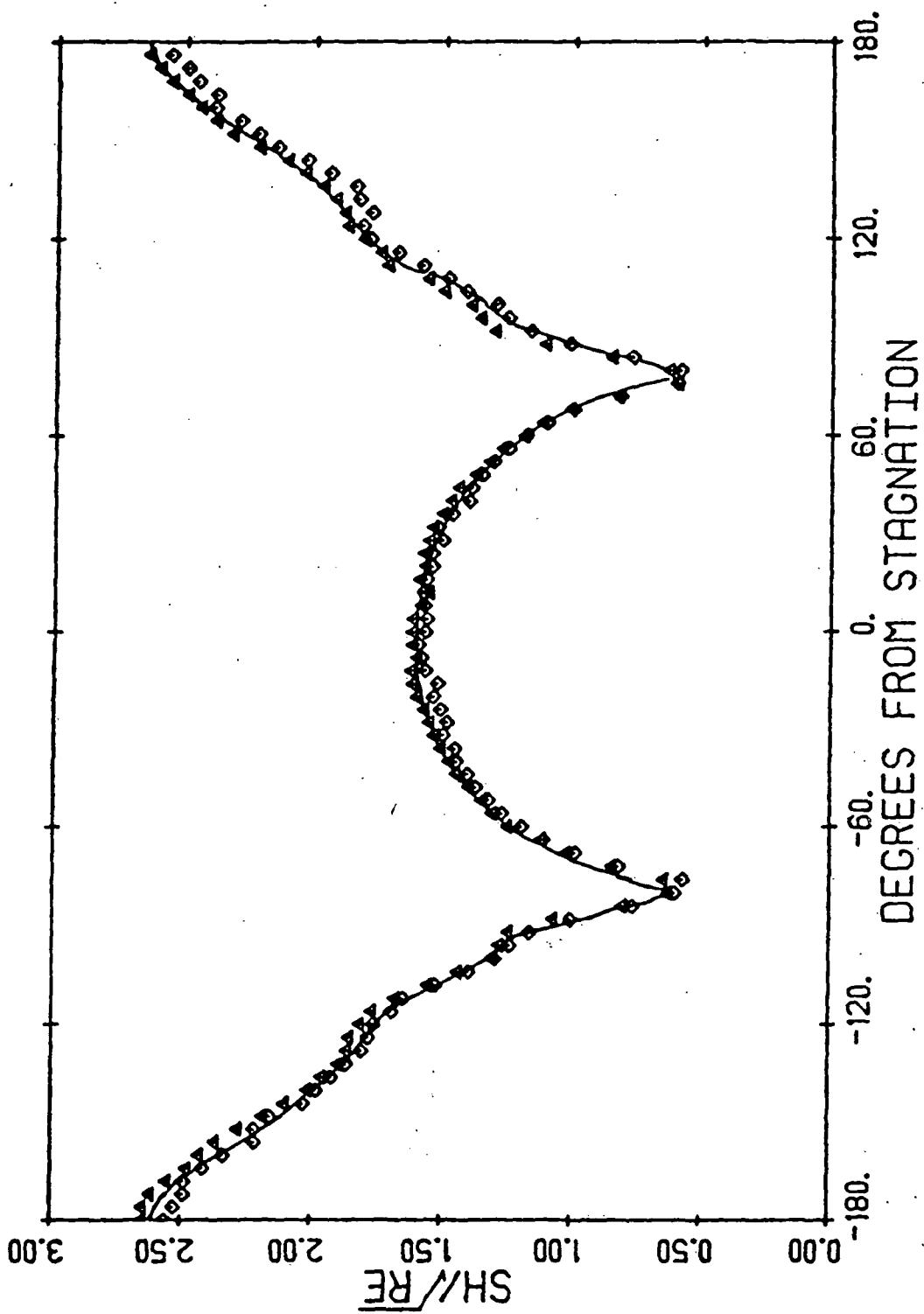


Figure 29. Mass transfer distribution ($Re = 125,000$)

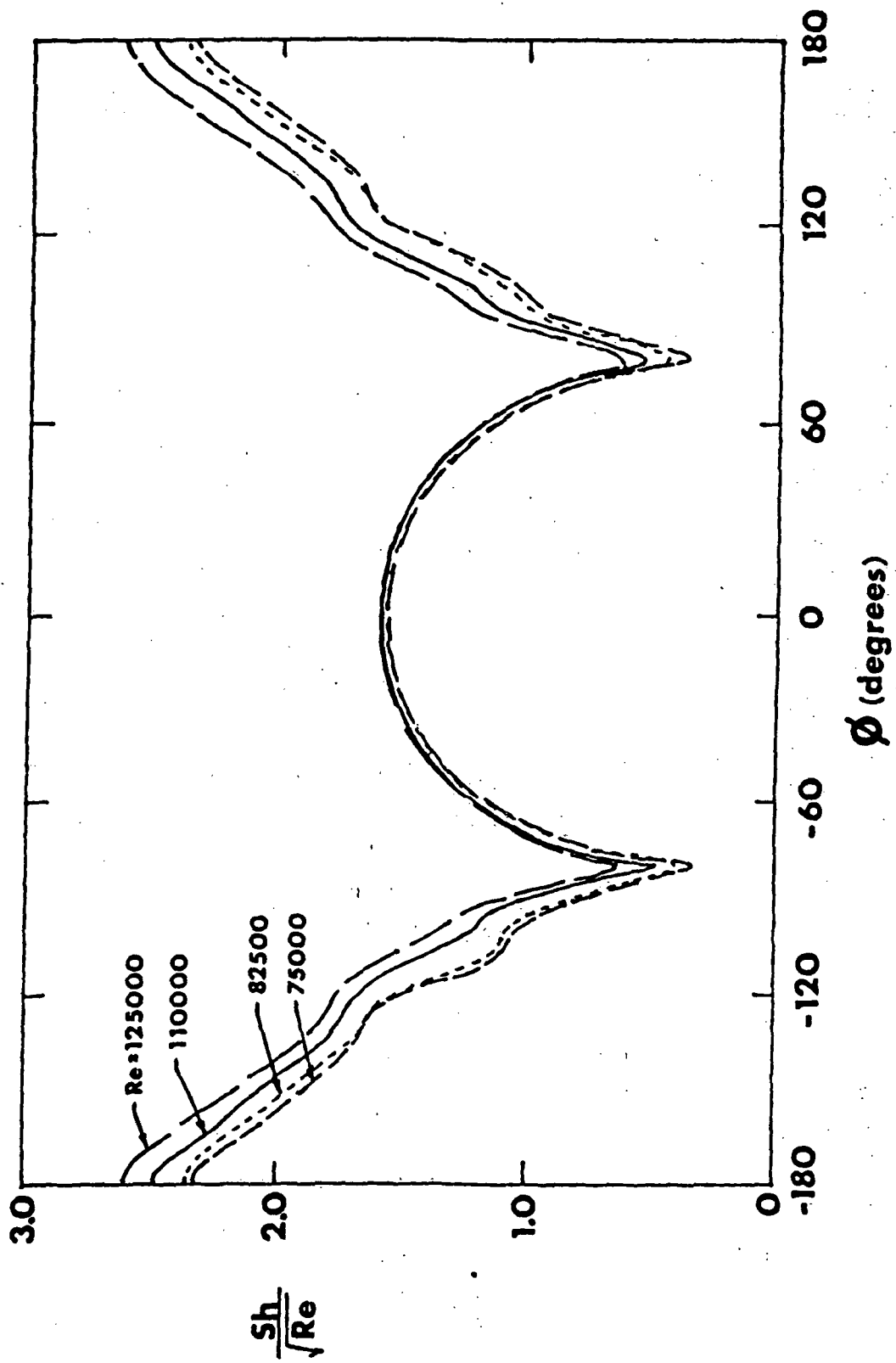


Figure 30. Comparison of low turbulence level results

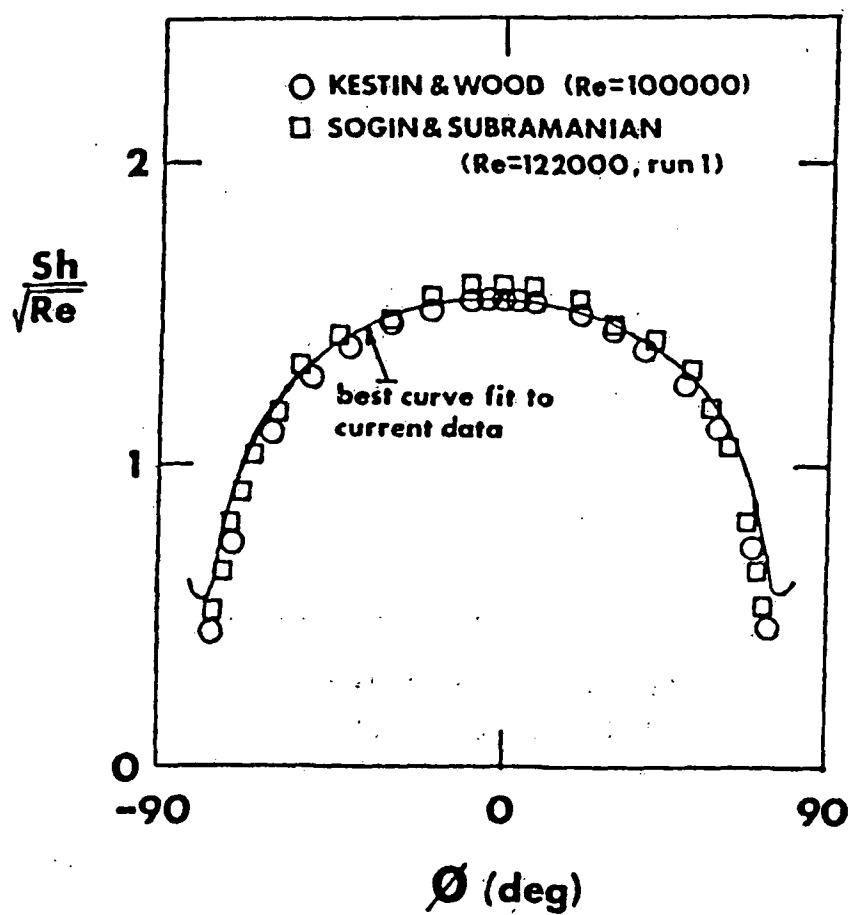


Figure 31. Comparison of leading edge results with previous measurements

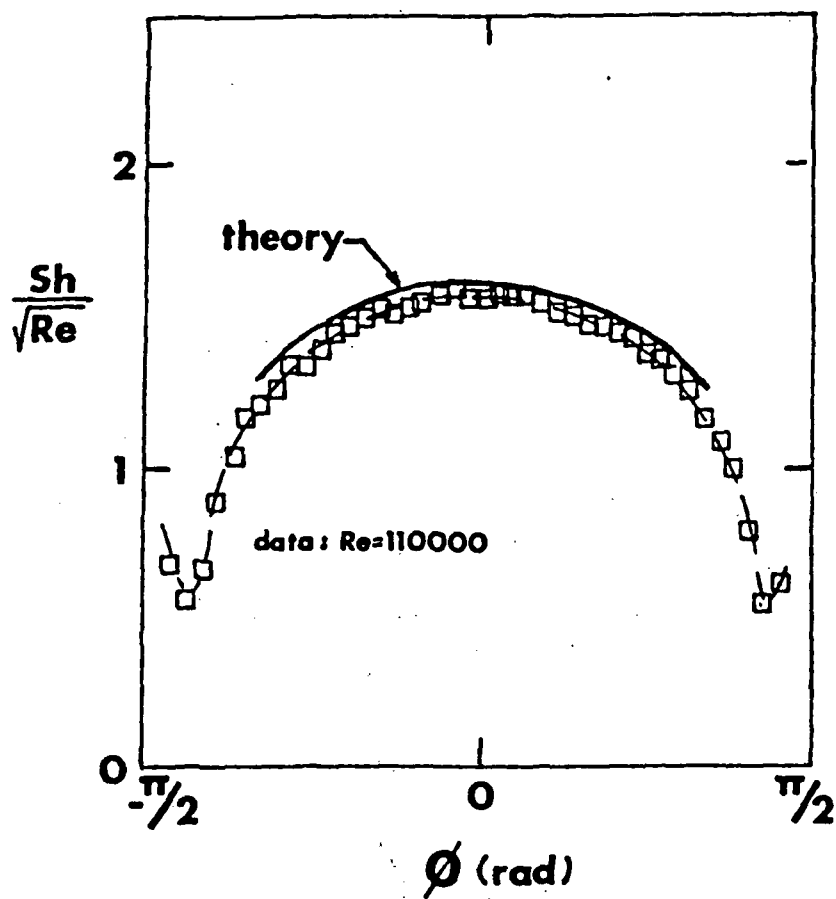


Figure 32. Comparison of leading edge results (Re = 110,000) with theory

of the local mass transfer rate at two spanwise positions were measured for incident Reynolds numbers of 75,000, 82,500, 110,000 and 125,000. The results are presented in Figs. 26 through 29. The distributions are compared in Fig. 30, where only a best curve fit to each set of data is shown for clarity. In the leading edge region up to separation, the results scaled by \sqrt{Re} are identical to within the $\pm 2\%$ measurement repeatability. After separation the values of Sh/\sqrt{Re} increase slightly with Reynolds number.

In Fig. 31 the results in the leading edge region for $Re = 110K$ are compared with the mass transfer results obtained by Sogin and Subramanian [31] and Kestin and Wood [14] for similar incident flow conditions. Near the stagnation point, a good agreement is seen. In the separation region, the current data deviates slightly from the other results and indicates that flow separation occurs further downstream. This is an effect of the high blockage ratio (cylinder diameter / tunnel width) of .2 used in the present investigation, Kestin and Wood used a blockage ratio of .12 and Sogin and Subramanian used a ratio of .13.

The low turbulence level data can also be compared with a theoretical laminar result obtained by a series solution to the boundary layer equations similar to Froessling's [1] but using a Schmidt number of 2.5. The calculation procedure developed by Childs [30] was used in combination with the experimentally determined distribution of the free stream velocity around the test cylinder, U_ϕ . The theory predicts a distribution of the local mass transfer rate given by

$$\frac{Sh}{\sqrt{Re}} = 1.612 - 0.253\phi^2 - .00216\phi^4$$

where ϕ is measured in radians. This theoretical result is plotted along with the experimental results for $Re = 110,000$ in Fig. 32. The slight discrepancy between the theory and the data is presently attributed to inaccuracies in the Schmidt number and vapor density relation. If the error is assumed to be caused only by the uncertainty in the Schmidt number, a value of 2.55 is required to make the theory and experiment correspond. This is within the error of experimentally and theoretically determined values.

Since the mass transfer surface occupies only 3" of the 18" span of the test cylinder, it would be expected that some spanwise transport of mass occurs. To ascertain the degree to which the results were affected by the experimental configuration, an additional low turbulence level experiment was performed in which the entire test cylinder was coated with naphthalene. A Reynolds number of 110,000 was used. The transfer rate on the insert was measured in the spanwise direction on the front and rear stagnation lines and near separation. The results are shown in Fig. 33 along with results obtained without full body naphthalene coating. The results on the front stagnation line and near separation are seen to be unchanged. The results along the rear stagnation line are about 8% lower than the previous measurements. This would be expected due to the large scale transport by the turbulent eddies found in the wake. This effect is of little importance to the current research which is primarily concerned with transfer rates in the leading edge region. Also, the data measured along the rear portions of the cylinder is probably of little use for comparison with other investigations since one would expect the transfer rate there to be a strong function of the blockage ratio.

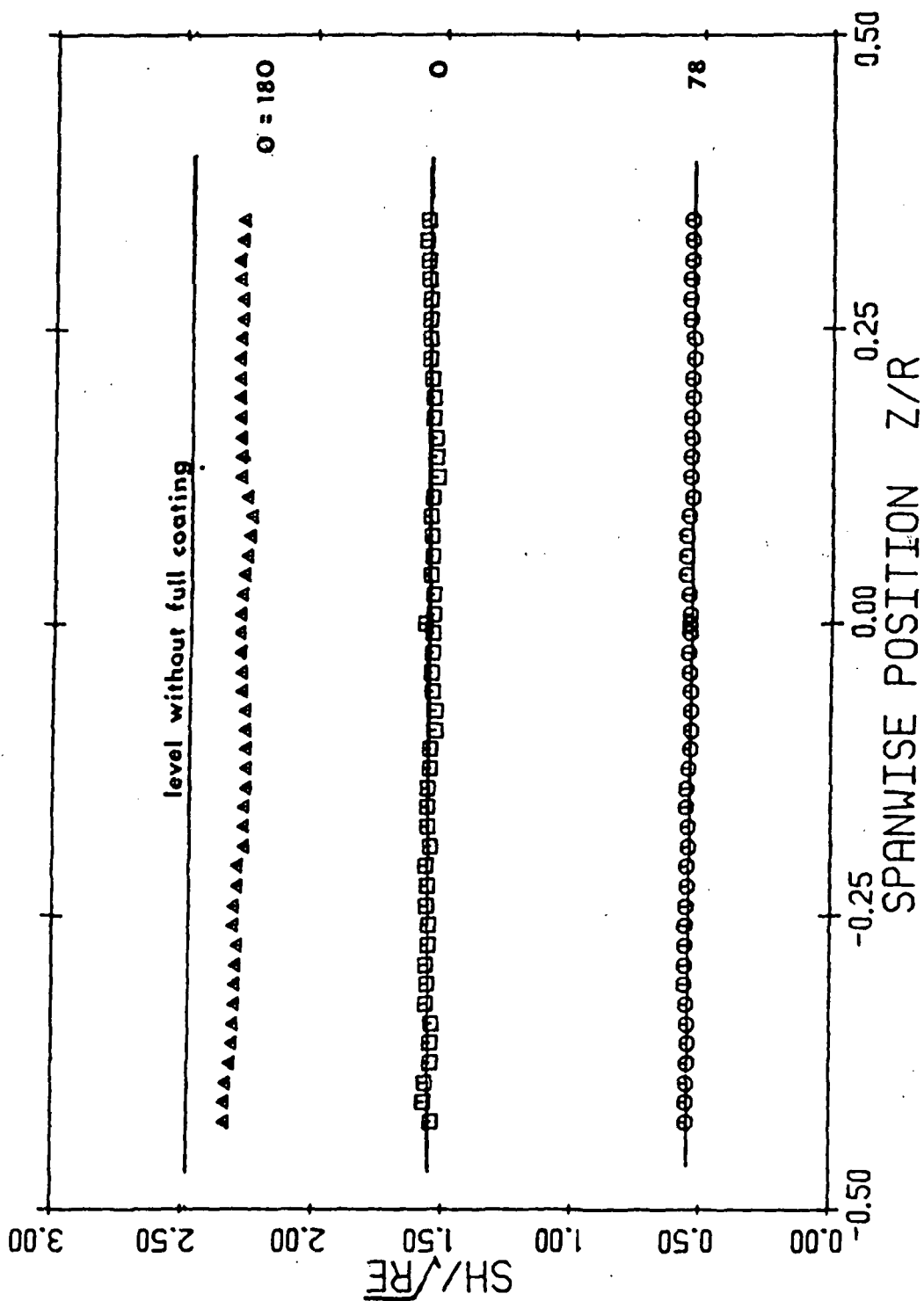


Figure 33. Comparison with results obtained with test cylinder fully coated with naphthalene (Re = 110000)

The results of the steady-state experiments performed behind turbulence generating grids are presented in Figs. 34 through 38. To demonstrate the effect of turbulence on the distribution of the local mass transfer rate, the results of the tests performed at $Re = 110,000$ are compared in Fig. 39. For clarity, a best curve fit to each data set is shown. From this figure the well-known effects of turbulence are readily evident. In the stagnation region, the mass transfer rate increases substantially as the incident turbulence level is increased, with augmentations as high as 30% being demonstrated by the current results. Further, the incident turbulence significantly alters the character of the flow near and after separation. For low turbulence levels, the transfer rate distributions along one side of the cylinder have a single minimum which occurs near the separation of the laminar boundary layer. At higher incident turbulence levels, the transfer rate distributions exhibit two minimum points, indicating that transition from a laminar to a turbulent boundary layer occurs before separation. After transition there is a rapid increase in the local transfer rate. In the present results, values for Sh/\sqrt{Re} as high as 3.5 were observed in the region between transition and separation. It should also be noted that the results observed at large turbulence levels are characteristic of low turbulence results measured at higher incident Reynolds numbers, and hence in simplistic terms, increases in the incident turbulence level can be viewed as a change in the effective Reynolds number of the flow.

In Fig. 40, the steady-state results at stagnation are plotted as a function of $Tu\sqrt{Re}$. For comparison with the heat transfer measurements

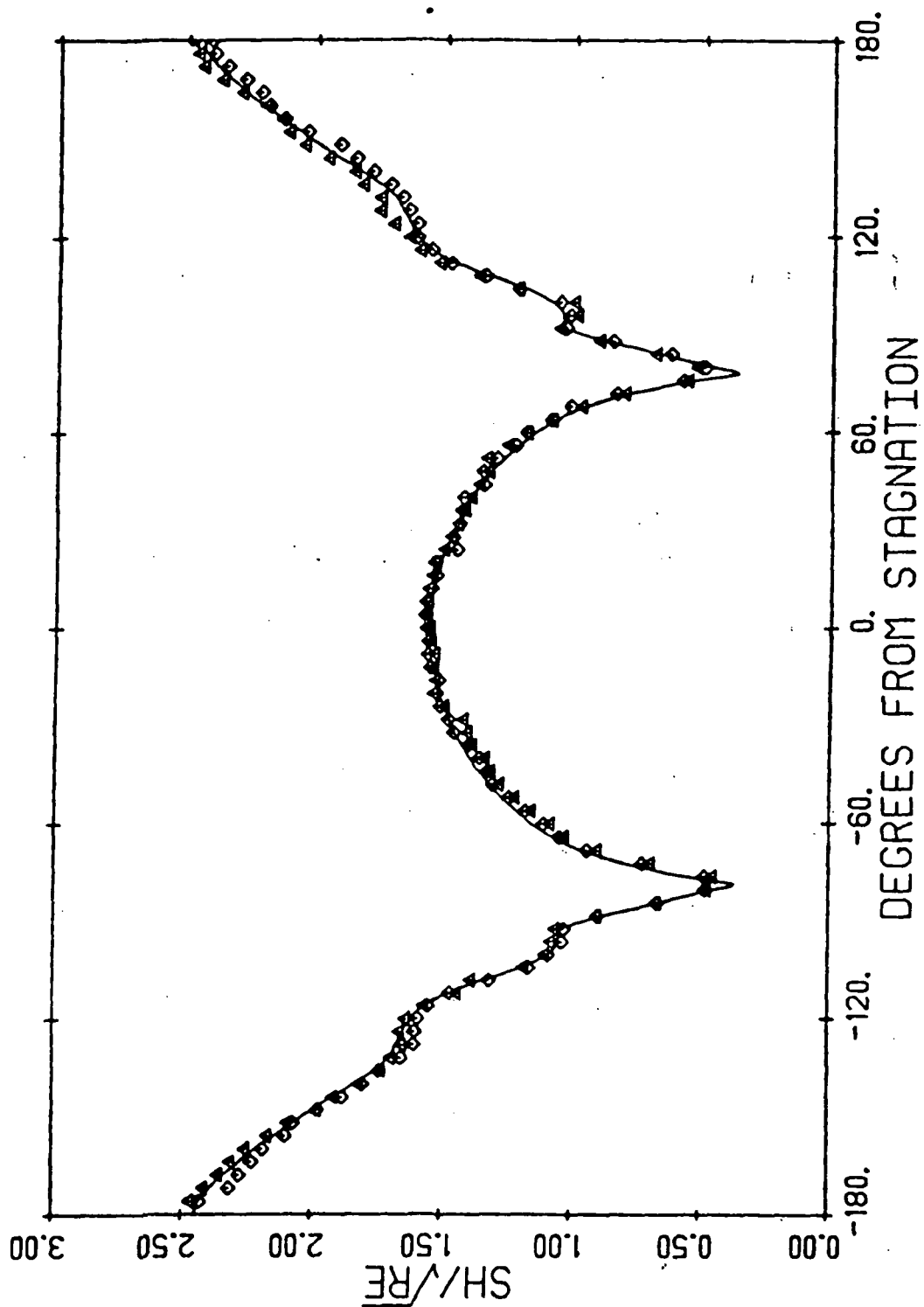


Figure 34. Mass transfer distribution
($Re = 110000$, $Tu = .34\%$, $L/D = .028$)

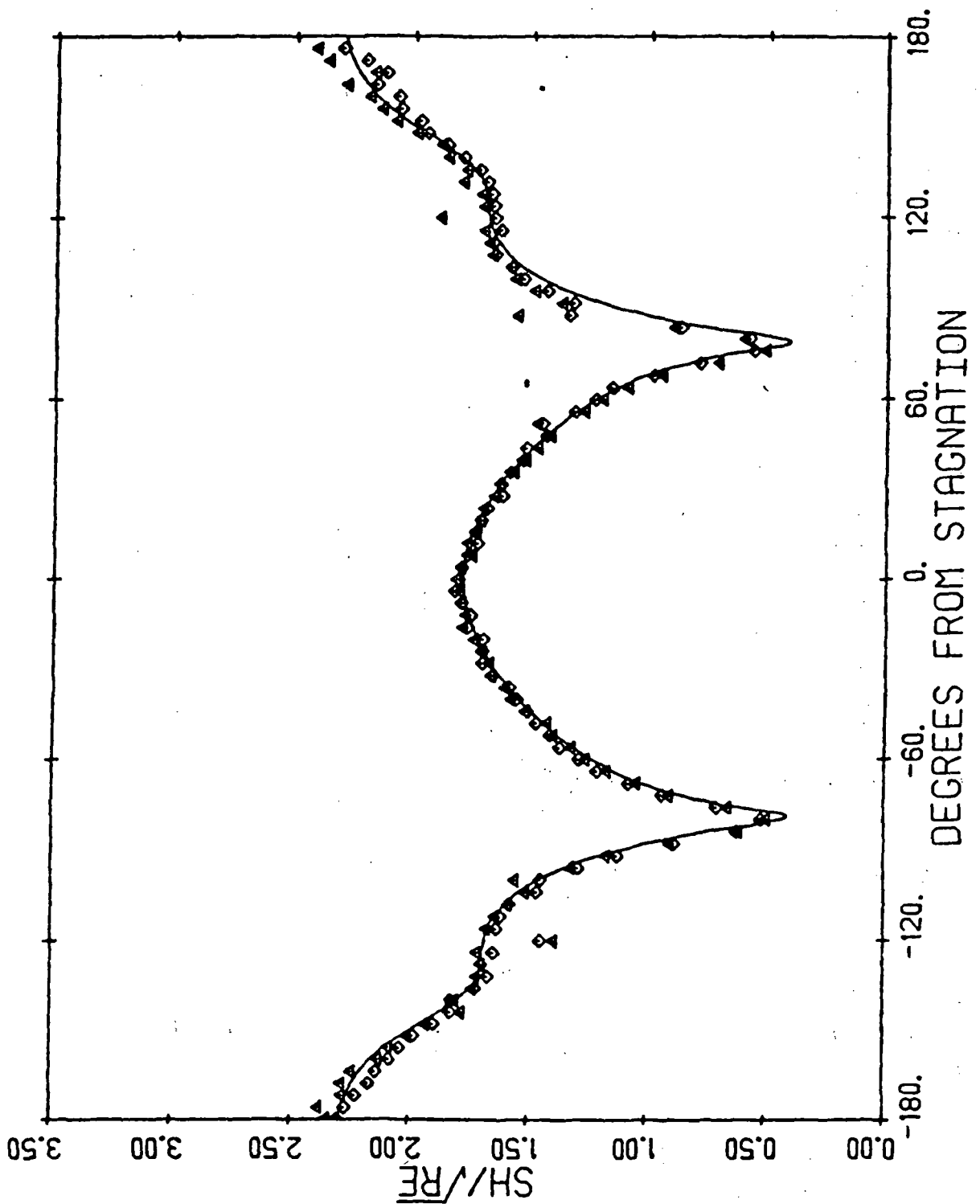


Figure 35. Mass transfer distribution
 ($Re = 110000$, $Tu = 1.18\%$, $L/D = .050$)

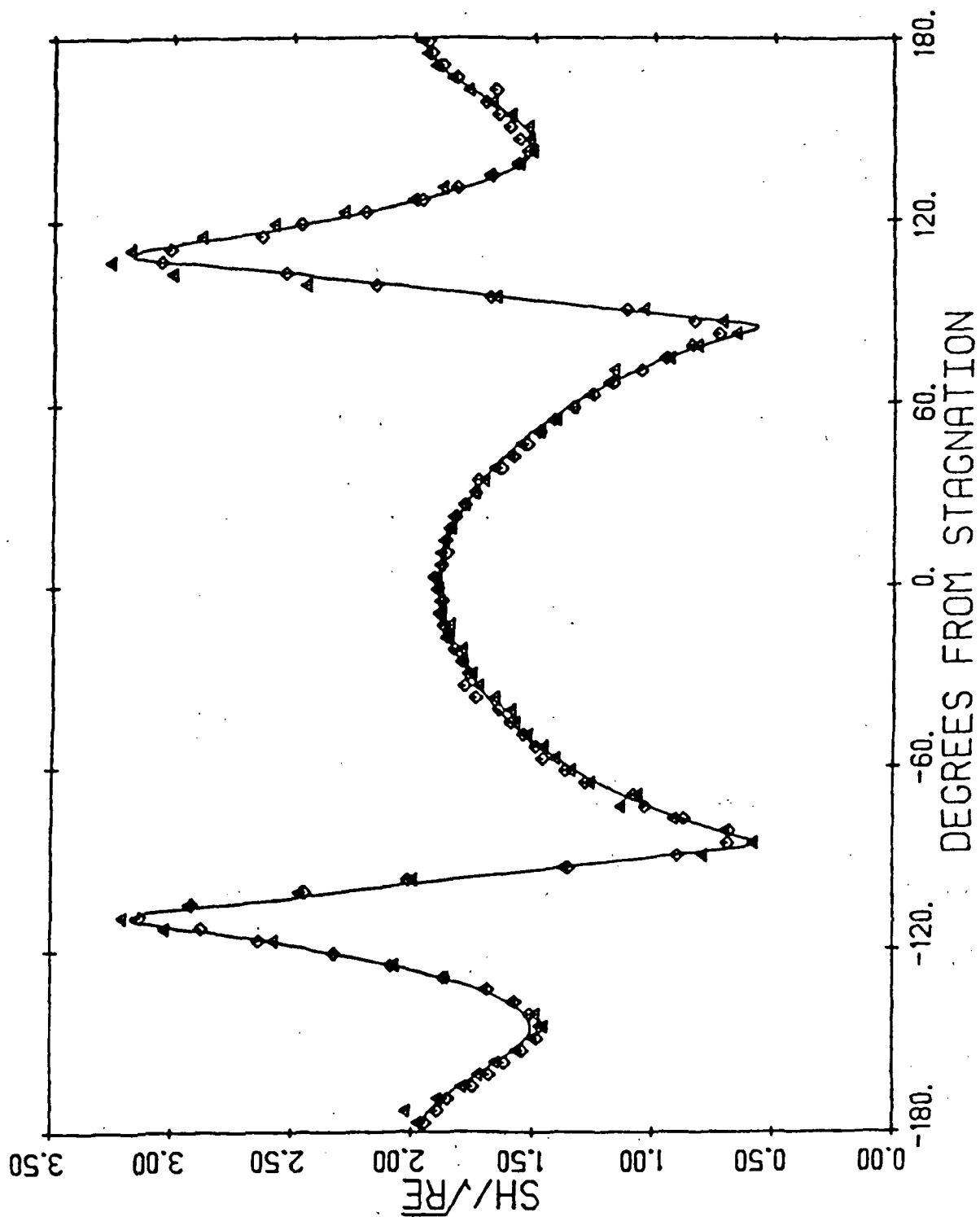


Figure 36. Mass transfer distribution
 ($Re = 110000$, $Tu = 1.80\%$, $L/D = .038$)

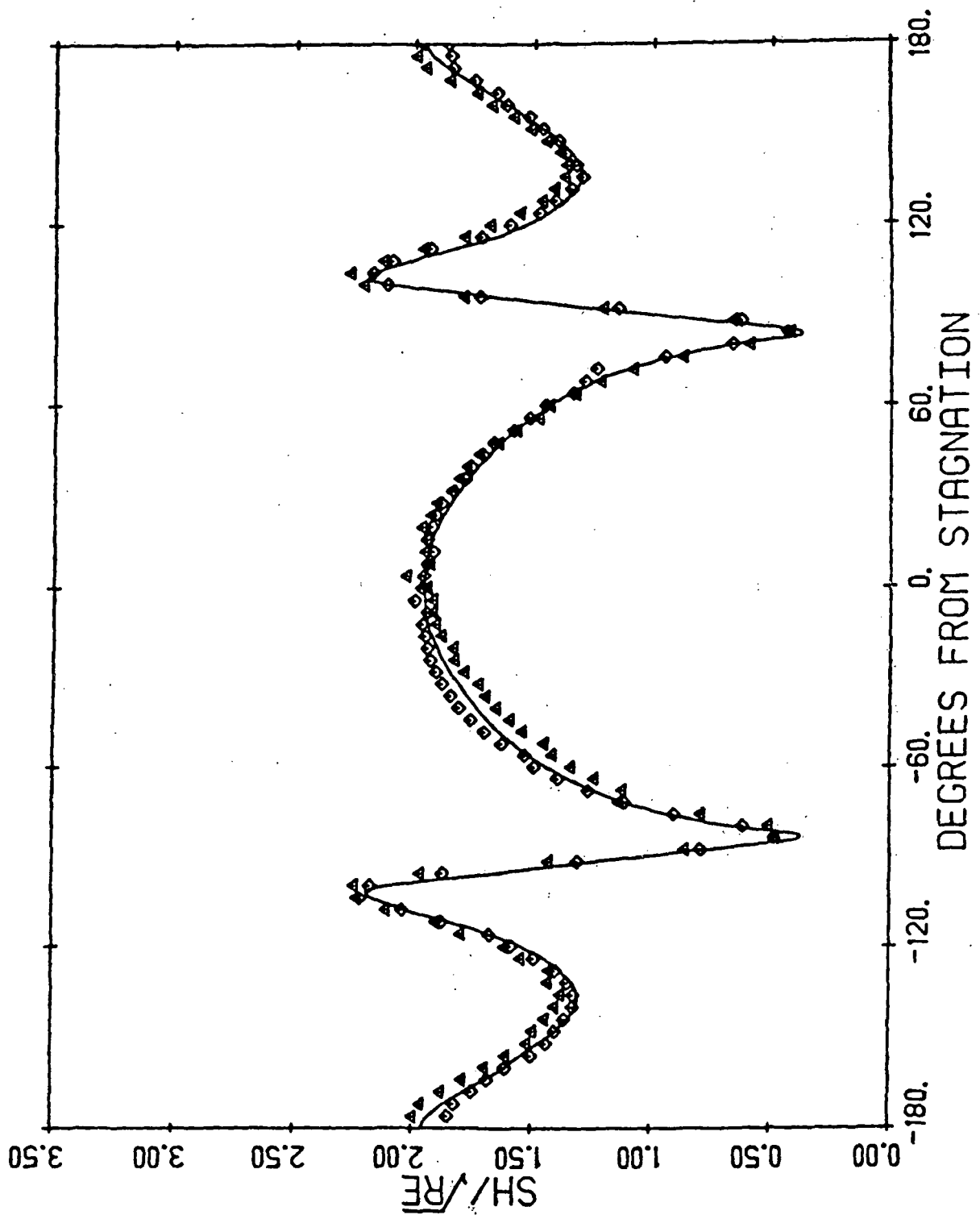


Figure 37. Mass transfer distribution
 ($Re = 75000$, $Tu = 2.65\%$, $L/D = .030$)

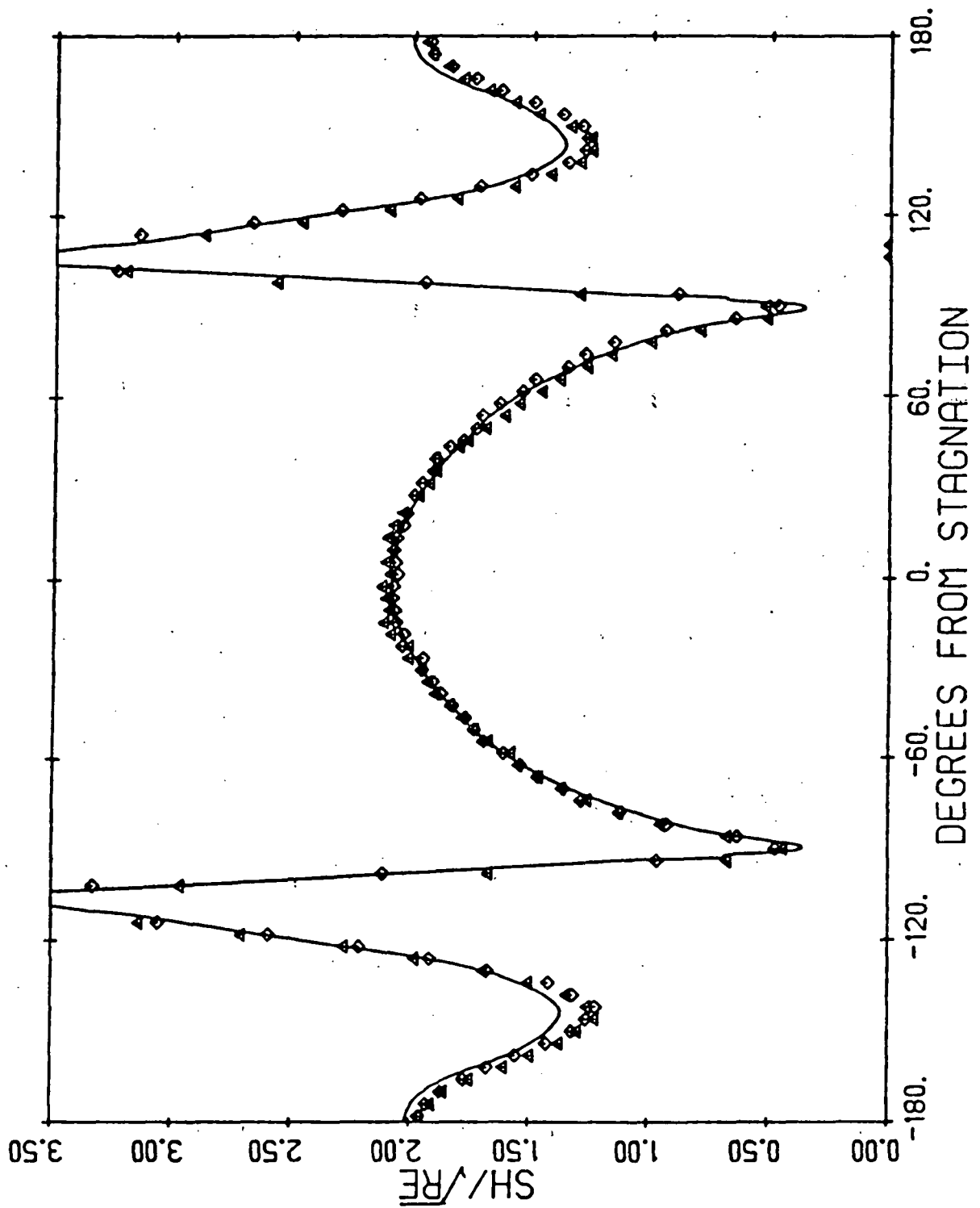


Figure 38. Mass transfer distribution
 ($Re = 110000$, $Tu = 2.65\%$, $L/D = .030$)

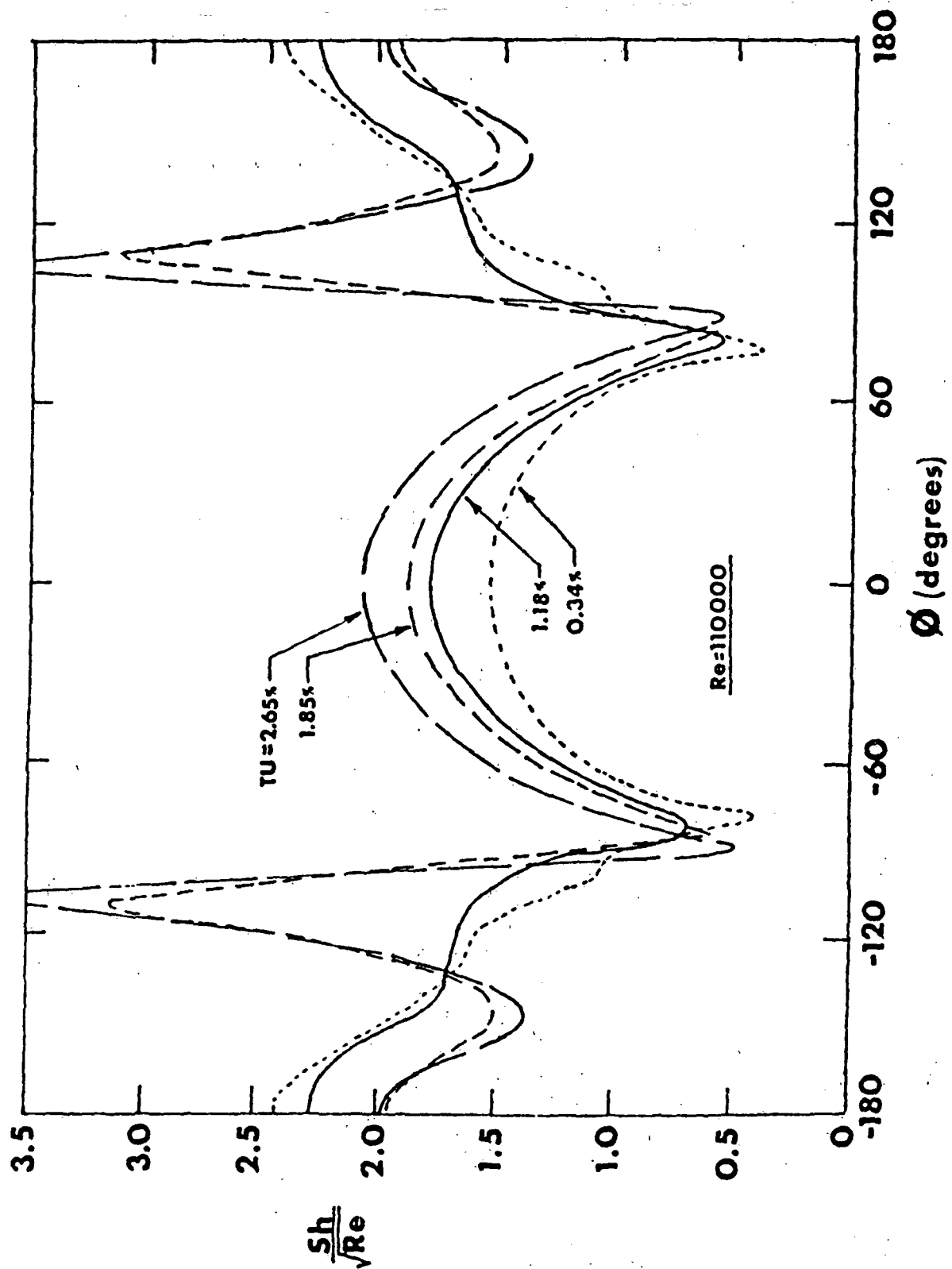


Figure 39. Comparison of elevated turbulence level results ($Re = 110,000$)

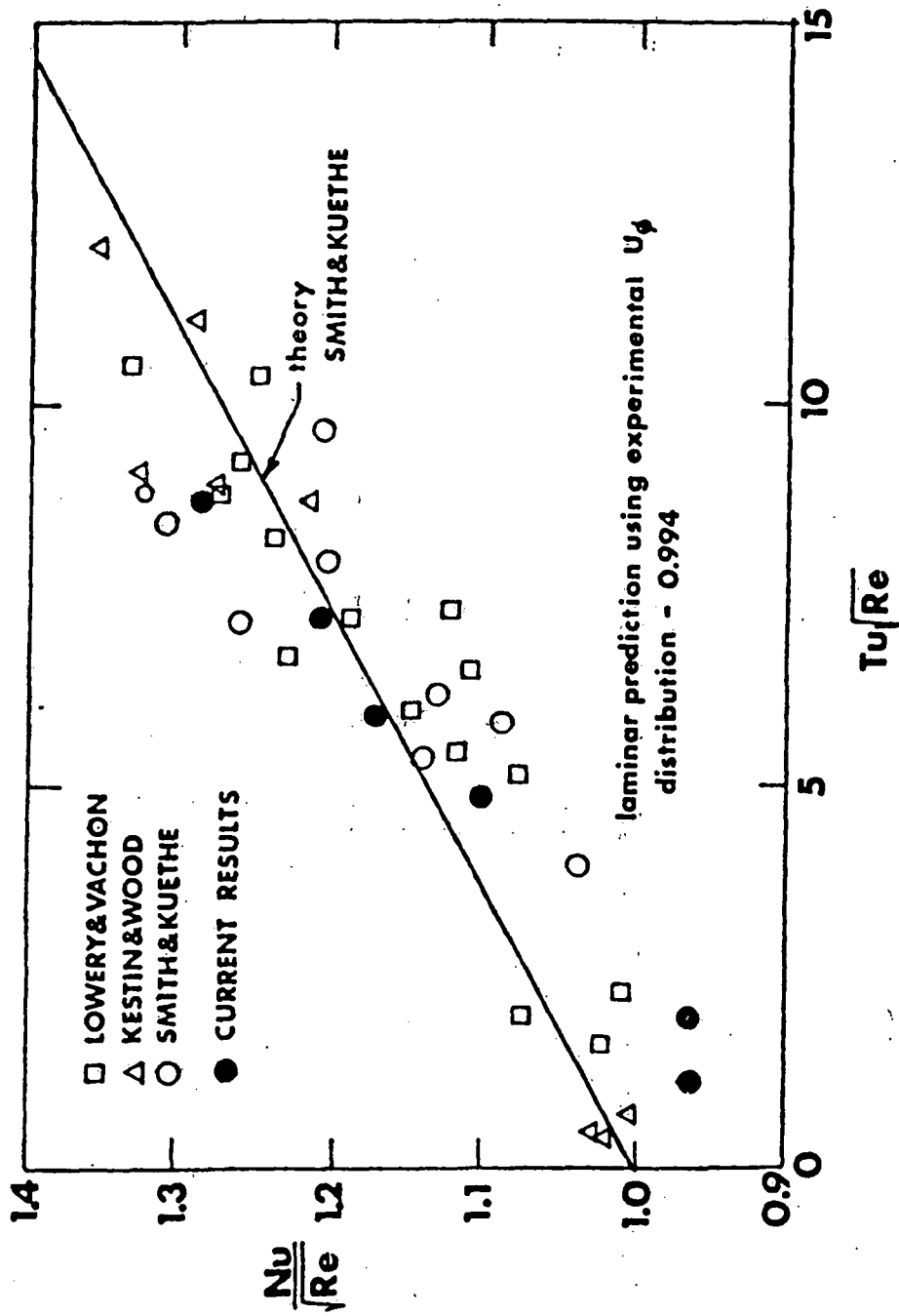


Figure 40. Comparison of stagnation point results with the results of other investigators

of other investigators, equivalent Nusselt numbers have been calculated from the mass transfer results through the use of the heat-mass transfer analogy. Due to the wide discrepancies in the methods used to report and measure turbulence levels, this figure should be viewed only as an indication of general trends, and not as a basis for the establishment of precise empirical correlations. The figure does, however, demonstrate that the current results are well within the band of scatter of the data from other investigations, although they appear to be somewhat low at low turbulence levels. This may be due to inaccuracies in the Schmidt number and vapor density relation, or it may be due to the difficulties presented by the rather high levels of ambient noise in the tunnel, which made the measurement of low turbulence levels more prone to error.

5.3 Mass Transfer Measurements - Oscillating Cylinder

In the oscillation study, each of the flow situations which produced nominally two-dimensional mass transfer results were repeated. Circumferential distributions of the time averaged local mass transfer rate were measured. For each case, the effects of oscillation on the transfer rate are evaluated by comparing the unsteady results to a "quasi-steady" curve calculated from the steady-state results obtained with an identical flow. Physically, the quasisteady distributions represent the results which would be obtained from a cylinder oscillating at an infinitely small frequency. In this situation the surface velocity of the cylinder is negligible and the effect of oscillation is a simple averaging of the transfer rates seen by a particular point at particular times, i.e.

$$Sh_{\text{quasisteady}}(\phi) = \frac{1}{2\pi} \int_{-\pi}^{\pi} Sh_{\text{steady}}(\phi + \phi_0 \sin \omega) d\omega$$

The quasisteady curves thus establish the "no effect" level for the oscillation tests. It should be noted that since the oscillation amplitudes used in the experiments are small, the quasisteady curve is essentially identical to the steady-state distribution in the stagnation zone and that it varies substantially only for the region around separation.

A summary of the oscillation tests performed is given in Table 3. Only two of the incident turbulence conditions used provided results which demonstrated a measurable effect of oscillation. The results for the other cases lie essentially, to within the limits of experimental error, on the quasisteady curves. The only substantial deviations from these curves are in the regions around separation. This effect was observed in all of the oscillation tests performed. The results which did demonstrate an effect of oscillation are presented and discussed below. To insure that the results of the investigation were reproducible, most of the tests described were repeated; in some cases many times. For brevity, only one representative set of data is presented for each case discussed. The full set of experimental data is available in Appendix A.

All of the results which show an effect of oscillation were obtained from tests performed downstream of the 7/8" mesh turbulence generating grid. Tests were performed for all three available positions of the grid, $x/R = 6.0$, 11.2 , and 18.7 where x is the distance upstream from the cylinder's axis, at a Reynolds number of $110,000$, an oscillation amplitude of 6° , and a Strouhal number of 0.0639 . The latter corresponds to the maximum available operating frequency. The results obtained with the grid installed at $x/R = 18.7$, which corresponds to $Tu = 1.182$ and $\frac{L}{D} = .050$ showed no effect of oscillation. The results for $x/R = 11.2$,

Table 3. Summary of oscillation tests performed

Re=110000				
Tu=.52%	= .34%	= 1.18%	= 1.80%	= 2.65%
L/D=.087	= .028	= .050	= .038	= .030
				= 4.9%
				= .188
St=.0071			Fig.43	no effect
			(2)	(1)
St=.0213			Fig.44	no effect
			(2)	(1)
St=.0355			Fig.45	no effect
			(2)	(1)
St=.0497			Fig.46	no effect
			(4)	(1)
St=.0639	no effect (2)	no effect (1)	Fig.47	no effect
			(3)	(1)
St=.0781			Fig.48	
$\phi_o = 12^\circ$			(1)	
St=.0213			Fig.52	
Re=75000			(1)	
St=.0417			Fig.49	
			(1)	
St=.1041			Fig.50	
Re=50000			(1)	
St=.1460			Fig.51	
			(1)	

number of tests performed for each case is written in parentheses

which corresponds to $Tu = 1.801\%$ and $\frac{L}{D} = .038$, are shown in Fig. 41. In this case a small effect of oscillation is discernible. The mass transfer rate at leading edge is about 3% higher than that suggested by the quasisteady curve. It is important to note, however, that this increase is barely above the 2% limit of experimental repeatability. The mass transfer measurements for the closest installation position of the grid, $x/R = 6.0$, are given in Fig. 42. In this case the measured incident turbulence level and integral length scale were 2.65% and $.03D$, respectively. The mass transfer rate at stagnation is, for this position of the grid, about 10% above the quasisteady transfer rate. Since this was the largest observed effect of oscillation, the turbulence field generated by this position of the $7/8"$ mesh grid was used for the remainder of the investigation.

In the next series of mass transfer experiments, the effect of Strouhal number was examined. Maintaining an oscillation amplitude of $\phi_0 = 6^\circ$ and a Reynolds number of 110,000; tests were performed for Strouhal numbers ranging from 0.007 to 0.0781. The results are presented in Figs. 43 through 48. Each case exhibited a small effect of oscillation, with increases in the mass transfer rate ranging from 3% to 10%, however, perhaps the most remarkable aspect of the results is the fact that an effect was observed even in the lowest frequency case, $St = 0.0071$.

The effects of oscillations at Strouhal numbers higher than 0.0781 were also examined. Since the actual maximum oscillation frequency was constrained by the physical limitations of the oscillation mechanism, the Strouhal number, $\frac{fD}{U}$, was increased by lowering the flow velocity. It should be noted that this has the unfortunate consequence of lowering the

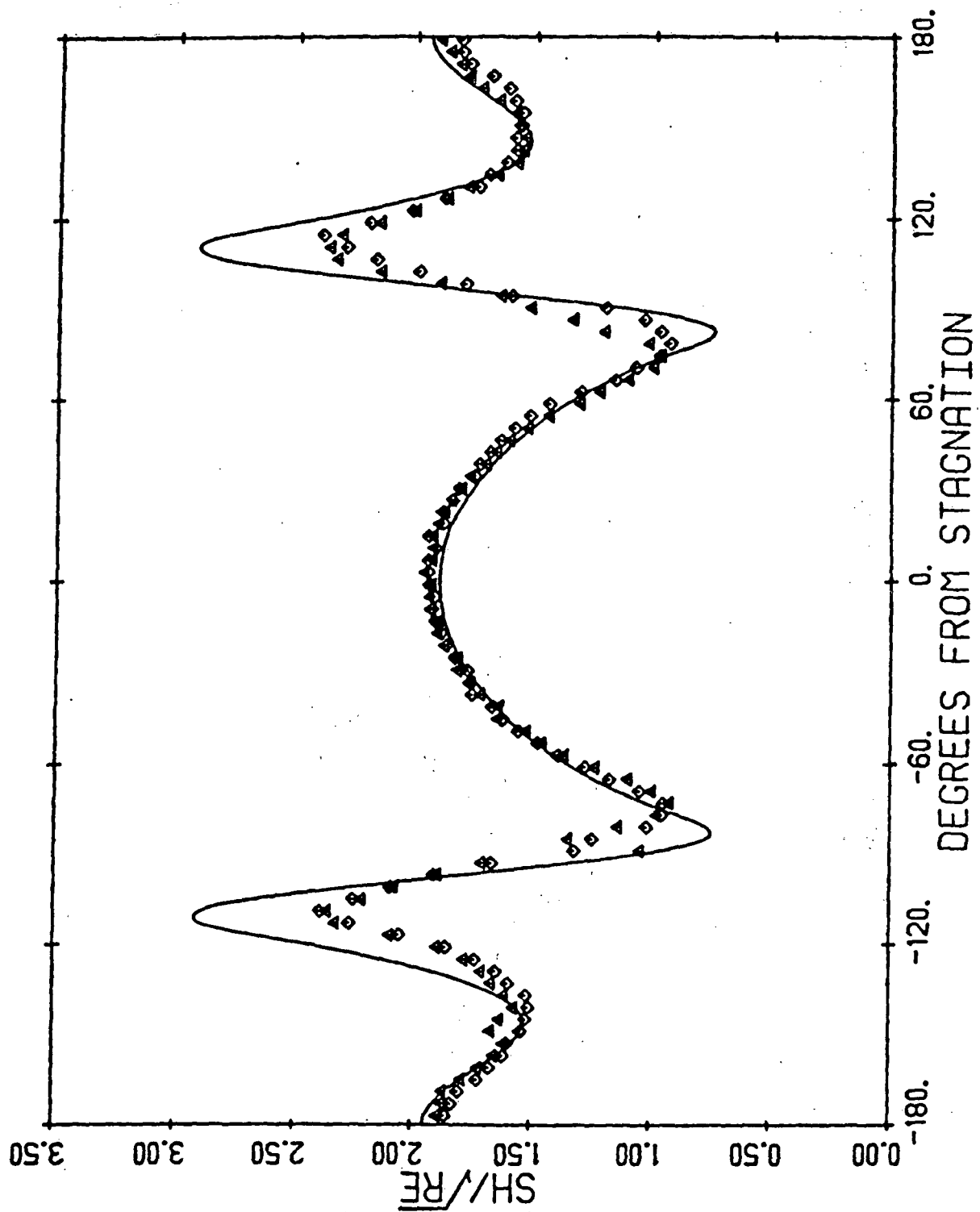


Figure 41. Mass transfer distribution with oscillation
 ($Re = 110000$, $Tu = 1.80\%$, $L/D = .038$, $St = .0639$)

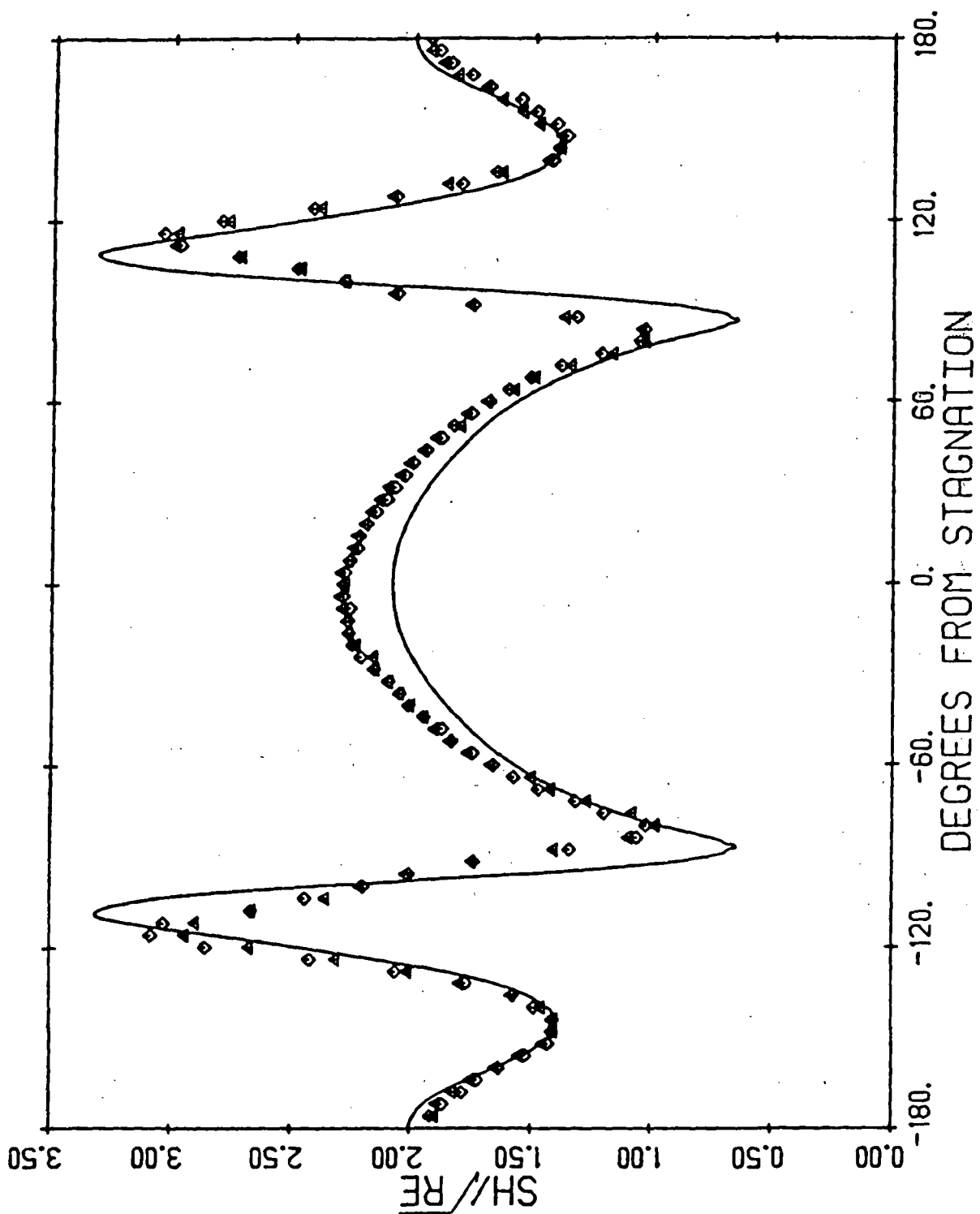


Figure 42. Mass transfer distribution with oscillation
 (Re = 110000, Tu = 2.65%, L/D = .030, St = .0639)

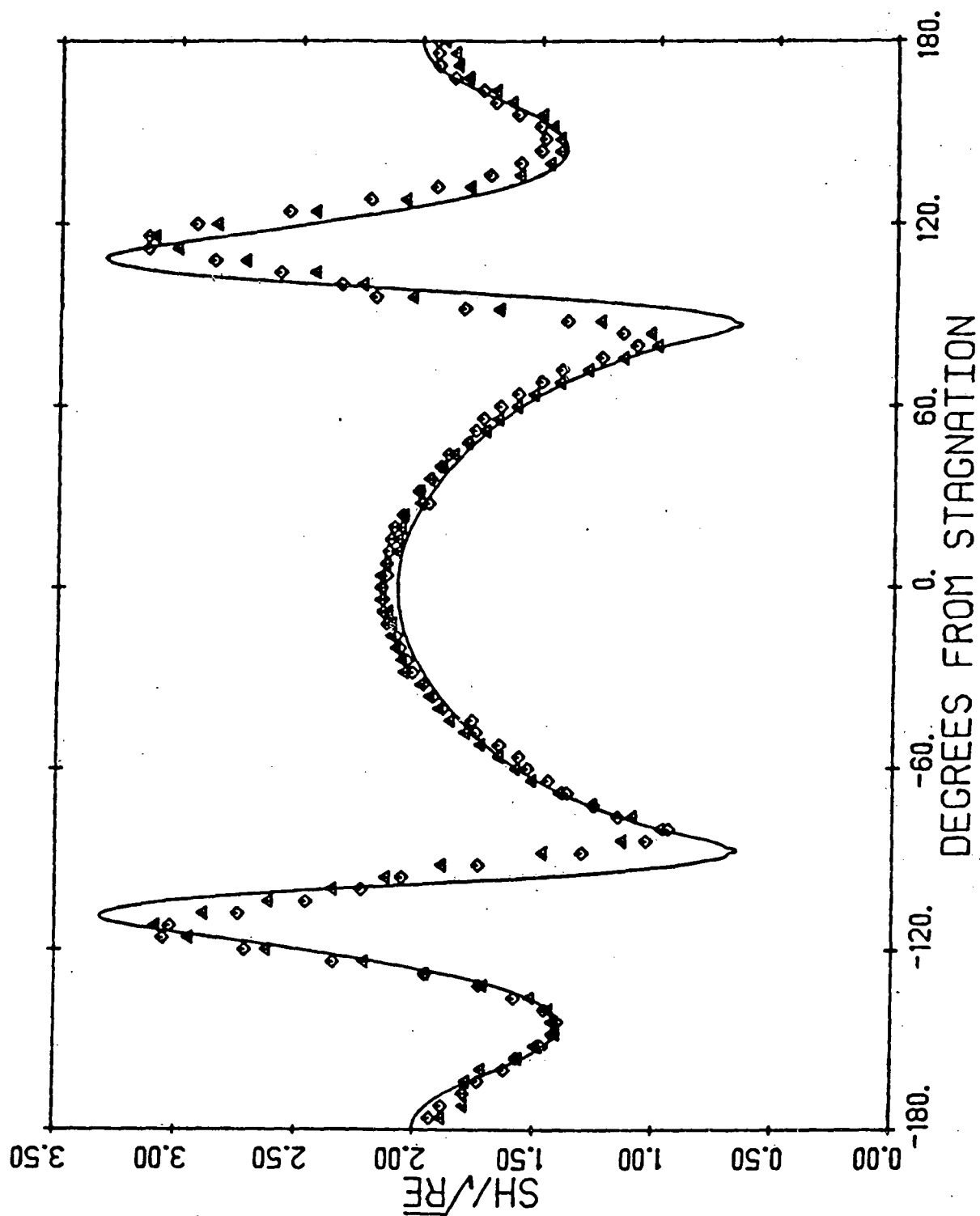


Figure 43. Mass transfer distribution with oscillation
 ($Re = 110000$, $Tu = 2.65\%$, $L/D = .030$, $St = .0071$)

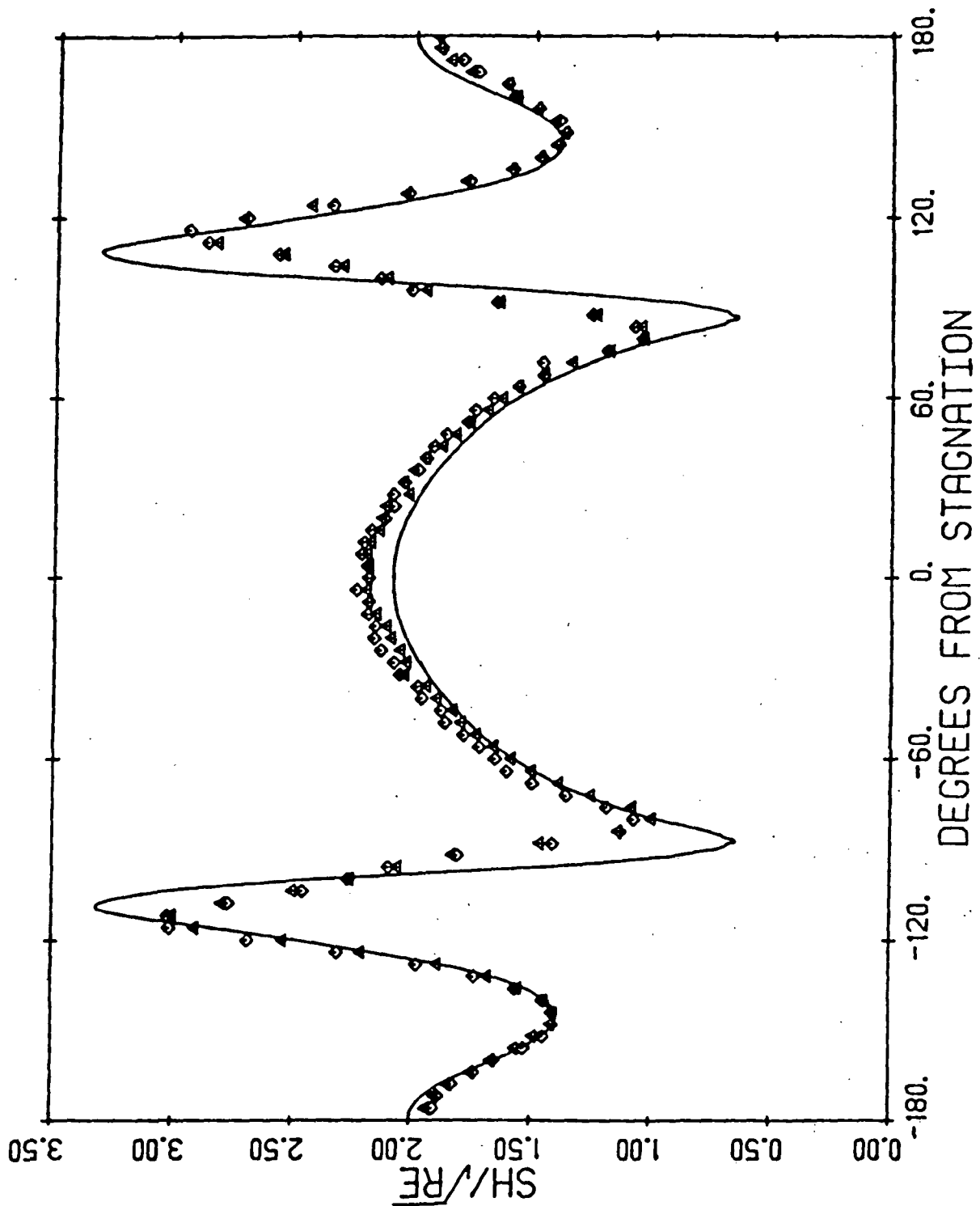


Figure 44. Mass transfer distribution with oscillation
 ($Re = 110000$, $Tu = 2.65\%$, $L/D = .030$, $St = .0213$)

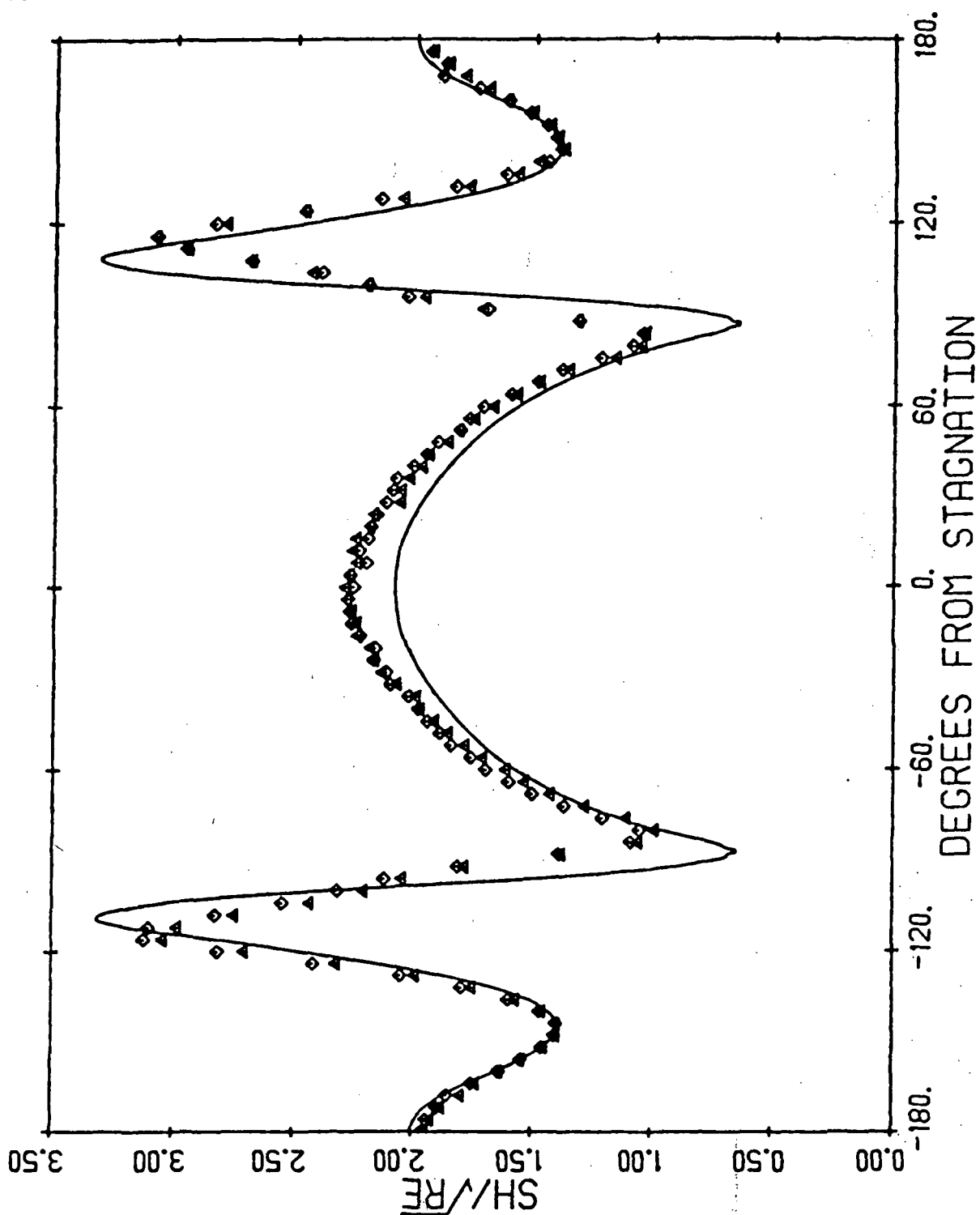


Figure 45. Mass transfer distribution with oscillation
 ($Re = 110000$, $Tu = 2.65\%$, $L/D = .030$, $St = .0355$)

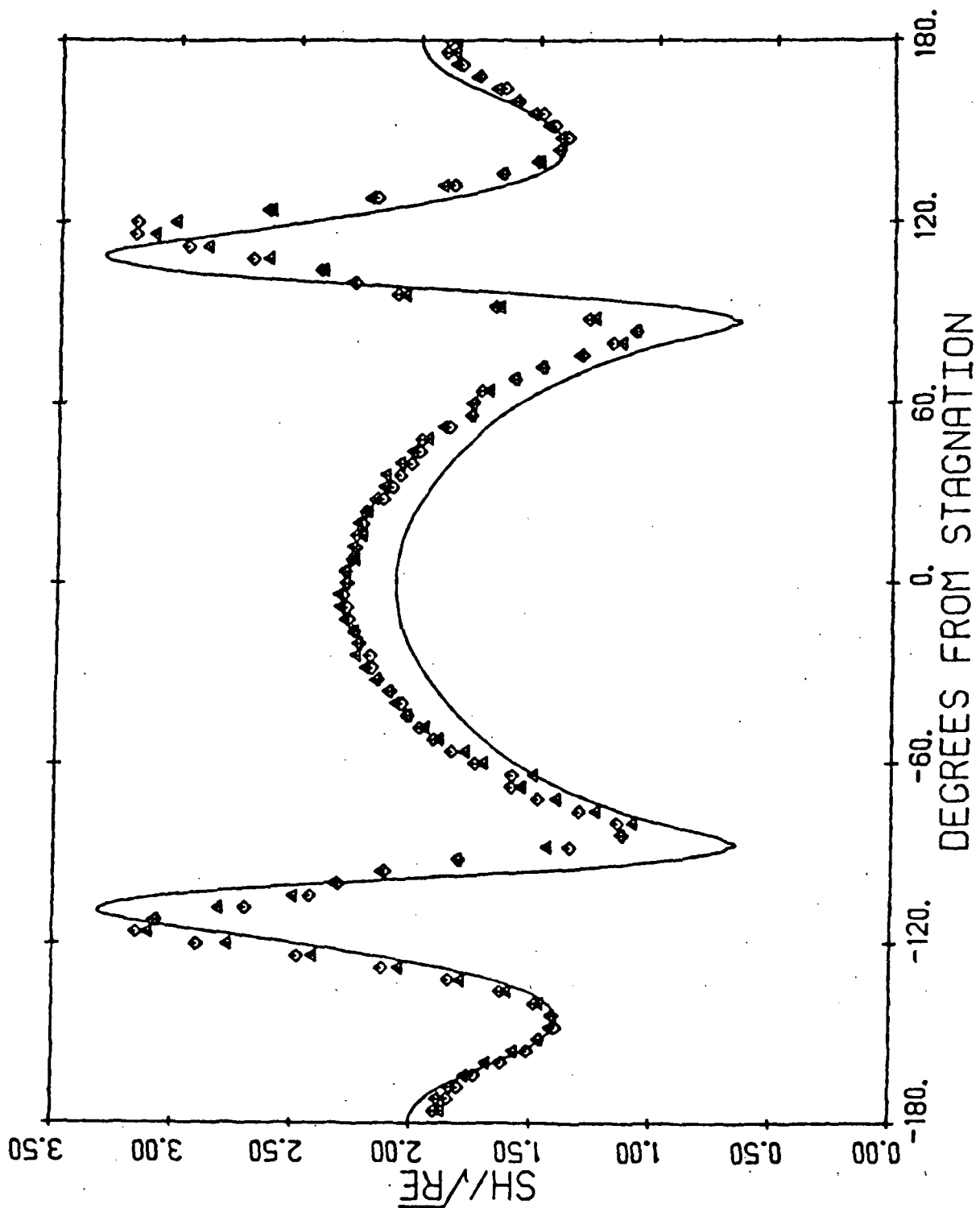


Figure 46. Mass transfer distribution with oscillation
 ($Re = 110000$, $Tu = 2.65\%$, $L/D = .030$, $St = .0497$)

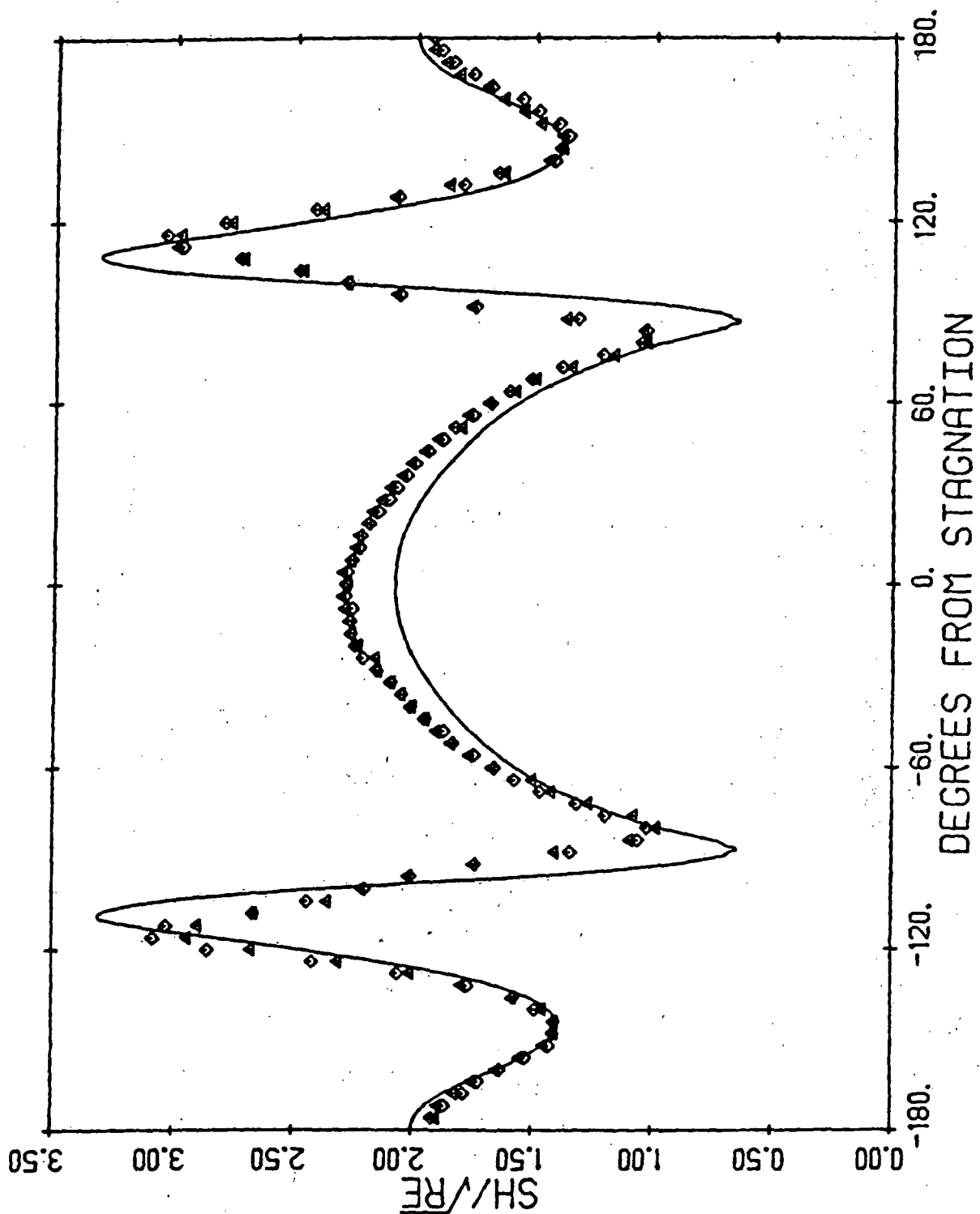


Figure 47. Mass transfer distribution with oscillation
 ($Re = 110000$, $Tu = 2.65\%$, $L/D = .030$, $St = .0639$)

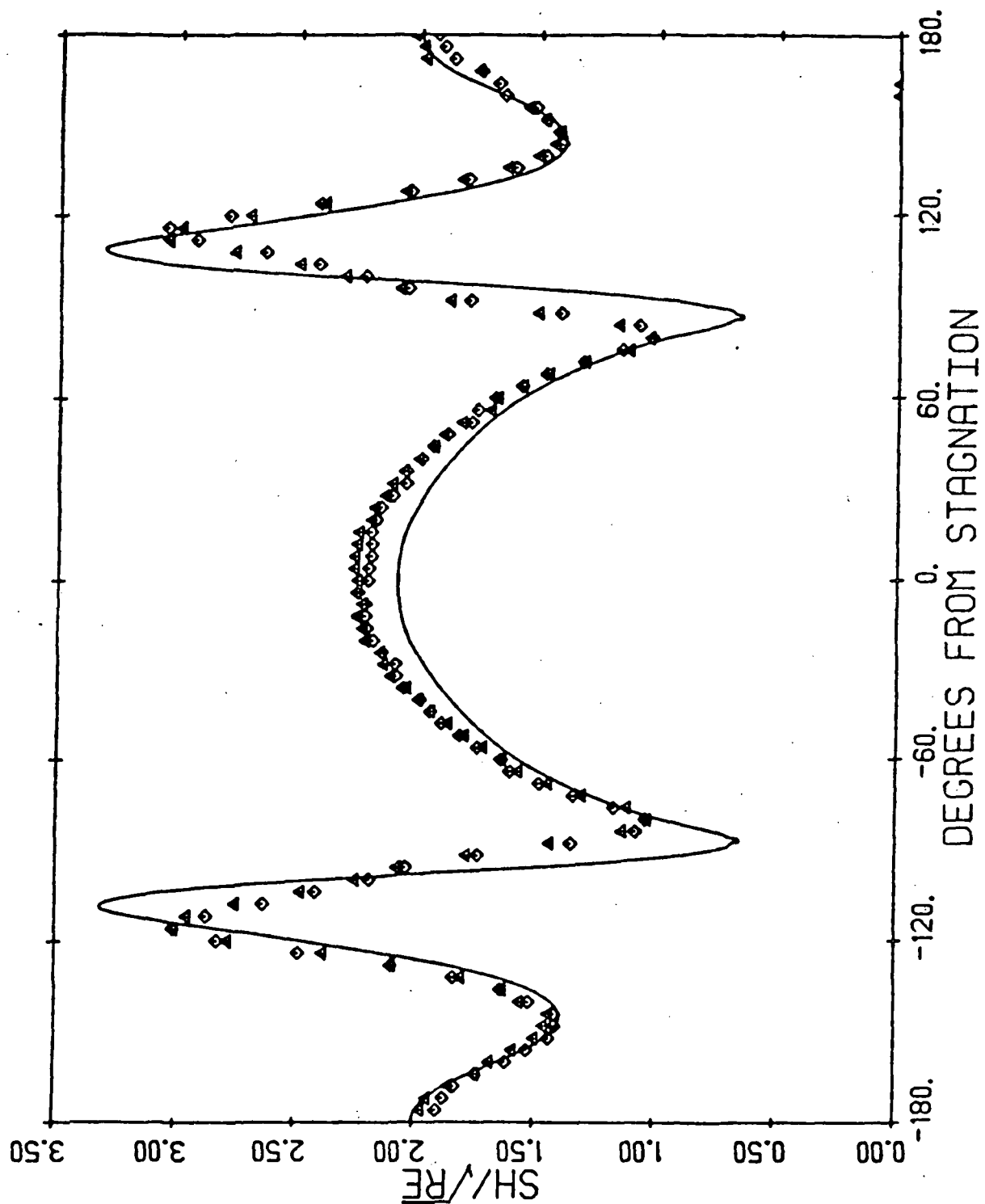


Figure 48. Mass transfer distribution with oscillation
 ($Re = 110000$, $Tu = 2.65\%$, $L/D = .030$, $St = .0781$)

effects of the incident turbulence level since the transfer rate depends in some manner on $Tu\sqrt{Re}$. The results of these tests performed at Reynolds numbers of 75,000 and 50,000 are given in Figs. 49, 50 and 51. In the $Re = 50,000$ case the results of the measurements at the two spanwise positions differed by approximately 7%. This difference was observed in both the steady and the oscillation tests; however, when the oscillation data at each position is scaled to the quasisteady curve obtained for that position, the effect measured by the two gauges is essentially identical. The spanwise discrepancy in these tests was generated by skew in the incident velocity caused by operation of the tunnel in an off-design mode.

As a final oscillation test, the effect of changing the oscillation amplitude was investigated. Unfortunately, the vibration forces generated by the oscillation increase drastically with amplitude, severely limiting the maximum available frequency. A mass transfer test was performed for the intensively studied case of $Tu = 2.65\%$, $\frac{L}{D} = .03$, at a Reynolds number of 110,000. An oscillation amplitude of $\phi = 12^\circ$ and a Strouhal number = .0213 were used. The results are presented in Fig. 52. The observed augmentation at stagnation is about 5% and is approximately equal to that measured at the previous oscillation amplitude.

The results of the unsteady tests performed for an incident turbulence level of 2.65% and an integral length scale of .03D are correlated in Fig. 53. The augmentation ratio, that is the unsteady mass transfer rate divided by the quasisteady mass transfer rate for similar flow conditions, is plotted as a function of Strouhal number at the stagnation point. The augmentation is seen to initially increase with Strouhal number reaching a maximum value of 1.1 at $St \approx .06$.

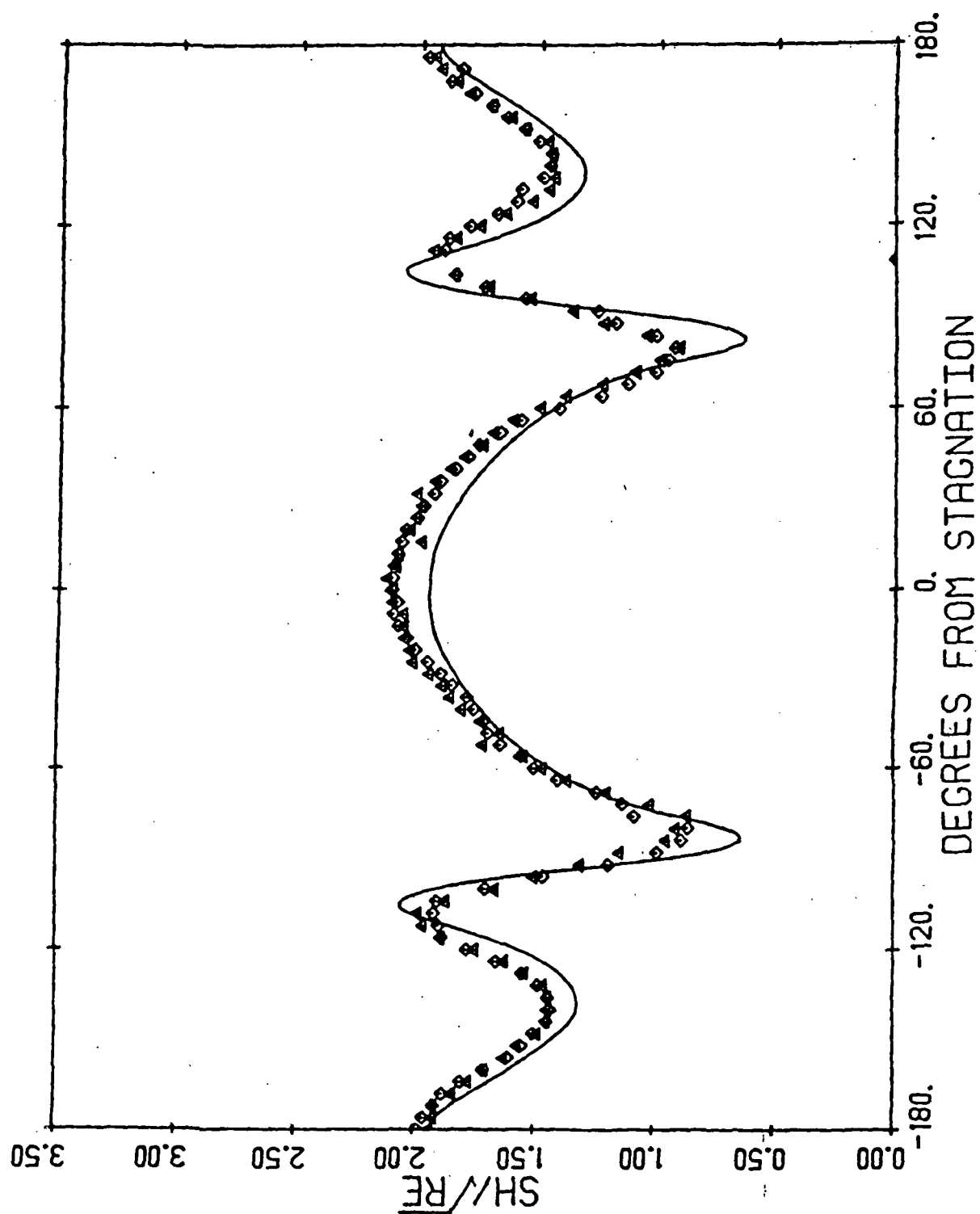


Figure 49. Mass transfer distribution with oscillation
 ($Re = 75000$, $Tu = 2.65\%$, $L/D = .030$, $St = .0417$)

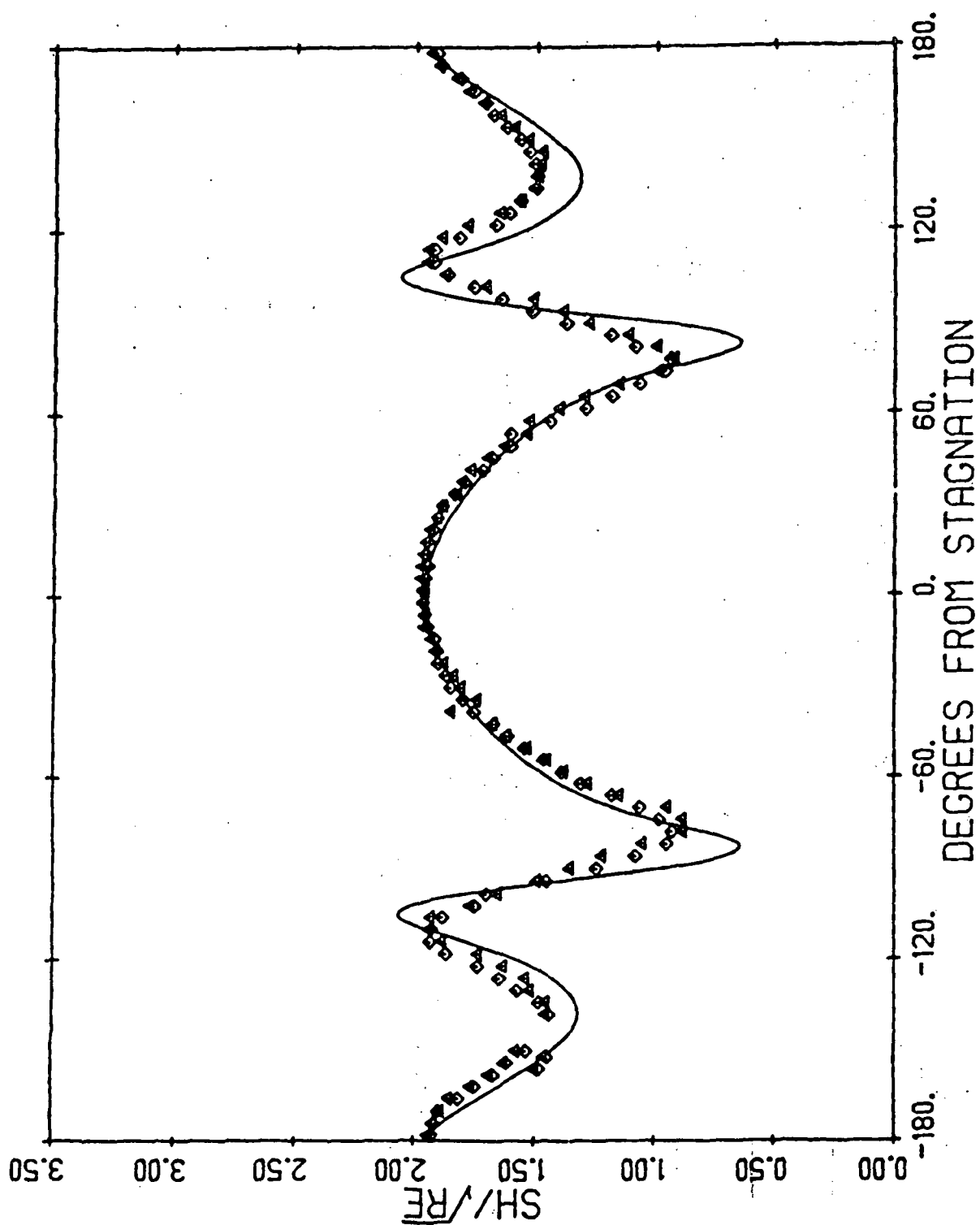


Figure 50. Mass transfer distribution with oscillation
 ($Re = 75000$, $Tu = 2.65\%$, $L/D = .030$, $St = .1041$)

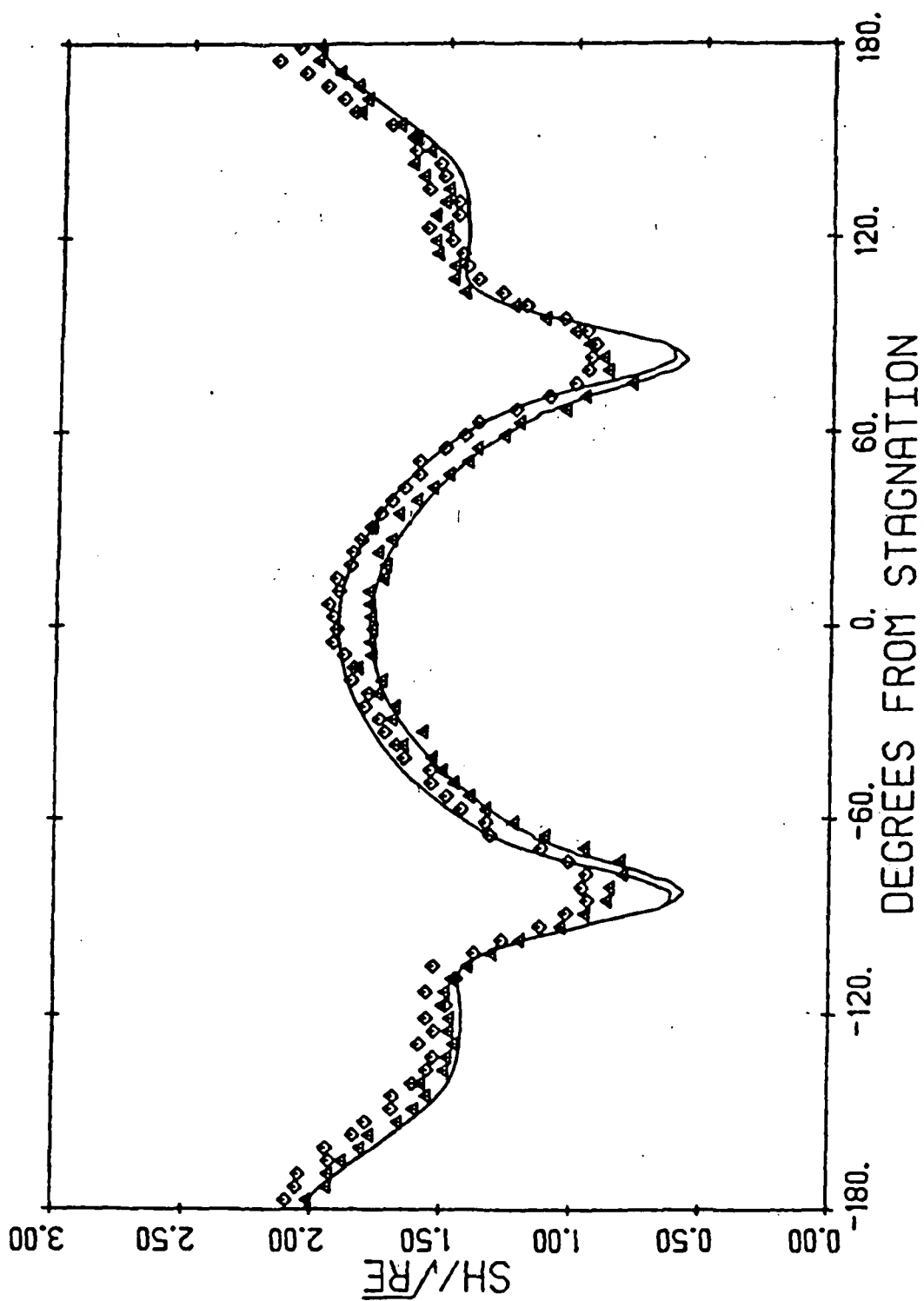


Figure 51. Mass transfer distribution with oscillation
 ($Re = 50000$, $Tu = 2.65\%$, $L/D = .030$, $St = .1406$)

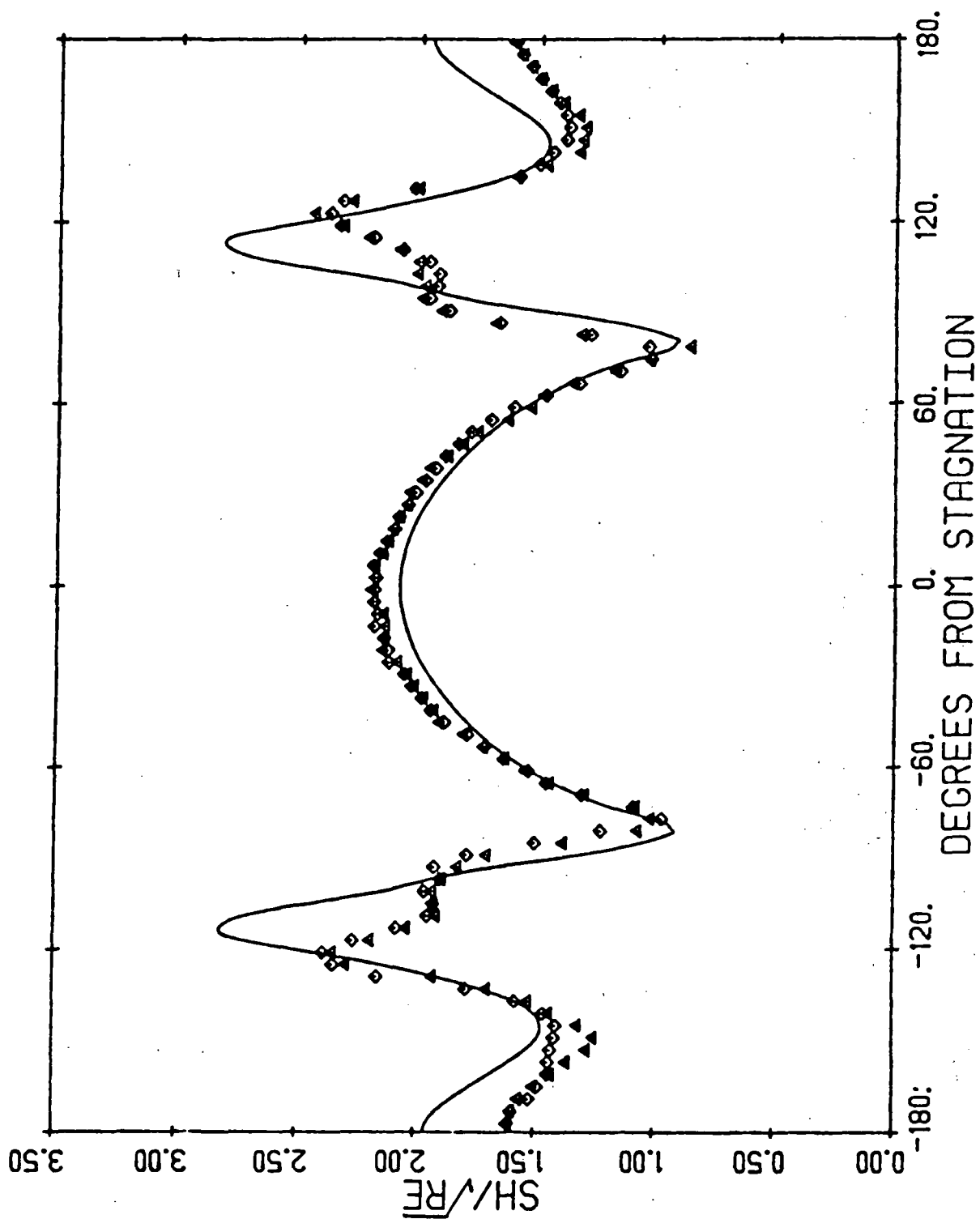


Figure 52. Results obtained with increased amplitude of oscillation ($Re = 110000$, $Tu = 2.65\%$, $L/D = .030$, $St = .0639$, $\phi_o = 12$)

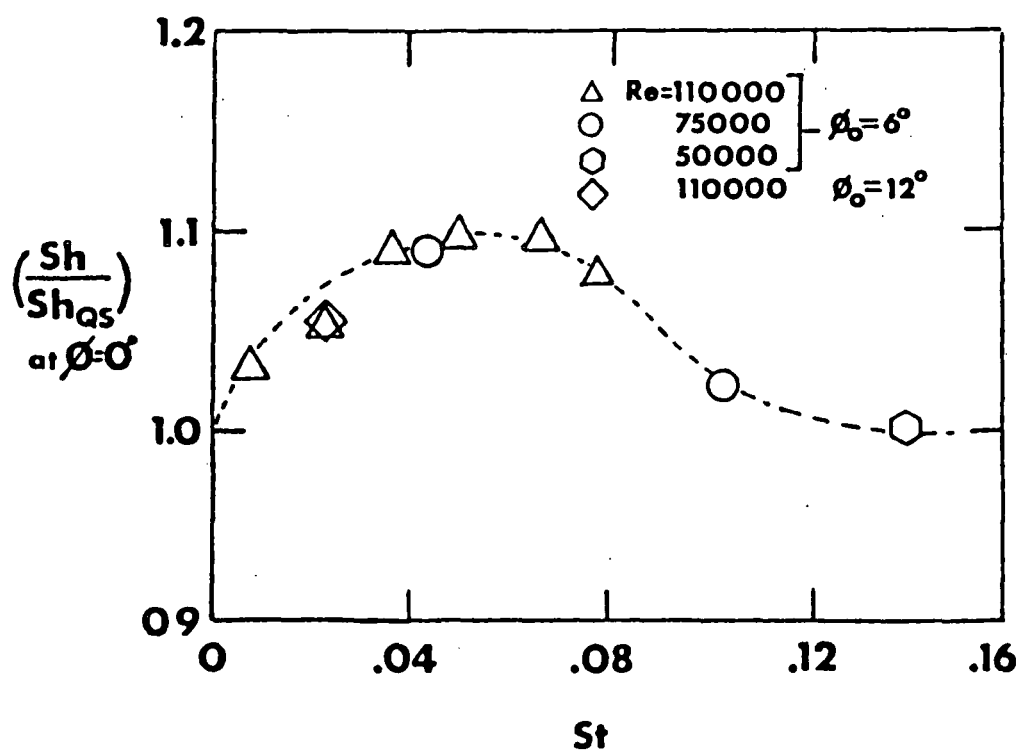


Figure 53. Correlation of oscillation results
($Re = 110000$, $Tu = 2.65\%$, $L/D = .030$)

For larger Strouhal numbers, the data suggests that the augmentation ratio decreases asymptotically back to 1.0, the no-effect level. It must, however, be noted that the data in this range was obtained at lower Reynolds numbers and that the effects of turbulence are hence decreased. Also of interest is the fact that the result obtained with the increased oscillation amplitude falls along the curve suggested by the other data.

5.4 Investigation into Spanwise Variations in Mass Transfer

As a portion of the unsteady investigation, a series of steady-state mass transfer experiments were performed under a variety of turbulence conditions. To establish the degree of two dimensionality of the results, measurements were taken in the spanwise direction at a number of circumferential positions on the test cylinder. The results of these experiments have been condensed in Figs. 54 through 60, where particular traverses have been selected from the full data set given in Appendix D. The results indicate that for certain turbulence conditions, which are associated with various combinations of generating screens and positions, the local mass transfer rate varied substantially across the span, while for other cases the mass transfer rate was nominally constant in the spanwise direction. In particular, the results presented in Figs. 57, 58, 59 and 60 are definitely three dimensional in nature. The measurements taken behind the 16-mesh screen are the most remarkable of these cases, exhibiting a regular wavelike behavior with a wavelength of about .15R. China clay flow visualizations performed across the full span of the test body indicated that the spanwise variations in the other cases were also somewhat periodic; however, the wavelengths for these cases were too large

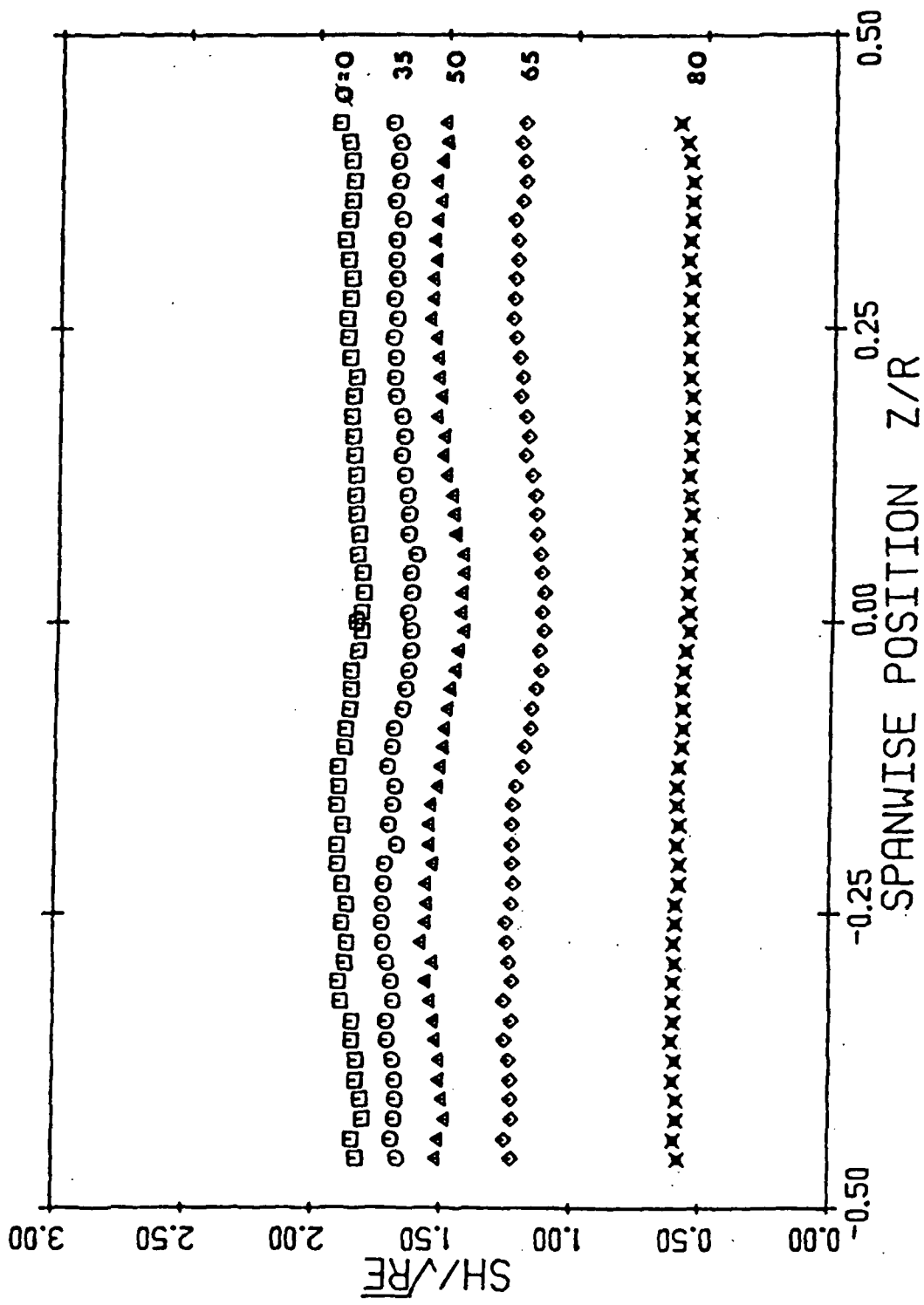


Figure 54. Spanwise mass transfer distributions behind generating grid ($M = 0.875$, $x/R = 18.7$, $Re = 110000$)

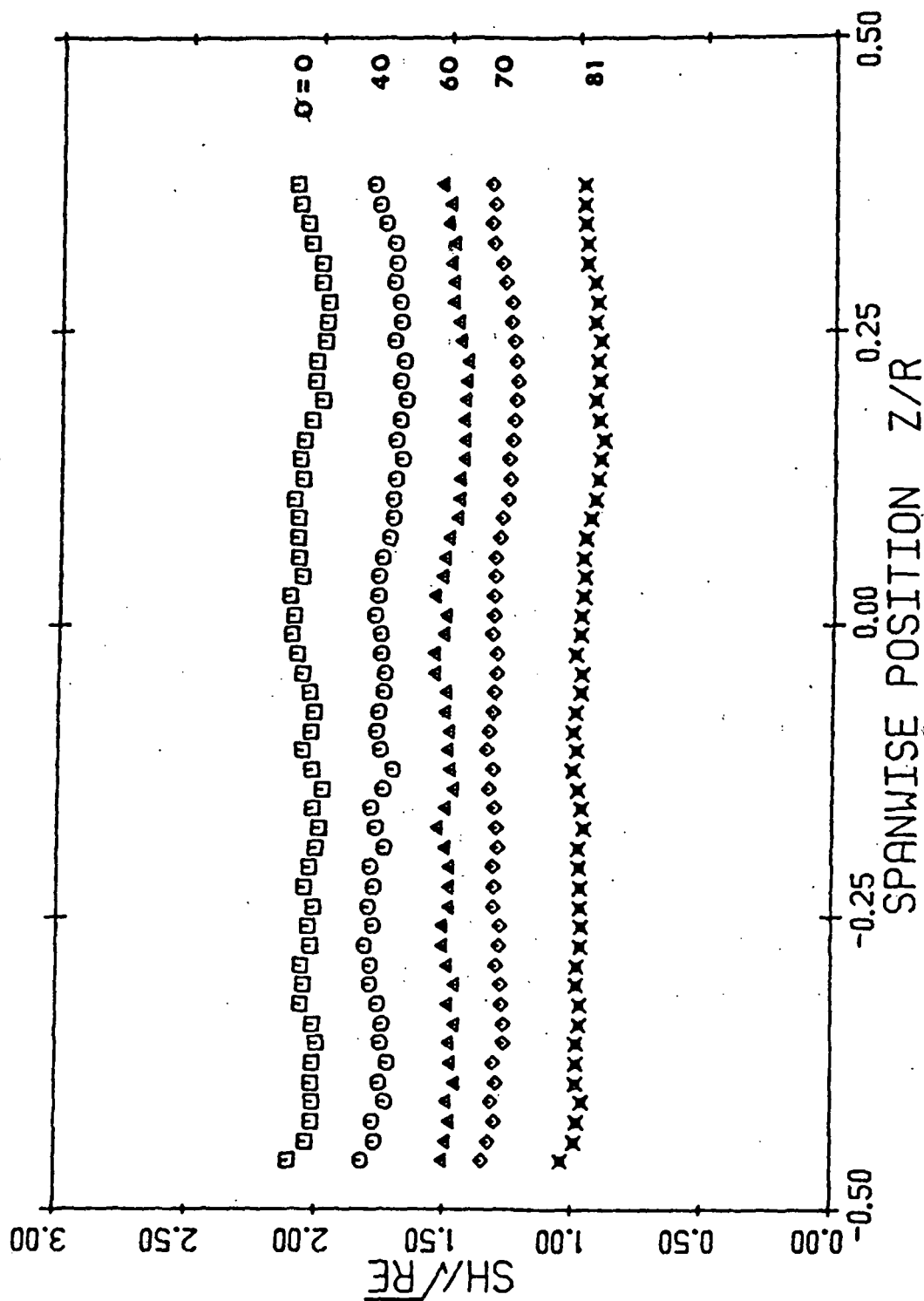


Figure 55. Spanwise mass transfer distributions behind generating grid ($M = .875$, $x/R = 6.0$, $Re = 110000$)

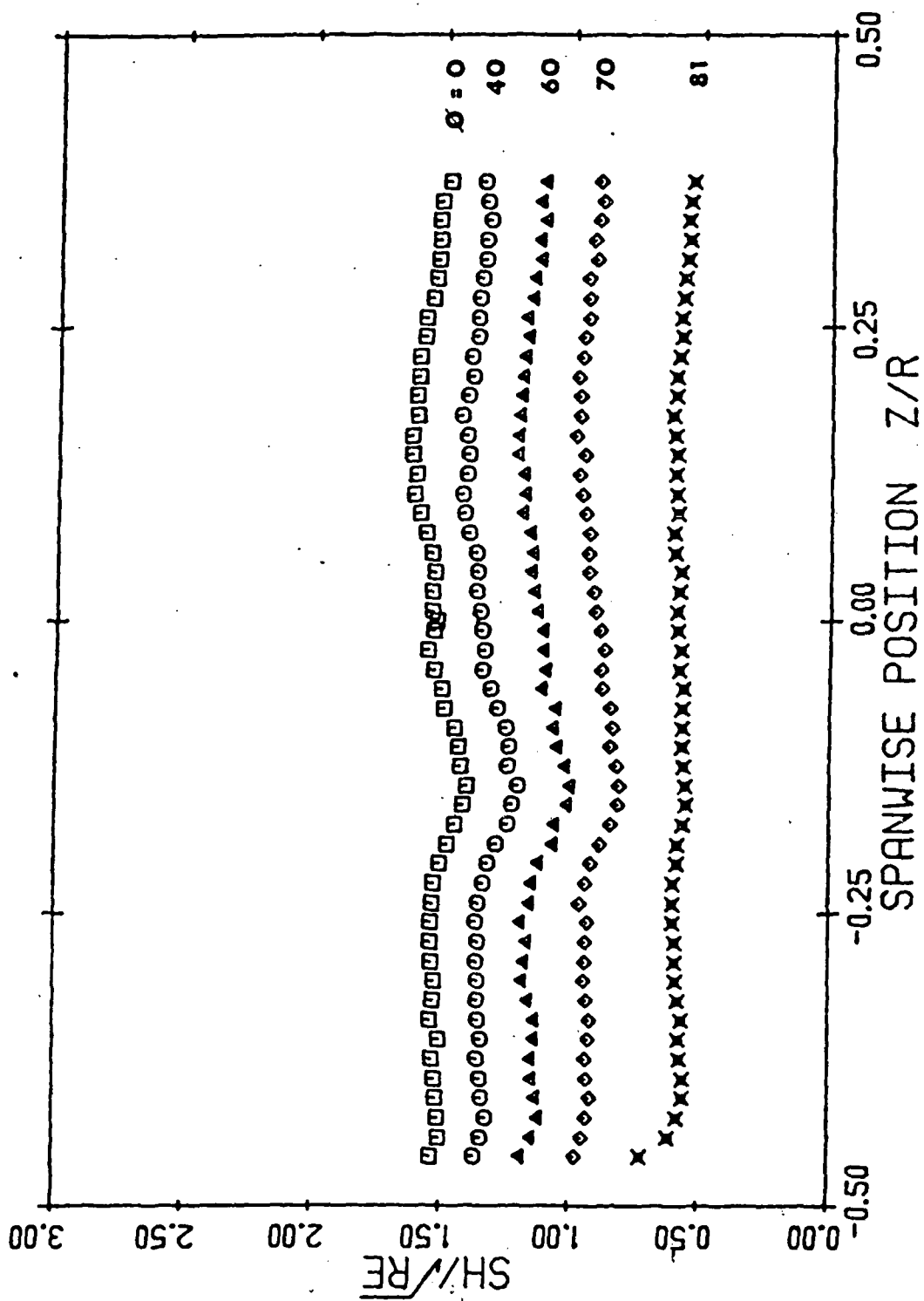


Figure 56. Spanwise mass transfer distributions behind generating grid ($M = .125$ ", $x/R = 18.7$, $Re = 110000$)

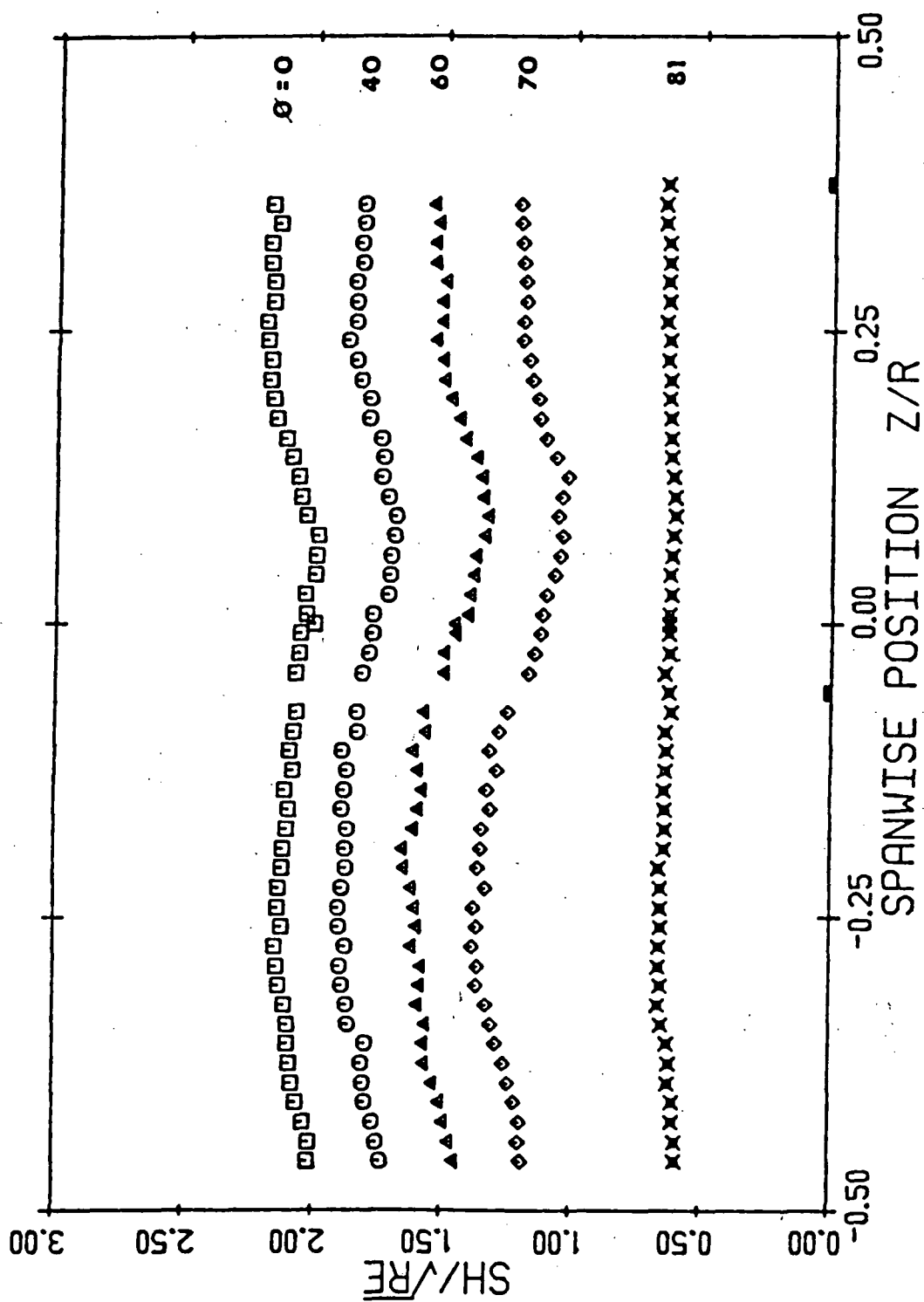


Figure 57. Spanwise mass transfer distributions behind generating grid ($M = .621$, $x/R = 11.2$, $Re = 110000$)

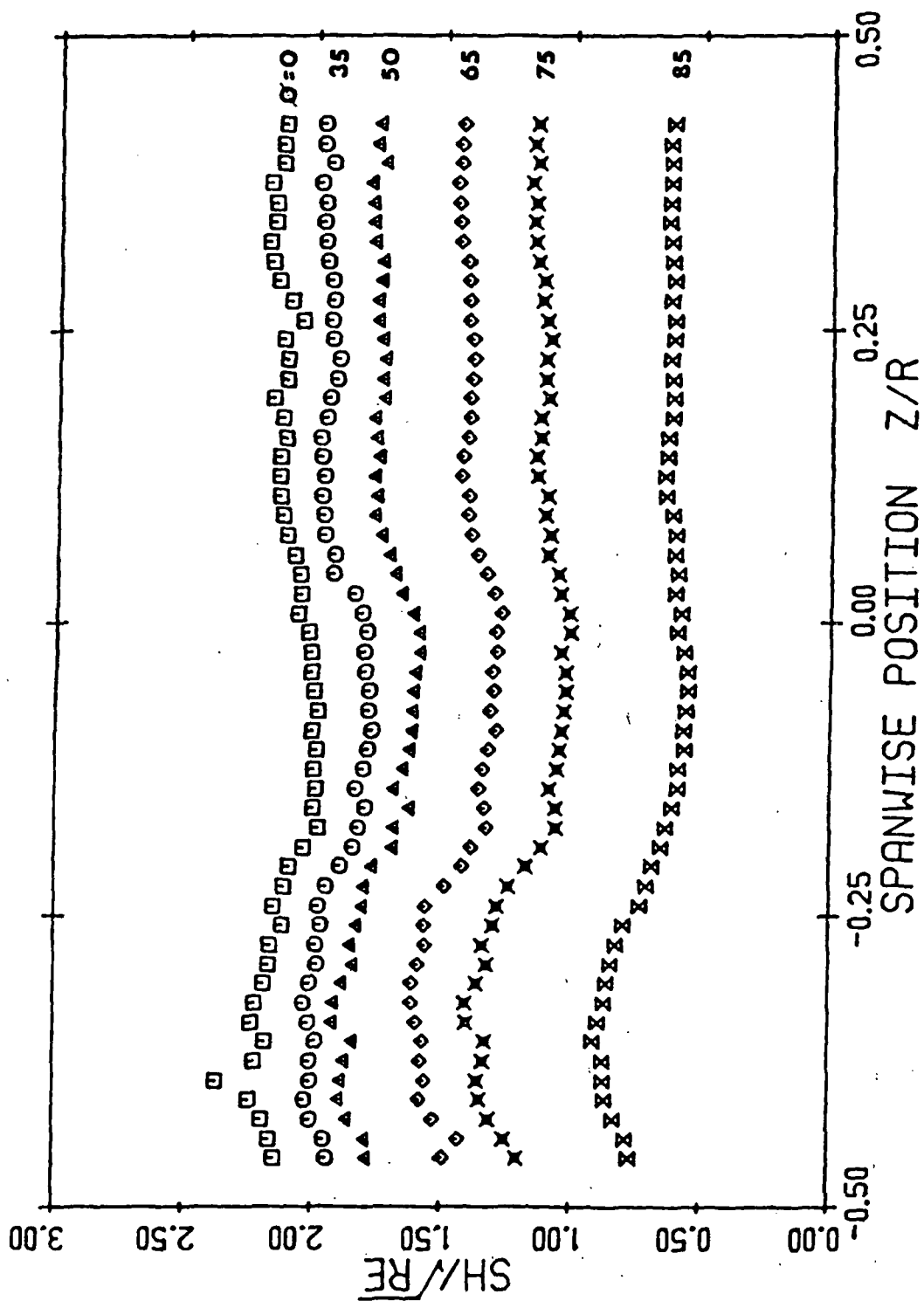


Figure 58. Spanwise mass transfer distributions behind generating grid ($M = 0.621$, $x/R = 6.0$, $Re = 110000$)

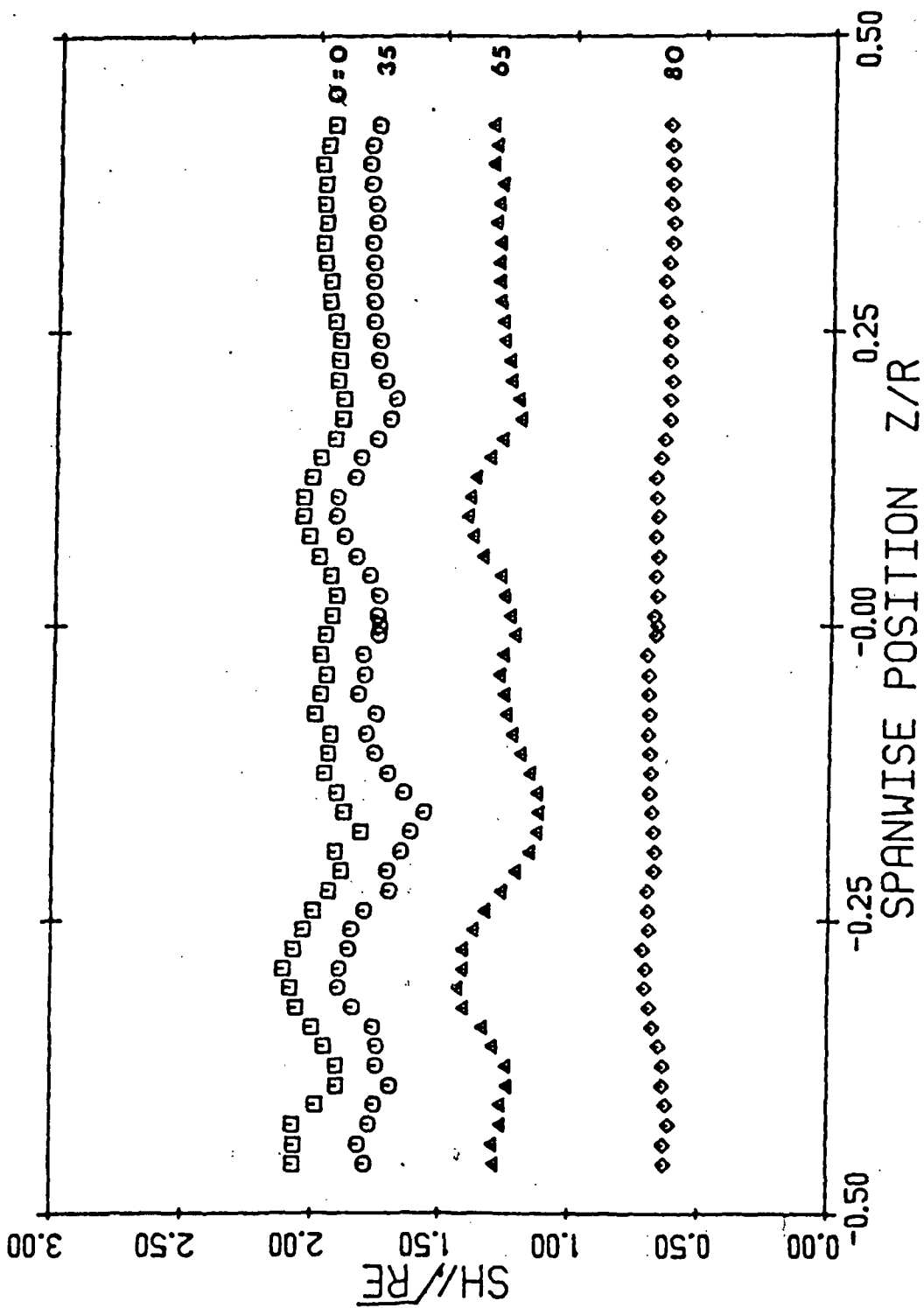


Figure 59. Spanwise mass transfer distributions behind generating grid ($M = .125$, $x/R = 6.0$, $Re = 110000$)

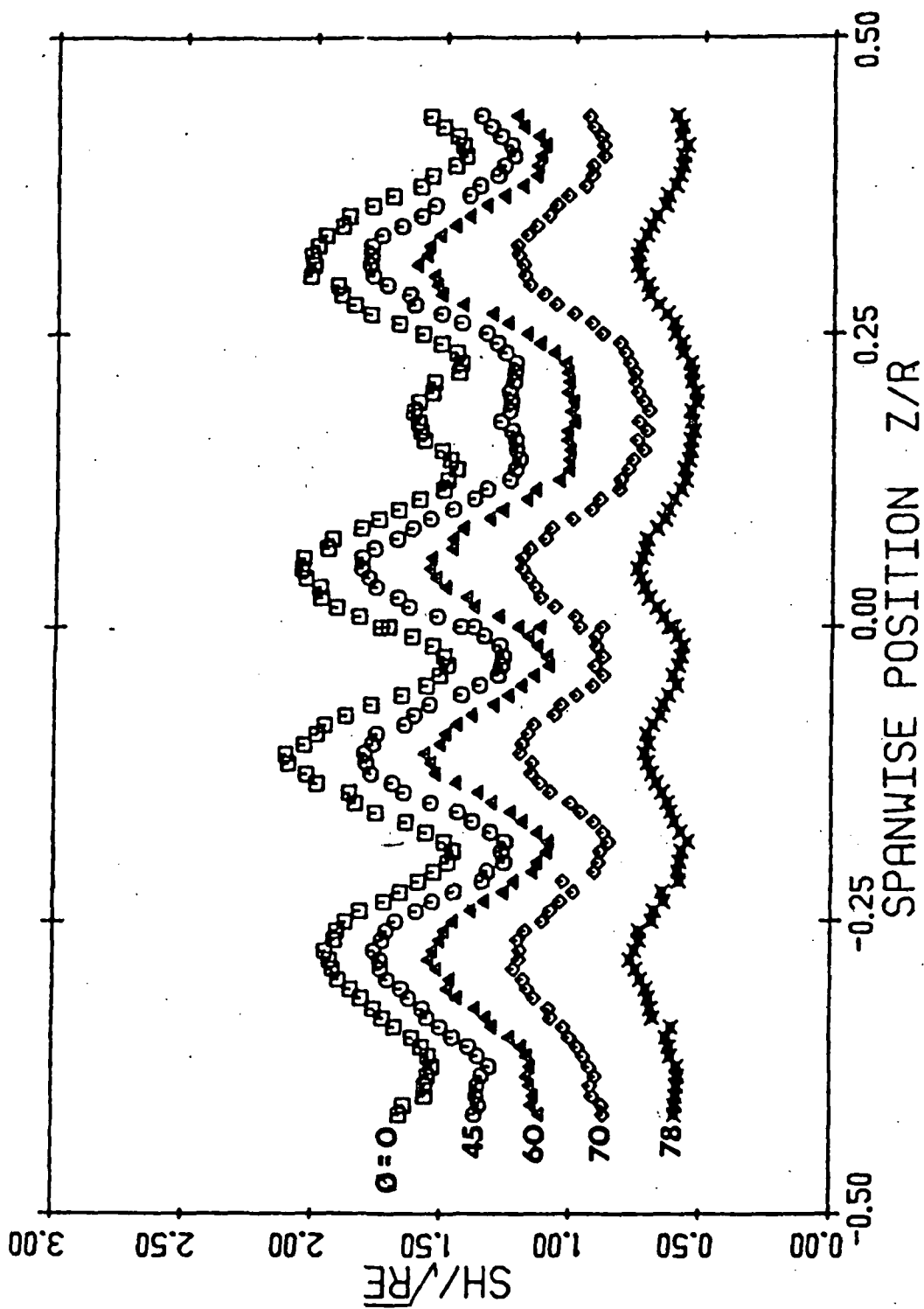


Figure 60. Spanwise mass transfer distributions behind generating grind ($M = .0625$ ", $x/R = 18.7$, $Re = 110000$)

to be visible on the 3"-mass transfer surface.

For further comparison of these mass transfer results, the spanwise averaged transfer rates at the stagnation line are plotted as a function of $Tu\sqrt{Re}$ in Fig. 61. As seen by this figure, the results for the cases which exhibited substantial spanwise variations are on the order of 20% higher than the general trend indicated by the other results. This dramatic increase and the rather remarkable three-dimensional behavior of the results obtained with a "nominally" uniform incident flow necessitated further investigation. Since the results measured behind the 16-mesh screen exhibited the most regular behavior, this screen was used in the study.

To begin the investigation, the effect of altering the position of the 16-mesh screen was examined. First, the streamwise position of the screen was changed from $\frac{x}{R} = 6.0$, to $\frac{x}{R} = 11.2$; where x is the distance upstream of the cylinder's axis, with care taken to preserve the orientation and vertical position of the screen with respect to the test cylinder. The spanwise distributions of the mass transfer rate at the leading edge are compared for the two screen positions in Fig. 62. The general curve shapes obtained from the tests are seen to be similar in nature, with the peaks of the distributions occurring at about the same spanwise positions. From this result it is evident that the vertical position of the waves is either fixed with respect to the tunnel or fixed with respect to the screen.

To ascertain the importance of the generating screen, an additional experiment was performed with the screen at $x/R = 6.0$, but shifted vertically upward $\frac{1}{4}$ ", approximately half of the observed wavelength. The spanwise variation in the mass transfer rate was observed to in turn

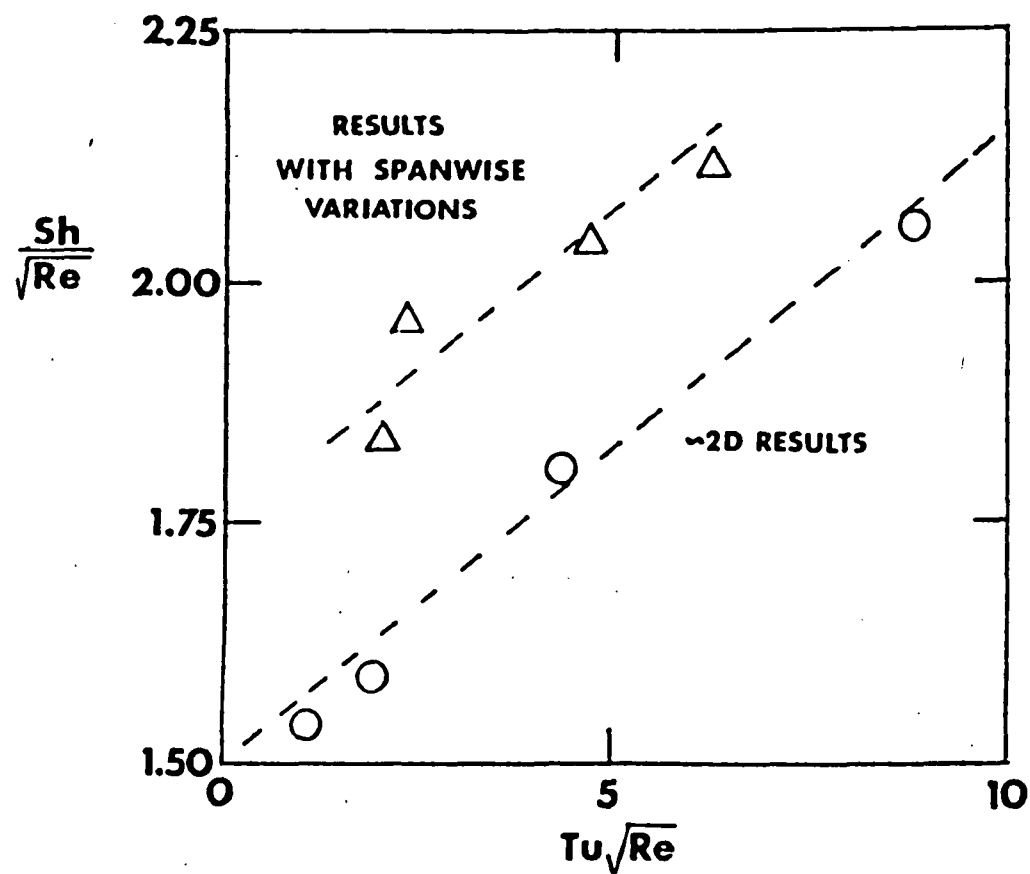


Figure 61. Comparison of average results obtained at stagnation point with and without spanwise variations

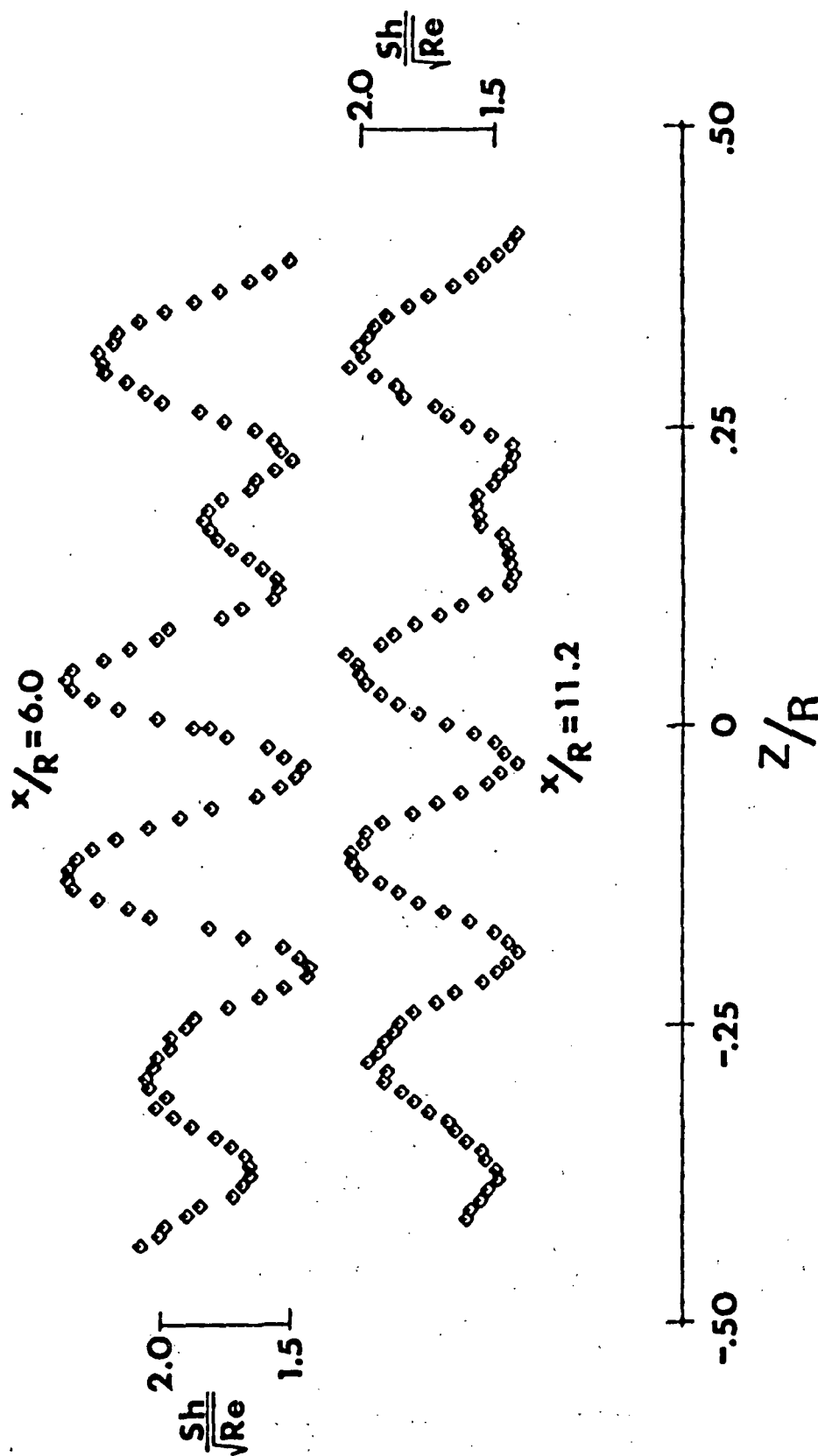


Figure 62. Spanwise mass transfer distributions at two positions downstream of 16 mesh screen ($x/R = 6.0, 11.2$)

shift upward the same distance, remaining in all other respects identical to the previous measurements. A comparison of the results at the leading edge for the two tests performed with the screen in a position $x/R = 2.5$ is given in Fig. 63, where the data is plotted as a function of position with respect to the screen

Since the phenomena being observed in the mass transfer tests exhibited a wavelength on the order of 15% of the span of the naphthalene test surface, it was also necessary to ascertain the degree to which the results were affected by the spanwise transport of mass. For this purpose, an experiment was performed with the test body fully coated with naphthalene. The results are shown in Fig. 64, where spanwise traverses taken along front stagnation line and near separation are presented. For comparison similar measurements obtained from a test without full body coating are also presented. (It should be noted that the shapes of the curves in these results differ from those previously presented. This was probably caused by physical abuse of the screen in the interval between the tests.) It is evident from the figure that only the two waves at the edges of the naphthalene strip are affected by the experimental configuration and that even in these regions the effect is small.

The mass transfer tests performed with various positions of the generating screen demonstrated that the spanwise variations in the local transfer rate were in some manner caused by the screen. Since it was known that the flow through the tunnel without generating screens was rather uniform and contained no wavelike disturbances, a full study of the flow field behind the 16-mesh turbulence generating screen was undertaken. Spanwise distributions of $\overline{u'^2}$, $\overline{w'^2}$, $\overline{u'w'}$ and U were measured at

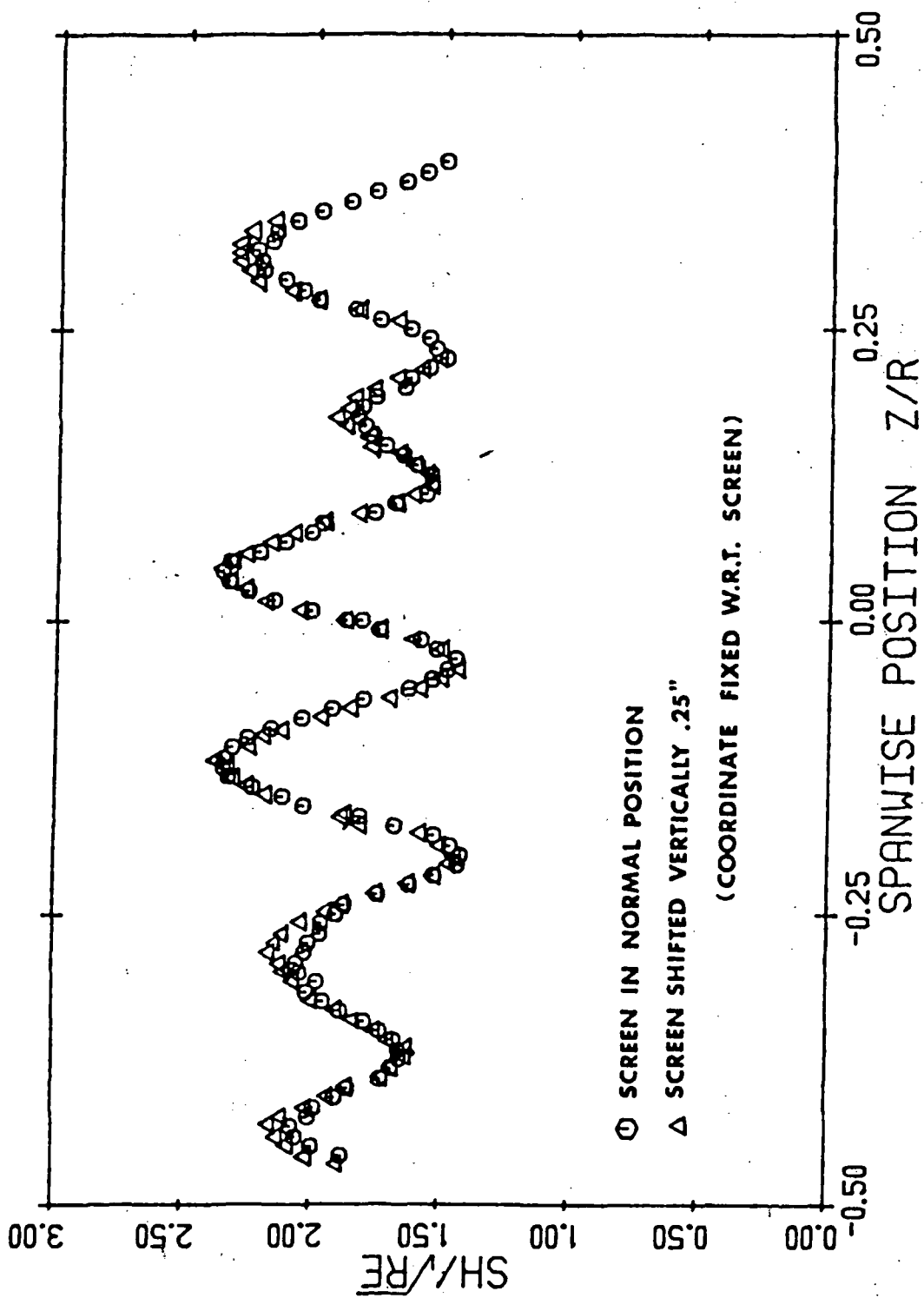


Figure 63. Spanwise mass transfer distributions with two positions of 16 mesh screen ($x/R = 6.0$)

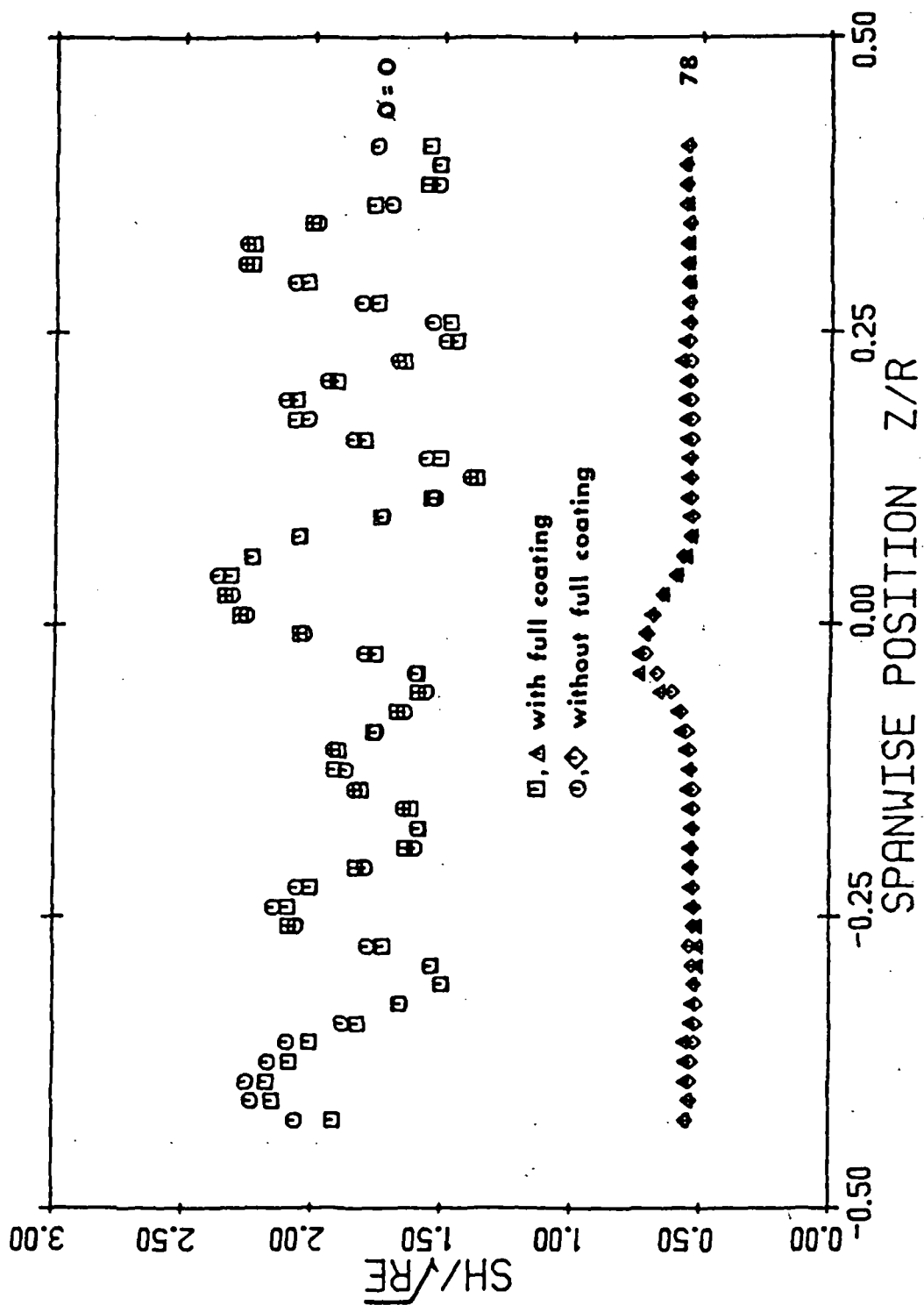


Figure 64. Comparison with results obtained with test cylinder fully coated with naphthalene ($x/R = 11.2$)

various locations upstream of the test cylinder in the stagnation plane. The profiles were measured both with and without the cylinder installed in the tunnel. For the purpose of comparison, the spanwise range corresponding to the location of the mass transfer surface was covered.

The results of the flow traverses with the cylinder removed from the tunnel are presented in Figs. 65 through 70. In Fig. 65, the spanwise distributions of the mean velocity at various distances downstream of the screen are presented. The velocity is shown as a percent variation about the spanwise averaged velocity, \bar{U} . The spanwise distance, z , is measured from a horizontal line which corresponds to the center of the mass transfer surface when the test cylinder is installed. The streamwise distance downstream of the screen, X , is given in mesh lengths. For later comparison, the spanwise distance is given in terms of the cylinder's radius, R ; as is the distance upstream of the cylinder's axis position, x . Also shown in this figure is the spanwise variation of the screen's mesh size, M , the vertical distance between individual wires. This was measured with a set of machinist's wire gauges of various diameters. From these measurements a periodic pattern can be identified. As shown in Fig. 65, this pattern induces a small magnitude wavelike disturbance in the mean velocity which persists for large distances downstream of the screen.

The decay in the amplitude of the mean velocity variations is shown in Fig. 66, where the average spanwise value of the half peak-to-peak amplitude is plotted as a function of distance downstream of the screen. According to Townsend [42], the amplitude of a periodic disturbance in mean velocity should decay as

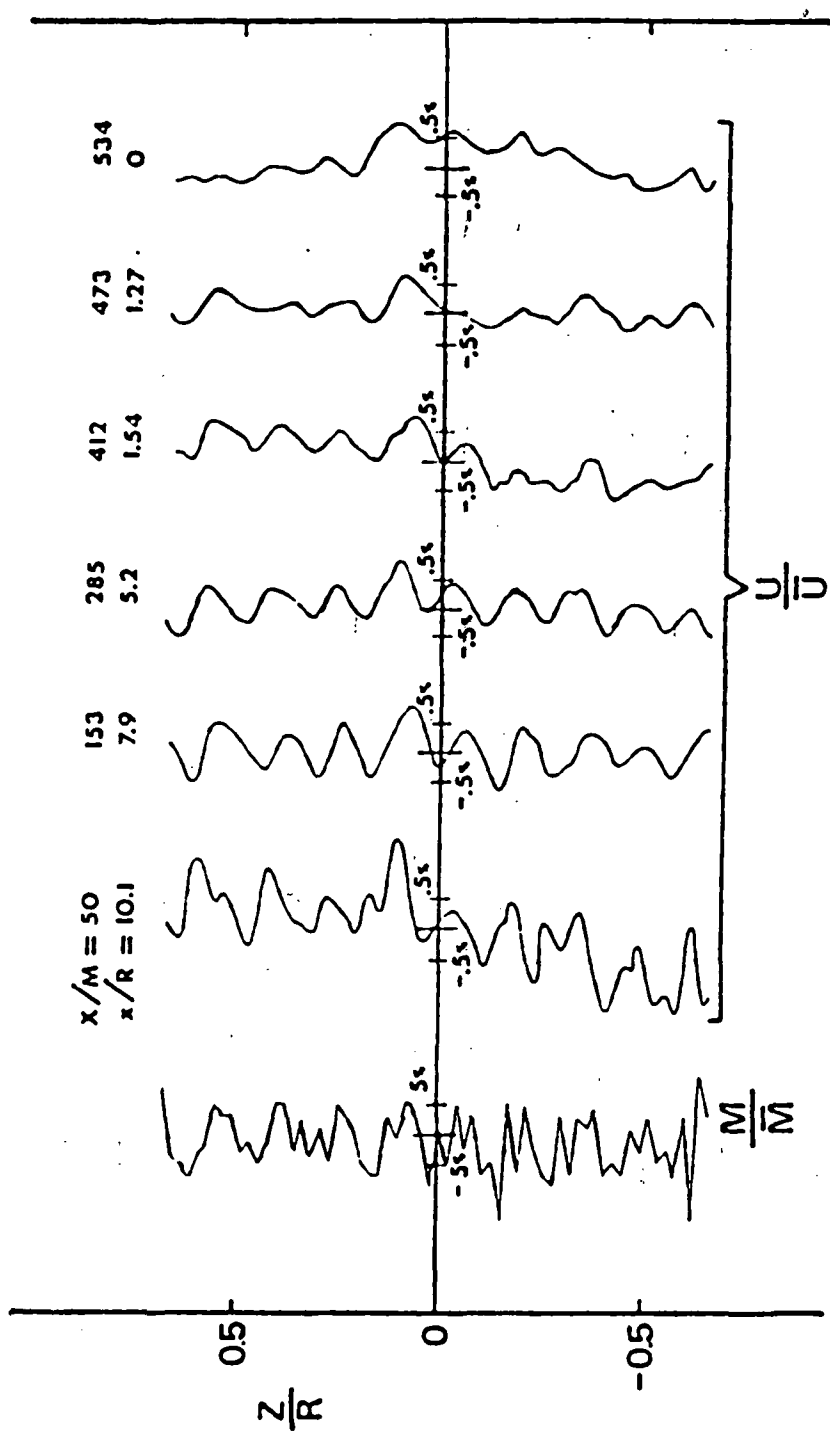


Figure 65. Spanwise distributions of mean velocity without test cylinder

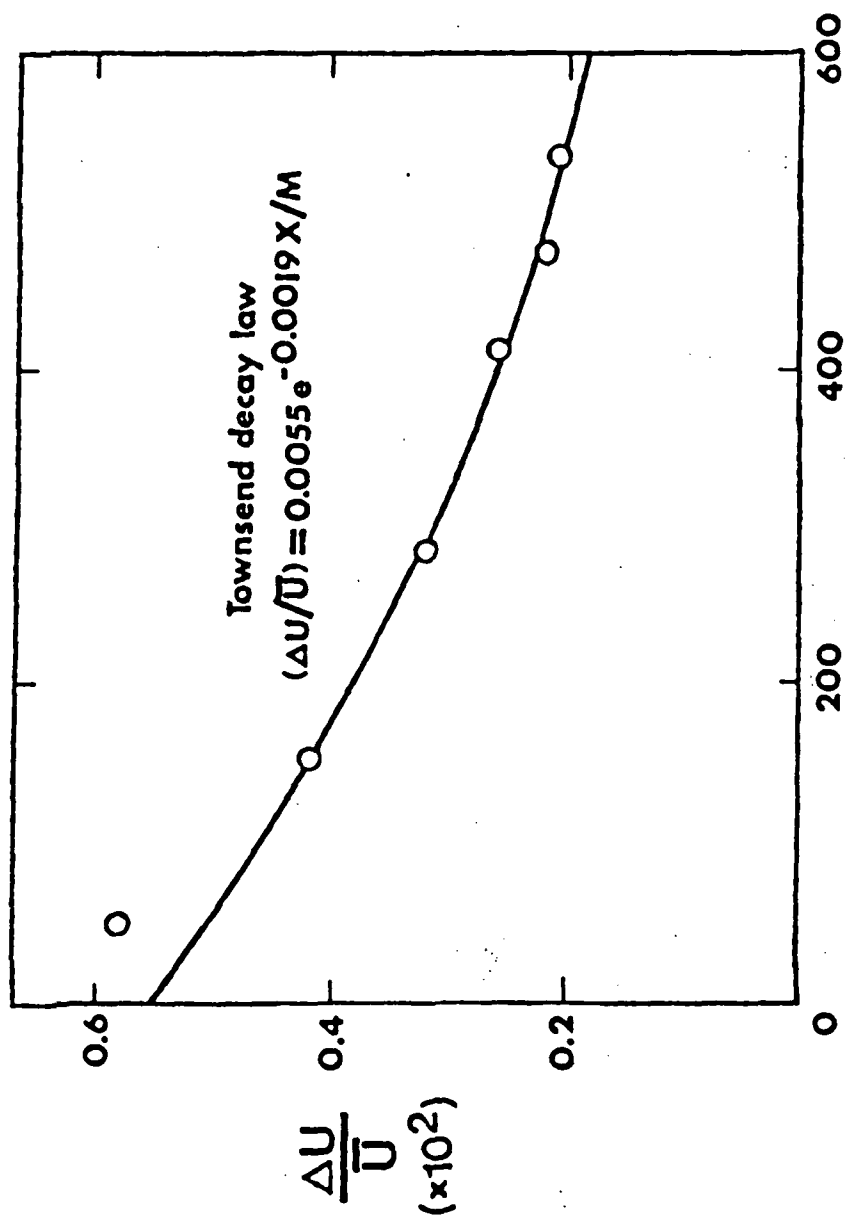


Figure 66. Streamwise distribution of the average perturbation in mean velocity without test cylinder

$$\frac{\Delta U}{U} \propto \exp \left[\frac{-v_T}{\nu} \left(\frac{2\pi M}{\lambda} \right)^2 \left(\frac{\nu}{UM} \right) \frac{X}{M} \right]$$

where λ is the wavelength of the disturbance and v_T is the eddy viscosity. For the present experiments $\frac{UM}{\nu} = 1146$ and $\lambda/M = 7.3$. This decay law is also shown in Fig. 66, where the constant of proportionality and a value of v_T/ν have been chosen to provide a best fit to the data. The latter value was $v_T/\nu = 2.94$, a surprisingly small ratio when compared to the values of about 150 quoted by Townsend for flow behind parallel rods. Kellogg and Corsin [43], however, found a value of $v_T/\nu = 3.5$ for a situation similar to that in the present experiments. Estimates of the eddy viscosity, v_T , made from the measured mean velocity and turbulent shear stress (\overline{uw}) also provided a ratio of v_T/ν between 2 and 3.

The spanwise variations of the turbulence quantities without the cylinder are shown in Figs. 67 through 69. The periodic behavior is obvious in all, particularly the $\overline{u'w'}$ distribution, and all have the same wavelength. A careful comparison between Figs. 65 and 69 will show a 90° phase shift between the $\overline{u'w'}$ and mean velocity distributions as one might expect.

The streamwise decay of the turbulence quantities is provided in Fig. 70. Spanwise averaged values of the relative intensities, $\overline{u'^2}$ and $\overline{w'^2}$, are presented along with the average peak amplitude of $\overline{u'w'}$, the spanwise average of which is virtually zero. The decay in the streamwise component of turbulence behind the screen could be fitted by the decay law

$$\frac{\overline{u'^2}}{\overline{u'^2}_0} \propto (X + X_0)/M$$

where a value of $X_0 = 113 M$ gave the best fit. When the cylinder was

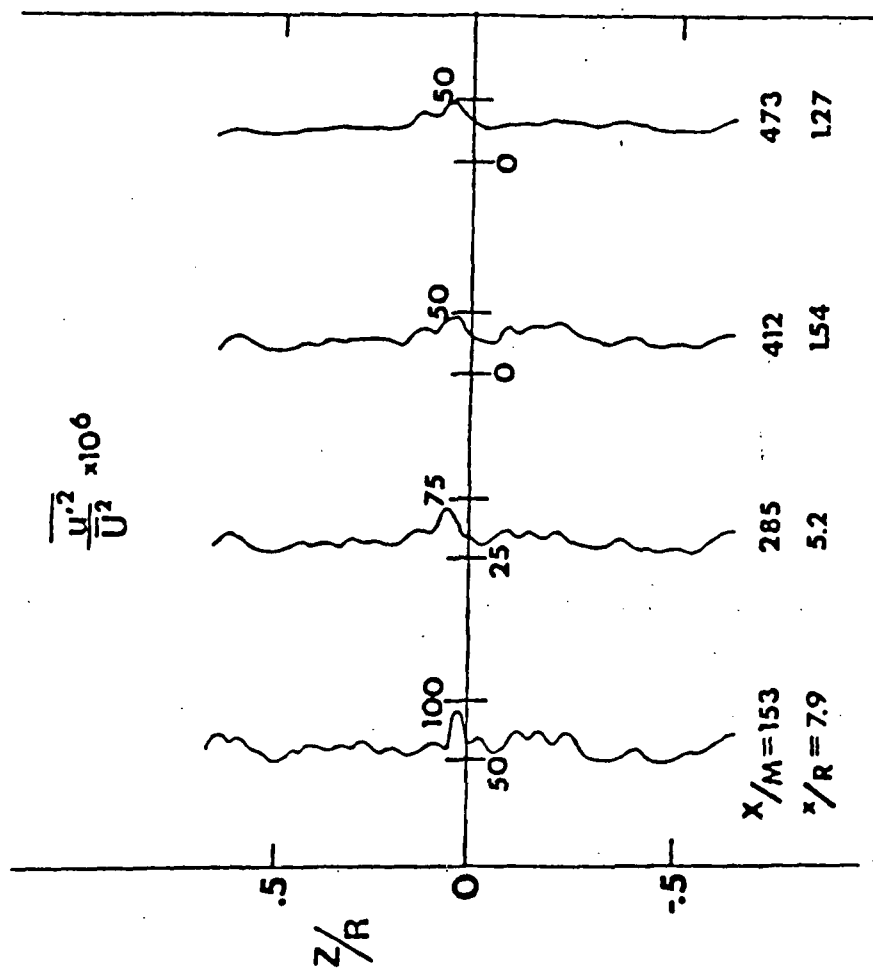


Figure 67. Spanwise distributions of $\frac{u'^2}{U^2}$ without test cylinder

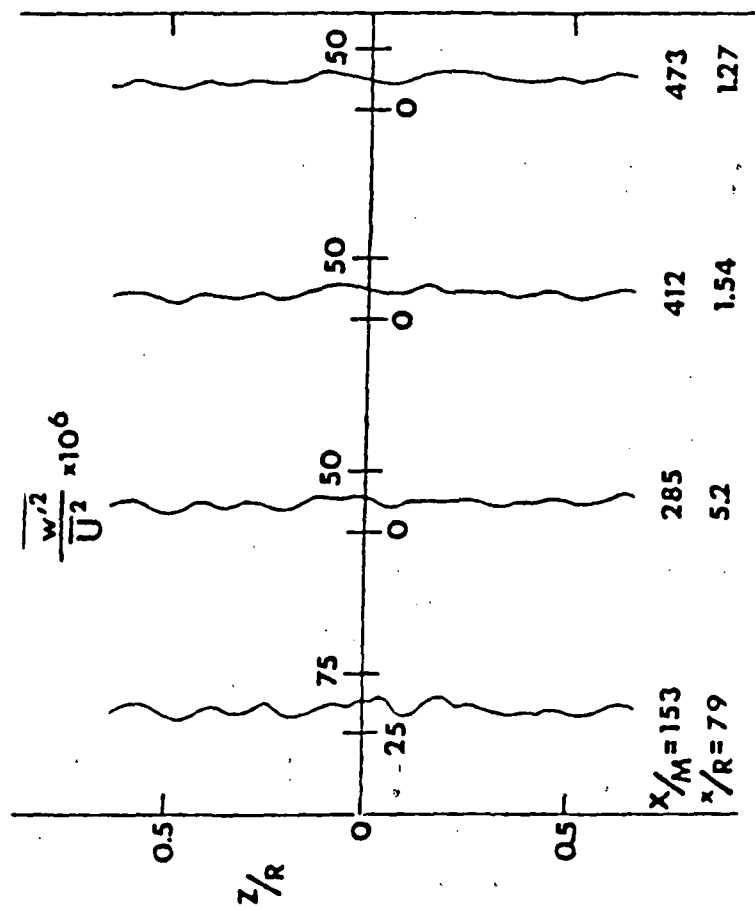


Figure 68. Spanwise distribution of w'^2 without test cylinder

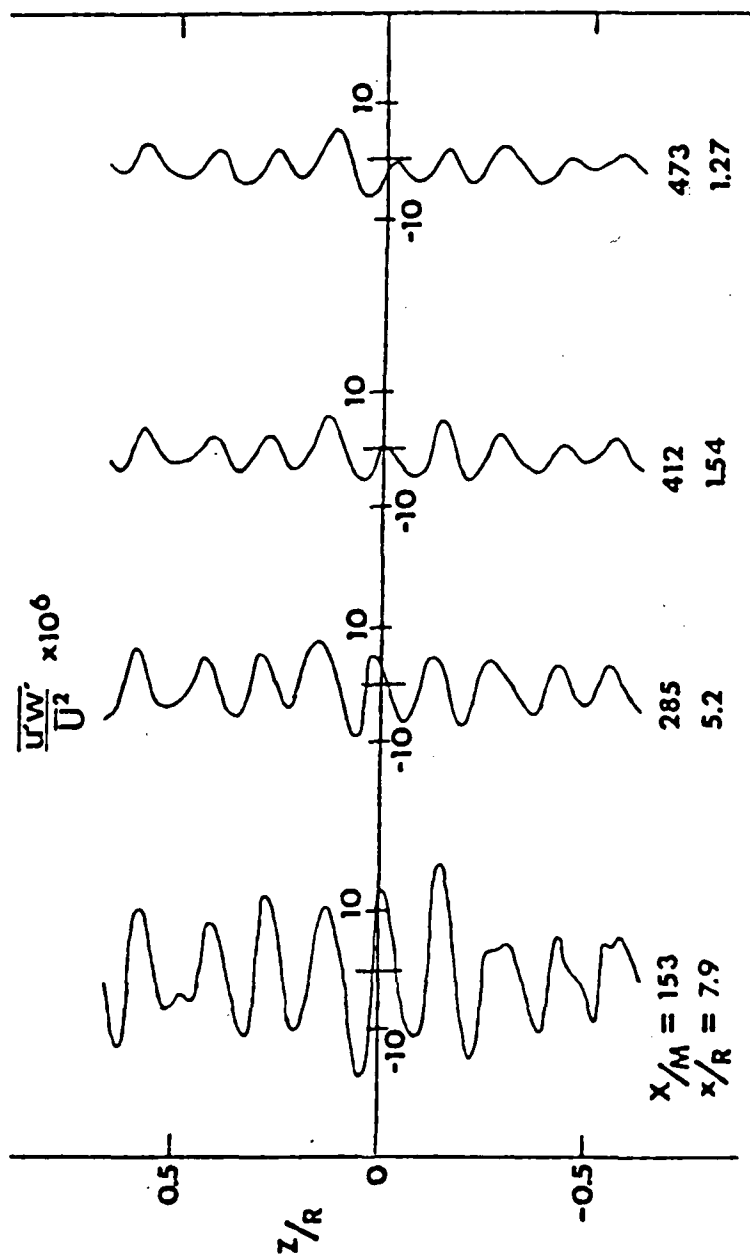


Figure 69. Spanwise distributions of $\overline{u'w'}$ without test cylinder

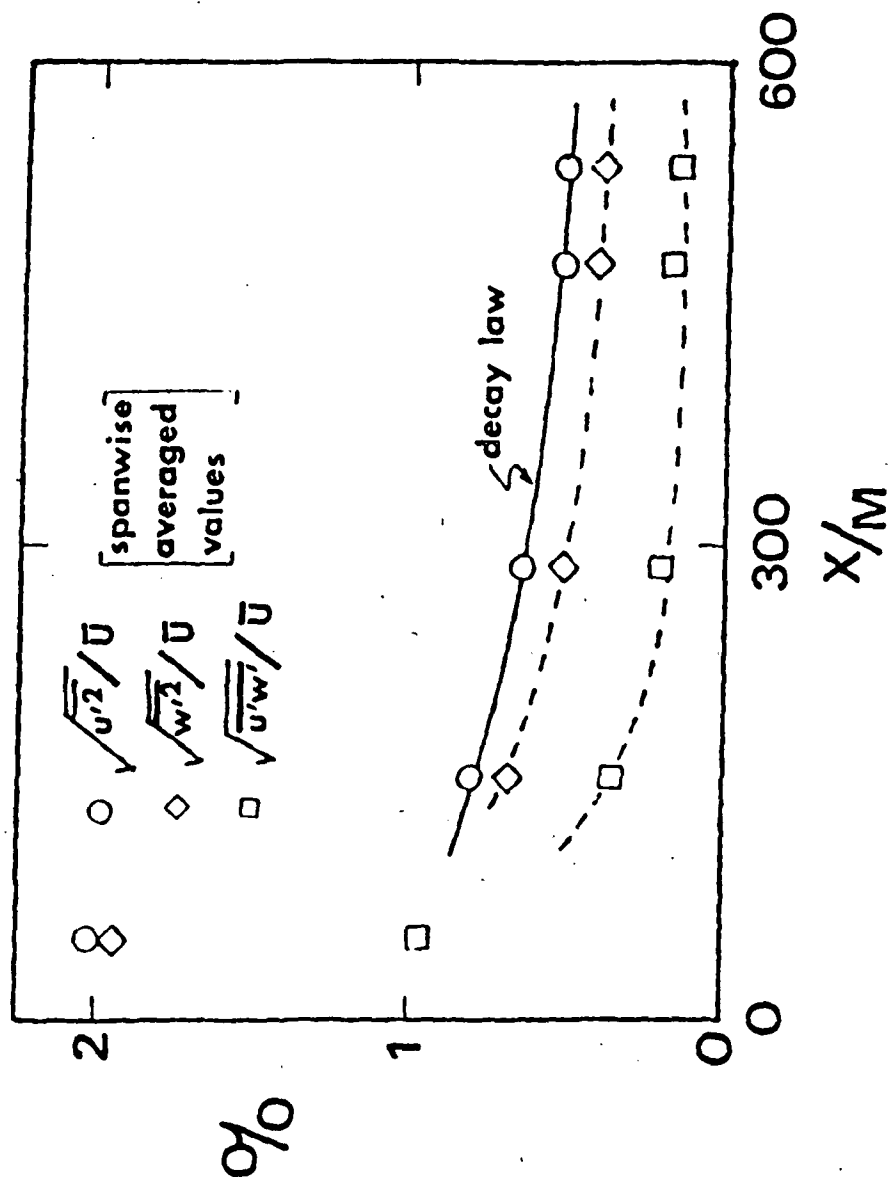


Figure 70. Streamwise distribution of average turbulence quantities without test cylinder

installed for measurements its leading edge position was $x/M = 488$.

Although this is a large distance in terms of mesh size, it is almost an order of magnitude smaller in terms of the wavelength of the screen's pattern, viz. $x/\lambda = 69$. Interestingly, a comparison of the amplitude of the spanwise variation in the mean velocity to the turbulence level at this position, 0.2 and 0.5%, respectively, shows that the mean velocity disturbance is "buried" in turbulence. In fact, in the initial profile measurements obtained without traversing continuously, the mean velocity was found to be "nominally" uniform. This has important implications with respect to stagnating flows as will be seen shortly.

The results of the incident flow traverses with the cylinder in place are shown in Figs. 71 through 76. The spanwise distributions of mean velocity are presented in Fig. 71. In this figure, the velocity is shown as a percent variation about the local mean velocity, which was found to vary in the manner predicted by potential flow. Comparing the distributions to those taken without the cylinder in place, Fig. 65, make the effect of the cylinder quite evident. At the position nearest the cylinder, a threefold increase in the relative amplitude is found, with correspondingly smaller increases further from the cylinder. The closest position, $x/R = 1.28$, is about 35 boundary layer thicknesses away.

The result is more graphic in Fig. 72 where the amplitudes of the mean velocity variation with the cylinder in place are plotted. Here the coordinate system associated with the cylinder is used. According to Sadeh et al. [22] the amplitude of a periodic disturbance in the velocity incident to a circular cylinder should vary as

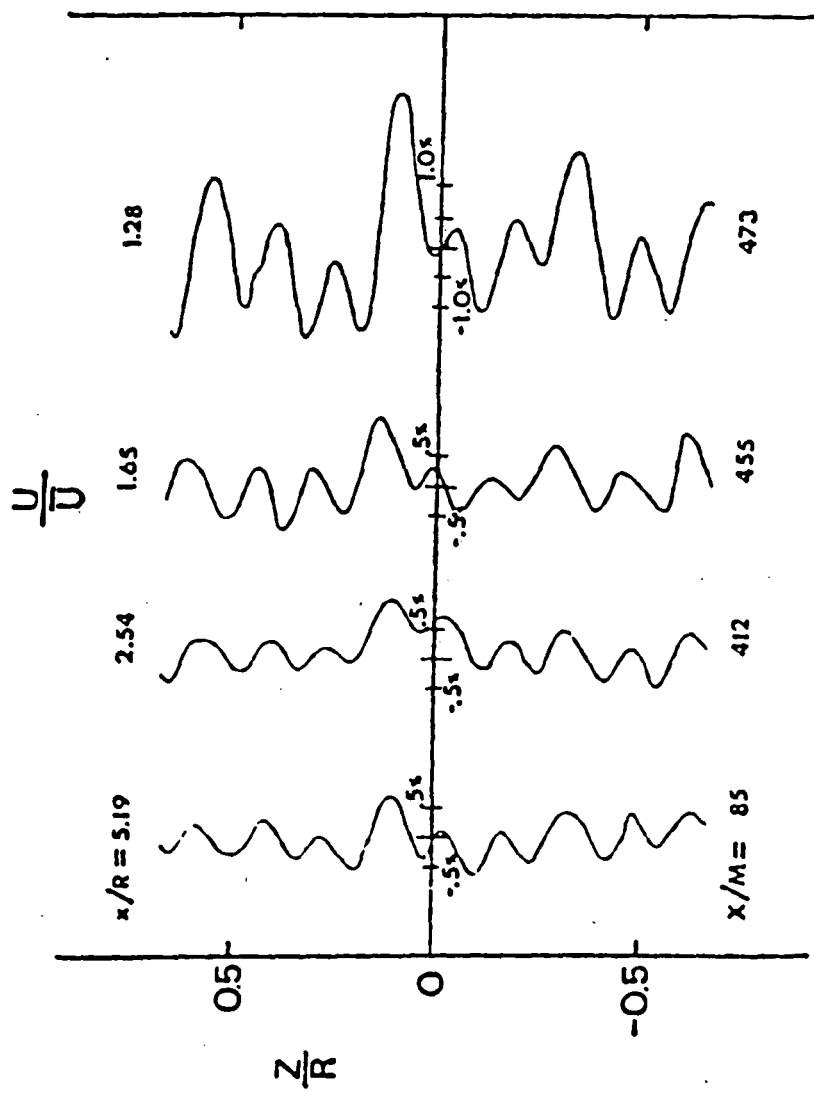


Figure 71. Spanwise distributions of mean velocity ahead of test cylinder

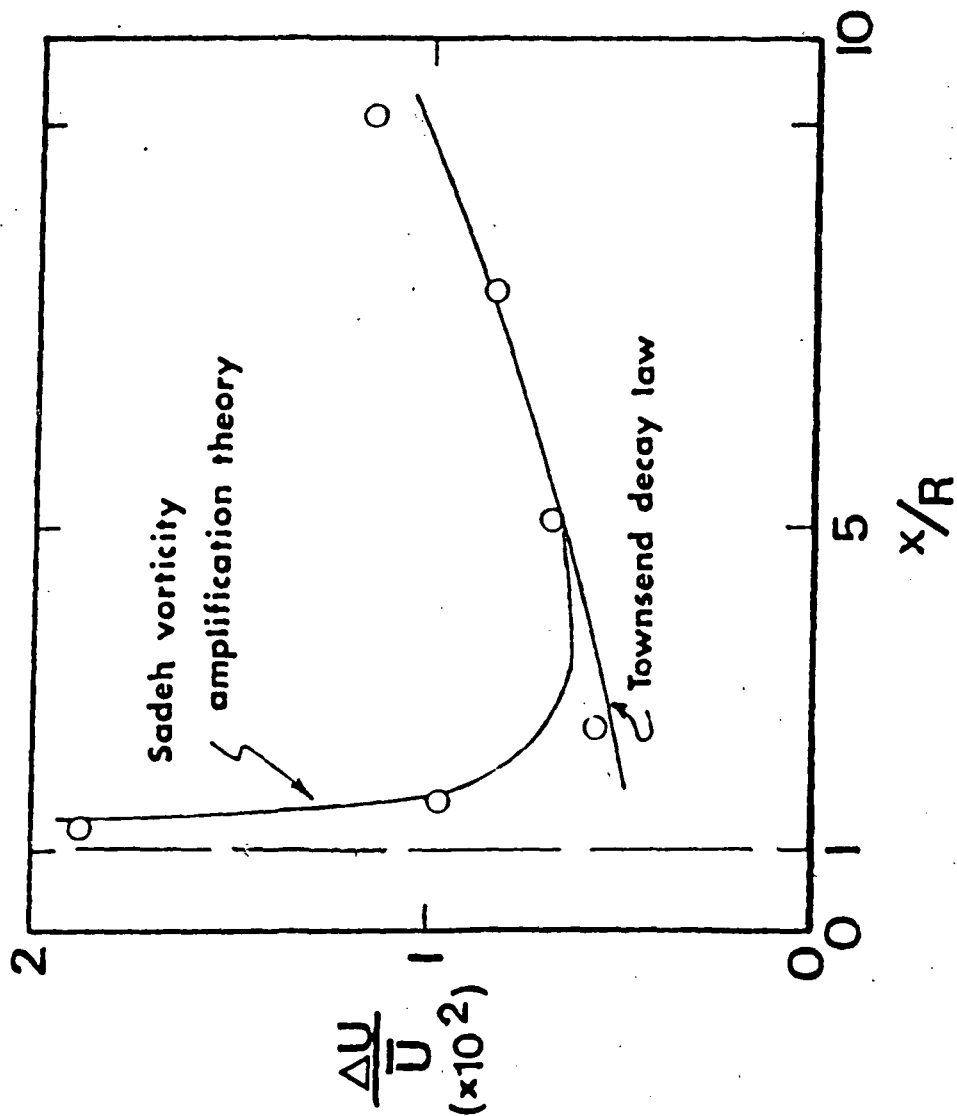


Figure 72. Streamwise distribution of the average perturbation in mean velocity ahead of test cylinder.

$$\frac{U}{\bar{U}} \propto \left[\frac{x^2}{x^2 - R^2} \right]^2 \left(\frac{x - R}{x + R} \right)^{\frac{1}{2}} \left(\frac{2\pi}{\lambda} \right)^2 \frac{v_T R}{U_\infty} \exp \left[\left(\frac{2\pi}{\lambda} \right)^2 \frac{v_T x}{U_\infty} \right]$$

This expression was evaluated using the values for v_T/ν and the constant of proportionality determined from the previous fit to the Townsend decay law, since for large x/R the relationship decays into the Townsend curve, and is plotted in the figure. Neither changing the kinematic viscosity nor the constant of proportionality provided a good fit over the entire range, indicating that as the cylinder is approached the structure of turbulence changes and cannot be modeled using the concept of an eddy viscosity. If only the behavior near the cylinder is of interest, the expression can fit to the data - but so can the expression one obtains from Bernoulli's equation, viz. $\Delta U \propto 1/U$.

The spanwise distributions of the turbulence quantities ahead of the cylinder are presented in Figs. 73 through 75. The wavelike disturbances in these quantities are also seen to be amplified as the cylinder is approached. The streamwise variations are given in Fig. 76 where spanwise averaged values of $\overline{u'^2}$, $\overline{w'^2}$ and the average peak amplitude of $\overline{u'w'}$ are plotted. The increase in the relative turbulent intensities as the cylinder is approached is apparent. This behavior was also obtained by Sadeh, Suter and Maeder [22] who showed that the intensities continue to increase up to the boundary layer substantially modifying the "free stream" flow conditions there.

To establish an accurate comparison between the mass transfer variations and the disturbances in the flow quantities, an additional mass transfer test was performed. The results of this test are shown in

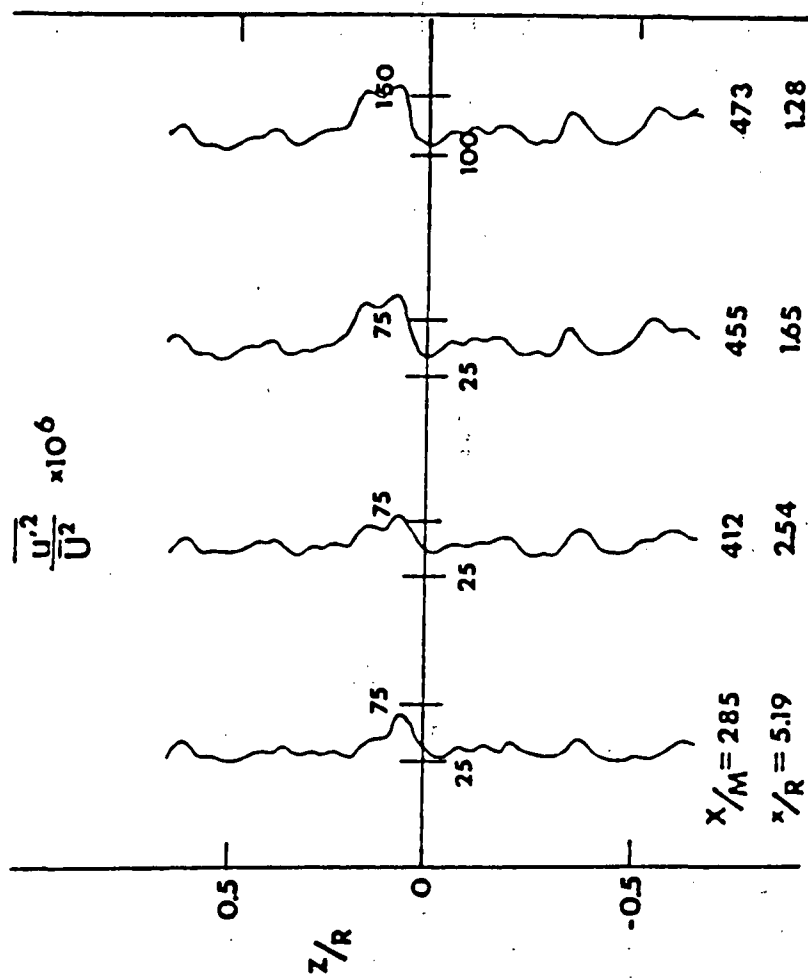


Figure 73. Spanwise distributions of $\frac{u'^2}{U^2}$ ahead of test cylinder

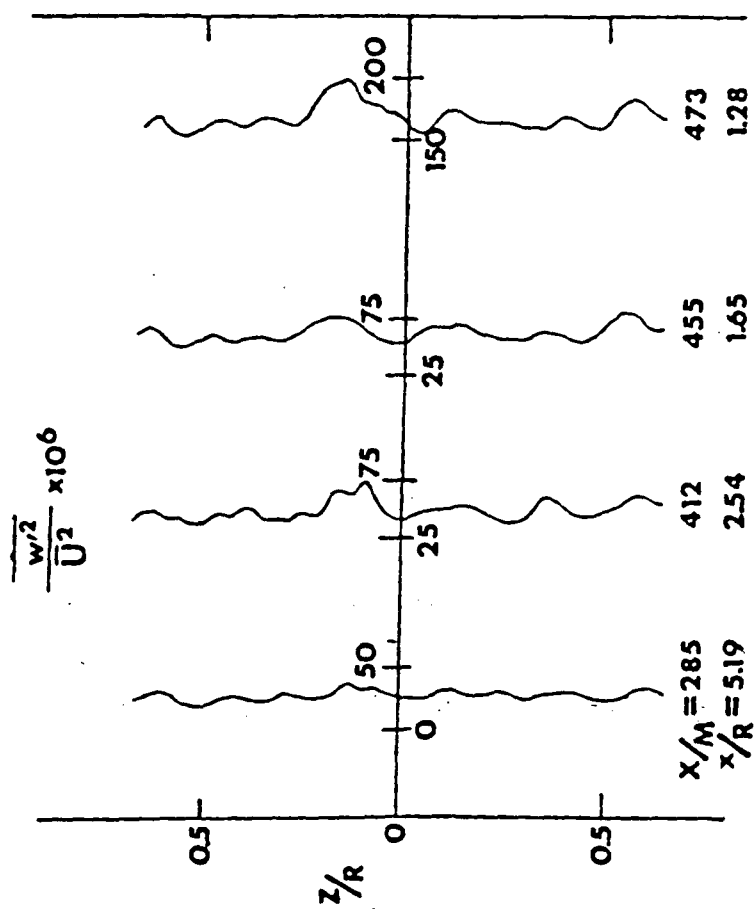


Figure 74. Spanwise distributions of w'^2 ahead of test cylinder

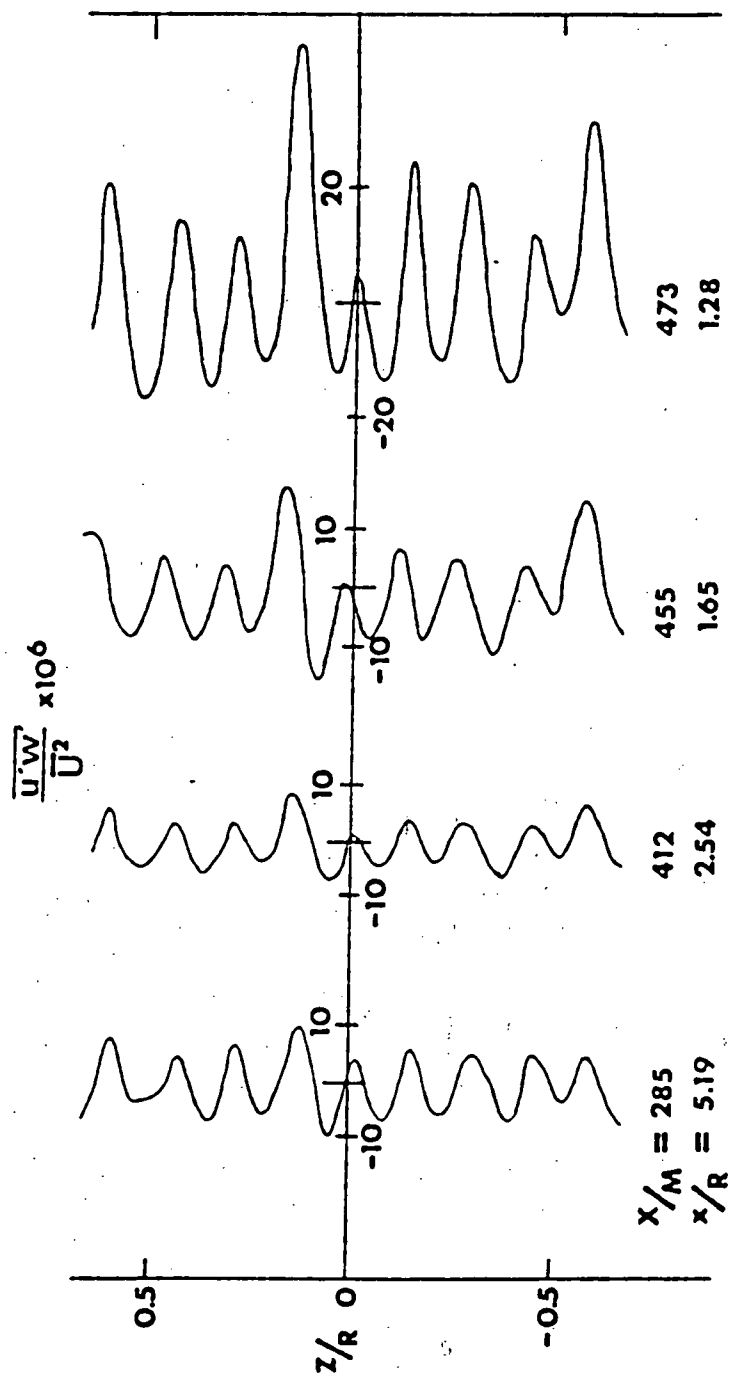


Figure 75. Spanwise distributions of $\overline{u'w'}$ ahead of test cylinder

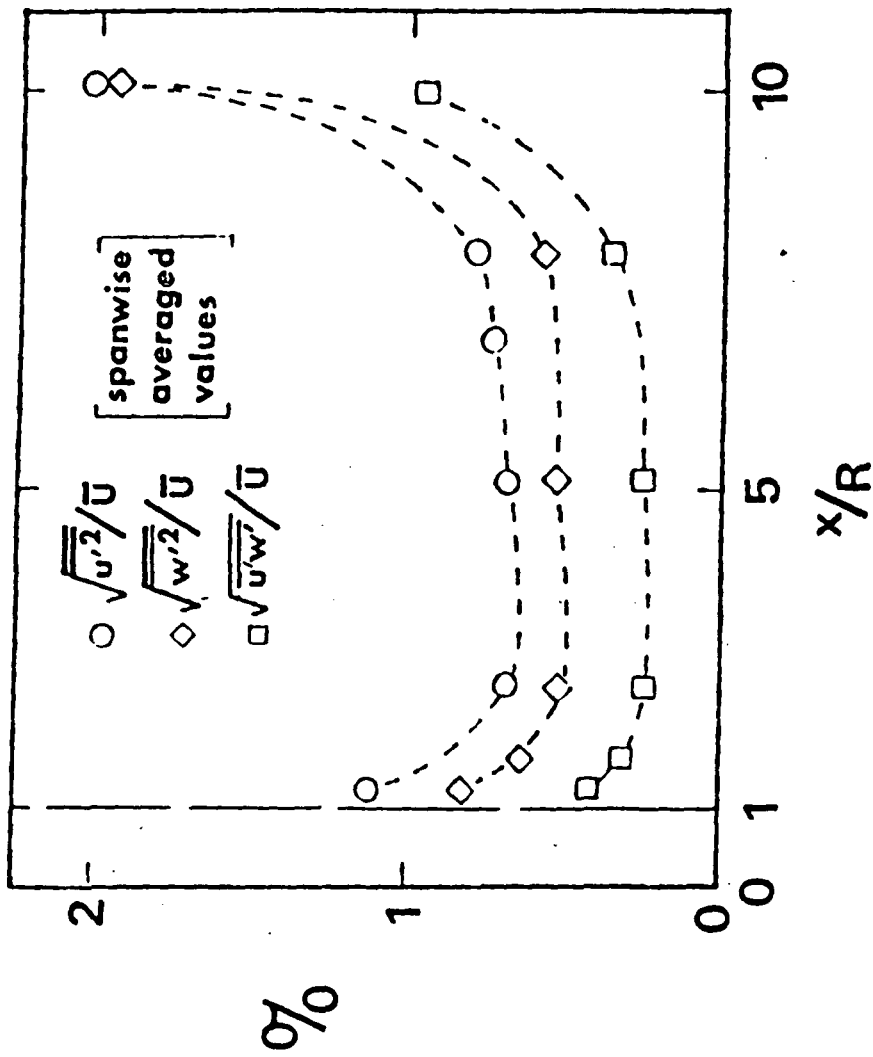


Figure 76. Streamwise distribution of averaged turbulence quantities ahead of test cylinder

Fig. 77, where the spanwise distribution of the local mass transfer rate is given at a number of degree positions. It should be noted that the wave shapes of this test are substantially different than those measured behind the 16-mesh screen in the initial phases of the investigation. This was felt to be due to disturbance of the screen's mesh pattern by various attempts to measure the mesh size distribution. As in the previous measurements a regular wavelike pattern was obtained. This periodic nature of the results is unmistakable even up to separation, which occurs at $\phi = 79^\circ$. Perhaps the most surprising result of this investigation is, however, the disproportionately large magnitude of the mass transfer variations, which are on the order of 15% generated by a 0.2 - 0.4% variation in the incident mean velocity.

Correlation of the results is made in Fig. 78 where the spanwise distributions of the Sherwood number at the leading edge, the mean velocity variation at $x/R = 1.28$, and the distribution of the mesh size have been assembled. Not only is it seen that the patterns are similar, but one finds that the position of a high mass transfer rate corresponds to that of a high mean velocity - while that for a low rate corresponds to that for a low velocity. This observation is in qualitative agreement with the vorticity amplification models presented by Suter et al. [20, 21] where the spanwise variation in the total pressure of the incident flow causes a periodic vortical motion around the cylinder. Under these circumstances, fluid moves toward the surface of the cylinder in regions of high velocity, increasing the transfer rate there, and away from the surface in low velocity regions decreasing the transfer rate there.

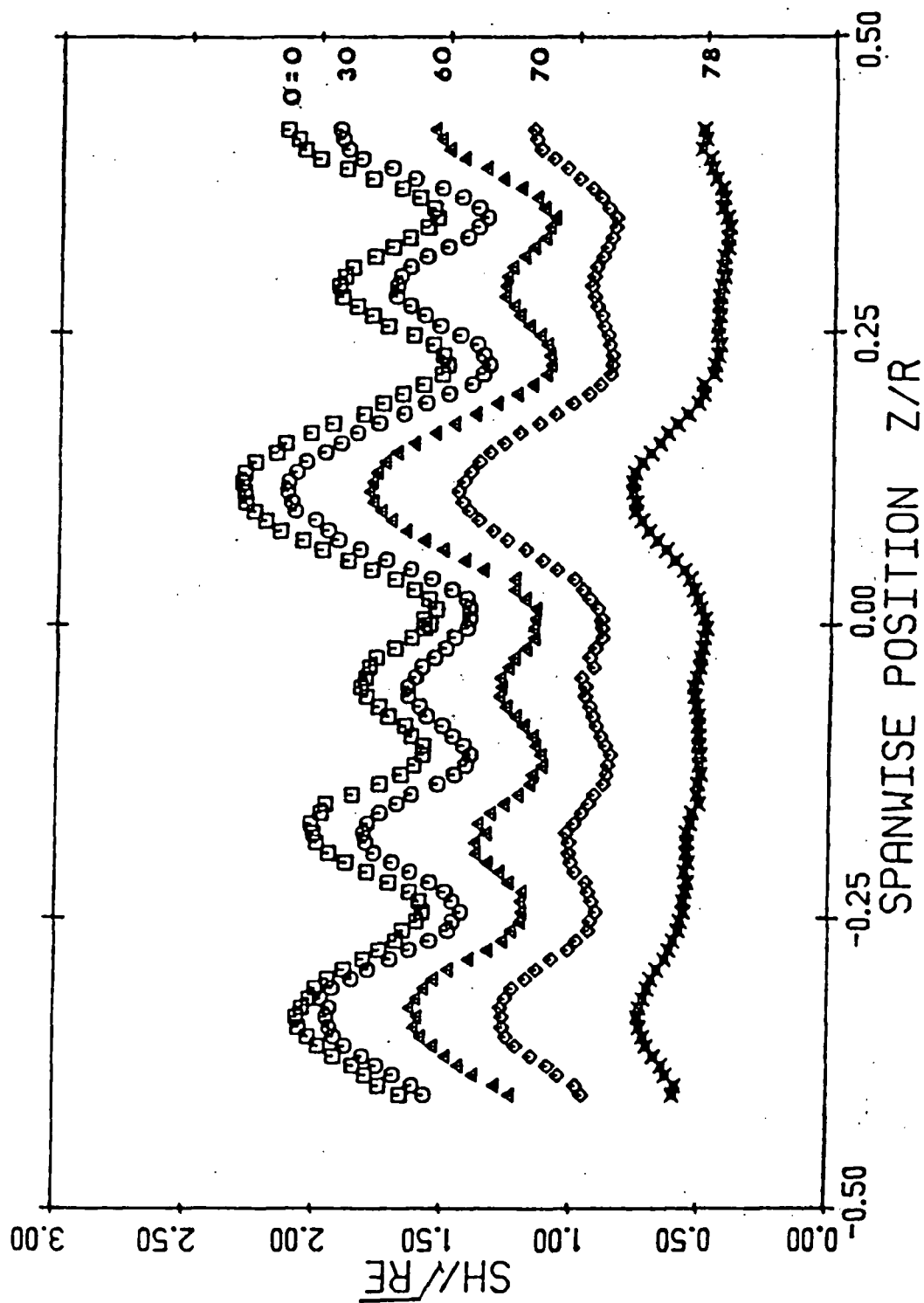


Figure 77. Spanwise distributions of mass transfer behind 16M screen ($x/R = 11.2$)

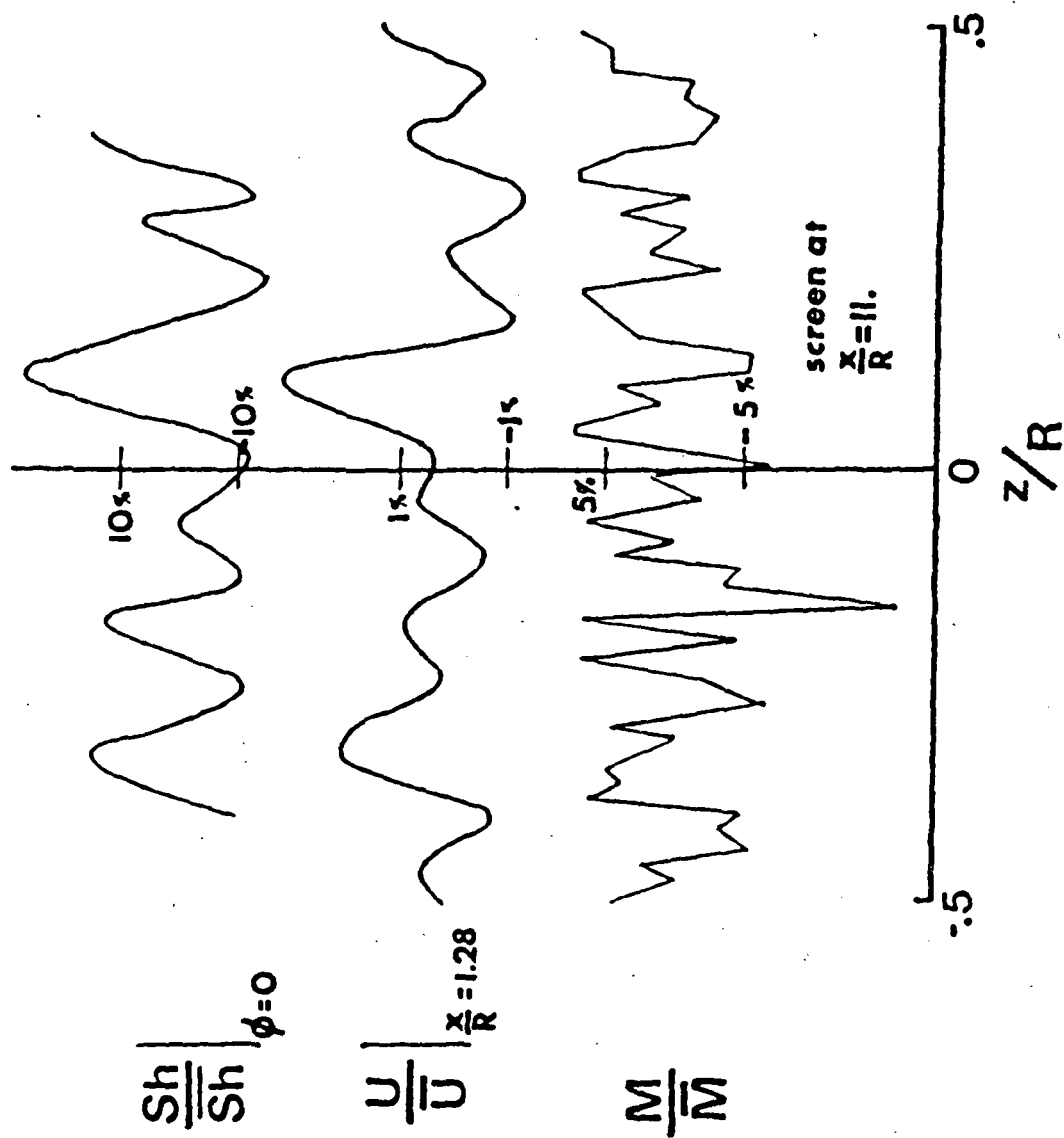


Figure 78. Correlation of results

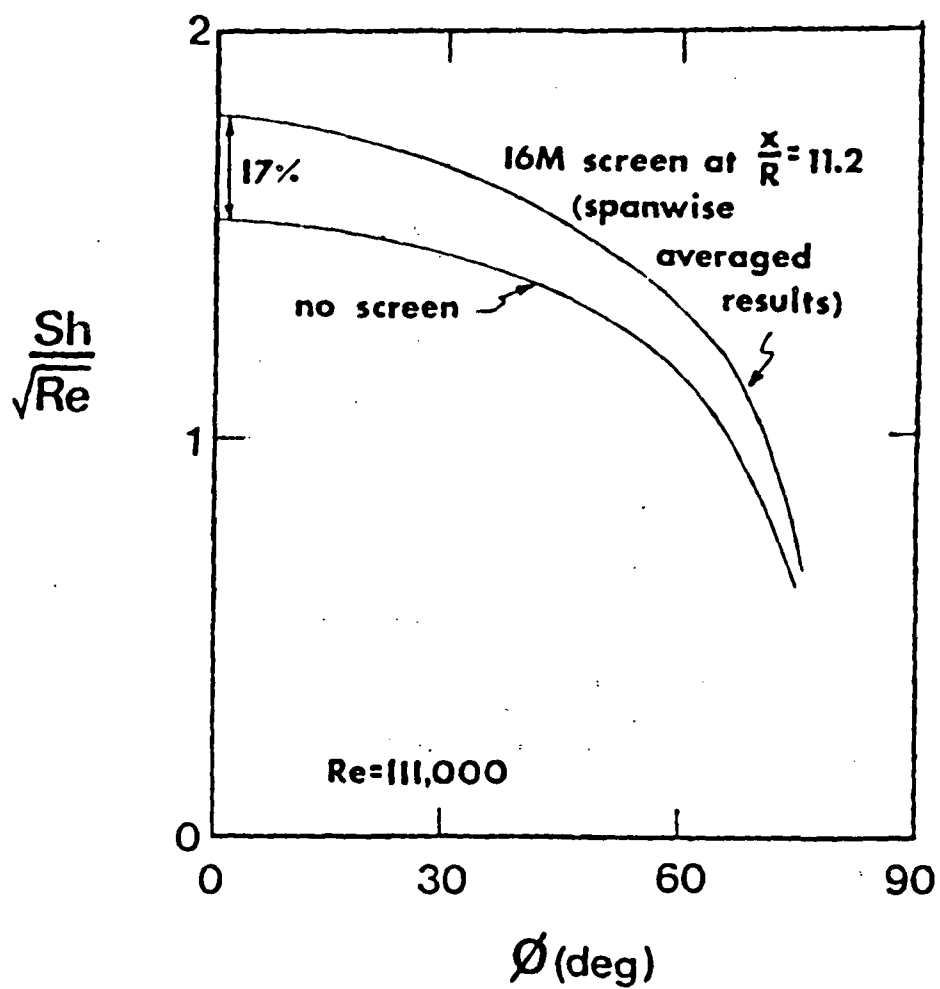


Figure 79. Effect of 16M screen on spanwise average mass transfer

The overall effect of the screen on the mass transfer rate is shown in Fig. 79, where the circumferential distributions in the Sherwood number with and without the screen are presented. That with the screen corresponds to spanwise averaged results, while that without is a best fit curve to the no-screen data presented elsewhere in this report. The effects of the screen are seen to increase the mass transfer rate over the whole leading edge surface. At stagnation the mass transfer rate is augmented by 17%. At this time it is difficult to ascertain how much of this increase is due to the variations in mean velocity and how much is attributable to the effects of turbulence. By comparing the present results through the heat-mass transfer analogy to those obtained from heat transfer experiments, it appears that the division is about equal.

PART 6

CONCLUSIONS

6.1 Steady-State Experiments

a) The mass transfer technique developed as a part of the reported research effort was found to yield results which were repeatable to within $\pm 2\%$. Although precise values for the diffusion coefficient and vapor pressure relation are not currently available, those given by Sogin [33] were found to provide results which compared well with the heat and mass transfer measurements of previous investigators and with a theoretical calculation.

b) Before an accurate empirical correlation between the turbulence characteristics of the incident flow and the stagnation region transfer rate can be established, a drastic improvement must be made in the methods used to measure and report turbulence. Current techniques for the measurement of turbulence levels and scales involve inherent uncertainties on the order of $\pm 20\%$. Reported measurements typically lack information concerning the decay length of the turbulence and the signal conditioning used in the measurements. Also, there seems to be no existing convention for reporting turbulence quantities, with definitions of the "incident" characteristics varying widely among experimental investigators. In some cases, the measurements are taken without the cylinder in place, using positions which correspond to either its leading edge or its axis, while in others the measurements are made ahead of the installed cylinder. A comparison of measured transfer rates is difficult under such circumstances. Future transfer rate measurements should be accompanied by

a complete description of the incident turbulent field. Values of the turbulence level and integral length scale at the leading edge position of the test body should be reported along with their respective rate of decay or growth.

6.2 Oscillation Experiments

a) For the range of significant parameters considered in the experiments, the effect of rotational oscillation of the test cylinder on the distribution of the local transfer rate over the leading edge region is small. The largest observed effect was a 10% augmentation of the transfer rate at stagnation. Since the range of parameters used was chosen to model an actual turbine situation, the results suggest that the heat load in the leading edge region of a turbine blade is not significantly affected by the variation in the angle of attack of the incident flow generated by airfoil wakes. The implication of the measurements is that, for the Strouhal number range of interest, the residence time during which a fluid particle passes over the surface is small with respect to the period of the unsteadiness in the incident flow. This would further suggest that not only are the effects of variation of the incident angle of the flow small, but also the effects of variation of the flow magnitude since the Strouhal number is identical. Hence, the uncertainty in leading edge heat load predictions due to the unsteady effects of airfoil is only on the order of 10%. Increases as large as 40% can be attributed to turbulence in the incident flow. The remainder of the 70% uncertainty in the predictions may be attributable to three-dimensional effects generated by small nonuniformities in the incident flow of the type observed in the current research.

b) The magnitude of the oscillation effects is intimately connected to the level and scale of the incident turbulence. For the range of St and Re used in the investigation and for turbulence scales on the order of $L/D \approx .02$, the effect seems to increase with turbulence level. For turbulence levels below 1.5% no effect was observed while increasing the turbulence level to 1.8% and 2.6% gave increases at stagnation of 3% and 7%, respectively. However, a larger length scale of $L/D = .18$, gave no effect even though the turbulence level was higher, $Tu = 4.9\%$, indicating the importance of the scale to the observed results. Interestingly, the length scale at which significant effects are evident is about eight boundary layer thicknesses and of the order of the value of $L/\delta \approx 10$ which produces the maximum transfer rate for a steady flow according to Yardi and Sukhatme.

c) At the incident turbulence conditions which demonstrate a significant effect of oscillation, $Tu = 2.65\%$, $L/D = .03$, the magnitude of the augmentation initially increases with Strouhal number reaching a maximum at $St \approx 0.056$ after which the effect decreases. This would suggest that some type of interaction between the turbulent eddies and the oscillation velocities occurs for a narrow range of the ratio of the characteristic incident turnover frequency of a turbulent eddy to the frequency of oscillation, i.e.

$$\left(\frac{Tu U_{\infty}}{L_T} \right) / \left(\frac{St U_{\infty}}{D} \right) = R_T$$

The maximum effect occurs at $R_T \approx 16$. This parameter is, however, significant only when the scale of turbulence is of the proper magnitude, $L/D \approx .03$.

Since the scale of a turbulent eddy changes as the stagnation point is approached, this may be the incident eddy size which generates eddies at stagnation of a scale on the order of the boundary layer thickness.

6.3 Investigation into the Observed Spanwise Variation of Mass Transfer

a) Small irregularities in a screen produced long-lived spanwise perturbations in the mean velocity which were "buried" in the turbulence generated by the screen itself. Although the amplitude of these perturbations could be correlated using Townsend's decay law, it implied that the apparent kinematic eddy viscosity was of the order of the molecular viscosity.

b) With the cylinder in place, the mean-velocity perturbations amplified as one approached stagnation. Within this region, about one diameter from the cylinder, the turbulence quantities were also amplified similar to that previously shown by Sadeh et al. [22], although to a much lesser extent than the perturbations in the mean velocity. Apparently, this is a result of a change in the turbulent structure and the added importance of the dissipation of turbulent energy.

c) The most surprising result perhaps is the disproportionately larger spanwise variation in the mass transfer caused by the mean-velocity perturbations. Here an initial 0.2 to 0.4% perturbation was responsible for a 15% variation.

d) Finally, the screen produced a spanwise averaged mass transfer rate which was 17% greater than that obtained at the base turbulence level of the tunnel.

In the present case it appears that the increase in mass transfer found with the screen is caused by two mechanisms. The first is amplification

of the spanwise mean-velocity perturbations (incident flow vorticity) in the stagnation region by the divergent flow there. This produced a large scale, spanwise periodic vortical motion around the cylinder's leading edge having the same wavelength as that in the incident flow. Where the fluid moved toward the surface the mass transfer increased, and where it moved away the mass transfer decreased, producing a spanwise regular pattern of mass transfer around the leading edge. As a note, no such pattern was found after separation. Interestingly, the wavelength imposed by the screen just happened to be about twenty boundary layer thicknesses, i.e., $\lambda/\delta \approx 20$, which gives a single vortex cell size equal to the turbulence length scale that produces the greatest heat transfer rate according to Yardi and Sukhatme. Also, since the vortex scale is large compared to the boundary layer thickness, this mechanism is mainly an inviscid one.

The second mechanism involved in the increase of mass transfer is the amplification of the incident turbulence in the stagnation region, again by the divergent flow. However, in this case it appears that the scale is smaller than that associated with the vortex motion and that it is random in nature. As such, it can be considered to be convected by the vortex motion, further increasing the mass transfer from the surface, in addition to being produced, diffused and dissipated.

Presently, it is difficult to say how much of the increase is caused by each mechanism and, indeed, it now appears difficult to say exactly how much of the previously published data was affected in the same way.

PART 7

LITERATURE CITED

- [1] Frössling, N., "Verdunstung, Wärmeübertragung und Geschwindigkeitsverteilung bei Zweidimensionaler und Rotationssymmetrischer Grenzschichtströmung," *Acta Univ. Jund* 2(4), 36(1940) (see also NACA TM1432).
- [2] Merk, H. J., "Rapid Calculation of Boundary Layer Transfer Using Wedge Solutions and Asymptotic Expansion," *Journal Fluid Mech.*, 5, pp. 460-480 (1959).
- [3] Drew, T. and Ryan, W., "The Mechanism of Heat Transmission: Distribution of Heat Flow About the Circumference of a Pipe in a Stream of Fluid," *Trans. Am. Inst. Chem. Engr.*, 26, pp. 118-147 (1931).
- [4] Small, J., "The Average and local Rates of Heat Transfer from the Surface of a Hot Cylinder in a Transverse Stream of Fluid," *Phil. Mag.* 19, pp. 251-260 (1935).
- [5] Schmidt, E. and Wenner, K., "Heat Transfer over the Circumference of a Heated Cylinder in Transverse Flow," *Forsch. Geb. Ing. Wes.* 12, pp. 65-73 (1941).
- [6] Comings, E., Clap, J. and Taylor, J., "Air Turbulence and Transfer Processes," *Ind. Engrg. Chem.*, 40(6), pp. 1076-1082 (1948).
- [7] Bollen, W., "Effect of Turbulence on Local Heat Transfer Coefficient Distributions Around a Cylinder Normal to Air Flow," Master's Thesis, Oregon State College (1949).
- [8] Zapp, G., Jr., "The Effect of Turbulence on Local Heat Transfer Coefficients Around a Cylinder Normal to an Air Stream," Master's Thesis Oregon State College (1950).
- [9] Schnautz, J., "Effect of Turbulence Intensity on Mass Transfer from Plates, Cylinders and Spheres in Air Streams," Doctoral Dissertation, Oregon State Univ. (1958).
- [10] Seban, R., "The Influence of Turbulence on Laminar Skin Friction and Heat Transfer," *Physics Fluids*, 9, pp. 2337-2344 (1966).
- [11] Kestin, J., Maeder, P. F. and Sogin, H., "The Influence of Turbulence on the Heat Transfer from Cylinders Near the Stagnation Point," *Z. Agnew. Math. Phys.* 12, pp. 115-132 (1969).
- [12] Appelqvist, B., "The Influence of Turbulence on the Local Heat Transfer from a Cylinder Normal to an Air Stream, Including Further Development of a Method for Local Heat Transfer Measurements," Doctoral Dissertation, Institute of Applied Thermo and Fluid Dynamics, Chalmers University of Technology, Gothenburg (1965).

- [13] Smith, M. and Kuethe, A., "Effects of Turbulence on Laminar Skin Friction and Heat Transfer," *Physics Fluids*, 9, pp. 2337-2344 (1966).
- [14] Kestin, J. and Wood, R., "The Influence of Turbulence on the Mass Transfer from Cylinders," *Journal Heat Transfer*, 93C, pp. 321-327 (1971).
- [15] Kayalar, L., "Experimentelle and Theoretische Untersuchungen über den Einfluss des Turbulenzgrades auf den Wärmeübergang in der Umgebung des Staupunktes eines Kreiszylinders," *Forsh. Geb. IngWes.*, 35, pp. 157-167 (1969).
- [16] Dyban, E. and Epick, E., "Some Heat Transfer Features in the Air Flow of Intensified Turbulence," in Proc. of the Fourth Int. Heat Transfer Conf., Paris (1970).
- [17] Lowery, G. W. and Vachon, R. I., "The Effect of Turbulence on Heat Transfer from Heated Cylinders," *Int. J. Heat Mass Transfer*, 18, pp. 1229-1242 (1975).
- [18] Yardi, N. R. and Sukhatme, S. P., "Effects of Turbulence Intensity and Integral Length Scale of a Turbulent Free Stream on Forced Convection Heat Transfer from a Circular Cylinder in Cross Flow," Proc. Sixth Int. Heat Transfer Conf., Toronto, Canada, Vol. 5, FC(b)-29, pp. 347-352 (1978).
- [19] Traci, R. M. and Willcox, D. C., "Freestream Turbulence Effects on Stagnation Point Heat Transfer," *AIAA Journal*, 13, pp. 890-896 (1965).
- [20] Sutera, S. P., Maeder, P. F. and Kestin, J., "On the Sensitivity of Heat Transfer on the Stagnation Point Boundary Layer to Free Stream Vorticity," *Journal Fluid Mechanics*, 16/4, pp. 497-520 (1963).
- [21] Sutera, S. P., "Vorticity Amplification in Stagnation Point Flow and Its Effect on Heat Transfer," *Journal Fluid Mechanics*, 21/3, pp. 513-534 (1965).
- [22] Sadeh, W. Z., Sutera, S. P. and Maeder, P. F., "Analysis of Vorticity Amplification in the Flow Approaching a Two-Dimensional Stagnation Point," *Z. Angew Math. Phys.*, 21, pp. 691-742 (1970).
- [23] Colak-Antic, P., "Visuelle Untersuchungen von Langswirbeln im Staupunktgebiet eines Kreiszylinders bei Turbulenter Anströmung," DLR Mitteilung 71-13, Bericht über die DGLR-Fachausschuss-Sitzung, "Laminare and Turbulente Grenzschichtung," Göttingen, pp. 194-220 (1971).
- [24] Nagib, H. M. and Hodson, P. R., "Vortices Induced in Stagnation Region by Wakes; Aerodynamic Heating and Thermal Protection Systems," L. S. Fletcher, ed., 59, pp. 66-90, *Progress in Aeronautics and Astronautics*, AIAA (1977).

- [25] Hassler, H., "Hitzdrahtmessungen von Langwirbelartigen Instabilitäterscheinungen in Staupunktgebiet Eines Kreiszylinders in Turbulenter Anströmung," DLR Mitteilung 71-13, Bericht Über Die DGLR-Fachausschus-sitzung, *Laminare and Turbulente Grenzschichtung*, "Gottingen, pp. 221-239 (1971).
- [26] Morkovin, M., "On the Question of Instabilities Upstream of Cylindri-cal Bodies," NASA CR3231 (1979).
- [27] Lighthill, M. J., "The Response of Laminar Skin Friction and Heat Trans-fer to Fluctuations in the Stream Velocity," *Proc. Roy. Soc. A224*, pp. 1-23 (1954).
- [28] Rott, M., "Unsteady Viscous Flow in the Vicinity of a Stagnation Point," *Quart. Appl. Math.*, 13, pp. 444-451 (1956).
- [29] Glauert, M. B., "The Laminar Boundary Layer on Oscillating Plates and Cylinders," *Journal Fluid Mechanics*, 1, pp. 97-110 (1956).
- [30] Childs, E. P., Jr., "Analysis of the Response of Laminar Skin Friction and Heat Transfer to the Rotational Oscillation of a Circular Cylinder in a Steady Stream," Master's Thesis, Rensselaer Polytechnic Institute (1980).
- [31] Sogin, H. H. and Subramanian, V. S., "Local Mass Transfer from Circular Cylinders in Cross Flow," *Trans. ASME, Journal Heat Transfer*, pp. 483-493 (1961).
- [32] Taylor, J., Master's Thesis, Univ. of Minn. (1975).
- [33] Sogin, H. H., "Sublimation from Disks to Air Streams Flowing Normal to Their Surface," *Trans. ASME*, 80, p. 61 (1958).
- [34] Skelland, A.H.P., *Diffusional Mass Transfer*, Wiley & Sons, New York, pp. 49-54 (1974).
- [35] Washburn, E. W., ed., *International Critical Tables, Vol. III*, McGraw-Hill, New York, p. 208 (1928).
- [36] Bedingfield, C. H., Jr., and Drew, T. B., "Analogy between Heat and Mass Transfer: A Psychrometric Study," *Ind. and Engrg. Chem.*, 42, Pt. 1, pp. 1165-1173 (1950).
- [37] Bradshaw, P., *An Introduction to Turbulence and Its Measurement*, Pergamon Press, New York.
- [38] Taylor, G. I., "The Spectrum of Turbulence," *Proc. Roy. Soc.*, 164A, p. 476 (1938).
- [39] Nagib, H. M., private communication.

- [40] Hinze, J. O., *Turbulence*, McGraw-Hill, New York,
- [41] Dryden, H. L., Schubauer, W. C., Mock, W. C., Jr. and Skramstad, H. K., "Measurements of Intensity and Scale of Wind Tunnel Turbulence and Their Relation to the Critical Reynolds Numbers of Spheres," NACA TR581 (1937).
- [42] Townsend, A. A., *The Structure of Turbulent Shear Flow*, Cambridge Univ. Press, Cambridge, England, pp. 56-63 (1956).
- [43] Kellog, R. M. and Corşin, S., "Evolution of a Spectrally Local Disturbance in Grid Generated, Nearly Isotropic Turbulence," *Journal of Fluid Mechanics*, 96/4, pp. 641-669 (1980).
- [44] Abramowitz and Stegun, *Handbook of Mathematical Functions*, Dover Publications, New York (1972).

APPENDIX A

Procedure for the Setup of the Measuring Table

As pointed out in the discussion of the measurement procedure, accurate determination of the local mass loss of the naphthalene surface is to some degree dependent upon the precise configuration of the measurement apparatus. To avoid unnecessary measurement errors a detailed procedure was developed for the setup and positioning of the various components of the table. This procedure is outlined below.

To avoid overranging of the displacement transducers during a measurement traverse, it is necessary that the test section be accurately leveled and centered on the rotary table. Leveling adjustments are provided by the holding pins on the alignment fixture plate and the section can be centered by adjustment of the clamp heads which hold the fixture plate onto the rotary table. To calibrate these adjustments the test section and one of the displacement transducers are used. The section is installed onto the fixture plate and, through the use of the clamp head screws, roughly centered by eye. To level the section, the transducer is positioned on the upper face of the test section near the edge. The table is rotated and the reading of the gauge when above each of the three holding pins is recorded. The reading above one of the pins is arbitrarily chosen as the reference reading. The table is again rotated to place each of the other two pins in turn underneath the gauge needle. The height of each pin is adjusted until the reference reading is obtained. The entire leveling procedure is then repeated until the section is as level as possible. In this manner, the section can be leveled to within 5×10^{-4} inches.

Centering of the section is accomplished in a similar manner. The displacement transducer is positioned against the vertical face of the upper steel rim of the test section and used to indicate off-center runout. The table is rotated and the reading is recorded at four 90° intervals which correspond to positions directly across from or over the brass positioning screws. The four readings are averaged to provide the reference reading which approximately corresponds to a centered section. The table is again rotated to position each of the clamp heads in turn across from the gauge and the clamp head screws are adjusted until the reference reading is obtained. Repetition of this procedure can center the section to within $1(10^{-4})$ inches.

When the test section is accurately centered and leveled, the four displacement transducers can be positioned in the desired measurement configuration. For accurate results, the points at which the gauges contact the surface must lie approximately along a common vertical line and the line of action of each gauge needle must be approximately perpendicular to the surface of the test section. To accurately position the gauge heads, the test section with a cast naphthalene surface is used. With a machinist's square, a true vertical is marked across the cylindrical face of the test section, using a fine point scribe along the naphthalene insert and a sharp pencil on the steel rims. The desired contact points for the four gages are indicated by cross hatches. The table is rotated to place this spanwise line at the desired contact position and the gauges are approximately configured by visual inspection. Their clamps are tightened just enough to avoid slippage and yet allow for slight positional adjustments. A perpendicular line of action of the

gauge needles can be roughly approximated at this point by rotating the gauge heads until their bodies are square with respect to the cylindrical face of the test section. When the gauges are in place, the test section is removed from the table, noting the reading of the lowest gauge, which is used as a reference to later reinstall the section in a centered position. The line of action of the upper three gauges can now be accurately adjusted to a position perpendicular with respect to the cylindrical surface. (The lower gauge is adjusted later.) For this purpose a Starrett height transfer gauge is used. This gauge consists of two similar triangles which are stacked together to provide two parallel surfaces whose separation distance is adjustable. The gauge is used as a reference to position the lines of action of the displacement transducers parallel to the surface of the rotary table, which is perpendicular to the face of a leveled and centered test section. The height transfer gauge is positioned just in front of and below each needle in turn and the gap between the needle and the gauge is observed as the needle is moved in and out. (Although the range of the transducers is only 20 mils, a clutch mechanism allows the needles to be moved a substantial distance.) The gauge heads are adjusted with light twisting actions until there is no visible variation of the gap. The test section is then reinstalled on the table with the gauges contacting the marked spanwise line. The position of the upper gauge is checked by visual inspection and if necessary adjusted with light hand pressure. The correct position of the two naphthalene gauges is obtained by "feeling out" the scribed lines with the respective gauge reading and continuous hand pressure. With care the angular orientation of the transducer heads will be unaltered by this

procedure. When the upper three gauges are accurately positioned, they are tightly clamped in place. A similar procedure is then followed to adjust the angular orientation and position of the remaining gauge, using the reading of the uppermost gauge as a reference for the removal and insertion of the test section.

When this procedure is complete, one final set of adjustments is made to move the operating range of each gauge inward or outward into an optimum position. This is done through the use of the fine adjustment screws on the gauge mounts. The two outer reference gauges are positioned such that their readings on a centered test section are approximately zero, the center of the operating range. The two measuring gauges are positioned farther inward, since their range must reach the depths of a sublimated surface. The gauges are positioned to give readings of approximately -5.0 mils on the centered test section (where the largest position reading corresponds to the most inward position). The measuring apparatus is then ready for use.

APPENDIX B

Measurements of Length Scales Using the Correlation Function

The reported values of the integral length scales of turbulence, L , were determined by fitting a measured spectral distribution to a theoretical distribution. Attempts were also made to determine the integral length scales from measurements of the lateral correlation function in the manner discussed by Hinze [40], however, the values determined using this technique were found to be drastically different from those obtained using the spectral distributions, which compare well with the previous measurements of Dryden et al. [41]. Also, due to the high levels of ambient noise in the wind tunnel and the electronic operations necessary to determine the correlation function, the former method was found to be highly prone to error. A discussion of the techniques used to determine the correlation function is given below, along with the results obtained.

The lateral correlation function is defined as

$$g(z_1) = \frac{u'(z_0) u'(z_0 + z_1)}{\sqrt{u'^2(z_0)} \sqrt{u'^2(z_0 + z_1)}}$$

where z is the lateral (spanwise) coordinate. The integral length scale is given in terms of this function by

$$L = \int_0^{\infty} g(z_1) dz_1$$

The correlation function can be measured experimentally using two hot wires whose separation distance is variable. The configuration is illustrated in Fig. 19a. The length scale is determined by numerical integration of a curve fit to the correlation measured at a number of separation distances, z_1 .

The correlation function is determined from combinations of the AC outputs of the two wires. Assuming that the turbulence field is uniform in the average sense, the terms in the denominator are constant across the span and equal to the measured turbulence level, Tu , i.e.

$$(Tu)^2 = \sqrt{u'^2(z_0)} \sqrt{u'^2(z_0 + z_1)}$$

If the system is noise-free and the wires are of matched response characteristics, the turbulent velocities are given by

$$u'(z_0) = \frac{\partial U}{\partial E} e_1$$

$$u'(z_0 + z_1) = \frac{\partial U}{\partial E} e_2$$

and the correlation term $\overline{u'(z_0) u'(z_0 + z_1)}$ can be determined by differencing the mean square sum and mean square difference of the signals, i.e.

$$\overline{u'(z_0) u'(z_0 + z_1)} = \frac{1}{4} \left(\frac{\partial U}{\partial E} \right)^2 \left[\overline{(e_1 + e_2)^2} - \overline{(e_1 - e_2)^2} \right].$$

In the actual flow there were, however, significant levels of pressure and electrical noise present. Since both wires and hence both available anemometer channels were required for the determination of the correlation function, this noise could not be directly eliminated. Further, frequency filtering of the noise is improper since this would significantly alter the correlation distribution. The ambient noise was hence read along with the true turbulence outputs and later eliminated mathematically. The actual wire outputs are

$$e_1 = e_{T_1} + e_{C_1} + e_P$$

$$e_2 = e_{T_2} + e_{C_2} + e_P$$

where the subscript T denotes AC components due to true turbulence, the subscript C denotes AC components due to electrical noise, and the subscript P denotes those due to pressure noise. The apparent value for $\overline{u'(z_0) u'(z_0 + z_1)}$ is then given by

$$\begin{aligned} u'(z_0) u'(z_0 + z_1)_{app} &= u'(z_0) u'(z_0 + z_1)_{actual} \\ &+ \frac{1}{4} \left(\frac{\partial U}{\partial E} \right)^2 \left[\overline{e_{C_1}^2} + \overline{e_{C_2}^2} + 4\overline{e_P^2} \right] \end{aligned}$$

The last term due to noise should be approximately constant across the flow, and hence its value can be determined by measuring the apparent level of $\overline{u'(z_0) u'(z_0 + z_1)}$ at a large value of z , for which the actual correlation term is zero. The equation for the correlation function is then

$$g(z_1) = \frac{1}{4} \left(\frac{U}{E} \right)^2 \left(\frac{1}{Tu} \right)^2 \left[\overline{(e_1 + e_2)^2} - \overline{(e_1 - e_2)^2} - (\overline{e_{C_1}^2} + \overline{e_{C_2}^2} + 4\overline{e_P^2}) \right]$$

Determination of the correlation function in this manner requires extensive use of electronic mean square operations. With the equipment used in the reported measurements, the repeatability of such operations was found to be about +15%. This large level of uncertainty significantly affects the determination of the correlation function allowing for possible errors on the order of +30%.

The length scales determined from measured correlation functions are given in Table A1 along with the previously reported values obtained with the spectral technique. In general, the values obtained from the two methods compare poorly. In some cases, the discrepancy is larger than that allowed by the estimated uncertainties of each method. At present, further explanation of the discrepancy is unavailable. Since the values obtained from the spectral technique compared well with those suggested by the results of Dryden et al. [41], they were accepted as the most representative results.

Table A1. Comparison of length scales measured with correlation function to those determined from spectral distributions

Screen	Pos-X/M	(L/D) _{corr}	(L/D) _{spec}
M=.125"	144	.005	.012
	268	.013	.017
	448	.015	.028
M=.621"	29.0	.027	.018
	53.9	.035	.022
	90.2	.043	.030
M=.875"	20.6	.048	.030
	38.3	.063	.038
	64.0	.098	.050

APPENDIX C

Theoretical Considerations of the Amplification of Flow Nonuniformities in a Stagnation Zone

A number of theoretical investigations have been conducted to examine the amplification of a periodic variation superimposed on a uniform mean flow as a stagnation zone is approached. Suter et al. [20] and Suter [21] have presented a model for the amplification within the region of the boundary layer normally associated with a two-dimensional stagnation point. In their analyses the relevant equations are not explicitly solved but rather used in an analog computer to obtain approximate distributions for the variables of interest. Sadeh, Suter and Maeder [22] have attempted to extend the treatment beyond the boundary layer region. An equation for the distribution of vorticity along the stagnation plane is presented; however, the variation of the streamwise velocity component is not obtained. In an attempt to examine the nature of the assumptions made in these treatments and the validity of the results, the problem is developed below in a somewhat more rigorous manner than the previous investigations. Although a valid solution is not obtained, the analysis demonstrates some of the basic aspects of the mathematical structure of the problem and identifies some inherent invalidities on the previously presented solutions.

Consider an infinitely long cylinder immersed in a cross stream whose velocity profile contains a uniform component and a component which varies periodically in the spanwise direction as shown in Fig. A1. For mathematical simplicity the variation is assumed to be sinusoidal. To model the situation investigated by the current experiments, the wavelength

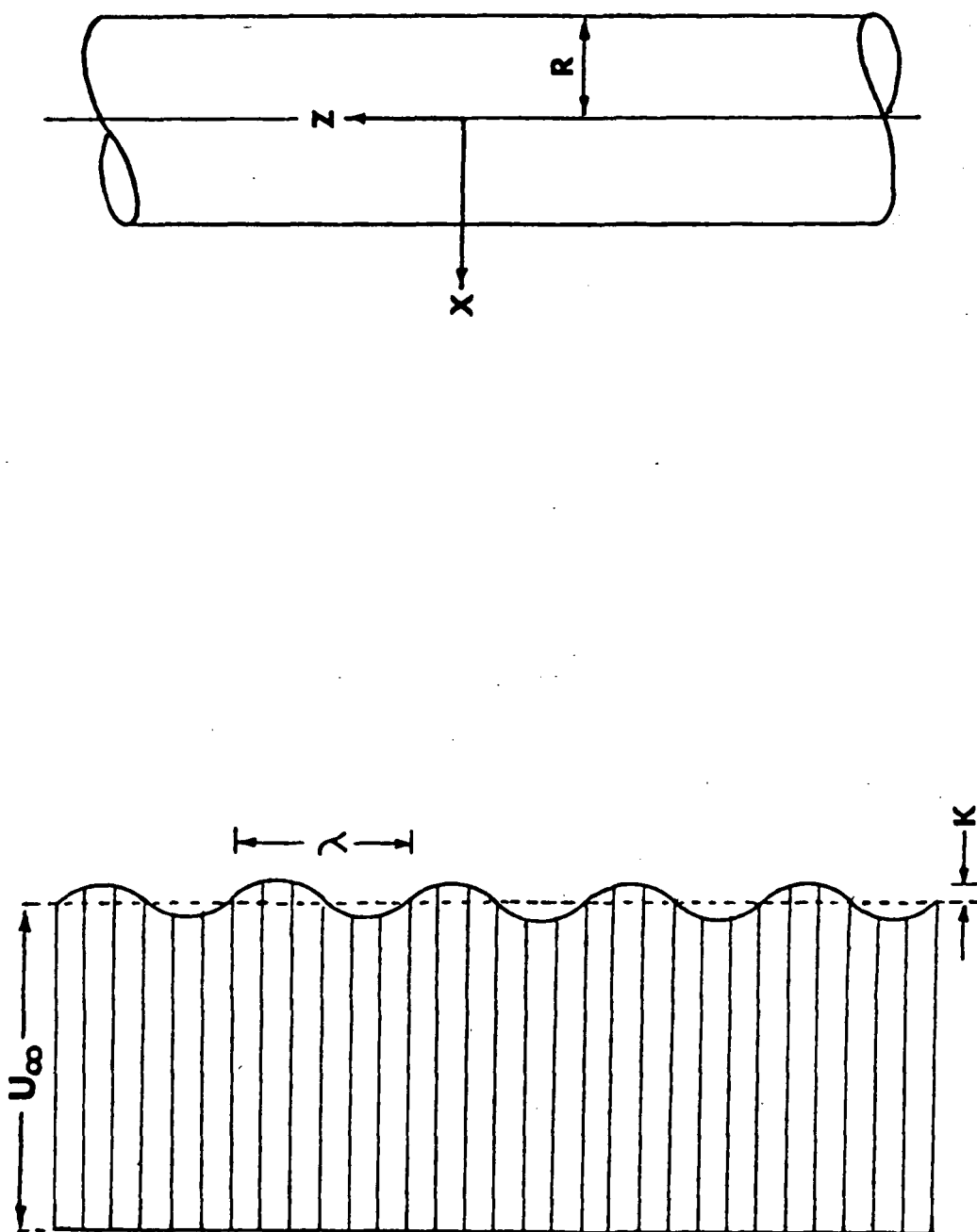


Figure A1. Periodically perturbed mean velocity incident to a circular cylinder

is assumed to be large with respect to the boundary layer thickness normally associated with two-dimensional stagnation on a cylinder. Then, if only the external flow region is considered, the effects of viscosity can be neglected and the appropriate equations of motion are

$$\bar{U} \frac{\partial \bar{U}}{\partial \bar{x}} + \bar{V} \frac{\partial \bar{U}}{\partial \bar{y}} + \bar{W} \frac{\partial \bar{U}}{\partial \bar{z}} = \frac{-1}{\rho} \frac{\partial \bar{P}}{\partial \bar{x}}$$

$$\bar{U} \frac{\partial \bar{V}}{\partial \bar{x}} + \bar{V} \frac{\partial \bar{V}}{\partial \bar{y}} + \bar{W} \frac{\partial \bar{V}}{\partial \bar{z}} = \frac{-1}{\rho} \frac{\partial \bar{P}}{\partial \bar{y}}$$

$$\bar{U} \frac{\partial \bar{W}}{\partial \bar{x}} + \bar{V} \frac{\partial \bar{W}}{\partial \bar{y}} + \bar{W} \frac{\partial \bar{W}}{\partial \bar{z}} = \frac{-1}{\rho} \frac{\partial \bar{P}}{\partial \bar{z}}$$

$$\frac{\partial \bar{U}}{\partial \bar{x}} + \frac{\partial \bar{V}}{\partial \bar{y}} + \frac{\partial \bar{W}}{\partial \bar{z}} = 0$$

where the bars denote dimensional variables and the coordinate system shown in Fig. A1 is used. With the assumed form of the incident velocity the boundary conditions far away from the cylinder are

$$\left. \begin{aligned} \bar{U}(\bar{x}, \bar{y}, \bar{z}) &\rightarrow U_{\infty} + K \cos \bar{z}/\lambda \\ \bar{V}(\bar{x}, \bar{y}, \bar{z}) &\rightarrow 0 \\ \bar{W}(\bar{x}, \bar{y}, \bar{z}) &\rightarrow 0 \end{aligned} \right\} \begin{array}{l} \text{as } \bar{x} \rightarrow \pm \infty \\ \text{or} \\ \text{as } \bar{y} \rightarrow \pm \infty \end{array}$$

It will also be assumed for the moment that the interaction of the inviscid region with the internal viscous region will be of the type normally used in two-dimensional boundary layer analysis; the components of velocity normal to the surface are zero, i.e.

$$\bar{U} \frac{\bar{x}}{R} + \bar{V} \frac{\bar{y}}{R} = 0 \quad \text{on} \quad \bar{x}^2 + \bar{y}^2 = R^2.$$

In addition to these conditions the equations necessitate conditions in the spanwise (\bar{z}) direction. Since we are considering a cylinder of infinite length, the relevant condition will be periodicity in \bar{z} . Further, a physical consideration of the flow field will demonstrate that there is no existing mechanism for a change in wavelength. (Such a change would have to occur in a continuous manner, the wavelength stretching about some point; however, the choice for this point would be arbitrary. Physically, there is no justification for the existence of such a point - hence, stretching of the wavelength cannot occur. This does not imply, however, that the velocity profile remains sinusoidal.) The conditions in the z direction are then

$$\left. \begin{aligned} \bar{U}(\bar{x}_0, \bar{y}_0, \bar{z}_0) &= \bar{U}(\bar{x}_0, \bar{y}_0, \bar{z}_0 + 2\pi n\lambda) \\ \bar{V}(\bar{x}_0, \bar{y}_0, \bar{z}_0) &= \bar{V}(\bar{x}_0, \bar{y}_0, \bar{z}_0 + 2\pi n\lambda) \\ \bar{W}(\bar{x}_0, \bar{y}_0, \bar{z}_0) &= \bar{W}(\bar{x}_0, \bar{y}_0, \bar{z}_0 + 2\pi n\lambda) \end{aligned} \right\} \begin{array}{l} \text{for any } x_0, y_0, z_0 \\ \text{and integer values} \\ \text{of } n. \end{array}$$

It is proper to nondimensionalize the equations and boundary conditions and for this purpose the following nondimensional variables are defined:

$$\begin{aligned} x &= \bar{x}/R & U &= \bar{U}/U_\infty \\ y &= \bar{y}/R & V &= \bar{V}/U_\infty & P &= \frac{\bar{P}}{\rho U_\infty^2} \\ z &= \bar{z}/\lambda & W &= \bar{W}/U_\infty \\ a &= R/\lambda & \delta &= K/U_\infty \end{aligned}$$

Using these variables the equations of motion and the boundary conditions are

$$U \frac{\partial U}{\partial x} + V \frac{\partial U}{\partial y} + aW \frac{\partial U}{\partial z} = -\frac{\partial P}{\partial x}$$

$$U \frac{\partial V}{\partial x} + V \frac{\partial V}{\partial y} + aW \frac{\partial V}{\partial z} = -\frac{\partial P}{\partial y}$$

$$U \frac{\partial W}{\partial x} + V \frac{\partial W}{\partial y} + aW \frac{\partial W}{\partial z} = -a \frac{\partial P}{\partial z}$$

$$\left. \begin{array}{l} U \rightarrow 1 + \delta \cos z \\ V \rightarrow 0 \\ W \rightarrow 0 \end{array} \right\} \begin{array}{l} \text{as } x \rightarrow \pm \infty \\ \text{or} \\ y \rightarrow \pm \infty \end{array}$$

$$U_x + V_y = 0 \quad \text{on } x^2 + y^2 = 1$$

$$\left. \begin{array}{l} U(x_0, y_0, z_0) = U(x_0, y_0, z_0 + 2\pi n) \\ V(x_0, y_0, z_0) = V(x_0, y_0, z_0 + 2\pi n) \\ W(x_0, y_0, z_0) = W(x_0, y_0, z_0 + 2\pi n) \end{array} \right\} \begin{array}{l} \text{for any } x_0, y_0, z_0 \\ \text{and integer values} \\ \text{of } n \end{array}$$

Since the incident flow field in the experiments is nominally uniform with a variation in magnitude of less than $\pm 0.2\%$, the problem can be considered in the form of a perturbation about δ which is assumed to be much less than 1. (It should be noted that Sadeh et al. [22] use a similar technique. Suter et al. [20] and Suter [21] do not explicitly state their equations in a perturbation form; however, they do assume that the velocity field is that for two-dimensional flow with a superimposed three-dimensional variation. Since the superimposed flow is not allowed to alter the mean flow structure, their assumption is equivalent to the use of a perturbation analysis.) The solution for the velocities is then assumed to be in the form of a perturbation series, i.e.

$$U = U_0(x, y, z) + \delta U_1(x, y, z) + \delta^2 U_2(x, y, z) + \dots$$

$$V = V_0(x, y, z) + \delta V_1(x, y, z) + \delta^2 V_2(x, y, z) + \dots$$

$$W = W_0(x, y, z) + \delta W_1(x, y, z) + \delta^2 W_2(x, y, z) + \dots$$

Substituting these expressions into the equations of motion and examining the first-order terms, it is obvious that the first term in each series is simply the appropriate velocity for two-dimensional potential flow around a cylinder, i.e.

$$U_0 = 1 - \frac{x^2 - y^2}{(x^2 + y^2)^2}, \quad V_0 = \frac{-2xy}{(x^2 + y^2)^2}, \quad W_0 = 0$$

The equations for the terms of order δ are then

$$U_1 \frac{\partial U_0}{\partial x} + U_0 \frac{\partial U_1}{\partial x} + V_1 \frac{\partial U_0}{\partial y} + V_0 \frac{\partial U_1}{\partial y} = \frac{-\partial P_1}{\partial x}$$

$$U_1 \frac{\partial V_0}{\partial x} + U_0 \frac{\partial V_1}{\partial x} + V_1 \frac{\partial V_0}{\partial y} + V_0 \frac{\partial V_1}{\partial y} = \frac{-\partial P_1}{\partial y}$$

$$U_0 \frac{\partial W_1}{\partial x} + V_0 \frac{\partial W_1}{\partial y} = -a \frac{\partial P_1}{\partial z}$$

$$\frac{\partial U_1}{\partial x} + \frac{\partial V_1}{\partial y} + \frac{\partial W_1}{\partial z} = 0$$

and the appropriate boundary conditions are

$$\left. \begin{array}{l} U_1 \rightarrow \cos z \\ V_1 \rightarrow 0 \\ W_1 \rightarrow 0 \end{array} \right\} \begin{array}{l} \text{as } x \rightarrow \pm \infty \\ \text{or} \\ \text{as } y \rightarrow \pm \infty \end{array}$$

$$U_1 x + V_1 y = 0 \quad \text{on } x^2 + y^2 = 1$$

$$\left. \begin{aligned} U_1(x_o, y_o, z_o) &= U_1(x_o, y_o, z_o + 2\pi n) \\ V_1(x_o, y_o, z_o) &= V_1(x_o, y_o, z_o + 2\pi n) \\ W_1(x_o, y_o, z_o) &= W_1(x_o, y_o, z_o + 2\pi n) \end{aligned} \right\} \begin{array}{l} \text{for any } x_o, y_o, z_o \\ \text{and integer} \\ \text{values of } n \end{array}$$

In an effort to simplify the problem, these equations can be considered for a small region near the stagnation plane, that is for $y \approx 0$. (Sadeh et al. [22], Suter [21] and Suter et al. [20] considered similar regions in their analyses.) If the functions are assumed to be analytic at $y = 0$, the velocities can be expanded in Taylor series in y . It should be noted that since the flow field is symmetric about the stagnation plane,

$$V(x, 0, z) = 0 \quad \text{and} \quad \frac{\partial U}{\partial y}(x, 0, z) = 0$$

Expanding the velocities using these conditions

$$\begin{aligned} U_1(x, y, z) &= U_1(x, 0, z) + y \frac{\partial U_1}{\partial y}(x, 0, z) + \dots \\ V_1(x, y, z) &= y \frac{\partial V_1}{\partial y}(x, 0, z) + \frac{y^2}{2} \frac{\partial^2 V_1}{\partial y^2}(x, 0, z) + \dots \\ W_1(x, y, z) &= W_1(x, 0, z) + y \frac{\partial W_1}{\partial y}(x, 0, z) + \dots \\ P_1(x, y, z) &= P_1(x, 0, z) + y \frac{\partial P_1}{\partial y}(x, 0, z) + \dots \end{aligned}$$

For clarity, the following set of functions is defined:

$$\begin{aligned} F_U(x, z) &= U_1(x, 0, z) & F_P(x, z) &= P_1(x, 0, z) \\ F_V(x, z) &= \frac{\partial V_1}{\partial y}(x, 0, z) & F_{P'}(x, z) &= \frac{\partial P_1}{\partial y}(x, 0, z) \\ F_W(x, z) &= W_1(x, 0, z) \end{aligned}$$

Substituting the Taylor expansions into the equations of motions and keeping only first-order terms yields

$$F_U \frac{\partial U_o}{\partial x} + U_o \frac{\partial F_U}{\partial x} = \frac{-\partial F_P}{\partial x}$$

$$0 = \frac{-\partial F_P}{\partial y}$$

$$U_o \frac{\partial F_W}{\partial x} = -a \frac{\partial F_P}{\partial z}$$

$$\frac{\partial F_U}{\partial x} + a \frac{\partial F_U}{\partial z} = -F_V$$

The second equation of this set provides no useful information and is dropped. The first and third equations can be combined to eliminate F_P giving the equation

$$\frac{\partial U_o}{\partial x} \left(\frac{\partial F_U}{\partial z} - \frac{1}{a} \frac{\partial F_W}{\partial x} \right) = -U_o \frac{\partial}{\partial x} \left(\frac{\partial F_U}{\partial z} - \frac{1}{a} \frac{\partial F_W}{\partial x} \right)$$

This can be integrated with respect to x to yield

$$\frac{\partial F_U}{\partial z} - \frac{1}{a} \frac{\partial F_W}{\partial x} = \frac{K(z)}{U_o(x)}$$

where $K(z)$ is a function of integration. Hence the problem statement becomes

$$\frac{\partial F_U}{\partial z} - \frac{1}{a} \frac{\partial F_W}{\partial x} = \frac{K(z)}{U_0(x)}$$

$$\frac{\partial F_U}{\partial x} + a \frac{\partial F_W}{\partial z} = -F_{V'}$$

$$\left. \begin{array}{l} F_U(x, z) \rightarrow \cos z \\ F_W(x, z) \rightarrow 0 \end{array} \right\} \text{ as } x \rightarrow \infty$$

$$F_U(1, z) = 0$$

$$\left. \begin{array}{l} F_U(x_0, z_0) = F_U(x_0, z_0 + 2\pi n) \\ F_W(x_0, z_0) = F_W(x_0, z_0 + 2\pi n) \end{array} \right\} \text{ for any } x_0, z_0 \text{ and integer values of } n.$$

An examination of these equations immediately demonstrates that the problem is now underspecified: there are three unknowns, F_U , F_W and $F_{V'}$, and only two equations. In order to solve for the U and W velocity components, $F_{V'}$, the gradient in the cross stream velocity V at the stagnation plane, must be specified. In past investigations the assumption used was

$$F_{V'} = y F_V(x)$$

Sadeh's solution shows that $F_V(x)$ decreases rapidly to zero as the cylinder is approached. Since the cross stream velocity must also go to zero at distances far from the cylinder, it will be assumed here that

$$F_{V'} \approx 0$$

With this assumption, an explicit solution to the stated equations can be obtained in the form of a Fourier series

$$F_U = \sum_{n=0}^{\infty} \left\{ \begin{aligned} & -A_n + \frac{1}{4} a n A_n E_1[an(x+1)] e^{an(x+1)} \\ & + \frac{1}{4} a n A_n E_i[an(x+1)] e^{-an(x+1)} \\ & - \frac{1}{4} a n A_n E_1[an(x+1)] e^{an(x-1)} \\ & - \frac{1}{4} a n A_n E_i[an(x-1)] e^{-an(x-1)} \\ & + C_{1n} e^{anx} + C_{2n} e^{-anx} \end{aligned} \right\} \cos nz$$

$$F_W = \frac{1}{a} \sum_{n=0}^{\infty} \left\{ \begin{aligned} & -\frac{1}{4} a^2 n A_n E_1[an(x+1)] e^{an(x+1)} \\ & - \frac{1}{4} a^2 n A_n E_i[an(x+1)] e^{-an(x+1)} \\ & + \frac{1}{4} a^2 n A_n E_1[an(x-1)] e^{an(x-1)} \\ & + \frac{1}{4} a^2 n A_n E_i[an(x-1)] e^{-an(x-1)} \\ & + C_{1n} a e^{anx} - C_{2n} a e^{-anx} \end{aligned} \right\} \sin nz$$

where A_n , C_{1n} and C_{2n} are constants of integration. E_i and E_1 denote exponential integral functions as defined by Abramowitz and Stegun [44], i.e.

$$E_i(r) = \int_{-\infty}^r \frac{e^t}{t} dt \quad (r > 0)$$

$$E_1(r) = \int_r^{\infty} \frac{e^{-t}}{t} dt \quad (\arg r < \pi)$$

Imposing the boundary conditions at infinity gives

$$C_{1n} = 0 \quad \text{for all } n$$

$$A_1 = 1$$

$$A_n = 0 \quad \text{for } n \neq 1$$

Further imposition of the boundary conditions at $x=1$ gives

$$C_{2n} = 0 \quad \text{for all } n$$

The streamwise component of velocity is then

$$F_U = \left\{ -1 + \frac{1}{4} a E_1[a(x+1)] e^{a(x+1)} - \frac{1}{4} E_1[a(x-1)] e^{a(x-1)} + \frac{1}{4} a E_1[a(x+1)] e^{-a(x+1)} - \frac{1}{4} a E_1[a(x-1)] e^{-a(x-1)} \right\} \cos z$$

$$= u_1(x, y, z) \text{ for small } y.$$

An examination of this solution will demonstrate that the assumptions made in the formulation of the problem are violated. Specifically, the assumed perturbation structure is invalid near the surface, since

$$\lim_{x \rightarrow 0} \left(\frac{U_1}{U_0} \right) \rightarrow \infty$$

This result is somewhat expected since the equation for F_U obtained by cross differentiation

$$\frac{\partial^2 F_U}{\partial x^2} + a^2 \frac{\partial^2 F_U}{\partial z^2} = \frac{a^2}{U_0} \frac{dK}{dz}$$

is singular at $x=1$ where $U_0 = 0$. This result would suggest that some type of inner-outer matching procedure is required to solve the stated perturbation problem. This is, however, somewhat of an anomaly since the equations do not exhibit the reduction of order for large x characteristic of typical inner-outer perturbation problems, and hence an attempted solution would result in an unspecified set of constants.

It should also be noted that the flow structure observed in the experiments of Nagib and Hodson [25] demonstrate that regions of flow

reversal exist near the surface of the cylinder. Mathematically this requires that $\delta U_1 > U_0$ for some region near the surface, and hence the assumed form for the external (outer) flow region must be invalid for some inner region. This violation of assumptions also occurs in the previously presented models of Sadeh et al. [22], Sutera et al. [20] and Sutera [21].

APPENDIX D

Tabular Listing of Mass Transfer Data

In the following pages a full tabular listing of the reported mass transfer measurements is given. For brevity only the calculated transfer rates are reported. The actual experimental loss depths in mils can be calculated using the "multiplier" and "loss correction" included with each data set, i.e.

$$\text{Depth (mils)} = \frac{Sh}{\sqrt{Re}} \div \text{multiplier} + \text{loss correction.}$$

For convenience, the figure in which each data set is plotted is also given in the listings. An index to the data table is given below.

Data Index

Circumferential data

No screen,	Re = 75000,	St = 0.0
	Re = 82500,	St = 0.0
	Re = 110000,	St = 0.0	(3 runs).....
	Re = 110000,	St = 0.0639	(2 runs).....
	Re = 125000,	St = 0.0
Tu = 0.34%,	Re = 110000,	St = 0.0
		St = 0.0639
Tu = 1.182%,	Re = 110000,	St = 0.0
		St = 0.0639
Tu = 1.801%,	Re = 110000,	St = 0.0
		St = 0.0639
Tu = 2.651%,	Re = 50000,	St = 0.0
		St = 0.1406
	Re = 75000,	St = 0.0	(2 runs).....
		St = 0.0417
		St = 0.1041
	Re = 110000,	St = 0.0	(2 runs).....
		St = 0.0071	(2 runs).....
		St = 0.0213	(2 runs).....
		St = 0.0213	($\phi_o = 12^\circ$).....
		St = 0.0355	(2 runs).....
		St = 0.0497	(4 runs).....
		St = 0.0639	(3 runs).....
		St = 0.0781
Tu = 4.9%,	Re = 110000,	St = 0.0
		St = 0.0071
		St = 0.0213
		St = 0.0355
		St = 0.0497
		St = 0.0639

Spanwise Data (Re = 110000)

No screen (Full body naphthalene coating).....
M=0.0625", x/R = 6.0.....
 x/R = 6.0 (screen shifted upward 0.25")...
 x/R = 11.2 (2 runs).....
 x/R = 11.2 (Full body naphthalene coating).
M = 0.125", x/R = 6.0.....
 x/R = 18.7.....
M = 0.621", x/R = 6.0.....
 x/R = 11.2.....
M = 0.875", x/R = 6.0.....
 x/R = 18.7.....

NO SCREEN RE= 75000, ST=0.0
MULTIPLIER=0.28138 /MIL

(FIG 26)
LOSS CORRECTION=0.067 MILS

DEG	SH/ \sqrt{RE} Z=-.5"	SH/ \sqrt{RE} Z=+.5"	DEG	SH/ \sqrt{RE} Z=-.5"	SH/ \sqrt{RE} Z=+.5"
-176	2.339	2.351	4	1.567	1.564
-172	2.315	2.324	8	1.549	1.568
-168	2.244	2.240	12	1.550	1.561
-164	2.177	2.158	16	1.539	1.535
-160	2.072	2.085	20	1.523	1.552
-156	2.016	2.001	24	1.494	1.501
-152	1.960	1.938	30	1.493	1.503
-148	1.923	1.903	34	1.463	1.479
-144	1.856	1.827	38	1.430	1.438
-140	1.762	1.743	42	1.398	1.387
-136	1.703	1.690	46	1.367	1.359
-132	1.646	1.650	48	1.327	1.333
-128	1.648	1.643	52	1.290	1.287
-124	1.607	1.586	56	1.261	1.245
-120	1.563	1.540	60	1.193	1.167
-116	1.476	1.430	64	1.127	1.101
-112	1.346	1.300	68	0.996	0.972
-108	1.188	1.155	72	0.888	0.827
-104	1.084	1.062	76	0.672	0.574
-100	1.028	1.027	80	0.458	0.458
-96	1.013	1.003	84	0.506	0.563
-92	0.943	0.916	88	0.662	0.758
-88	0.805	0.744	92	0.817	0.907
-84	0.628	0.570	96	0.955	0.977
-80	0.468	0.435	100	1.001	1.021
-76	0.465	0.550	104	1.013	1.063
-72	0.704	0.778	108	1.092	1.139
-68	0.910	0.963	112	1.209	1.263
-64	1.037	1.081	116	1.351	1.411
-60	1.134	1.156	120	1.481	1.526
-56	1.200	1.200	124	1.544	1.564
-52	1.268	1.380	128	1.597	1.621
-48	1.310	1.309	132	1.590	1.636
-44	1.348	1.355	136	1.660	1.679
-40	1.369	1.390	140	1.720	1.760
-36	1.392	1.432	144	1.789	1.823
-32	1.416	1.447	148	1.833	1.894
-28	1.436	1.486	152	1.926	1.956
-24	1.471	1.500	156	1.976	2.005
-20	1.513	1.528	160	2.013	2.007
-16	1.532	1.557	164	2.119	2.157
-12	1.562	1.580	168	2.188	2.239
-8	1.551	1.574	172	2.263	2.305
-4	1.556	1.577	176	2.292	2.321
0	1.558	1.561	180	2.334	2.361

NO SCREEN RE= 82500, ST=0.0
MULTIPLIER=0.19925 /MIL

(FIG 27)
LOSS CORRECTION=0.110 MILS

DEG	SH/ \sqrt{RE} Z=-.5"	SH/ \sqrt{RE} Z=+.5"	DEG	SH/ \sqrt{RE} Z=-.5"	SH/ \sqrt{RE} Z=+.5"
-176	2.368	2.355	4	1.539	1.588
-172	2.369	2.354	8	1.546	1.591
-168	2.232	2.287	12	1.553	1.576
-164	2.192	2.222	16	1.525	1.557
-160	2.117	2.096	20	1.509	1.544
-156	2.083	2.067	24	1.479	1.525
-152	2.032	1.980	28	1.469	1.518
-148	1.961	1.891	32	1.434	1.500
-144	1.890	1.834	36	1.431	1.493
-140	1.831	1.748	40	1.399	1.459
-136	1.748	1.717	44	1.326	1.410
-132	1.660	1.679	48	1.337	1.358
-128	1.648	1.623	52	1.326	1.333
-124	1.641	1.625	56	1.257	1.260
-120	1.558	1.548	60	1.215	1.163
-116	1.477	1.428	64	1.107	1.069
-112	1.354	1.290	68	0.999	0.950
-108	1.239	1.159	72	0.863	0.755
-104	1.122	1.075	76	0.585	0.515
-100	1.087	1.031	80	0.446	0.473
-96	1.048	0.992	84	0.585	0.613
-92	0.961	0.881	88	0.779	0.794
-88	0.780	0.710	92	0.894	0.946
-84	0.592	0.553	96	1.049	1.063
-80	0.449	0.404	100	1.064	1.048
-76	0.526	0.571	104	1.107	1.162
-72	0.780	0.818	108	1.200	1.234
-68	0.950	0.985	112	1.315	1.355
-64	1.062	1.083	116	1.427	1.498
-60	5.000	5.000	120	1.518	1.591
-56	1.236	1.232	124	1.613	1.656
-52	1.305	1.316	128	1.610	1.659
-48	1.330	1.354	132	1.626	1.682
-44	1.347	1.392	136	1.687	1.714
-40	1.399	1.427	140	1.727	1.794
-36	1.438	1.472	144	1.831	1.873
-32	1.431	1.493	148	1.932	1.967
-28	1.497	1.518	152	2.010	1.953
-24	1.506	1.518	156	2.027	2.077
-20	1.528	1.560	160	2.113	2.144
-16	1.544	1.566	164	2.157	2.207
-12	1.548	1.574	168	2.226	2.328
-8	1.554	1.574	172	2.336	2.371
-4	1.548	1.572	176	2.348	2.373
0	1.556	1.580	180	2.383	2.385

NO SCREEN RE=110000, ST=0.0
MULTIPLIER=0.32443 /MIL

(RUN 1, FG 28)
LOSS CORRECTION=0.042 MILS

DEG	SH//RE Z=0	DEG	SH//RE Z=0
-179	2.551	1	1.553
-175	2.533	5	1.562
-171	2.487	9	1.556
-167	2.385	13	1.562
-163	2.319	17	1.541
-159	2.225	21	1.492
-155	2.201	25	1.483
-151	2.144	29	1.453
-147	2.041	33	1.450
-143	1.975	37	1.432
-139	1.887	41	1.417
-135	1.809	45	1.366
-131	1.767	49	1.342
-127	1.743	53	1.281
-123	1.704	57	1.245
-119	1.676	61	1.146
-115	1.592	65	1.076
-111	1.474	69	0.959
-107	1.342	73	0.775
-103	1.236	77	0.558
-99	1.173	81	0.603
-95	1.134	85	0.757
-91	1.040	89	1.019
-87	0.856	93	1.107
-83	0.669	97	1.158
-79	0.549	101	1.245
-75	0.639	105	1.348
-71	0.880	109	1.450
-67	1.019	113	1.571
-63	1.167	117	1.658
-59	1.206	121	1.719
-55	1.254	125	1.737
-51	1.330	129	1.785
-47	1.330	133	1.791
-43	1.393	139	1.860
-39	1.432	143	1.927
-35	1.456	147	2.020
-31	1.495	151	2.117
-27	1.526	155	2.159
-23	1.502	157	2.219
-19	1.526	161	2.276
-15	1.532	165	2.373
-11	1.571	169	2.406
-7	1.595	173	2.460
-3	1.559	177	2.472

NO SCREEN RE=110000, ST=0.0
MULTIPLIER=0.30095 /MIL

(RUN 2, FIG 28)
LOSS CORRECTION=0.053 MILS

DEG	SH/ \sqrt{RE} Z=0	DEG	SH/ \sqrt{RE} Z=0
-179	2.537	1	1.552
-175	2.387	5	1.576
-171	2.363	9	1.558
-167	2.307	13	1.555
-163	2.252	17	1.540
-159	2.146	21	1.525
-155	2.123	25	1.521
-151	2.044	29	1.514
-147	1.992	33	1.534
-143	1.925	37	1.472
-139	1.848	41	1.438
-135	1.821	45	1.426
-131	1.763	49	1.408
-127	1.723	53	1.326
-123	1.727	57	1.264
-119	1.698	61	1.221
-115	1.655	65	1.130
-111	1.549	69	0.998
-107	1.417	73	0.808
-103	1.270	77	0.582
-99	1.191	81	0.576
-95	1.166	85	0.777
-91	1.107	89	0.992
-87	0.922	93	1.110
-83	0.710	97	1.200
-79	0.563	101	1.258
-75	0.630	105	1.377
-71	0.854	109	1.481
-67	1.077	113	1.610
-63	1.114	117	1.649
-59	1.200	121	1.704
-55	1.251	125	1.769
-51	1.312	129	1.716
-47	1.347	133	1.736
-41	1.371	137	1.778
-37	1.399	141	1.848
-33	1.429	145	1.912
-29	1.463	149	2.017
-25	1.490	153	2.093
-23	1.525	157	2.204
-19	1.511	161	2.182
-15	1.549	165	2.246
-11	1.564	169	2.332
-7	1.561	173	2.473
-3	1.555	177	2.375

NO SCREEN RE=110000, ST=0.0
MULTIPLIER=0.23443 /MIL

(RUN 3, FIG 28)
LOSS CORRECTION=0.044 MILS

DEG	SH/ \sqrt{RE} Z=0	DEG	SH/ \sqrt{RE} Z=0
-179	2.445	1	1.586
-175	2.463	5	1.580
-171	2.406	9	1.577
-167	2.370	13	1.550
-163	2.267	17	1.541
-159	2.204	21	1.529
-155	2.189	25	1.508
-151	2.111	29	1.502
-147	2.038	33	1.450
-143	1.960	37	1.423
-139	1.887	41	1.405
-135	1.818	45	1.369
-131	1.764	49	1.339
-127	1.764	53	1.290
-123	1.640	57	1.257
-119	1.574	61	1.191
-115	1.508	65	1.098
-111	1.511	69	0.980
-107	1.366	73	0.781
-103	1.257	77	0.561
-99	1.170	81	0.606
-95	1.140	85	0.766
-91	1.049	89	0.950
-87	0.914	93	1.076
-83	0.690	97	1.137
-79	0.543	101	1.185
-75	0.648	105	1.254
-71	0.914	109	1.414
-67	1.031	113	1.535
-63	1.143	117	1.622
-59	1.221	121	1.701
-55	1.290	125	1.743
-51	1.336	129	1.764
-47	1.345	133	1.746
-43	1.408	139	1.815
-39	1.432	143	1.918
-35	1.474	147	2.005
-31	1.495	151	2.050
-27	1.514	155	2.108
-23	1.529	157	2.189
-19	1.526	161	2.216
-15	1.556	165	2.204
-11	1.565	169	2.406
-7	1.601	173	2.448
-3	1.580	177	2.484

NO SCREEN RE=110000, ST=0.0639 (RUN 1)
MULTIPLIER=0.23235 /MIL LOSS CORRECTION=0.034 MILS

DEG	SH/ \sqrt{RE} Z=-.5"	SH/ \sqrt{RE} Z=+.5"	DEG	SH/ \sqrt{RE} Z=-.5"	SH/ \sqrt{RE} Z=+.5"
-178	2.476	2.496	2	1.558	1.592
-174	2.472	2.451	6	1.560	1.569
-170	2.465	2.460	10	1.558	1.565
-166	2.390	2.391	14	1.537	1.566
-162	2.305	2.323	18	1.522	1.563
-158	2.243	2.278	22	1.516	1.539
-154	2.202	2.191	26	1.484	1.770
-150	2.107	2.096	30	1.505	1.481
-146	2.040	2.024	34	1.444	1.455
-142	1.952	1.974	40	1.421	1.446
-138	1.891	1.980	44	1.378	1.391
-134	1.818	1.857	48	1.363	1.346
-130	1.810	1.801	52	1.302	1.298
-126	1.716	1.739	56	1.247	1.239
-122	1.667	1.660	58	1.178	1.152
-118	1.649	1.580	62	1.077	1.028
-114	1.514	1.490	66	0.949	0.928
-110	1.434	1.433	70	0.876	0.866
-106	1.342	1.346	74	0.832	0.833
-102	1.255	1.182	78	0.828	0.845
-98	1.102	1.097	82	0.831	0.843
-94	0.989	0.969	86	0.832	0.856
-90	0.872	0.859	90	0.892	0.955
-86	0.837	0.831	94	0.995	1.052
-82	0.821	0.823	98	1.145	1.220
-78	0.801	0.820	102	1.257	1.310
-74	0.823	0.829	106	1.347	1.397
-70	0.867	0.884	110	1.429	1.470
-66	0.961	1.000	114	1.531	1.559
-62	1.076	1.112	118	1.608	1.642
-58	1.176	1.216	122	1.668	1.722
-54	1.240	1.273	126	1.745	1.800
-50	1.280	1.315	130	1.792	1.850
-46	1.339	1.379	134	1.844	1.892
-42	1.391	1.432	138	1.911	1.950
-38	1.398	1.436	142	1.975	2.009
-34	1.454	1.501	146	2.009	2.045
-30	1.453	1.509	150	2.092	2.153
-26	1.509	1.530	154	2.191	2.225
-22	1.530	1.538	158	2.218	2.328
-18	1.535	1.538	162	2.315	2.355
-14	1.556	1.592	166	2.350	2.413
-10	1.607	1.554	170	2.400	2.462
-6	1.541	1.592	174	2.441	2.517
-2	1.566	1.591	178	2.491	2.522

NO SCREEN RE=110000, ST=0.0639 (RUN 2)
MULTIPLIER=0.26083 /MIL LOSS CORRECTION=0.060 MILS

DEG	SH/ \sqrt{RE} Z=-.5"	SH/ \sqrt{RE} Z=+.5"	DEG	SH/ \sqrt{RE} Z=-.5"	SH/ \sqrt{RE} Z=+.5"
-176	2.472	2.468	4	1.572	1.568
-172	2.438	2.434	8	1.544	1.540
-168	2.416	2.412	12	1.528	1.524
-164	2.358	2.354	16	1.520	1.516
-160	2.332	2.328	20	1.525	1.521
-156	2.271	2.267	24	1.515	1.511
-152	2.178	2.174	28	1.505	1.501
-148	2.097	2.093	32	1.471	1.467
-144	2.008	2.004	36	1.423	1.419
-140	1.936	1.932	42	1.390	1.386
-136	1.938	1.934	46	1.372	1.368
-132	1.848	1.844	50	1.334	1.330
-128	1.790	1.786	54	1.286	1.282
-124	1.725	1.721	58	1.211	1.207
-120	1.683	1.679	60	1.137	1.133
-116	1.619	1.615	64	1.038	1.034
-112	1.554	1.550	68	0.907	0.903
-108	1.442	1.438	72	0.826	0.822
-104	1.345	1.341	76	0.773	0.769
-100	1.273	1.269	80	0.760	0.756
-96	1.130	1.126	84	0.784	0.780
-92	1.017	1.013	88	0.814	0.810
-88	0.908	0.904	92	0.831	0.827
-84	0.847	0.843	96	0.951	0.947
-80	0.857	0.853	100	1.080	1.076
-76	0.852	0.848	104	1.202	1.198
-72	0.867	0.863	108	1.319	1.315
-68	0.891	0.887	112	1.396	1.392
-64	0.947	0.943	116	1.495	1.491
-60	1.081	1.077	120	1.551	1.547
-56	1.172	1.168	124	1.616	1.612
-52	1.271	1.267	128	1.698	1.694
-48	1.305	1.301	132	1.764	1.760
-44	1.336	1.332	136	1.810	1.806
-40	1.384	1.380	140	1.836	1.832
-36	1.397	1.393	144	1.916	1.912
-32	1.424	1.420	148	1.989	1.985
-28	1.468	1.464	152	2.062	2.058
-24	1.480	1.476	156	2.138	2.134
-20	1.523	1.519	160	2.213	2.209
-16	1.532	1.528	164	2.268	2.264
-12	1.522	1.518	168	2.310	2.306
-8	1.550	1.546	172	2.378	2.374
-4	1.585	1.581	176	2.448	2.444
0	1.555	1.551	180	2.445	2.441

NO SCREEN RE=125000, ST=0.0
MULTIPLIER=0.25859 /MIL

(FIG 29)
LOSS CORRECTION=0.049 MILS

DEG	SH//RE Z=-.5"	SH//RE Z=+.5"	DEG	SH//RE Z=-.5"	SH//RE Z=+.5"
-176	2.526	2.646	4	1.565	1.617
-172	2.488	2.615	8	1.573	1.583
-168	2.486	2.550	12	1.577	1.554
-164	2.415	2.475	16	1.566	1.590
-160	2.335	2.427	20	1.545	1.569
-156	2.217	2.366	24	1.545	1.574
-152	2.217	2.278	28	1.505	1.552
-148	2.156	2.184	32	1.524	1.538
-144	2.028	2.100	36	1.469	1.503
-140	1.978	2.010	40	1.403	1.471
-136	1.921	1.956	44	1.393	1.441
-132	1.862	1.891	48	1.354	1.375
-128	1.806	1.861	52	1.310	1.324
-124	1.779	1.852	56	1.252	1.275
-120	1.759	1.810	60	1.186	1.189
-116	1.690	1.765	64	1.103	1.119
-112	1.645	1.676	68	1.004	1.011
-108	1.522	1.548	72	0.822	0.825
-104	1.394	1.435	76	0.601	0.596
-100	1.295	1.304	80	0.589	0.631
-96	1.237	1.275	84	0.775	0.852
-92	1.161	1.242	88	1.017	1.109
-88	1.003	1.069	92	1.171	1.307
-84	0.764	0.801	96	1.258	1.362
-80	0.600	0.624	100	1.302	1.395
-76	0.569	0.641	104	1.417	1.503
-72	0.818	0.843	108	1.492	1.565
-68	0.987	1.018	112	1.587	1.721
-64	1.108	1.113	116	1.684	1.748
-60	1.192	1.245	120	1.792	1.814
-56	1.270	1.305	124	1.821	1.874
-52	1.323	1.344	128	1.787	1.888
-48	1.370	1.396	132	1.835	1.923
-44	1.402	1.445	136	1.848	1.972
-40	1.445	1.472	140	1.945	2.038
-36	1.453	1.506	144	2.036	2.109
-32	1.499	1.531	148	2.150	2.218
-28	1.483	1.548	152	2.224	2.323
-24	1.508	1.568	156	2.294	2.385
-20	1.535	1.596	160	2.390	2.441
-16	1.521	1.614	164	2.383	2.495
-12	1.567	1.620	168	2.456	2.555
-8	1.583	1.598	172	2.497	2.602
-4	1.595	1.616	176	2.560	2.643
0	1.570	1.616	180	2.561	2.645

TU=0.339%, L/D=0.028, RE=110000, ST=0.0
MULTIPLIER=0.19724 /MIL

(FIG 34)
LOSS CORRECTION=0.180 MILS

DEG	SH/ \sqrt{RE} Z=-.5"	SH/ \sqrt{RE} Z=+.5"	DEG	SH/ \sqrt{RE} Z=-.5"	SH/ \sqrt{RE} Z=+.5"
-176	2.429	2.465	4	1.572	1.563
-172	2.314	2.411	8	1.568	1.560
-168	2.276	2.355	12	1.550	1.557
-164	2.226	2.306	16	1.532	1.544
-160	2.184	2.250	20	1.536	1.529
-156	2.098	2.165	24	1.452	1.499
-152	2.066	2.088	28	1.469	1.471
-148	1.974	1.973	32	1.443	1.445
-144	1.876	1.909	36	1.433	1.419
-140	1.799	1.810	40	1.424	1.393
-136	1.736	1.726	44	1.348	1.364
-132	1.651	1.688	48	1.351	1.326
-128	1.602	1.646	52	1.299	1.334
-124	1.598	1.654	56	1.227	1.254
-120	1.588	1.631	60	1.183	1.178
-116	1.548	1.563	64	1.088	1.082
-112	1.464	1.435	68	1.014	0.968
-108	1.314	1.383	72	0.838	0.803
-104	1.162	1.180	76	0.581	0.559
-100	1.086	1.097	80	0.496	0.524
-96	1.034	1.075	84	0.628	0.684
-92	1.026	1.057	88	0.854	0.903
-88	0.897	0.896	92	1.034	1.057
-84	0.669	0.666	96	1.019	0.987
-80	0.481	0.473	100	1.058	1.000
-76	0.485	0.452	104	1.220	1.216
-72	0.726	0.692	108	1.348	1.370
-68	0.938	0.898	112	1.484	1.526
-64	1.046	1.025	116	1.560	1.602
-60	1.106	1.079	120	1.615	1.641
-56	1.178	1.154	124	1.614	1.701
-52	1.241	1.217	128	1.646	1.754
-48	1.305	1.278	132	1.672	1.750
-44	1.326	1.311	136	1.719	1.821
-40	1.355	1.333	140	1.783	1.854
-36	1.400	1.383	144	1.851	1.954
-32	1.455	1.401	148	1.913	2.049
-28	1.478	1.417	152	2.041	2.109
-24	1.511	1.491	156	2.133	2.139
-20	1.526	1.533	160	2.191	2.199
-16	1.517	1.527	164	2.220	2.291
-12	1.550	1.534	168	2.282	2.369
-8	1.560	1.532	172	2.352	2.441
-4	1.559	1.546	176	2.402	2.462
0	1.563	1.550	180	2.417	2.485

TU=0.339%, L/D=0.028, RE=110000, ST=0.0639

MULTIPLIER=0.19396 /MIL

LOSS CORRECTION=0.168 MILS

DEG	SH/ \sqrt{RE} Z=-.5"	SH/ \sqrt{RE} Z=+.5"	DEG	SH/ \sqrt{RE} Z=-.5"	SH/ \sqrt{RE} Z=+.5"
-176	2.319	2.387	4	1.557	1.536
-172	2.263	2.313	8	1.548	1.482
-168	2.295	2.311	12	1.544	1.508
-164	2.216	2.256	16	1.515	1.490
-160	2.172	2.196	20	1.512	1.486
-156	2.102	2.193	24	1.476	1.473
-152	2.022	2.079	28	1.416	1.432
-148	1.928	2.004	32	1.405	1.422
-144	1.899	1.921	36	1.380	1.375
-140	1.804	1.855	40	1.362	1.341
-136	1.720	1.821	44	1.318	1.309
-132	1.724	1.765	48	1.269	1.282
-128	1.656	1.702	52	1.243	1.227
-124	1.622	1.651	56	1.174	1.162
-120	1.534	1.562	60	1.074	1.084
-116	1.454	1.476	64	0.983	0.975
-112	1.380	1.397	68	0.858	0.855
-108	1.334	1.330	72	0.792	0.819
-104	1.250	1.259	76	0.770	0.779
-100	1.172	1.162	80	0.728	0.794
-96	1.029	1.033	84	0.733	0.793
-92	0.898	0.910	88	0.741	0.796
-88	0.804	0.813	92	0.806	0.863
-84	0.799	0.785	96	0.923	0.994
-80	0.818	0.797	100	0.951	0.999
-76	0.815	0.794	104	1.113	1.198
-72	0.814	0.779	108	1.236	1.265
-68	0.869	0.850	112	1.300	1.349
-64	0.967	0.927	116	1.394	1.447
-60	1.078	1.064	120	1.461	1.565
-56	1.171	1.136	124	1.476	1.612
-52	1.216	1.201	128	1.594	1.679
-48	1.294	1.263	132	1.657	1.730
-44	1.400	1.296	136	1.704	1.751
-40	1.367	1.300	140	1.871	1.846
-36	1.410	1.368	144	1.832	1.905
-32	1.444	1.398	148	1.903	1.971
-28	1.422	1.446	152	1.962	2.032
-24	1.501	1.442	156	2.043	2.153
-20	1.492	1.466	160	2.125	2.203
-16	1.483	1.475	164	2.198	2.260
-12	1.502	1.478	168	2.248	2.289
-8	1.544	1.525	172	2.301	2.332
-4	1.557	1.539	176	2.311	2.376
0	1.563	1.545	180	2.350	2.378

TU=1.182%, L/D=0.050, RE=110000, ST=0.0 (FIG 35)
 MULTIPLIER=0.19834 /MIL LOSS CORRECTION=0.170 MILS

DEG	SH//RE Z=-.5"	SH//RE Z=+.5"	DEG	SH//RE Z=-.5"	SH//RE Z=+.5"
-176	2.267	2.378	4	1.794	1.792
-172	2.224	2.280	8	1.770	1.747
-168	2.166	2.279	12	1.724	1.765
-164	2.137	2.238	16	1.735	1.726
-160	2.081	2.126	20	1.713	1.710
-156	2.039	2.083	24	1.686	1.698
-152	1.980	2.005	28	1.623	1.654
-148	1.895	1.929	32	1.627	1.630
-144	1.824	1.778	36	1.589	1.570
-140	1.823	1.805	40	1.537	1.522
-136	1.721	1.731	44	1.522	1.471
-132	1.669	1.716	48	1.437	1.417
-128	1.695	1.695	52	1.456	1.476
-124	1.647	1.714	56	1.316	1.274
-120	1.450	1.391	60	1.231	1.195
-116	1.633	1.674	64	1.158	1.089
-112	1.617	1.638	68	0.984	0.946
-108	1.582	1.584	72	0.791	0.710
-104	1.466	1.513	76	0.561	0.510
-100	1.449	1.556	80	0.580	0.598
-96	1.289	1.319	84	0.870	0.895
-92	1.123	1.170	88	1.341	1.559
-88	0.888	0.903	92	1.326	1.373
-84	0.623	0.614	96	1.438	1.488
-80	0.518	0.493	100	1.537	1.567
-76	0.706	0.657	104	1.588	1.588
-72	0.936	0.906	108	1.658	1.666
-68	1.078	1.044	112	1.669	1.681
-64	1.213	1.171	116	1.636	1.702
-60	1.290	1.261	120	1.660	1.886
-56	1.373	1.321	124	1.666	1.704
-52	1.414	1.399	128	1.673	1.713
-48	1.474	1.426	132	1.693	1.792
-44	1.513	1.517	136	1.726	1.777
-40	1.557	1.579	140	1.793	1.855
-36	1.591	1.607	144	1.864	1.886
-32	1.661	1.663	148	1.947	1.988
-28	1.702	1.671	152	1.977	2.075
-24	1.705	1.701	156	2.060	2.137
-20	1.700	1.735	160	2.071	2.189
-16	1.767	1.787	164	2.164	2.287
-12	1.753	1.773	168	2.122	2.166
-8	1.792	1.788	172	2.205	2.361
-4	1.820	1.796	176	2.305	2.414
0	1.806	1.813	-180	2.297	2.344

TU=1.182%, L/D=0.050, RE=110000, ST=0.0639

MULTIPLIER=0.21396 /MIL

LOSS CORRECTION=0.020 MILS

DEG	SH/ \sqrt{RE} Z=-.5"	SH/ \sqrt{RE} Z=+.5"	DEG	SH/ \sqrt{RE} Z=-.5"	SH/ \sqrt{RE} Z=+.5"
-176	2.190	2.359	4	1.765	1.832
-172	2.133	2.450	8	1.772	1.818
-168	2.097	2.364	12	1.739	1.797
-164	2.016	2.233	16	1.712	1.765
-160	1.999	2.150	20	1.692	1.766
-156	1.950	2.051	24	1.677	1.753
-152	1.912	2.027	28	1.653	1.693
-148	1.861	1.999	32	1.626	1.666
-144	1.822	1.903	36	1.559	1.631
-140	1.772	1.848	40	1.517	1.577
-136	1.730	1.809	44	1.431	1.519
-132	1.718	1.808	48	1.416	1.453
-128	1.715	1.769	52	1.329	1.371
-124	1.690	1.729	56	1.257	1.319
-120	1.621	1.681	60	1.133	1.174
-116	1.617	1.659	64	1.017	1.044
-112	1.588	1.664	68	0.897	0.904
-108	1.497	1.584	72	0.825	0.846
-104	1.472	1.478	76	0.758	0.830
-100	1.349	1.418	80	0.799	0.872
-96	1.194	1.262	84	0.800	0.905
-92	1.060	1.080	88	0.867	0.969
-88	0.898	0.950	92	0.988	1.088
-84	0.823	0.889	96	1.172	1.265
-80	0.805	0.843	100	1.332	1.430
-76	0.782	0.838	104	1.422	1.535
-72	0.797	0.855	108	1.510	1.627
-68	0.865	0.924	112	1.581	1.659
-64	0.984	1.053	116	1.604	1.704
-60	1.110	1.173	120	1.653	1.717
-56	1.212	1.280	124	1.650	1.763
-52	1.287	1.369	128	1.693	1.777
-48	1.383	1.409	132	1.714	1.816
-44	1.439	1.496	136	1.752	1.864
-40	1.508	1.578	140	1.825	1.898
-36	1.574	1.586	144	1.847	1.961
-32	1.549	1.646	148	1.900	2.033
-28	1.625	1.666	152	1.985	2.085
-24	1.666	1.732	156	2.002	2.152
-20	1.694	1.774	160	2.072	2.240
-16	1.693	1.756	164	2.154	2.335
-12	1.730	1.790	168	2.206	2.329
-8	1.763	1.806	172	2.201	2.365
-4	1.782	1.811	176	2.207	2.368
0	1.764	1.831	180	2.192	2.339

TU=1.801%, L/D=0.038, RE=110000, ST=0.0
 MULTIPLIER=0.18572 /MIL

(FIG 36)
 LOSS CORRECTION=0.095 MILS

DEG	SH/ \sqrt{RE} Z=-.5"	SH/ \sqrt{RE} Z=+.5"	DEG	SH/ \sqrt{RE} Z=-.5"	SH/ \sqrt{RE} Z=+.5"
-177	1.942	1.971	3	1.915	1.898
-173	1.892	2.022	7	1.886	1.888
-169	1.851	1.888	11	1.862	1.885
-165	1.748	1.789	15	1.868	1.870
-161	1.679	1.722	19	1.852	1.842
-157	1.614	1.649	23	1.831	1.836
-153	1.541	1.562	27	1.792	1.787
-149	1.479	1.494	31	1.745	1.745
-145	1.467	1.450	35	1.734	1.705
-141	1.511	1.483	39	1.639	1.663
-137	1.574	1.585	43	1.589	1.600
-133	1.687	1.699	47	1.530	1.554
-129	1.868	1.863	51	1.481	1.474
-125	2.086	2.069	55	1.422	1.408
-121	2.322	2.326	59	1.342	1.339
-117	2.635	2.571	63	1.258	1.269
-113	2.876	3.022	67	1.172	1.189
-109	3.132	3.202	71	1.056	1.164
-105	2.919	2.925	75	0.955	0.934
-101	2.445	2.466	79	0.848	0.818
-97	2.018	1.995	83	0.732	0.655
-93	1.354	1.373	87	0.835	0.714
-89	0.899	0.788	91	1.117	1.041
-85	0.687	0.576	95	1.686	1.659
-81	0.683	0.697	99	2.156	2.443
-77	0.874	0.914	103	2.532	2.999
-73	1.034	1.132	107	3.049	3.259
-69	1.081	1.060	111	3.016	3.178
-65	1.283	1.260	115	2.634	2.876
-61	1.368	1.342	119	2.471	2.577
-57	1.462	1.408	123	2.205	2.290
-53	1.491	1.456	127	1.970	2.005
-49	1.545	1.522	131	1.824	1.879
-45	1.600	1.577	135	1.680	1.687
-41	1.649	1.595	139	1.573	1.561
-37	1.744	1.661	143	1.533	1.509
-33	1.790	1.728	147	1.567	1.520
-29	1.773	1.754	151	1.608	1.526
-25	1.802	1.795	155	1.655	1.600
-21	1.833	1.796	159	1.709	1.680
-17	1.862	1.850	163	1.667	1.776
-13	1.879	1.849	167	1.826	1.840
-9	1.896	1.884	171	1.886	1.911
-5	1.884	1.890	175	1.933	1.950
-1	1.902	1.893	179	1.946	1.968

TU=1.801%, L/D=0.038, RE=110000, ST=0.0639 (FIG 41)
 MULTIPLIER=0.18564 /MIL LOSS CORRECTION=0.092 MILS

DEG	SH/ \sqrt{RE} Z=-.5"	SH/ \sqrt{RE} Z=+.5"	DEG	SH/ \sqrt{RE} Z=-.5"	SH/ \sqrt{RE} Z=+.5"
-177	1.853	1.887	3	1.943	1.957
-173	1.830	1.866	7	1.944	1.924
-169	1.800	1.864	11	1.913	1.921
-165	1.720	1.784	15	1.943	1.920
-161	1.670	1.715	19	1.881	1.900
-157	1.614	1.650	23	1.886	1.873
-153	1.597	1.610	27	1.844	1.845
-149	1.538	1.662	31	1.816	1.802
-145	1.521	1.628	35	1.751	1.768
-141	1.508	1.568	39	1.730	1.702
-137	1.518	1.608	43	1.686	1.658
-133	1.593	1.662	47	1.640	1.601
-129	1.648	1.707	51	1.584	1.528
-125	1.735	1.779	55	1.521	1.439
-121	1.856	1.893	59	1.440	1.310
-117	2.053	2.093	63	1.308	1.224
-113	2.264	2.321	67	1.163	1.108
-109	2.389	2.355	71	1.078	1.002
-105	2.248	2.210	75	0.978	0.970
-101	2.092	2.073	79	0.934	1.021
-97	1.910	1.891	83	0.975	1.208
-93	1.667	1.707	87	1.043	1.341
-89	1.320	1.043	91	1.203	1.518
-85	1.246	1.345	95	1.600	1.644
-81	1.018	1.135	99	1.795	1.897
-77	0.954	0.976	103	1.989	2.149
-73	0.948	0.919	107	2.170	2.333
-69	1.048	0.997	111	2.296	2.365
-65	1.174	1.095	115	2.395	2.312
-61	1.277	1.234	119	2.198	2.154
-57	1.392	1.363	123	2.023	2.005
-53	1.477	1.458	127	1.886	1.870
-49	1.558	1.523	131	1.742	1.783
-45	1.624	1.643	135	1.698	1.660
-41	1.668	1.639	139	1.626	1.578
-37	1.757	1.719	143	1.584	1.556
-33	1.766	1.760	147	1.588	1.545
-29	1.775	1.815	151	1.568	1.574
-25	1.831	1.814	155	1.561	1.587
-21	1.864	1.871	159	1.592	1.656
-17	1.887	1.899	163	1.618	1.728
-13	1.913	1.897	167	1.688	1.783
-9	1.927	1.934	171	1.783	1.818
-5	1.915	1.936	175	1.815	1.863
-1	1.939	1.924	179	1.818	1.903

TU=2.651%, L/D=0.030, RE= 50000, ST=0.0

MULTIPLIER=0.29838 /MIL

LOSS CORRECTION=0.060 MILS

DEG	SH/ \sqrt{RE} Z=-.5"	SH/ \sqrt{RE} Z=+.5"	DEG	SH/ \sqrt{RE} Z=-.5"	SH/ \sqrt{RE} Z=+.5"
-176	2.036	2.004	4	1.908	1.801
-172	1.983	1.944	8	1.917	1.756
-168	1.925	1.885	12	1.901	1.751
-164	1.790	1.809	16	1.876	1.734
-160	1.709	1.731	20	1.880	1.703
-156	1.652	1.690	24	1.828	1.696
-152	1.595	1.645	28	1.840	1.672
-148	1.530	1.582	32	1.839	1.682
-144	1.513	1.501	36	1.735	1.630
-140	1.425	1.467	40	1.693	1.580
-136	1.408	1.447	44	1.657	1.509
-132	1.441	1.447	48	1.565	1.437
-128	1.439	1.458	52	1.537	1.417
-124	1.438	1.444	56	1.492	1.352
-120	1.440	1.439	60	1.397	1.267
-116	1.427	1.447	64	1.324	1.165
-112	1.404	1.458	68	1.225	1.040
-108	1.406	1.474	72	1.094	0.911
-104	1.382	1.471	76	0.890	0.694
-100	1.298	1.384	80	0.612	0.468
-96	1.161	1.223	84	0.488	0.473
-92	0.943	0.972	88	0.646	0.702
-88	0.708	0.692	92	0.918	1.001
-84	0.516	0.492	96	1.142	1.266
-80	0.584	0.506	100	1.302	1.425
-76	0.852	0.717	104	1.381	1.484
-72	1.090	0.910	108	1.419	1.472
-68	1.242	1.061	112	1.419	1.467
-64	1.324	1.176	116	1.427	1.431
-60	1.405	1.242	120	1.426	1.456
-56	1.492	1.318	124	1.428	1.469
-52	1.528	1.384	128	1.453	1.459
-48	1.592	1.463	132	1.437	1.439
-44	1.636	1.497	136	1.404	1.428
-40	1.672	1.556	140	1.408	1.459
-36	1.697	1.594	144	1.456	1.507
-32	1.759	1.613	148	1.539	1.558
-28	1.780	1.628	152	1.585	1.625
-24	1.845	1.738	156	1.664	1.687
-20	1.907	1.713	160	1.714	1.753
-16	1.889	1.793	164	1.764	1.820
-12	1.895	1.802	168	1.883	1.906
-8	1.895	1.778	172	1.939	1.994
-4	1.880	1.775	176	2.028	2.048
0	1.928	1.825	-180	2.029	2.005

TU=2.651%, L/D=0.030, RE= 50000, ST=0.1406 (FIG 51)
 MULTIPLIER=0.27880 /MIL LOSS CORRECTION=0.105 MILS

DEG	SH/ \sqrt{RE} Z=-.5"	SH/ \sqrt{RE} Z=+.5"	DEG	SH/ \sqrt{RE} Z=-.5"	SH/ \sqrt{RE} Z=+.5"
-177	2.096	2.008	3	1.932	1.782
-173	2.056	1.933	7	1.949	1.785
-169	2.047	1.929	11	1.910	1.789
-165	1.927	1.873	15	1.922	1.736
-161	1.943	1.804	19	1.865	1.725
-157	1.837	1.771	23	1.859	1.759
-153	1.789	1.660	27	1.829	1.706
-149	1.689	1.599	31	1.787	1.780
-145	1.684	1.550	35	1.753	1.679
-141	1.606	1.572	39	1.709	1.609
-137	1.552	1.481	43	1.659	1.546
-133	1.530	1.470	47	1.604	1.485
-129	1.585	1.446	51	1.602	1.410
-125	1.528	1.466	55	1.503	1.377
-121	1.559	1.464	59	1.430	1.273
-117	1.481	1.496	63	1.378	1.215
-113	1.561	1.481	67	1.233	1.036
-109	1.443	1.456	71	1.103	0.960
-105	1.533	1.395	75	1.003	0.778
-101	1.374	1.302	79	0.954	0.872
-97	1.268	1.194	83	0.940	0.889
-93	1.121	1.037	87	0.924	0.947
-89	1.020	0.943	91	0.962	1.006
-85	0.939	0.860	95	1.050	1.121
-81	0.961	0.848	99	1.199	1.243
-77	0.943	0.797	103	1.290	1.434
-73	1.013	0.808	107	1.384	1.476
-69	1.117	0.946	111	1.427	1.473
-65	1.314	1.097	115	1.446	1.537
-61	1.332	1.221	119	1.487	1.546
-57	1.428	1.329	123	1.581	1.503
-53	1.486	1.393	127	1.462	1.546
-49	1.545	1.453	131	1.465	1.512
-45	1.548	1.499	135	1.580	1.498
-41	1.651	1.539	139	1.518	1.596
-37	1.680	1.649	143	1.535	1.638
-33	1.726	1.575	147	1.630	1.571
-29	1.748	1.695	151	1.640	1.625
-25	1.803	1.681	155	1.726	1.689
-21	1.789	1.750	159	1.867	1.844
-17	1.857	1.735	163	1.912	1.817
-13	1.849	1.830	167	1.982	1.857
-9	1.888	1.779	171	2.064	1.928
-5	1.933	1.783	175	2.173	2.015
-1	1.917	1.775	179	2.089	2.004

TU=2.651%, L/D=0.030, RE= 75000, ST=0.0 (RUN 1, FIG 37)
 MULTIPLIER=0.19694 /MIL LOSS CORRECTION=0.295 MILS

DEG	SH/ \sqrt{RE} Z=-.5"	SH/ \sqrt{RE} Z=+.5"	DEG	SH/ \sqrt{RE} Z=-.5"	SH/ \sqrt{RE} Z=+.5"
-176	1.847	1.993	4	1.958	2.028
-172	1.819	1.958	8	1.944	1.930
-168	1.745	1.875	12	1.918	1.952
-164	1.682	1.786	16	1.941	1.940
-160	1.605	1.690	20	1.923	1.962
-156	1.497	1.601	24	1.906	1.925
-152	1.434	1.512	28	1.883	1.902
-148	1.398	1.490	32	1.834	1.839
-144	1.358	1.438	36	1.784	1.809
-140	1.324	1.398	40	1.759	1.776
-136	1.322	1.374	44	1.707	1.724
-132	1.348	1.427	48	1.664	1.643
-128	1.396	1.420	52	1.582	1.567
-124	1.486	1.540	56	1.515	1.475
-120	1.583	1.607	60	1.448	1.428
-116	1.673	1.792	64	1.333	1.320
-112	1.875	1.899	68	1.282	1.216
-108	2.041	2.107	72	1.233	1.079
-104	2.219	2.230	76	0.947	0.871
-100	2.176	2.239	80	0.667	0.592
-96	1.871	1.964	84	0.436	0.421
-92	1.307	1.427	88	0.631	0.663
-88	0.792	0.855	92	1.145	1.207
-84	0.482	0.476	96	1.725	1.791
-80	0.615	0.504	100	2.114	2.209
-76	0.902	0.788	104	2.176	2.269
-72	1.108	1.132	108	2.093	2.130
-68	1.261	1.118	112	1.934	1.962
-64	1.390	1.236	116	1.720	1.786
-60	1.489	1.333	120	1.602	1.681
-56	1.527	1.411	124	1.478	1.557
-52	1.623	1.445	128	1.413	1.466
-48	1.697	1.536	132	1.344	1.412
-44	1.756	1.591	136	1.300	1.369
-40	1.807	1.648	140	1.326	1.361
-36	1.841	1.692	144	1.369	1.387
-32	1.878	1.722	148	1.399	1.445
-28	1.903	1.783	152	1.468	1.513
-24	1.927	1.823	156	1.524	1.584
-20	1.941	1.830	160	1.616	1.675
-16	1.951	1.880	164	1.657	1.737
-12	1.962	1.903	168	1.750	1.852
-8	1.942	1.916	172	1.841	1.952
-4	1.995	1.916	176	1.850	1.992
0	1.964	1.939	180	1.864	1.973

TU=2.651%, L/D=0.030, RE= 75000, ST=0.0 (RUN 2)
 MULTIPLIER=0.19726 /MIL LOSS CORRECTION=0.030 MILS

DEG	SH/ \sqrt{RE} Z=-.5"	SH/ \sqrt{RE} Z=+.5"	DEG	SH/ \sqrt{RE} Z=-.5"	SH/ \sqrt{RE} Z=+.5"
-176	1.743	1.977	4	1.980	1.955
-172	1.699	1.912	8	1.963	1.960
-168	1.634	1.834	12	1.940	1.957
-164	1.586	1.737	16	1.924	1.941
-160	1.482	1.652	20	1.899	1.926
-156	1.407	1.525	24	1.906	1.908
-152	1.337	1.495	28	1.825	1.871
-148	1.265	1.375	32	1.781	1.831
-144	1.235	1.308	36	1.744	1.778
-140	1.213	1.282	40	1.681	1.766
-136	1.186	1.260	44	1.695	1.692
-132	1.235	1.291	48	1.560	1.651
-128	1.304	1.341	52	1.481	1.593
-124	1.379	1.431	56	1.390	1.485
-120	1.445	1.536	60	1.303	1.415
-116	1.613	1.616	64	1.240	1.321
-112	1.776	1.812	68	1.180	1.209
-108	1.984	1.984	72	1.078	1.076
-104	2.145	2.150	76	0.898	0.880
-100	2.112	2.177	80	0.605	0.621
-96	1.859	1.923	84	0.370	0.457
-92	1.318	1.411	88	0.530	0.694
-88	0.792	0.825	92	0.999	1.243
-84	0.499	0.448	96	1.521	1.796
-80	0.613	0.446	100	1.966	2.191
-76	0.936	0.702	104	2.106	2.267
-72	1.140	0.939	108	1.971	2.128
-68	1.297	1.073	112	1.778	1.953
-64	1.392	1.203	116	1.612	1.798
-60	1.451	1.292	120	1.478	1.658
-56	1.517	1.384	124	1.370	1.574
-52	1.576	1.437	128	1.299	1.466
-48	1.622	1.516	132	1.228	1.416
-44	1.664	1.565	136	1.178	1.373
-40	1.712	1.614	140	1.186	1.379
-36	1.759	1.661	144	1.200	1.378
-32	1.789	1.672	148	1.242	1.445
-28	1.836	1.758	152	1.311	1.502
-24	1.868	1.787	156	1.364	1.578
-20	1.904	1.838	160	1.464	1.656
-16	1.923	1.857	164	1.548	1.757
-12	1.952	1.903	168	1.592	1.789
-8	1.966	1.918	172	1.678	1.832
-4	1.970	1.947	176	1.721	1.919
0	1.975	1.946	-180	1.745	1.986

TU=2.651%, L/D=0.030, RE= 75000, ST=0.0417 (FIG 49)
 MULTIPLIER=0.20291 /MIL LOSS CORRECTION=0.030 MILS

DEG	SH/ \sqrt{RE} Z=-.5"	SH/ \sqrt{RE} Z=+.5"	DEG	SH/ \sqrt{RE} Z=-.5"	SH/ \sqrt{RE} Z=+.5"
-176	1.957	1.914	4	2.108	2.131
-172	1.918	1.914	8	2.105	2.093
-168	1.880	1.838	12	2.086	2.083
-164	1.805	1.774	16	2.071	1.987
-160	1.710	1.704	20	2.053	2.034
-156	1.607	1.623	24	2.006	2.011
-152	1.551	1.569	28	1.981	1.988
-148	1.504	1.485	32	1.937	2.004
-144	1.449	1.449	36	1.912	1.932
-140	1.434	1.444	40	1.848	1.870
-136	1.442	1.441	44	1.797	1.809
-132	1.485	1.460	48	1.752	1.734
-128	1.551	1.538	52	1.662	1.690
-124	1.659	1.625	56	1.576	1.608
-120	1.782	1.746	60	1.417	1.495
-116	1.887	1.887	64	1.241	1.387
-112	1.900	1.965	68	1.130	1.232
-108	1.921	1.987	72	1.012	1.094
-104	1.907	1.871	76	0.962	0.994
-100	1.705	1.665	80	0.936	0.915
-96	1.465	1.505	84	1.016	1.050
-92	1.194	1.309	88	1.185	1.231
-88	0.990	1.145	92	1.259	1.359
-84	0.889	0.952	96	1.564	1.540
-80	0.861	0.910	100	1.734	1.715
-76	1.085	0.863	104	1.859	1.860
-72	1.135	1.019	108	0.0	0.0
-68	1.244	1.201	112	1.904	1.948
-64	1.408	1.365	116	1.885	1.851
-60	1.506	1.470	120	1.798	1.755
-56	1.562	1.549	124	1.682	1.645
-52	1.649	1.721	128	1.603	1.534
-48	1.701	1.650	132	1.583	1.465
-44	1.722	1.732	136	1.493	1.442
-40	1.759	1.811	140	1.464	1.457
-36	1.790	1.861	144	1.457	1.451
-32	1.856	1.894	148	1.510	1.469
-28	1.904	1.949	152	1.571	1.567
-24	1.956	2.016	156	1.645	1.624
-20	2.009	2.030	160	1.709	1.706
-16	2.045	2.052	164	1.781	1.798
-12	2.082	2.057	168	1.881	1.853
-8	2.103	2.059	172	1.837	1.920
-4	2.086	2.106	176	1.979	1.946
0	2.112	2.106	-180	1.983	1.933

TU=2.651%, L/D=0.030, RE= 75000, ST=0.1041 (FIG 50)
 MULTIPLIER=0.20290 /MIL LOSS CORRECTION=0.030 MILS

DEG	SH/ \sqrt{RE} Z=-.5"	SH/ \sqrt{RE} Z=+.5"	DEG	SH/ \sqrt{RE} Z=-.5"	SH/ \sqrt{RE} Z=+.5"
-178	1.926	1.940	2	1.970	1.959
-174	1.918	1.917	6	1.961	1.977
-170	1.896	1.885	10	1.949	1.974
-166	1.813	1.852	14	1.958	1.963
-162	1.745	1.761	18	1.950	1.957
-158	1.666	1.684	22	1.928	1.938
-154	1.612	1.622	26	1.911	1.909
-150	1.532	1.574	30	1.893	1.888
-156	1.479	1.497	34	1.841	1.828
-152	1.446	1.458	38	1.799	1.807
-138	1.440	1.454	42	1.724	1.771
-134	1.481	1.452	46	1.681	1.700
-130	1.572	1.518	50	1.607	1.631
-126	1.645	1.537	54	1.608	1.539
-122	1.735	1.628	58	1.443	1.526
-118	1.866	1.732	62	1.294	1.401
-114	1.931	1.881	66	1.184	1.297
-110	1.927	1.935	70	1.067	1.152
-106	1.880	1.928	74	0.962	0.988
-102	1.746	1.763	78	0.940	0.922
-98	1.700	1.653	82	1.086	0.993
-94	1.451	1.491	86	1.189	1.114
-90	1.243	1.352	90	1.376	1.279
-86	1.080	1.220	94	1.517	1.386
-82	0.947	1.050	98	1.646	1.513
-78	0.924	0.880	102	1.762	1.710
-74	0.979	0.883	106	1.870	1.878
-70	1.062	0.946	110	1.927	1.954
-66	1.176	1.145	114	1.925	1.951
-62	1.306	1.279	118	1.824	1.893
-58	1.388	1.376	122	1.673	1.788
-54	1.464	1.449	126	1.616	1.653
-50	1.544	1.532	130	1.572	1.567
-46	1.614	1.616	134	1.506	1.514
-42	1.673	1.672	138	1.500	1.493
-38	1.754	1.848	142	1.509	1.483
-34	1.800	1.743	146	1.533	1.475
-30	1.853	1.810	150	1.568	1.533
-26	1.873	1.839	154	1.626	1.593
-22	1.905	1.881	158	1.683	1.651
-18	1.911	1.917	162	1.715	1.721
-14	1.923	1.935	166	1.761	1.784
-10	1.951	1.965	170	1.818	1.832
-6	1.962	1.960	174	1.898	1.903
-2	1.971	1.964	178	1.916	1.937

TU=2.651%, L/D=0.030, RE=110000, ST=0.0 (RUN 1, FIG 38)
 MULTIPLIER=0.19374 /MIL LOSS CORRECTION=0.056 MILS

DEG	SH/ \sqrt{RE} Z=-.5"	SH/ \sqrt{RE} Z=+.5"	DEG	SH/ \sqrt{RE} Z=-.5"	SH/ \sqrt{RE} Z=+.5"
-178	1.960	1.957	2	2.062	2.091
-174	1.929	1.906	6	2.071	2.106
-170	1.868	1.853	10	2.077	2.079
-166	1.771	1.745	14	2.065	2.099
-162	1.674	1.602	18	2.039	2.074
-158	1.555	1.492	22	2.026	2.038
-154	1.424	1.368	28	1.994	1.970
-150	1.318	1.293	32	1.962	1.926
-146	1.259	1.221	36	1.914	1.898
-142	1.220	1.252	40	1.903	1.904
-138	1.314	1.339	44	1.846	1.803
-134	1.418	1.500	46	1.789	1.765
-130	1.676	1.689	50	1.734	1.691
-126	1.918	1.979	54	1.710	1.611
-122	2.213	2.273	58	1.635	1.548
-118	2.595	2.706	62	1.541	1.456
-114	3.056	3.134	66	1.488	1.379
-110	3.526	3.584	70	1.351	1.268
-106	3.880	3.739	74	1.278	1.163
-102	3.328	2.963	78	1.157	0.999
-98	2.117	1.671	82	0.942	0.794
-94	0.966	0.671	86	0.652	0.515
-90	0.471	0.436	90	0.471	0.521
-86	0.630	0.670	94	0.891	1.298
-82	0.925	0.950	98	1.954	2.572
-78	1.122	1.121	102	3.244	3.201
-74	1.283	1.256	106	0.0	0.0
-70	1.359	1.363	110	0.0	0.0
-66	1.466	1.461	114	3.148	2.876
-62	1.542	1.548	118	2.679	2.468
-58	1.610	1.576	122	2.306	2.099
-54	1.694	1.672	126	1.978	1.817
-50	1.736	1.732	130	1.725	1.576
-46	1.775	1.784	134	1.512	1.423
-42	1.832	1.835	138	1.353	1.299
-38	1.878	1.900	142	1.282	1.250
-34	1.913	1.932	146	1.274	1.254
-30	1.960	1.957	150	1.296	1.341
-26	1.954	2.013	154	1.376	1.473
-22	2.040	2.011	158	1.498	1.575
-18	2.035	2.085	162	1.638	1.685
-14	2.068	2.115	166	1.747	1.792
-10	2.073	2.094	170	1.849	1.859
-6	2.082	2.106	174	1.926	1.925
-2	2.079	2.123	178	1.938	1.948

TU=2.651%, L/D=0.030, RE=110000, ST=0.0 (RUN 2)
 MULTIPLIER=0.20601 /MIL LOSS CORRECTION=0.076 MILS

DEG	SH/ \sqrt{RE} Z=-.5"	SH/ \sqrt{RE} Z=+.5"	DEG	SH/ \sqrt{RE} Z=-.5"	SH/ \sqrt{RE} Z=+.5"
-178	2.026	2.087	2	2.127	2.114
-174	2.011	2.017	6	2.082	2.099
-170	1.925	1.913	10	2.099	2.091
-166	1.821	1.811	14	2.055	2.079
-162	1.704	1.681	18	2.052	2.057
-158	1.588	1.570	22	2.045	2.022
-154	1.487	1.479	26	2.007	1.998
-150	1.363	1.405	30	1.964	1.981
-146	1.344	1.377	34	1.979	1.935
-142	1.384	1.404	38	1.914	1.893
-138	1.479	1.473	42	1.855	1.842
-134	1.647	1.649	46	1.827	1.779
-130	1.840	1.840	50	1.791	1.715
-126	2.111	2.103	54	1.720	1.650
-122	2.436	2.391	58	1.644	1.473
-118	2.811	2.790	62	1.587	1.498
-114	3.266	3.242	66	1.506	1.405
-110	3.455	3.483	70	1.390	1.314
-106	3.445	3.481	74	1.261	1.203
-102	2.751	3.119	78	1.073	1.036
-98	1.511	1.953	82	0.818	0.762
-94	0.631	0.921	86	0.550	0.492
-90	0.400	0.492	90	0.885	0.760
-86	0.709	0.742	94	1.887	1.731
-82	0.987	1.076	98	3.201	3.015
-78	1.166	1.237	102	3.752	3.634
-74	1.254	1.378	106	3.762	3.655
-70	1.362	1.480	110	3.384	3.336
-66	1.454	1.520	114	2.961	2.899
-62	1.526	1.573	118	2.579	2.517
-58	1.609	1.632	122	2.210	2.166
-54	1.646	1.681	126	1.932	1.877
-50	1.715	1.764	130	1.753	1.634
-46	1.764	1.801	134	1.584	1.460
-42	1.812	1.888	138	1.475	1.383
-38	1.845	1.925	142	1.450	1.348
-34	1.914	1.966	146	1.467	1.373
-30	1.954	1.986	150	1.534	1.419
-26	1.990	2.008	154	1.646	1.549
-22	2.021	2.030	158	1.742	1.677
-18	2.045	2.068	162	1.867	1.830
-14	2.075	2.087	166	1.932	1.934
-10	2.110	2.097	170	2.012	2.028
-6	2.091	2.098	174	2.049	2.015
-2	2.103	2.113	178	2.064	2.011

TU=2.651%, L/D=0.030, RE=110000, ST=0.0071 (RUN 1, FIG 43)
 MULTIPLIER=0.20525 /MIL LOSS CORRECTION=0.004 MILS

DEG	SH//RE Z=-.5"	SH//RE Z=+.5"	DEG	SH//RE Z=-.5"	SH//RE Z=+.5"
-176	1.930	1.880	4	2.131	2.154
-172	1.882	1.786	8	2.134	2.132
-168	1.790	1.789	12	2.123	2.082
-164	1.729	1.777	16	2.114	2.081
-160	1.621	1.714	20	2.099	2.067
-156	1.568	1.559	24	2.066	2.057
-152	1.463	1.490	28	1.957	1.989
-148	1.417	1.402	32	1.999	1.993
-144	1.398	1.420	36	1.949	1.952
-140	1.453	1.432	40	1.908	1.897
-136	1.582	1.511	44	1.875	1.849
-132	1.726	1.708	48	1.795	1.794
-128	1.954	1.952	52	1.763	1.719
-124	2.342	2.208	56	1.732	1.667
-120	2.712	2.620	60	1.661	1.589
-116	3.052	2.943	64	1.587	1.517
-112	3.023	3.080	68	1.490	1.408
-108	2.740	2.882	72	1.404	1.291
-104	2.459	2.612	76	1.237	1.141
-100	2.225	2.344	80	1.089	0.998
-96	2.056	2.120	84	1.149	1.028
-92	1.736	1.887	88	1.382	1.240
-88	1.301	1.464	92	1.817	1.668
-84	1.031	1.130	96	2.188	2.031
-80	0.937	0.971	100	2.332	2.240
-76	1.151	1.086	104	2.589	2.439
-72	1.255	1.257	108	2.862	2.731
-68	1.365	1.397	112	3.138	3.012
-64	1.446	1.511	116	3.137	3.107
-60	1.533	1.580	120	2.938	2.849
-56	1.570	1.650	124	2.556	2.441
-52	1.653	1.729	128	2.215	2.063
-48	1.749	1.792	132	1.938	1.796
-44	1.767	1.856	136	1.716	1.589
-40	1.889	1.902	140	1.590	1.462
-36	1.930	1.943	144	1.505	1.421
-32	1.973	1.982	148	1.486	1.419
-28	2.019	2.053	152	1.507	1.450
-24	2.043	2.062	156	1.600	1.494
-20	2.073	2.087	160	1.696	1.624
-16	2.091	2.107	164	1.748	1.690
-12	2.127	2.104	168	1.868	1.806
-8	2.144	2.121	172	1.932	1.849
-4	2.146	2.153	176	1.938	1.862
0	2.154	2.150	180	1.938	1.906

TU=2.651%, L/D=0.030, RE=110000, ST=0.0071 (RUN 2)

MULTIPLIER=0.22151 /MIL

LOSS CORRECTION=0.068 MILS

DEG	SH/ \sqrt{RE} Z=-.5"	SH/ \sqrt{RE} Z=+.5"	DEG	SH/ \sqrt{RE} Z=-.5"	SH/ \sqrt{RE} Z=+.5"
-178	1.898	1.928	2	2.210	2.275
-174	1.866	1.878	6	2.211	2.263
-170	1.832	1.839	10	2.204	2.263
-166	1.729	1.770	14	2.199	2.242
-162	1.634	1.675	18	2.097	2.228
-158	1.543	1.562	22	2.165	2.206
-154	1.465	1.458	26	2.116	2.152
-150	1.390	1.400	30	2.106	2.131
-146	1.394	1.381	34	2.060	2.090
-142	1.445	1.425	38	2.037	2.007
-138	1.550	1.530	42	1.993	1.953
-134	1.736	1.685	46	1.948	1.947
-130	2.005	1.928	50	1.866	1.898
-126	2.311	2.249	54	1.797	1.799
-122	2.702	2.596	58	1.735	1.775
-118	3.020	2.978	62	1.687	1.684
-114	3.015	3.035	66	1.590	1.570
-110	2.746	2.828	70	1.436	1.451
-106	2.475	2.541	74	1.268	1.276
-102	2.278	2.342	78	1.107	1.094
-98	2.107	2.143	82	1.052	1.053
-94	1.747	1.849	86	1.268	1.240
-90	1.336	1.425	90	1.710	1.660
-86	1.067	1.101	94	2.052	2.078
-82	1.050	1.047	98	2.304	2.287
-78	1.225	1.169	102	2.489	2.490
-74	1.409	1.346	106	2.786	2.773
-70	1.516	1.484	110	3.084	3.082
-66	1.627	1.595	114	3.107	3.163
-62	1.697	1.667	118	2.872	2.873
-58	1.762	1.737	122	2.449	2.501
-54	1.869	1.822	126	2.069	2.112
-50	1.903	1.853	130	1.770	1.826
-46	1.935	1.953	134	1.589	1.624
-42	1.984	1.969	138	1.474	1.480
-38	2.046	2.032	142	1.407	1.414
-34	2.082	2.090	146	1.388	1.400
-30	2.122	2.105	150	1.413	1.435
-26	2.148	2.158	154	1.502	1.503
-22	2.165	2.180	158	1.600	1.604
-18	2.169	2.240	162	1.744	1.715
-14	2.207	2.269	166	1.817	1.774
-10	2.207	2.268	170	1.854	1.880
-6	2.199	2.270	174	1.900	1.933
-2	2.214	2.270	178	1.922	1.929

TU=2.651%, L/D=0.030, RE=110000, ST=0.0213 (RUN 1, FIG 44)
 MULTIPLIER=0.20256 /MIL LOSS CORRECTION=0.102 MILS

DEG	SH/ \sqrt{RE} Z=-.5"	SH/ \sqrt{RE} Z=+.5"	DEG	SH/ \sqrt{RE} Z=-.5"	SH/ \sqrt{RE} Z=+.5"
-176	1.904	1.932	4	2.194	2.183
-172	1.884	1.895	8	2.218	2.193
-168	1.825	1.842	12	2.206	2.177
-164	1.734	1.745	16	2.178	2.142
-160	1.652	1.659	20	2.122	2.133
-156	1.527	1.563	24	2.085	2.118
-152	1.447	1.487	28	2.087	2.020
-148	1.409	1.414	32	2.042	2.041
-144	1.411	1.402	36	1.982	2.001
-140	1.446	1.439	40	1.952	1.949
-136	1.563	1.549	44	1.917	1.881
-132	1.733	1.676	48	1.866	1.823
-128	1.976	1.888	52	1.777	1.766
-124	2.307	2.207	56	1.747	1.691
-120	2.686	2.537	60	1.671	1.633
-116	3.010	2.904	64	1.568	1.568
-112	3.018	2.998	68	1.464	1.459
-108	2.767	2.792	72	1.466	1.342
-104	2.457	2.497	76	1.195	1.183
-100	2.265	2.255	80	1.049	1.040
-96	2.095	2.056	84	1.080	1.051
-92	1.808	1.831	88	1.259	1.240
-88	1.413	1.464	92	1.659	1.646
-84	1.130	1.137	96	2.014	1.951
-80	1.073	0.996	100	2.145	2.114
-76	1.187	1.078	104	2.339	2.301
-72	1.356	1.253	108	2.575	2.551
-68	1.500	1.386	112	2.871	2.831
-64	1.606	1.501	116	2.945	3.912
-60	1.655	1.586	120	2.708	2.720
-56	1.719	1.658	124	2.346	2.434
-52	1.785	1.730	128	2.031	2.042
-48	1.864	1.796	132	1.778	1.790
-44	1.882	1.831	136	1.598	1.602
-40	1.963	1.897	140	1.478	1.482
-36	1.981	1.942	144	1.409	1.416
-32	2.055	2.035	148	1.379	1.383
-28	2.081	2.027	152	1.406	1.419
-24	2.135	2.052	156	1.492	1.495
-20	2.163	2.091	160	1.591	1.580
-16	2.159	2.111	164	1.622	1.618
-12	2.189	2.151	168	1.744	1.774
-8	2.186	2.188	172	1.810	1.856
-4	2.238	2.194	176	1.899	1.904
0	2.188	2.189	180	1.911	1.909

TU=2.651%, L/D=0.030, RE=110000, ST=0.0213 (RUN 2)

MULTIPLIER=0.20509 /MIL

LOSS CORRECTION=0.065 MILS

DEG	SH/ \sqrt{RE} Z=-.5"	SH/ \sqrt{RE} Z=+.5"	DEG	SH/ \sqrt{RE} Z=-.5"	SH/ \sqrt{RE} Z=+.5"
-178	1.875	1.935	2	2.154	2.121
-174	1.818	1.855	6	2.151	2.122
-170	1.759	1.809	10	2.135	2.119
-166	1.689	1.756	14	2.112	2.082
-162	1.597	1.674	18	2.077	2.099
-158	1.526	1.587	22	2.065	2.063
-154	1.442	1.469	26	2.012	1.999
-150	1.368	1.401	30	1.976	1.981
-146	1.397	1.384	34	1.950	1.937
-142	1.468	1.416	38	1.873	1.886
-138	1.574	1.529	42	1.795	1.850
-134	1.728	1.676	46	1.810	1.776
-130	1.972	1.908	50	1.723	1.662
-126	2.287	2.180	54	1.646	1.630
-122	2.619	2.537	58	1.600	1.562
-118	2.963	2.896	62	1.509	1.502
-114	2.922	3.018	66	1.451	1.368
-110	2.617	2.834	70	1.312	1.255
-106	2.448	2.546	74	1.172	1.117
-102	2.251	2.242	78	1.045	0.977
-98	2.050	2.111	82	0.956	0.964
-94	1.794	1.844	86	1.355	1.292
-90	1.428	1.478	90	1.752	1.667
-86	1.128	1.148	94	2.092	1.995
-82	1.039	0.966	98	2.241	2.203
-78	1.162	1.056	102	2.470	2.413
-74	1.321	1.214	106	2.729	2.699
-70	1.437	1.369	110	2.965	3.084
-66	1.534	1.453	114	3.029	2.997
-62	1.614	1.534	118	2.807	2.712
-58	1.688	1.602	122	2.439	2.387
-54	1.733	1.704	126	2.083	2.055
-50	1.847	1.707	130	1.827	1.766
-46	1.851	1.820	134	1.624	1.586
-42	1.889	1.855	138	1.445	1.468
-38	1.941	1.860	142	1.434	1.410
-34	1.974	1.904	146	1.432	1.390
-30	1.983	1.958	150	1.432	1.462
-26	2.048	2.020	154	1.524	1.515
-22	2.080	2.059	158	1.595	1.635
-18	2.093	2.078	162	1.689	1.669
-14	2.114	2.099	166	1.769	1.747
-10	2.110	2.105	170	1.840	1.831
-6	2.142	2.115	174	1.863	1.941
-2	2.162	2.119	178	1.895	1.926

TU=2.651%, L/D=0.030, RE=110000, ST=0.0213 (FIG 52)
 MULTIPLIER=0.23927 /MIL LOSS CORRECTION=0.068 MILS
 OSCILLATION AMPLITUDE INCREASED TO 12 DEGREES

DEG	SH/ \sqrt{RE} Z=-.5"	SH/ \sqrt{RE} Z=+.5"	DEG	SH/ \sqrt{RE} Z=-.5"	SH/ \sqrt{RE} Z=+.5"
-177	1.608	1.603	3	2.177	2.180
-173	1.592	1.591	7	2.189	2.178
-169	1.519	1.562	11	2.162	2.146
-165	1.484	1.500	15	2.132	2.123
-161	1.442	1.427	19	2.101	2.104
-157	1.440	1.363	23	2.084	2.078
-153	1.429	1.278	27	2.046	2.047
-149	1.415	1.249	31	2.012	2.035
-145	1.409	1.317	35	1.971	1.983
-141	1.462	1.437	39	1.930	1.952
-137	1.580	1.524	43	1.892	1.879
-133	1.785	1.697	47	1.837	1.815
-129	2.159	1.925	51	1.783	1.752
-125	2.343	2.287	55	1.701	1.627
-121	2.385	2.344	59	1.605	1.531
-117	2.259	2.186	63	1.474	1.482
-113	2.081	2.036	67	1.333	1.359
-109	1.950	1.912	71	1.161	1.180
-105	1.928	1.923	75	1.033	1.034
-101	1.963	1.929	79	1.043	0.866
-97	1.898	1.888	83	1.287	1.324
-93	1.923	1.824	87	1.668	1.682
-89	1.787	1.703	91	1.879	1.909
-85	1.505	1.385	95	1.962	1.990
-81	1.228	1.072	99	1.930	1.978
-77	0.973	1.017	103	1.924	2.011
-73	1.092	1.079	107	1.963	2.005
-69	1.307	1.293	111	2.078	2.086
-65	1.458	1.441	115	2.197	2.216
-61	1.532	1.544	119	2.338	2.321
-57	1.634	1.628	123	2.377	2.442
-53	1.717	1.718	127	2.325	2.284
-49	1.789	1.803	131	2.030	2.010
-45	1.886	1.905	135	1.595	1.601
-41	1.943	1.927	139	1.510	1.476
-37	1.982	1.973	143	1.453	1.338
-33	2.026	2.012	147	1.398	1.325
-29	2.057	2.043	151	1.384	1.314
-25	2.121	2.083	155	1.399	1.344
-21	2.125	2.146	159	1.428	1.407
-17	2.143	2.137	163	1.464	1.459
-13	2.182	2.136	167	1.507	1.502
-9	2.169	2.143	171	1.546	1.543
-5	2.184	2.184	175	1.587	1.583
-1	2.183	2.194	179	1.611	1.617

TU=2.651%, L/D=0.030, RE=110000, ST=0.0355 (RUN 1, FIG 45)
 MULTIPLIER=0.21920 /MIL LOSS CORRECTION=0.070 MILS

DEG	SH/ \sqrt{RE} Z=-.5"	SH/ \sqrt{RE} Z=+.5"	DEG	SH/ \sqrt{RE} Z=-.5"	SH/ \sqrt{RE} Z=+.5"
-176	1.942	1.921	4	2.271	2.268
-172	1.895	1.876	8	2.204	2.241
-168	1.854	1.794	12	2.232	2.256
-164	1.751	1.732	16	2.197	2.245
-160	1.637	1.635	20	2.187	2.187
-156	1.544	1.542	24	2.163	2.171
-152	1.459	1.449	28	2.122	2.060
-148	1.407	1.399	32	2.094	2.057
-144	1.399	1.396	36	2.078	2.021
-140	1.467	1.456	40	2.008	1.969
-136	1.599	1.568	44	1.954	1.940
-132	1.796	1.751	48	1.907	1.862
-128	2.051	1.988	52	1.815	1.815
-124	2.416	2.317	56	1.773	1.749
-120	2.816	2.704	60	1.715	1.670
-116	3.120	3.039	64	1.601	1.574
-112	3.100	2.980	68	1.489	1.477
-108	2.826	2.745	72	1.386	1.355
-104	2.550	2.432	76	1.224	1.159
-100	2.316	2.204	80	1.091	1.053
-96	2.120	2.044	84	1.049	1.036
-92	1.814	1.784	88	1.320	1.320
-88	1.390	1.378	92	1.700	1.719
-84	1.088	1.054	96	2.036	1.960
-80	1.054	0.989	100	2.200	2.199
-76	1.211	1.107	104	2.393	2.431
-72	1.369	1.280	108	2.691	2.687
-68	1.504	1.425	112	2.960	2.952
-64	1.603	1.533	116	3.080	3.083
-60	1.699	1.612	120	2.838	2.791
-56	1.761	1.708	124	2.467	2.463
-52	1.844	1.784	128	2.149	2.053
-48	1.891	1.854	132	1.837	1.776
-44	1.944	1.913	136	1.628	1.575
-40	1.985	1.973	140	1.450	1.487
-36	2.024	1.991	144	1.395	1.379
-32	2.102	2.073	148	1.417	1.404
-28	2.119	2.135	152	1.454	1.436
-24	2.172	2.166	156	1.527	1.513
-20	2.165	2.183	160	1.620	1.620
-16	2.228	2.235	164	1.744	1.696
-12	2.262	2.241	168	1.893	1.794
-8	2.273	2.263	172	1.879	1.865
-4	2.280	2.281	176	1.942	1.933
0	2.256	2.288	180	1.959	1.943

TU=2.651%, L/D=0.030, RE=110000, ST=0.0355 (RUN 2)

MULTIPLIER=0.23509 /MIL

LOSS CORRECTION=0.062 MILS

DEG	SH/ \sqrt{RE} Z=-.5"	SH/ \sqrt{RE} Z=+.5"	DEG	SH/ \sqrt{RE} Z=-.5"	SH/ \sqrt{RE} Z=+.5"
-176	1.930	1.920	4	2.308	2.249
-172	1.871	1.878	8	2.300	2.262
-168	1.778	1.787	12	2.293	2.280
-164	1.707	1.698	16	2.281	2.217
-160	1.555	1.598	20	2.240	2.219
-156	1.481	1.507	24	2.210	2.173
-152	1.455	1.453	28	2.246	2.144
-148	1.421	1.425	32	2.104	2.098
-144	1.455	1.434	36	2.026	2.003
-140	1.558	1.520	40	1.979	1.938
-136	1.659	1.631	44	1.941	1.890
-132	1.932	1.860	48	1.885	1.827
-128	2.228	2.123	52	1.818	1.617
-124	2.575	2.490	56	1.719	1.716
-120	2.935	2.811	60	1.693	1.608
-116	3.063	3.020	64	1.605	1.524
-112	2.883	2.919	68	1.476	1.425
-108	2.571	2.673	72	1.339	1.250
-104	2.338	2.353	76	1.153	1.079
-100	2.181	2.177	80	1.010	1.013
-96	1.948	1.952	84	1.179	1.171
-92	1.552	1.606	88	1.509	1.549
-88	1.187	1.233	92	1.949	1.901
-84	1.034	1.011	96	2.189	2.110
-80	1.238	1.070	100	2.358	2.330
-76	1.310	1.220	104	2.631	2.604
-72	1.469	1.401	108	2.941	2.903
-68	1.587	1.515	112	3.116	3.062
-64	1.674	1.617	116	3.018	2.925
-60	1.740	1.696	120	2.675	2.546
-56	1.808	1.777	124	2.264	2.192
-52	1.865	1.884	128	1.948	1.902
-48	1.905	1.915	132	1.703	1.688
-44	2.017	1.950	136	1.552	1.525
-40	2.037	2.031	140	1.422	1.452
-36	2.079	2.075	144	1.436	1.429
-32	2.141	2.091	148	1.433	1.472
-28	2.136	2.182	152	1.494	1.527
-24	2.193	2.216	156	1.591	1.617
-20	2.218	2.213	160	1.679	1.697
-16	2.245	2.268	164	1.776	1.799
-12	2.260	2.267	168	1.882	1.868
-8	2.285	2.285	172	1.895	1.954
-4	2.297	2.301	176	1.957	1.966
0	2.304	2.283	180	1.956	1.966

TU=2.651%, L/D=0.030, RE=110000, ST=0.0497 (RUN 1, FIG 46)
 MULTIPLIER=0.20514 /MIL LOSS CORRECTION=0.107 MILS

DEG	SH/ \sqrt{RE} Z=-.5"	SH/ \sqrt{RE} Z=+.5"	DEG	SH/ \sqrt{RE} Z=-.5"	SH/ \sqrt{RE} Z=+.5"
-176	1.899	1.871	4	2.296	2.290
-172	1.846	1.891	8	2.271	2.255
-168	1.801	1.838	12	2.257	2.266
-164	1.735	1.773	16	2.251	2.224
-160	1.621	1.683	20	2.228	2.243
-156	1.518	1.573	24	2.211	2.201
-152	1.465	1.467	28	2.143	2.177
-148	1.396	1.419	32	2.103	2.135
-144	1.410	1.413	36	2.071	2.128
-140	1.486	1.462	40	2.023	2.066
-136	1.627	1.599	44	1.990	2.017
-132	1.845	1.792	48	1.983	1.955
-128	2.125	2.052	52	1.864	1.890
-124	2.479	2.411	56	1.775	1.774
-120	2.901	2.770	60	1.768	1.771
-116	3.151	3.098	64	1.736	1.701
-112	3.070	3.074	68	1.598	1.597
-108	2.701	2.807	72	1.481	1.479
-104	2.430	2.498	76	1.314	1.323
-100	2.314	2.327	80	1.187	1.144
-96	2.116	2.130	84	1.090	1.087
-92	1.809	1.809	88	1.287	1.258
-88	1.345	1.435	92	1.678	1.657
-84	1.126	1.130	96	2.088	2.052
-80	1.147	1.079	100	2.266	2.279
-76	1.306	1.233	104	2.411	2.398
-72	1.480	1.399	108	2.693	2.625
-68	1.590	1.546	112	2.963	2.878
-64	1.588	1.497	116	3.185	3.102
-60	1.744	1.705	120	3.184	3.017
-56	1.841	1.783	124	2.630	2.618
-52	1.919	1.894	128	2.178	2.206
-48	1.975	1.952	132	1.858	1.900
-44	2.028	2.025	136	1.658	1.656
-40	2.049	2.075	140	1.508	1.497
-36	2.101	2.106	144	1.418	1.422
-32	2.154	2.160	148	1.382	1.413
-28	2.182	2.206	152	1.440	1.465
-24	2.189	2.245	156	1.489	1.529
-20	2.236	2.239	160	1.594	1.603
-16	2.258	2.251	164	1.646	1.682
-12	2.281	2.295	168	1.756	1.766
-8	2.289	2.317	172	1.831	1.855
-4	2.305	2.320	176	1.895	1.857
0	2.290	2.294	180	1.885	1.853

TU=2.651%, L/D=0.030, RE=110000, ST=0.0497 (RUN 2)

MULTIPLIER=0.22538 /MIL

LOSS CORRECTION=0.108 MILS

DEG	SH/ \sqrt{RE} Z=-.5"	SH/ \sqrt{RE} Z=+.5"	DEG	SH/ \sqrt{RE} Z=-.5"	SH/ \sqrt{RE} Z=+.5"
-176	1.905	1.930	4	2.318	2.335
-172	1.833	1.918	8	2.234	2.322
-168	1.785	1.777	12	2.307	2.321
-164	1.690	1.628	16	2.246	2.281
-160	1.593	1.568	20	2.238	2.240
-156	1.522	1.495	24	2.219	2.204
-152	1.452	1.409	28	2.168	2.131
-148	1.361	1.340	32	2.127	2.070
-144	1.443	1.436	38	2.022	2.029
-140	1.519	1.552	42	1.951	1.920
-136	1.686	1.736	46	1.963	1.872
-132	1.939	2.037	50	1.874	1.816
-128	2.240	2.340	54	1.810	1.770
-124	2.682	2.771	56	1.743	1.663
-120	3.051	3.078	60	1.744	1.624
-116	3.200	3.103	64	1.604	1.498
-112	2.891	2.916	68	1.467	1.383
-108	2.621	2.557	72	1.328	1.192
-104	2.198	2.182	76	1.215	1.019
-100	2.136	2.059	80	1.032	0.991
-96	1.916	1.725	84	1.090	1.197
-92	1.503	1.367	88	1.378	1.634
-88	1.114	1.034	92	1.838	2.037
-84	0.978	0.946	96	2.168	2.234
-80	1.056	1.039	100	2.355	2.469
-76	1.214	1.242	104	2.587	2.677
-72	1.385	1.343	108	2.835	2.990
-68	1.454	1.470	112	3.189	3.130
-64	1.600	1.622	116	3.234	2.987
-60	1.671	1.694	120	2.876	2.586
-56	1.751	1.769	124	2.516	2.180
-52	1.808	1.855	128	2.029	1.838
-48	1.923	1.943	132	1.780	1.598
-44	1.898	1.991	136	1.528	1.430
-40	1.992	2.070	140	1.443	1.411
-36	2.029	2.123	144	1.381	1.419
-32	2.074	2.112	148	1.357	1.410
-28	2.162	2.230	152	1.420	1.499
-24	2.223	2.257	156	1.510	1.549
-20	2.245	2.232	160	1.660	1.722
-16	2.297	2.249	164	1.755	1.800
-12	2.303	2.330	168	1.837	1.833
-8	2.285	2.318	172	1.854	1.904
-4	2.285	2.354	176	1.904	1.958
0	2.330	2.346	180	1.940	1.931

TU=2.651%, L/D=0.030, RE=110000, ST=0.0497 (RUN 3)

MULTIPLIER=0.23505 /MIL

LOSS CORRECTION=0.100 MILS

DEG	SH/ \sqrt{RE} Z=-.5"	SH/ \sqrt{RE} Z=+.5"	DEG	SH/ \sqrt{RE} Z=-.5"	SH/ \sqrt{RE} Z=+.5"
-176	1.875	2.006	4	2.311	2.298
-172	1.860	1.885	8	2.303	2.289
-168	1.760	1.820	12	2.277	2.259
-164	1.700	1.758	16	2.259	2.264
-160	1.618	1.654	20	2.250	2.251
-156	1.487	1.566	24	2.154	2.199
-152	1.430	1.466	28	2.124	2.140
-148	1.413	1.401	32	2.081	2.119
-144	1.384	1.397	36	2.057	2.070
-140	1.443	1.446	40	1.997	2.041
-136	1.378	1.347	44	1.981	1.977
-132	1.786	1.750	48	1.879	1.900
-128	2.058	2.041	52	1.865	1.860
-124	2.407	2.388	56	1.767	1.778
-120	2.837	2.785	60	1.692	1.719
-116	3.139	3.093	64	1.623	1.621
-112	3.045	3.113	68	1.550	1.532
-108	2.767	2.820	72	1.481	1.415
-104	2.515	2.520	76	1.305	1.250
-100	2.280	2.322	80	1.136	1.090
-96	2.124	2.128	84	1.025	0.992
-92	1.801	1.829	88	1.162	1.130
-88	1.347	1.410	92	1.567	1.529
-84	1.107	1.095	96	1.986	1.935
-80	1.112	1.020	100	2.207	2.165
-76	1.288	1.185	104	2.326	2.349
-72	1.444	1.342	108	2.594	2.597
-68	1.565	1.474	112	2.875	2.823
-64	1.668	1.576	116	3.030	3.078
-60	1.749	1.655	120	2.930	2.965
-56	1.841	1.764	124	2.595	2.600
-52	1.883	1.819	128	2.213	2.234
-48	1.924	1.888	132	1.865	1.870
-44	1.981	1.951	136	1.611	1.626
-40	2.043	2.002	140	1.457	1.457
-36	2.099	2.052	144	1.386	1.360
-32	2.176	2.107	148	1.353	1.329
-28	2.187	2.135	152	1.378	1.347
-24	2.265	2.192	156	1.439	1.434
-20	2.292	2.195	160	1.490	1.533
-16	2.302	2.234	164	1.621	1.635
-12	2.299	2.242	168	1.742	1.770
-8	2.321	2.290	172	1.801	1.821
-4	2.335	2.296	176	1.882	1.883
0	2.320	2.300	180	1.886	1.917

TU=2.651%, L/D=0.030, RE=110000, ST=0.0497 (RUN 4)
 MULTIPLIER=0.23679 /MIL LOSS CORRECTION=0.082 MILS

DEG	SH/ \sqrt{RE} Z=-.5"	SH/ \sqrt{RE} Z=+.5"	DEG	SH/ \sqrt{RE} Z=-.5"	SH/ \sqrt{RE} Z=+.5"
-176	1.873	1.887	4	2.311	2.301
-172	1.819	1.869	8	2.303	2.307
-168	1.786	1.828	12	2.294	2.323
-164	1.699	1.777	16	2.251	2.304
-160	1.626	1.736	20	2.226	2.274
-156	1.550	1.610	24	2.222	2.245
-152	1.442	1.526	28	2.172	2.189
-148	1.399	1.503	32	2.119	2.135
-144	1.436	1.473	36	2.094	2.108
-140	1.518	1.514	40	2.030	2.057
-136	1.637	1.664	44	2.011	2.026
-132	1.840	1.729	48	1.949	1.947
-128	2.095	1.988	52	1.898	1.876
-124	2.436	2.325	56	1.863	1.785
-120	2.851	2.787	60	1.745	1.726
-116	3.144	3.088	64	1.674	1.629
-112	3.037	3.088	68	1.556	1.533
-108	2.658	2.823	72	1.427	1.378
-104	2.408	2.549	76	1.261	1.196
-100	2.214	2.330	80	1.107	1.078
-96	2.057	2.112	84	1.146	1.148
-92	1.732	1.817	88	1.426	1.450
-88	1.333	1.429	92	1.850	1.841
-84	1.098	1.101	96	2.137	2.202
-80	1.098	1.039	100	2.376	2.414
-76	1.253	1.186	104	2.556	2.560
-72	1.423	1.375	108	2.753	2.762
-68	1.526	1.506	112	3.014	3.033
-64	1.639	1.608	116	3.175	3.101
-60	1.747	1.699	120	2.917	2.872
-56	1.808	1.784	124	2.508	2.454
-52	1.881	1.877	128	2.202	2.092
-48	1.947	1.957	132	1.913	1.835
-44	2.008	2.004	136	1.618	1.578
-40	2.042	2.066	140	1.510	1.466
-36	2.080	2.108	144	1.431	1.387
-32	2.143	2.171	148	1.435	1.489
-28	2.190	2.211	152	1.498	1.544
-24	2.209	2.258	156	1.542	1.599
-20	2.230	2.247	160	1.647	1.663
-16	2.270	2.278	164	1.689	1.733
-12	2.268	2.306	168	1.781	1.832
-8	2.293	2.305	172	1.905	1.952
-4	2.314	2.328	176	1.929	1.970
0	2.321	2.332	180	1.942	1.988

TU=2.651%, L/D=0.030, RE=110000, ST=0.0639 (RUN 1, FIG 47)
 MULTIPLIER=0.30104 /MIL LOSS CORRECTION=0.077 MILS

DEG	SH/ \sqrt{RE} Z=-.5"	SH/ \sqrt{RE} Z=+.5"	DEG	SH/ \sqrt{RE} Z=-.5"	SH/ \sqrt{RE} Z=+.5"
-176	1.918	1.898	4	2.283	2.300
-172	1.867	1.892	8	2.262	2.266
-168	1.787	1.824	12	2.231	2.246
-164	1.724	1.750	16	2.225	2.233
-160	1.635	1.645	20	2.193	2.201
-156	1.526	1.550	24	2.154	2.176
-152	1.429	1.450	28	2.109	2.139
-148	1.414	1.406	32	2.076	2.104
-144	1.410	1.403	36	2.036	2.054
-140	1.488	1.455	40	2.003	2.017
-136	1.578	1.582	44	1.948	1.961
-132	1.772	1.797	48	1.884	1.908
-128	2.065	2.012	52	1.836	1.806
-124	2.422	2.311	56	1.761	1.781
-120	2.857	2.675	60	1.689	1.697
-116	3.082	2.940	64	1.608	1.582
-112	3.029	2.897	68	1.516	1.496
-108	2.669	2.664	72	1.389	1.346
-104	2.444	2.357	76	1.219	1.170
-100	2.201	2.212	80	1.057	1.034
-96	2.013	2.020	84	1.037	1.048
-92	1.744	1.750	88	1.323	1.371
-88	1.344	1.407	92	1.754	1.765
-84	1.062	1.095	96	2.070	2.085
-80	1.023	0.981	100	2.291	2.287
-76	1.198	1.078	104	2.488	2.472
-72	1.319	1.269	108	2.733	2.719
-68	1.472	1.422	112	2.972	2.994
-64	1.579	1.502	116	3.040	2.980
-60	1.664	1.673	120	2.800	2.770
-56	1.749	1.769	124	2.421	2.387
-52	1.839	1.846	128	2.078	2.091
-48	1.876	1.907	132	1.806	1.863
-44	1.955	1.951	136	1.660	1.635
-40	2.016	2.009	140	1.427	1.447
-36	2.054	2.054	144	1.402	1.391
-32	2.100	2.098	148	1.367	1.392
-28	2.160	2.155	152	1.410	1.482
-24	2.216	2.163	156	1.494	1.552
-20	2.249	2.235	160	1.561	1.638
-16	2.267	2.264	164	1.692	1.705
-12	2.269	2.274	168	1.768	1.823
-8	2.260	2.292	172	1.853	1.884
-4	2.290	2.303	176	1.902	1.935
0	2.290	2.281	180	1.939	1.941

TU=2.651%, L/D=0.030, RE=110000, ST=0.0639 (RUN 2)

MULTIPLIER=0.19963 /MIL

LOSS CORRECTION=0.070 MILS

DEG	SH/ \sqrt{RE} Z=-.5"	SH/ \sqrt{RE} Z=+.5"	DEG	SH/ \sqrt{RE} Z=-.5"	SH/ \sqrt{RE} Z=+.5"
-178	1.872	1.847	2	2.270	2.251
-174	1.836	1.829	6	2.263	2.258
-170	1.773	1.747	10	2.248	2.242
-166	1.712	1.648	14	2.359	2.239
-162	1.631	1.563	18	2.227	2.242
-158	1.543	1.485	22	2.198	2.181
-154	1.456	1.417	26	2.157	2.122
-150	1.364	1.351	30	2.083	2.069
-146	1.332	1.329	34	2.066	2.075
-142	1.368	1.370	38	2.054	2.017
-138	1.498	1.525	42	2.001	1.952
-134	1.656	1.692	46	1.916	1.853
-130	1.881	1.948	50	1.858	1.774
-126	2.193	2.261	54	1.794	1.729
-122	2.570	2.267	58	1.686	1.690
-118	2.911	2.936	62	1.684	1.599
-114	2.981	2.872	66	1.568	1.486
-110	2.728	2.646	70	1.475	1.370
-106	2.486	2.409	74	1.307	1.219
-102	2.318	2.208	78	1.160	1.073
-98	2.124	2.032	82	1.051	1.021
-94	1.865	1.760	86	1.068	1.150
-90	1.494	1.372	90	1.356	1.542
-86	1.153	1.041	94	1.728	1.853
-82	1.058	1.016	98	1.985	2.060
-78	1.137	1.140	102	1.157	2.239
-74	1.314	1.315	106	2.338	2.437
-70	1.458	1.449	110	2.556	2.697
-66	1.561	1.555	114	2.818	2.961
-62	1.626	1.642	118	2.959	2.828
-58	1.714	1.625	122	2.669	2.401
-54	1.793	1.766	126	2.335	2.138
-50	1.871	1.833	130	1.995	1.850
-46	1.906	1.901	134	1.717	1.613
-42	1.946	1.992	138	1.525	1.458
-38	2.030	2.019	142	1.374	1.323
-34	2.062	2.046	146	1.337	1.344
-30	2.121	2.082	150	1.348	1.359
-26	2.162	2.178	154	1.379	1.452
-22	2.193	2.181	158	1.468	1.549
-18	2.207	2.200	162	1.560	1.614
-14	2.228	2.230	166	1.643	1.736
-10	2.232	2.308	170	1.710	1.782
-6	2.277	2.310	174	1.794	1.830
-2	2.294	2.304	178	1.853	1.866

TU=2.651%, L/D=0.030, RE=110000, ST=0.0639 (RUN 3)

MULTIPLIER=0.21404 /MIL

LOSS CORRECTION=0.030 MILS

DEG	SH/ \sqrt{RE} Z=-.5"	SH/ \sqrt{RE} Z=+.5"	DEG	SH/ \sqrt{RE} Z=-.5"	SH/ \sqrt{RE} Z=+.5"
-178	1.904	1.895	2	2.315	2.365
-174	1.866	1.873	6	2.324	2.393
-170	1.830	1.809	10	2.299	2.360
-166	1.737	1.745	14	2.281	2.389
-162	1.625	1.647	18	2.267	2.324
-158	1.581	1.518	22	2.233	2.298
-154	1.449	1.449	26	2.218	2.251
-150	1.398	1.411	30	2.164	2.225
-146	1.367	1.366	34	2.151	2.190
-142	1.401	1.426	40	2.092	2.128
-138	1.496	1.543	44	2.050	2.060
-134	1.662	1.730	48	2.018	1.981
-130	1.844	1.954	52	1.959	1.896
-126	2.227	2.323	56	1.869	1.872
-122	2.627	2.769	58	1.792	1.800
-118	2.971	3.025	62	1.742	1.706
-114	3.007	2.973	66	1.680	1.619
-110	2.755	2.733	70	1.168	1.248
-106	2.484	2.458	74	1.418	1.321
-102	2.303	2.245	78	1.231	1.162
-98	2.115	2.093	82	1.091	1.105
-94	1.873	1.829	86	1.083	1.240
-90	1.507	1.379	90	1.433	1.660
-86	1.130	1.064	94	1.863	2.024
-82	1.077	1.047	98	2.172	2.239
-78	1.152	1.184	102	2.291	2.380
-74	1.390	1.357	106	2.503	2.580
-70	1.541	1.503	110	2.726	2.888
-66	1.607	1.613	114	2.958	2.965
-62	1.716	1.660	118	2.984	2.939
-58	1.832	1.756	122	2.754	2.554
-54	1.907	1.870	126	2.372	2.110
-50	1.995	1.955	130	1.987	1.802
-46	1.996	2.012	134	1.719	1.573
-42	2.077	2.069	138	1.513	1.409
-38	2.130	2.096	142	1.386	1.366
-34	2.118	2.199	146	1.348	1.349
-30	2.175	2.236	150	1.354	1.420
-26	2.228	2.295	154	1.415	1.481
-22	2.236	2.314	158	1.487	1.556
-18	2.255	2.291	162	1.596	1.662
-14	2.290	2.362	166	1.670	1.740
-10	2.317	2.378	170	1.773	1.838
-6	2.333	2.402	174	1.864	1.901
-2	2.310	2.392	178	1.854	1.919

TU=2.651%, L/D=0.030, RE=110000, ST=0.0781 (FIG 49)
 MULTIPLIER=0.20449 /MIL LOSS CORRECTION=0.083 MILS

DEG	SH/ \sqrt{RE} Z=-.5"	SH/ \sqrt{RE} Z=+.5"	DEG	SH/ \sqrt{RE} Z=-.5"	SH/ \sqrt{RE} Z=+.5"
-176	1.903	1.966	4	2.206	2.262
-172	1.875	1.942	8	2.196	2.261
-168	1.830	1.851	12	2.192	2.249
-164	1.740	1.740	16	2.196	2.244
-160	1.616	1.680	20	2.176	2.194
-156	1.529	1.587	24	2.157	2.181
-152	1.439	1.496	28	2.106	2.135
-148	1.413	1.458	32	2.050	2.103
-144	1.415	1.437	36	2.051	2.056
-140	1.522	1.559	40	1.988	1.997
-136	1.640	1.630	44	1.939	1.931
-132	1.835	1.802	48	1.880	1.892
-128	2.094	2.089	52	1.780	1.818
-124	2.484	2.381	56	1.755	1.697
-120	2.827	2.781	60	1.681	1.669
-116	3.008	3.003	64	1.570	1.566
-112	2.872	2.951	68	1.471	1.457
-108	2.636	2.750	72	1.315	1.307
-104	2.417	2.475	76	1.152	1.120
-100	2.190	2.247	80	1.027	1.034
-96	2.038	2.071	84	1.082	1.166
-92	1.739	1.786	88	1.409	1.502
-88	1.351	1.439	92	1.788	1.869
-84	1.081	1.135	96	2.047	2.076
-80	1.038	1.030	100	2.225	2.305
-76	1.173	1.117	104	2.421	2.498
-72	1.342	1.306	108	2.644	2.770
-68	1.484	1.447	112	2.932	3.048
-64	1.607	1.571	116	3.053	2.994
-60	1.645	1.639	120	2.796	2.707
-56	1.744	1.719	124	2.415	2.393
-52	1.819	1.798	128	2.041	2.059
-48	1.896	1.868	132	1.800	1.823
-44	1.944	1.942	136	1.603	1.635
-40	1.989	1.992	140	1.476	1.504
-36	2.056	2.040	144	1.410	1.437
-32	2.087	2.108	148	1.425	1.417
-28	2.091	2.138	152	1.476	1.477
-24	2.147	2.152	156	1.520	1.549
-20	2.183	2.214	160	1.649	0.0
-16	2.211	2.225	164	1.678	0.0
-12	2.218	2.248	168	1.752	1.758
-8	2.221	2.228	172	1.864	1.981
-4	2.249	2.252	176	1.906	1.990
0	2.208	2.248	180	1.934	2.029

TU=4.9%, L/D=0.188, RE=110000, ST=0.0

MULTIPLIER=0.23086 /MIL

LOSS CORRECTION=0.035 MILS

DEG	SH/ \sqrt{RE} Z=-.5"	SH/ \sqrt{RE} Z=+.5"	DEG	SH/ \sqrt{RE} Z=-.5"	SH/ \sqrt{RE} Z=+.5"
-176	1.839	1.987	4	1.987	2.000
-172	1.737	1.927	8	1.977	1.999
-168	1.673	1.835	12	1.973	1.987
-164	1.515	1.696	16	1.963	1.981
-160	1.419	1.551	20	1.928	1.960
-156	1.290	1.341	24	1.922	1.932
-152	1.213	1.333	28	1.885	1.900
-148	1.194	1.281	32	1.846	1.890
-144	1.263	1.312	36	1.829	1.832
-140	1.418	1.425	40	1.772	1.745
-136	1.626	1.632	44	1.723	1.747
-132	1.887	1.898	48	1.680	1.647
-128	2.212	2.207	52	1.612	1.613
-124	2.550	2.583	56	1.548	1.567
-120	2.977	3.058	60	1.475	1.478
-116	3.575	3.453	64	1.407	1.425
-112	3.429	3.880	68	1.340	1.348
-108	3.523	3.444	72	1.263	1.284
-104	2.335	2.696	76	1.162	1.188
-100	1.089	1.350	80	1.001	1.058
-96	0.519	0.586	84	0.875	0.883
-92	0.543	0.484	88	0.707	0.659
-88	0.785	0.713	92	0.553	0.469
-84	0.931	0.917	96	0.725	0.740
-80	1.055	1.078	100	1.752	1.697
-76	1.262	1.204	104	3.080	3.091
-72	1.309	1.290	108	3.743	3.959
-68	1.366	1.347	112	3.536	3.831
-64	1.434	1.428	116	3.078	3.372
-60	1.504	1.506	120	2.670	2.924
-56	1.565	1.573	124	2.219	2.476
-52	1.617	1.616	128	1.887	2.124
-48	1.681	1.669	132	1.574	1.797
-44	1.728	1.719	136	1.370	1.564
-40	1.781	1.767	140	1.218	1.389
-36	1.827	1.771	144	1.124	1.265
-32	1.900	1.804	148	1.097	1.247
-28	1.908	1.875	152	1.129	1.273
-24	1.931	1.915	156	1.243	1.396
-20	1.958	1.902	160	1.401	1.539
-16	1.972	1.960	164	1.531	1.678
-12	1.973	1.956	168	1.666	1.813
-8	1.974	1.995	172	1.768	1.907
-4	1.984	1.987	176	1.840	1.958
0	1.988	2.015	-180	1.860	2.010

TU=4.9%, L/D=0.188, RE=110000, ST=0.0071

MULTIPLIER=0.23546 /MIL

LOSS CORRECTION=0.024 MILS

DEG	SH/ \sqrt{RE} Z=-.5"	SH/ \sqrt{RE} Z=+.5"	DEG	SH/ \sqrt{RE} Z=-.5"	SH/ \sqrt{RE} Z=+.5"
-178	1.724	1.780	2	1.983	1.991
-174	1.714	1.786	6	1.965	1.990
-170	1.673	1.758	10	1.966	1.983
-166	1.617	1.745	14	1.948	1.971
-162	1.554	1.583	18	1.933	1.951
-158	1.446	1.500	22	1.907	1.930
-154	1.369	1.410	26	1.877	1.890
-150	1.312	1.347	30	1.838	1.870
-146	1.274	1.328	34	1.800	1.824
-142	1.299	1.364	38	1.771	1.808
-138	1.375	1.418	42	1.727	1.777
-134	1.610	1.567	46	1.683	1.730
-130	1.757	1.832	50	1.637	1.658
-126	2.052	2.105	54	1.583	1.624
-122	2.385	2.457	58	1.523	1.557
-118	2.703	2.817	62	1.450	1.512
-114	2.786	2.988	66	1.409	1.449
-110	2.549	2.766	70	1.324	1.349
-106	2.330	2.524	74	1.234	1.263
-102	2.093	2.256	78	1.132	1.143
-98	1.864	2.057	82	0.974	1.021
-94	1.543	1.728	86	0.871	0.881
-90	1.108	1.256	90	0.877	0.851
-86	0.838	0.900	94	1.111	1.053
-82	0.862	0.844	98	1.493	1.434
-78	0.941	0.953	102	1.877	1.851
-74	1.109	1.103	106	2.088	2.151
-70	1.215	1.226	110	2.330	2.378
-66	1.329	1.321	114	2.576	2.619
-62	1.435	1.410	118	2.832	2.864
-58	1.491	1.454	122	2.898	2.916
-54	1.558	1.529	126	2.636	2.724
-50	1.621	1.564	130	2.226	2.389
-46	1.667	1.646	134	1.984	2.102
-42	1.739	1.682	138	1.684	1.726
-38	1.779	1.743	142	1.489	1.500
-34	1.818	1.781	146	1.346	1.341
-30	1.859	1.824	150	1.294	1.336
-26	1.893	1.860	154	1.263	1.283
-22	1.929	1.890	158	1.321	1.310
-18	1.944	1.929	162	1.374	1.395
-14	1.959	1.960	166	1.462	1.512
-10	1.969	1.974	170	1.565	1.586
-6	1.975	1.978	174	1.679	1.696
-2	1.982	1.997	178	1.707	1.745

TU=4.9%, L/D=0.188, RE=110000, ST=0.0213

MULTIPLIER=0.20143 /MIL

LOSS CORRECTION=0.030 MILS

DEG	SH/ \sqrt{RE} Z=-.5"	SH/ \sqrt{RE} Z=+.5"	DEG	SH/ \sqrt{RE} Z=-.5"	SH/ \sqrt{RE} Z=+.5"
-176	1.761	1.873	4	1.983	2.011
-172	1.765	1.824	8	1.965	2.014
-168	1.696	1.781	12	1.971	2.004
-164	1.606	1.714	16	1.969	1.977
-160	1.512	1.602	20	1.946	1.976
-156	1.454	1.483	24	1.903	1.928
-152	1.353	1.427	28	1.896	1.895
-148	1.361	1.376	32	1.850	1.887
-144	1.362	1.348	36	1.836	1.846
-140	1.407	1.403	40	1.759	1.786
-136	1.524	1.528	44	1.722	1.733
-132	1.693	1.725	48	1.649	1.699
-128	1.979	1.995	52	1.605	1.662
-124	2.285	2.322	56	1.552	1.604
-120	2.642	2.670	60	1.594	1.540
-116	2.875	2.932	64	1.457	1.484
-112	2.723	2.831	68	1.377	1.407
-108	2.540	2.554	72	1.283	1.320
-104	2.183	2.309	76	1.213	1.231
-100	2.027	2.112	80	1.070	1.116
-96	1.772	1.835	84	0.951	0.971
-92	1.365	1.469	88	0.870	0.889
-88	1.023	1.068	92	1.002	1.012
-84	0.825	0.879	96	1.385	1.377
-80	0.896	0.893	100	1.796	1.824
-76	1.025	1.032	104	2.104	2.116
-72	1.084	1.126	108	2.221	2.321
-68	1.217	1.226	112	2.516	2.548
-64	1.314	1.318	116	2.790	2.790
-60	1.405	1.397	120	2.926	3.009
-56	1.464	1.447	124	2.792	2.842
-52	1.530	1.512	128	2.422	2.610
-48	1.567	1.660	132	2.074	2.236
-44	1.629	1.620	136	1.831	1.877
-40	1.681	1.675	140	1.613	1.650
-36	1.728	1.771	144	1.464	1.467
-32	1.795	1.782	148	1.350	1.367
-28	1.846	1.838	152	1.323	1.330
-24	1.911	1.872	156	1.363	1.349
-20	1.876	1.923	160	1.406	1.418
-16	1.921	1.952	164	1.489	1.523
-12	1.928	1.965	168	1.558	1.603
-8	1.960	1.926	172	1.631	1.708
-4	1.915	2.007	176	1.695	1.811
0	1.999	2.022	180	1.750	1.848

TU=4.9%, L/D=0.188, RE=110000, ST=0.0355

MULTIPLIER=0.21068 /MIL

LOSS CORRECTION=0.010 MILS

DEG	SH/ \sqrt{RE} Z=-.5"	SH/ \sqrt{RE} Z=+.5"	DEG	SH/ \sqrt{RE} Z=-.5"	SH/ \sqrt{RE} Z=+.5"
-176	1.622	1.736	4	1.960	1.991
-172	1.605	1.759	8	1.931	1.986
-168	1.571	1.697	12	1.933	1.981
-164	1.504	1.616	16	1.933	1.974
-160	1.424	1.536	20	1.918	1.960
-156	1.358	1.440	24	1.896	1.941
-152	1.289	1.362	28	1.852	1.914
-148	1.229	1.318	32	1.833	1.889
-144	1.213	1.369	36	1.771	1.848
-140	1.227	1.333	40	1.752	1.811
-136	1.412	1.498	44	1.716	1.762
-132	1.656	1.657	48	1.685	1.720
-128	1.887	1.942	52	1.647	1.638
-124	2.225	2.277	56	1.587	1.585
-120	2.547	2.688	60	1.528	1.530
-116	2.762	2.891	64	1.448	1.441
-112	2.692	2.768	68	1.369	1.344
-108	2.516	2.529	72	1.286	1.255
-104	2.333	2.354	76	1.178	1.159
-100	2.068	2.157	80	1.077	1.135
-96	1.704	1.924	84	0.962	0.960
-92	1.212	1.532	88	0.931	0.858
-88	0.960	1.152	92	1.002	0.902
-84	0.906	0.877	96	1.235	1.172
-80	0.922	0.882	100	1.561	1.596
-76	1.058	1.042	104	1.984	1.950
-72	1.204	1.161	108	2.177	2.172
-68	1.304	1.281	112	2.411	2.312
-64	1.400	1.373	116	2.611	2.534
-60	1.484	1.426	120	2.769	2.772
-56	1.548	1.504	124	2.737	2.786
-52	1.649	1.596	128	2.601	2.479
-48	1.674	1.679	132	2.130	2.107
-44	1.733	1.728	136	1.806	1.888
-40	1.766	1.789	140	1.591	1.563
-36	1.803	1.827	144	1.394	1.372
-32	1.862	1.873	148	1.248	1.297
-28	1.861	1.900	152	1.229	1.201
-24	1.885	1.919	156	1.232	1.269
-20	1.906	1.939	160	1.264	1.333
-16	1.961	1.958	164	1.310	1.406
-12	1.958	1.972	168	1.361	1.506
-8	1.963	1.981	172	1.411	1.601
-4	1.947	1.977	176	1.538	1.672
0	1.952	1.999	180	1.579	1.730

TU=4.9%, L/D=0.188, RE=110000, ST=0.0497

MULTIPLIER=0.20682 /MIL

LOSS CORRECTION=0.015 MILS

DEG	SH/ \sqrt{RE} Z=-.5"	SH/ \sqrt{RE} Z=+.5"	DEG	SH/ \sqrt{RE} Z=-.5"	SH/ \sqrt{RE} Z=+.5"
-176	1.749	1.816	4	2.030	2.031
-172	1.717	1.884	8	2.034	2.026
-168	1.671	1.786	12	2.025	2.014
-164	1.610	1.721	16	2.003	2.011
-160	1.538	1.647	20	1.991	1.991
-156	1.471	1.545	24	1.965	1.957
-152	1.411	1.470	28	1.943	1.915
-148	1.432	1.435	32	1.927	1.868
-144	1.460	1.419	36	1.884	1.861
-140	1.411	1.463	40	1.851	1.836
-136	1.532	1.593	44	1.791	1.768
-132	1.828	1.794	48	1.716	1.713
-128	2.084	2.042	52	1.656	1.668
-124	2.458	2.542	56	1.581	1.642
-120	2.722	2.704	60	1.490	1.545
-116	2.846	2.966	64	1.387	1.478
-112	2.841	2.851	68	1.303	1.410
-108	2.685	2.667	72	1.232	1.330
-104	2.432	2.418	76	1.127	1.196
-100	2.111	2.182	80	1.033	1.092
-96	1.821	1.967	84	0.938	0.939
-92	1.605	1.618	88	0.897	0.881
-88	1.079	1.176	92	0.972	1.028
-84	0.921	0.934	96	1.204	1.382
-80	0.963	0.902	100	1.674	1.822
-76	1.070	1.030	104	1.957	2.011
-72	1.185	1.179	108	2.381	2.221
-68	1.287	1.306	112	2.565	2.482
-64	1.405	1.385	116	2.693	2.721
-60	1.492	1.474	120	2.697	2.914
-56	1.561	1.520	124	2.596	2.866
-52	1.634	1.595	128	2.253	2.481
-48	1.694	1.679	132	1.972	2.144
-44	1.741	1.708	136	1.727	1.859
-40	1.793	1.752	140	1.588	1.607
-36	1.830	1.819	144	1.445	1.485
-32	1.886	1.837	148	1.354	1.361
-28	1.910	1.887	152	1.330	1.321
-24	1.953	1.918	156	1.378	1.356
-20	2.000	1.963	160	1.475	1.415
-16	2.016	1.967	164	1.541	1.504
-12	2.021	2.022	168	0.0	1.656
-8	2.030	2.002	172	0.0	1.718
-4	2.032	2.033	176	1.736	1.799
0	2.041	2.028	180	1.764	1.815

TU=4.9%, L/D=0.188, RE=110000, ST=0.0639

MULTIPLIER=0.22453 /MIL

LOSS CORRECTION=0.020 MILS

DEG	SH/ \sqrt{RE} Z=-.5"	SH/ \sqrt{RE} Z=+.5"	DEG	SH/ \sqrt{RE} Z=-.5"	SH/ \sqrt{RE} Z=+.5"
-176	1.764	1.766	4	1.984	1.983
-172	1.749	1.755	8	1.986	1.966
-168	1.690	1.703	12	1.984	1.947
-164	1.634	1.659	16	1.975	1.942
-160	1.542	1.574	20	1.946	1.921
-156	1.453	1.441	24	1.913	1.967
-152	1.382	1.378	28	1.858	1.854
-148	1.324	1.288	32	1.833	1.840
-144	1.354	1.343	36	1.797	1.815
-140	1.403	1.392	40	1.760	1.759
-136	1.524	1.556	44	1.711	1.723
-132	1.722	1.732	48	1.655	1.672
-128	1.996	2.078	52	1.603	1.627
-124	2.323	2.311	56	1.557	1.528
-120	2.669	2.748	60	1.491	1.447
-116	2.919	2.973	64	1.409	1.415
-112	2.708	2.871	68	1.348	1.345
-108	2.544	2.608	72	1.287	1.282
-104	2.207	2.360	76	1.167	1.171
-100	2.045	2.097	80	1.086	1.072
-96	1.889	1.930	84	0.941	0.918
-92	1.415	1.567	88	0.795	0.859
-88	1.034	1.139	92	0.902	0.966
-84	0.858	0.909	96	1.254	1.295
-80	1.008	0.896	100	1.625	1.736
-76	1.131	1.003	104	1.996	2.026
-72	1.248	1.161	108	2.192	2.224
-68	1.331	1.264	112	2.393	2.428
-64	1.412	1.356	116	2.582	2.684
-60	1.471	1.434	120	2.801	2.903
-56	1.536	1.495	124	2.695	2.863
-52	1.603	1.563	128	2.399	2.590
-48	1.654	1.628	132	2.075	2.223
-44	1.670	1.679	136	1.759	1.892
-40	1.763	1.714	140	1.535	1.646
-36	1.791	1.750	144	1.395	1.468
-32	1.831	1.814	148	1.229	1.573
-28	1.865	1.802	152	1.287	1.329
-24	1.899	1.850	156	1.304	1.368
-20	1.917	1.892	160	1.345	1.395
-16	1.921	1.921	164	1.440	1.466
-12	1.953	1.940	168	1.541	1.548
-8	1.990	1.957	172	1.626	1.633
-4	1.993	1.965	176	1.703	1.717
0	1.998	1.981	-180	1.760	1.767

TRAVERSES WITHOUT SCREEN, WITH FULL BODY NAPHTHALENE COATING

RE=110000 (FIG. 33)
MULTIPLIER=0.20556 /MIL
LOSS CORRECTION=0.023 MILS

Z/R	0	78	180	0.225	1.556	0.546	2.292
-0.425	1.575	0.549	2.337	0.242	1.564	0.538	2.293
-0.408	1.542	0.552	2.335	0.258	1.563	0.538	2.288
-0.392	1.569	0.553	2.334	0.275	1.565	0.553	2.284
-0.375	1.565	0.553	2.330	0.292	1.564	0.554	2.284
-0.358	1.544	0.548	2.314	0.308	1.568	0.551	2.291
-0.342	1.546	0.548	2.307	0.325	1.571	0.547	2.295
-0.325	1.541	0.550	2.303	0.342	1.579	0.547	2.285
-0.308	1.563	0.554	2.298	0.358	1.572	0.546	2.278
-0.292	1.560	0.562	2.298				
-0.275	1.564	0.560	2.294				
-0.258	1.555	0.559	2.288				
-0.242	1.553	0.558	2.302				
-0.225	1.563	0.557	2.302				
-0.208	1.559	0.553	2.289				
-0.192	1.564	0.552	2.286				
-0.175	1.550	0.550	2.265				
-0.158	1.559	0.550	2.265				
-0.142	1.559	0.556	2.263				
-0.125	1.560	0.558	2.258				
-0.108	1.551	0.548	2.256				
-0.092	1.550	0.541	2.257				
-0.075	1.529	0.539	2.259				
-0.058	1.530	0.541	2.261				
-0.042	1.542	0.542	2.273				
-0.025	1.547	0.547	2.275				
-0.008	1.546	0.552	2.281				
0.008	1.546	0.548	2.286				
0.025	1.544	0.548	2.283				
0.042	1.545	0.553	2.278				
0.058	1.555	0.564	2.269				
0.075	1.551	0.565	2.261				
0.092	1.553	0.563	2.250				
0.108	1.557	0.555	2.244				
0.125	1.552	0.543	2.263				
0.142	1.530	0.548	2.284				
0.158	1.538	0.548	2.285				
0.175	1.541	0.547	2.288				
0.192	1.549	0.546	2.289				
0.208	1.549	0.542	2.291				

SPANWISE TRAVERSES WITH SCREEN
RE=110000 (FIGS. 62, 63) X/R=6.0

M=0.0625"

MULTIPLIER=0.22270 /MIL
LOSS CORRECTION=0.031 MILS

Z/R	SH/ \sqrt{RE}				
-0.458	1.812	-0.117	2.349	0.233	1.495
-0.450	1.875	-0.108	2.346	0.242	1.538
-0.442	1.993	-0.100	2.313	0.250	1.565
-0.433	2.056	-0.092	2.255	0.258	1.637
-0.425	2.074	-0.083	2.165	0.267	1.755
-0.417	2.005	-0.075	2.044	0.275	1.851
-0.408	1.981	-0.067	1.924	0.283	1.996
-0.400	1.897	-0.058	1.803	0.292	2.059
-0.392	1.848	-0.050	1.628	0.300	2.129
-0.383	1.722	-0.042	1.538	0.308	2.213
-0.375	1.682	-0.033	1.480	0.317	2.222
-0.367	1.652	-0.025	1.447	0.325	2.237
-0.358	1.655	-0.017	1.523	0.333	2.180
-0.350	1.673	-0.008	1.586	0.342	2.165
-0.342	1.728	-0.0	1.746	0.350	2.083
-0.333	1.788	0.008	1.875	0.358	1.984
-0.325	1.881	0.017	2.011	0.367	1.872
-0.317	1.948	0.025	2.159	0.375	1.773
-0.308	2.014	0.033	2.258	0.383	1.658
-0.300	1.975	0.042	2.334	0.392	1.580
-0.292	2.041	0.050	2.358	0.400	1.505
-0.283	2.053	0.058	2.334		
-0.275	2.023	0.067	2.216		
-0.267	2.011	0.075	2.117		
-0.258	1.963	0.083	2.014		
-0.250	1.960	0.092	1.972		
-0.242	1.900	0.100	1.767		
-0.233	1.869	0.108	1.688		
-0.225	1.740	0.117	1.568		
-0.217	1.616	0.125	1.550		
-0.208	1.523	0.133	1.553		
-0.200	1.432	0.142	1.607		
-0.192	1.423	0.150	1.661		
-0.183	1.462	0.158	1.728		
-0.175	1.526	0.167	1.779		
-0.167	1.679	0.175	1.812		
-0.158	1.812	0.183	1.836		
-0.150	2.035	0.192	1.818		
-0.142	2.117	0.200	1.767		
-0.133	2.234	0.208	1.655		
-0.125	2.328	0.217	1.634		
		0.225	1.562		

SPANWISE TRAVERSES WITH SCREEN
 RE=110000, SCREEN SHIFTED VERTICALLY UPWARD 0.25" M=0.0625" X/R=6.0
 (FIG. 63) Z/R GIVEN IN COORDINATES FIXED W.R.T. SCREEN

MULTIPLIER=0.00000 /MIL
 LOSS CORRECTION=0.000 MILS

Z/R	SH/√RE				
-0.508	0	-0.167	1.812	0.183	1.927
-0.500	1.966	-0.158	1.878	0.192	1.866
-0.492	1.788	-0.150	2.041	0.200	1.845
-0.483	1.676	-0.142	2.174	0.208	1.767
-0.475	1.652	-0.133	2.264	0.217	1.679
-0.467	1.701	-0.125	2.319	0.225	1.571
-0.458	1.794	-0.117	2.322	0.233	1.517
-0.450	1.903	-0.108	2.376	0.242	1.529
-0.442	2.020	-0.100	2.252	0.250	1.556
-0.433	2.092	-0.092	2.198	0.258	1.631
-0.425	2.138	-0.083	2.117	0.267	1.685
-0.417	2.171	-0.075	1.972	0.275	1.830
-0.408	2.126	-0.067	1.857	0.283	1.981
-0.400	2.023	-0.058	1.698	0.292	2.096
-0.392	1.924	-0.050	1.571	0.300	2.237
-0.383	1.851	-0.042	1.486	0.308	2.279
-0.375	1.722	-0.033	1.438	0.317	2.304
-0.367	1.691	-0.025	1.447	0.325	2.304
-0.358	1.646	-0.017	1.489	0.333	2.304
-0.350	1.637	-0.008	1.616	0.342	2.261
-0.342	1.698	0.0	1.749	0.350	2.165
-0.333	1.746	0.008	1.887		
-0.325	1.830	0.017	2.053		
-0.317	1.887	0.025	2.192		
-0.308	1.999	0.033	2.261		
-0.300	2.020	0.042	2.343		
-0.292	2.080	0.050	2.334		
-0.283	2.111	0.058	2.310		
-0.275	2.120	0.067	2.264		
-0.267	2.171	0.075	2.162		
-0.258	2.153	0.083	2.086		
-0.250	2.126	0.092	1.960		
-0.242	2.041	0.100	1.824		
-0.233	1.945	0.108	1.694		
-0.225	1.857	0.117	1.610		
-0.217	1.749	0.125	1.535		
-0.208	1.625	0.133	1.535		
-0.200	1.532	0.142	1.568		
-0.192	1.468	0.150	1.649		
-0.183	1.459	0.158	1.782		
-0.175	1.505	0.167	1.794		
	1.586	0.175	1.887		

SPANWISE TRAVERSES WITH SCREEN M=0.0625" X/R=11.2 RE=110000 (RUN 1, FIG. 60)

MULTIPLIER=0.20874 /MIL LOSS CORRECTION=0.099 MILS

Z/R	0	15	30	SH/ \sqrt{RE} 45	60	70	75	78
-0.416	1.713	1.664	1.511	1.384	1.122	0.886	0.684	0.612
-0.408	1.661	1.628	1.538	1.369	1.116	0.871	0.645	0.597
-0.400	1.643	1.613	1.544	1.351	1.146	0.874	0.675	0.594
-0.391	1.559	1.574	1.520	1.360	1.137	0.911	0.684	0.591
-0.383	1.559	1.544	1.492	1.357	1.152	0.920	0.672	0.588
-0.375	1.550	1.505	1.465	1.342	1.164	0.902	0.684	0.585
-0.366	1.532	1.514	1.456	1.309	1.149	0.923	0.709	0.588
-0.358	1.547	1.556	1.477	1.357	1.161	0.947	0.715	0.612
-0.350	1.574	1.568	1.489	1.393	1.185	0.971	0.733	0.618
-0.341	1.610	1.628	1.550	1.453	1.230	1.001	0.724	0.627
-0.333	1.679	1.670	1.595	1.502	1.296	1.025	0.784	0.609
-0.325	1.725	1.698	1.628	1.553	1.321	1.073	0.817	0.681
-0.316	1.761	1.767	1.701	1.571	1.366	1.082	0.838	0.690
-0.308	1.809	1.824	1.746	1.625	1.435	1.140	0.877	0.700
-0.300	1.851	1.872	1.830	1.655	1.474	1.167	0.889	0.709
-0.291	1.900	1.939	1.827	1.710	1.465	1.185	0.914	0.730
-0.283	1.921	1.927	1.857	1.734	1.514	1.221	0.935	0.748
-0.275	1.933	1.999	1.854	1.737	1.547	1.200	0.923	0.769
-0.266	1.951	1.960	1.887	1.761	1.532	1.197	0.950	0.754
-0.258	1.915	1.936	1.900	1.731	1.505	1.206	0.920	0.736
-0.250	1.906	1.900	1.903	1.713	1.486	1.176	0.871	0.736
-0.241	1.872	1.878	1.809	1.679	1.453	1.110	0.847	0.687
-0.233	1.815	1.827	1.770	1.598	1.384	1.079	0.787	0.678
-0.225	1.722	1.740	1.676	1.535	1.330	1.040	0.772	0.642
-0.216	1.661	1.670	1.604	1.453	1.257	0.992	0.730	0.648
-0.208	1.592	1.562	1.520	1.345	1.221	1.034	0.709	0.585
-0.200	1.532	1.505	1.450	1.324	1.146	0.911	0.678	0.588
-0.191	1.477	1.465	1.411	1.260	1.128	0.895	0.681	0.582
-0.183	1.459	1.423	1.384	1.269	1.091	0.889	0.669	0.576
-0.175	1.492	1.462	1.432	1.257	1.085	0.856	0.678	0.552
-0.166	1.562	1.514	1.462	1.312	1.128	0.877	0.669	0.579
-0.158	1.640	1.610	1.541	1.384	1.188	0.914	0.700	0.603
-0.150	1.758	1.710	1.619	1.441	1.233	0.965	0.718	0.618
-0.141	1.836	1.806	1.746	1.544	1.303	1.004	0.754	0.630
-0.133	1.860	1.881	1.791	1.649	1.357	1.082	0.793	0.651
-0.125	1.987	1.948	1.875	1.694	1.444	1.122	0.796	0.672
-0.116	2.026	2.023	1.936	1.776	1.523	1.155	0.847	0.690
-0.108	2.096	2.056	1.963	1.794	1.541	1.152	0.859	0.706
-0.100	2.108	2.059	1.990	1.800	1.565	1.200	0.892	0.718
-0.091	2.035	2.014	1.945	1.770	1.505	1.191	0.868	0.703
-0.083	1.987	2.002	1.936	1.755	1.483	1.167	0.868	0.709
-0.075	1.957	1.942	1.854	1.646	1.441	1.146	0.853	0.687
-0.066	1.875	1.827	1.785	1.610	1.384	1.067	0.811	0.660
-0.058	1.776	1.734	1.682	1.550	1.296	1.040	0.778	0.648
-0.050	1.658	1.643	1.592	1.429	1.242	0.983	0.742	0.627
-0.041	1.562	1.541	1.508	1.357	1.191	0.920	0.709	0.597
-0.033	1.511	1.489	1.438	1.284	1.140	0.877	0.709	0.609

-0.025	1.480	1.423	1.423	1.272	1.082	0.911	0.684	0.588
-0.016	1.495	1.474	1.408	1.266	1.091	0.877	0.675	0.579
-0.008	1.541	1.511	1.435	1.281	1.131	0.908	0.684	0.576
0.0	1.622	1.592	1.508	1.342	1.167	0.911	0.700	0.597
0.009	1.743	1.698	1.601	1.435	1.209	0.974	0.693	0.630
0.017	1.827	1.803	1.670	1.526	1.284	0.992	0.748	0.651
0.025	1.915	1.881	1.770	1.634	1.378	1.070	0.790	0.675
0.034	1.975	1.945	1.842	1.679	1.408	1.125	0.784	0.706
0.042	1.981	2.002	1.903	1.764	1.489	1.146	0.850	0.724
0.050	2.035	2.026	1.933	1.791	1.526	1.173	0.899	0.739
0.059	2.050	2.035	1.945	1.818	1.550	1.197	0.886	0.751
0.067	2.044	2.077	1.918	1.818	1.544	1.197	0.883	0.733
0.075	1.951	1.945	1.903	1.770	1.465	1.167	0.853	0.721
0.084	1.933	1.897	1.836	1.682	1.462	1.107	0.847	0.715
0.092	1.821	1.818	1.743	1.625	1.426	1.085	0.814	0.678
0.100	1.755	1.722	1.682	1.556	1.321	1.007	0.766	0.651
0.109	1.679	1.640	1.610	1.468	1.272	0.932	0.718	0.636
0.117	1.598	1.547	1.483	1.387	1.179	0.899	0.693	0.615
0.125	1.505	1.453	1.426	1.336	1.143	0.826	0.642	0.588
0.134	1.489	1.432	1.372	1.248	1.052	0.820	0.603	0.570
0.142	1.456	1.447	1.345	1.227	1.016	0.790	0.564	0.573
0.150	1.480	1.453	1.345	1.212	1.016	0.772	0.564	0.558
0.159	1.511	1.462	1.384	1.224	1.010	0.730	0.552	0.552
0.167	1.580	1.477	1.399	1.227	1.022	0.757	0.534	0.549
0.175	1.595	1.562	1.426	1.242	1.022	0.718	0.549	0.540
0.184	1.604	1.568	1.474	1.284	0.995	0.751	0.552	0.546
0.192	1.622	1.577	1.462	1.251	1.010	0.712	0.561	0.549
0.200	1.604	1.574	1.450	1.248	1.001	0.733	0.555	0.531
0.209	1.553	1.514	1.423	1.254	1.025	0.757	0.567	0.534
0.217	1.544	1.489	1.387	1.236	1.016	0.766	0.576	0.549
0.225	1.450	1.450	1.342	1.233	1.022	0.766	0.552	0.549
0.234	1.441	1.435	0.0	1.230	1.034	0.787	0.0	0.555
0.242	1.459	1.438	0.0	1.269	1.076	0.805	0.0	0.582
0.250	1.517	1.520	0.0	1.300	1.131	0.826	0.0	0.588
0.259	1.589	1.610	0.0	1.342	1.182	0.895	0.660	0.612
0.267	1.682	1.688	1.598	1.441	1.257	0.935	0.696	0.618
0.275	1.791	1.734	1.694	1.517	1.315	1.004	0.718	0.645
0.284	1.854	1.854	1.797	1.622	1.432	1.073	0.757	0.678
0.292	1.906	1.881	1.836	1.643	1.514	1.122	0.778	0.712
0.300	1.921	1.963	1.897	1.731	1.532	1.176	0.817	0.721
0.309	2.026	2.059	1.942	1.785	1.544	1.197	0.859	0.748
0.317	2.014	2.011	1.981	1.797	1.610	1.203	0.853	0.760
0.325	2.020	2.026	1.966	1.791	1.571	1.221	0.877	0.757
0.334	1.996	1.990	1.963	1.788	1.559	1.224	0.883	0.748
0.342	1.966	1.963	1.893	1.749	1.520	1.185	0.850	0.724
0.350	1.900	1.918	1.836	1.673	1.462	1.149	0.850	0.706
0.359	1.875	1.833	1.800	1.595	1.405	1.101	0.799	0.684
0.367	1.785	1.758	1.685	1.544	1.339	1.070	0.757	0.651
0.375	1.707	1.664	1.607	1.411	1.272	1.028	0.742	0.642
0.384	1.598	1.592	1.532	1.369	1.200	0.959	0.696	0.612
0.392	1.556	1.544	1.465	1.300	1.146	0.935	0.700	0.597
0.400	1.468	1.489	1.414	1.278	1.143	0.935	0.666	0.588
0.409	1.426	1.444	1.372	1.242	1.131	0.892	0.681	0.585

0.417	1.438	1.414	1.351	1.251	1.113	0.892	0.657	0.570
0.425	1.459	1.459	1.396	1.293	1.140	0.902	0.675	0.594
0.434	1.514	1.517	1.459	1.330	1.200	0.932	0.700	0.591
0.442	1.562	1.571	1.505	1.366	1.224	0.947	0.715	0.609

SPANWISE TRAVERSES WITH SCREEN M=0.0625" X/R=11.2 RE=110000 (RUN 2, FIG. 77)
 (FOR COMPARISON WITH FLOW FIELD TRAVERSES)
 MULTIPLIER=0.22904 /MIL LOSS CORRECTION=0.105 MILS

Z/R	0	30	60	\sin/\sqrt{RE}	70	75	78
-0.425	1.560	1.502	1.196	0.937	0.657	0.587	
-0.417	1.658	1.564	1.230	0.955	0.675	0.598	
-0.408	1.740	1.612	1.290	0.980	0.685	0.593	
-0.400	1.794	1.686	1.372	1.048	0.747	0.628	
-0.392	1.842	1.749	1.428	1.088	0.776	0.645	
-0.383	1.916	1.805	1.478	1.151	0.824	0.674	
-0.375	1.978	1.875	1.528	1.211	0.854	0.703	
-0.367	2.018	1.917	1.574	1.249	0.883	0.716	
-0.358	2.054	1.934	1.602	1.263	0.909	0.731	
-0.350	2.062	1.944	1.586	1.263	0.909	0.736	
-0.342	2.041	1.935	1.618	1.271	0.911	0.731	
-0.333	2.013	1.969	1.592	1.253	0.882	0.718	
-0.325	1.990	1.924	1.563	1.227	0.860	0.703	
-0.317	1.943	1.851	1.527	1.175	0.842	0.689	
-0.308	1.881	1.786	1.472	1.135	0.804	0.666	
-0.300	1.806	1.701	1.393	1.078	0.772	0.637	
-0.292	1.743	1.627	1.321	1.014	0.739	0.620	
-0.283	1.680	1.548	1.264	0.982	0.709	0.604	
-0.275	1.654	1.479	1.230	0.937	0.687	0.585	
-0.267	1.597	1.459	1.195	0.929	0.671	0.576	
-0.258	1.574	1.428	1.187	0.905	0.651	0.563	
-0.250	1.588	1.461	1.193	0.923	0.657	0.564	
-0.242	1.626	1.489	1.188	0.937	0.649	0.556	
-0.233	1.708	1.549	1.241	0.947	0.661	0.551	
-0.225	1.793	1.627	1.277	0.990	0.665	0.560	
-0.217	1.878	1.697	1.325	1.006	0.687	0.549	
-0.208	1.944	1.768	1.369	1.014	0.689	0.554	
-0.200	1.992	1.800	1.373	1.014	0.701	0.553	
-0.192	2.004	1.808	1.329	1.024	0.691	0.552	
-0.183	2.014	1.793	1.360	0.994	0.675	0.539	
-0.175	1.975	1.746	1.313	0.965	0.657	0.533	
-0.167	1.957	1.681	1.261	0.939	0.635	0.508	
-0.158	1.856	1.624	1.208	0.919	0.621	0.515	
-0.150	1.748	1.523	1.162	0.883	0.605	0.512	
-0.142	1.666	1.458	1.151	0.871	0.602	0.501	
-0.133	1.613	1.413	1.113	0.865	0.602	0.506	
-0.125	1.580	1.398	1.119	0.855	0.594	0.505	
-0.117	1.580	1.424	1.141	0.875	0.607	0.509	
-0.108	1.626	1.467	1.153	0.894	0.615	0.510	
-0.100	1.652	1.507	1.189	0.913	0.623	0.514	
-0.092	1.718	1.569	1.221	0.927	0.643	0.521	
-0.083	1.755	1.596	1.259	0.939	0.637	0.528	
-0.075	1.803	1.642	1.285	0.959	0.653	0.531	
-0.067	1.827	1.644	1.276	0.957	0.657	0.522	
-0.058	1.807	1.615	1.282	0.973	0.651	0.511	
-0.050	1.794	1.590	1.252	0.927	0.657	0.511	
-0.042	1.768	1.541	1.229	0.943	0.641	0.509	

-0.033	1.697	1.498	1.185	0.921	0.637	0.500
-0.025	1.630	1.463	1.152	0.893	0.629	0.495
-0.017	1.581	1.414	1.154	0.893	0.625	0.486
-0.008	1.581	1.406	1.148	0.893	0.629	0.491
0.0	1.536	1.407	1.144	0.910	0.635	0.508
0.008	1.563	1.419	1.188	0.943	0.655	0.521
0.017	1.622	1.477	1.230	0.971	0.683	0.536
0.025	1.698	1.556	1.230	1.005	0.731	0.553
0.033	1.790	1.638	1.354	1.073	0.761	0.576
0.042	1.883	1.734	1.426	1.129	0.813	0.613
0.050	1.981	1.835	1.509	1.194	0.871	0.646
0.058	2.057	1.921	1.581	1.266	0.921	0.683
0.067	2.145	1.960	1.653	1.322	0.961	0.716
0.075	2.203	2.010	1.711	1.377	1.005	0.745
0.083	2.247	2.090	1.751	1.415	1.023	0.768
0.092	2.281	2.105	1.781	1.441	1.051	0.769
0.100	2.285	2.121	1.797	1.457	1.075	0.780
0.108	2.292	2.116	1.783	1.433	1.061	0.779
0.117	2.284	2.085	1.766	1.408	1.036	0.772
0.125	2.245	2.047	1.736	1.376	1.010	0.747
0.133	2.162	1.972	1.690	1.334	0.970	0.711
0.142	2.128	1.913	1.623	1.279	0.925	0.674
0.150	2.029	1.850	1.542	1.221	0.870	0.645
0.158	1.946	1.766	1.469	1.146	0.832	0.609
0.167	1.825	1.671	1.389	1.082	0.781	0.568
0.175	1.752	1.584	1.308	1.017	0.717	0.528
0.183	1.677	1.497	1.229	0.957	0.682	0.509
0.192	1.596	1.410	1.170	0.914	0.640	0.510
0.200	1.525	1.367	1.118	0.874	0.632	0.469
0.208	1.503	1.344	1.100	0.868	0.605	0.465
0.217	1.520	1.366	1.105	0.866	0.607	0.452
0.225	1.558	1.389	1.113	0.876	0.603	0.445
0.233	1.634	1.455	1.141	0.881	0.615	0.452
0.242	1.735	1.533	1.185	0.899	0.619	0.453
0.250	1.795	1.593	1.223	0.907	0.630	0.448
0.258	1.857	1.650	1.245	0.929	0.626	0.451
0.267	1.915	1.706	1.281	0.939	0.626	0.448
0.275	1.928	1.702	1.279	0.949	0.616	0.441
0.283	1.906	1.689	1.273	0.941	0.619	0.433
0.292	1.875	1.650	1.252	0.931	0.607	0.436
0.300	1.788	1.587	1.206	0.905	0.599	0.431
0.308	1.721	1.506	1.169	0.889	0.597	0.418
0.317	1.655	1.431	1.127	0.870	0.598	0.417
0.325	1.586	1.390	1.108	0.858	0.590	0.414
0.333	1.549	1.357	1.090	0.856	0.602	0.423
0.342	1.563	1.391	1.132	0.886	0.606	0.440
0.350	1.617	1.453	1.160	0.914	0.618	0.437
0.358	1.687	1.531	1.222	0.950	0.642	0.443
0.367	1.799	1.637	1.292	1.001	0.666	0.465
0.375	1.902	1.727	1.355	1.047	0.698	0.480
0.383	2.004	1.843	1.441	1.099	0.730	0.490
0.392	2.064	1.897	1.499	1.149	0.760	0.522
0.400	2.090	1.918	1.531	1.169	0.780	0.508

0.408 2.132 1.928 1.555 1.177 0.793 0.515

21

EFFECT OF FULL BODY COATING AND COMPARISON TEST

$$Z/R$$

(FIG. 59)

RE=110000

X/R=6.0

M=0.125"

SPANWISE TRAVERSES WITH SCREEN

MULTIPLIER=0.17213 /MIL LOSS CORRECTION=0.126 MILS

Z/R	0	5	10	20	SH/RE	35	50	65	75	80	85	90	95
-0.458	2.056	2.014	2.032	1.900	1.749	1.640	1.625	1.290	0.742	0.672	1.013	1.511	1.893
-0.442	2.068	2.074	2.023	1.939	1.785	1.625	1.589	1.281	0.760	0.627	0.992	1.450	1.815
-0.425	2.065	2.017	2.014	1.909	1.812	1.589	1.556	1.281	0.739	0.630	0.959	1.399	1.734
-0.408	2.071	1.984	1.951	1.884	1.770	1.556	1.529	1.257	0.739	0.612	0.947	1.390	1.707
-0.392	1.981	1.960	1.869	1.839	1.749	1.529	1.514	1.257	0.748	0.621	0.932	1.378	1.688
-0.375	1.900	1.906	1.875	1.809	1.691	1.514	1.529	1.233	0.724	0.636	0.944	1.348	1.652
-0.358	1.900	1.860	1.872	1.809	1.743	1.529	1.562	1.236	0.760	0.633	0.947	1.296	1.619
-0.342	1.951	1.927	1.851	1.818	1.743	1.562	1.562	1.290	0.766	0.651	0.959	1.330	1.607
-0.325	1.996	2.002	1.984	1.939	1.755	1.628	1.628	1.327	0.787	0.675	0.965	1.306	1.565
-0.308	2.059	2.062	2.059	1.954	1.836	1.679	1.679	1.402	0.841	0.687	0.956	1.318	1.550
-0.292	2.083	2.114	2.077	2.008	1.893	1.752	1.752	1.423	0.847	0.706	0.977	1.309	1.520
-0.275	2.111	2.111	2.089	2.041	1.890	1.752	1.752	1.405	0.847	0.703	0.977	1.309	1.520
-0.258	2.071	2.035	2.050	1.972	1.854	1.749	1.749	1.405	0.823	0.715	0.971	1.284	1.499
-0.242	2.035	2.002	1.984	1.954	1.845	1.713	1.713	1.366	0.793	0.693	0.980	1.266	1.511
-0.225	1.996	1.990	1.906	1.863	1.794	1.670	1.670	1.321	0.763	0.696	0.998	1.269	1.468
-0.208	1.936	1.942	1.875	1.863	1.798	1.625	1.625	1.260	0.718	0.700	0.995	1.300	1.514
-0.192	1.884	1.906	1.860	1.854	1.704	1.559	1.559	1.203	0.669	0.672	0.983	1.281	1.480
-0.175	1.909	1.878	1.833	1.818	1.652	1.505	1.505	1.149	0.648	0.669	0.974	1.309	1.514
-0.158	1.809	1.839	1.785	1.788	1.616	1.468	1.468	1.122	0.627	0.681	1.007	1.312	1.477
-0.142	1.875	1.872	1.827	1.788	1.562	1.499	1.499	1.116	0.633	0.681	1.016	1.315	1.495
-0.125	1.906	1.963	1.863	1.830	1.643	1.538	1.538	1.122	0.633	0.693	1.031	1.321	1.508
-0.108	1.954	1.906	1.890	1.866	1.704	1.538	1.538	1.149	0.651	0.687	1.034	1.327	1.499
-0.092	1.942	1.975	1.954	1.912	1.758	1.583	1.583	1.188	0.666	0.693	1.031	1.333	1.499
-0.075	1.933	1.942	1.933	1.924	1.791	1.628	1.628	1.221	0.690	0.700	1.028	1.333	1.499
-0.058	1.996	1.987	1.972	1.936	1.755	1.655	1.655	1.245	0.690	0.696	1.025	1.333	1.502
-0.042	1.975	1.972	1.957	1.963	1.824	1.673	1.673	1.254	0.715	0.703	1.022	1.309	1.453
-0.025	1.954	1.984	1.972	1.945	1.803	1.670	1.670	1.275	0.712	0.703	1.025	1.327	1.474
-0.008	1.978	1.972	1.954	1.945	1.809	1.661	1.661	1.260	0.718	0.709	1.034	1.336	1.483
0.008	1.960	1.924	1.881	1.884	1.752	1.619	1.619	1.218	0.687	0.678	1.013	1.345	1.492
0.025	1.933	1.915	1.897	1.884	1.755	1.631	1.631	1.236	0.712	0.684	0.998	1.360	1.474
0.042	1.918	1.936	1.890	1.875	1.752	1.628	1.628	1.260	0.718	0.678	0.998	1.354	1.477
0.058	1.939	1.936	1.903	1.918	1.785	1.658	1.658	1.272	0.730	0.678	0.995	1.330	1.486
0.075	1.987	1.984	1.945	1.969	1.839	1.728	1.728	1.342	0.757	0.669	0.995	1.345	1.477
0.092	2.026	2.035	2.008	1.987	1.887	1.788	1.788	1.381	0.787	0.681	0.983	1.345	1.450
0.108	2.050	2.086	2.047	2.023	1.916	1.806	1.806	1.402	0.793	0.672	0.983	1.348	1.489
0.125	2.050	2.068	2.029	2.014	1.915	1.794	1.794	1.393	0.796	0.681	0.980	1.336	1.489
0.142	2.017	2.038	1.999	1.993	1.845	1.761	1.761	1.372	0.808	0.681	0.977	1.342	1.502
0.158	1.987	1.987	1.972	1.972	1.824	1.707	1.707	1.318	0.757	0.663	0.956	1.342	1.502
0.175	1.924	1.945	1.933	1.900	1.758	1.646	1.646	1.269	0.733	0.648	0.953	1.333	1.505
0.192	1.897	1.887	1.881	1.848	1.710	1.607	1.607	1.200	0.709	0.630	0.917	1.327	1.520
0.208	1.893	1.903	1.863	1.851	1.688	1.610	1.610	1.209	0.703	0.630	0.944	1.321	1.514
0.225	1.918	1.912	1.893	1.833	1.731	1.622	1.622	1.239	0.712	0.624	0.935	1.315	1.502
0.242	1.912	1.933	1.909	1.881	1.758	1.664	1.664	1.245	0.739	0.633	0.923	1.303	1.508
0.258	1.912	1.930	1.927	1.903	1.755	1.679	1.679	1.269	0.742	0.636	0.914	1.318	1.532
0.275	1.930	1.939	1.939	1.906	1.779	1.701	1.701	1.272	0.760	0.633	0.926	1.327	1.520
0.292	1.954	1.951	1.921	1.909	1.782	1.707	1.707	1.284	0.778	0.651	0.923	1.333	1.535
0.308	1.948	1.984	1.951	1.933	1.782	1.707	1.707	1.287	0.766	0.651	0.935	1.321	1.553

0.325	1.972	1.987	1.948	1.782	1.713	1.290	0.772	0.639	0.929	1.309	1.556
0.342	1.981	1.987	1.945	1.788	1.722	1.287	0.766	0.627	0.923	1.336	1.574
0.358	1.969	1.975	1.936	1.773	1.719	1.303	0.778	0.624	0.920	1.342	1.616
0.375	1.978	1.960	1.936	1.776	1.725	1.293	0.775	0.633	0.923	1.357	1.640
0.392	1.975	1.966	1.963	1.794	1.737	1.281	0.781	0.630	0.929	1.339	1.664
0.408	1.987	1.981	1.972	1.800	1.731	1.315	0.784	0.630	0.920	1.351	1.698
0.425	1.963	1.981	1.972	1.791	1.746	1.303	0.778	0.630	0.932	1.402	1.755
0.442	1.936	1.936	1.942	1.764	1.701	1.315	0.754	0.636	0.986	1.432	1.845

(FIG. 56)

RE=110000

M=0.125" X/R=18.7

SPANWISE TRAVERSES WITH SCREEN

MULTIPLIER=0.20798 /MIL LOSS CORRECTION=0.062 MILS

Z/R	0	20	40	60	SH/RE 70	75	78	81	100	120	150	180
-0.458	1.529	1.471	1.399	1.176	0.977	0.859	0.844	0.977	2.596	1.839	1.999	2.367
-0.442	1.535	1.477	1.366	1.185	0.974	0.760	0.675	0.721	2.442	1.761	1.930	2.307
-0.425	1.505	1.471	1.342	1.146	0.950	0.745	0.624	0.615	2.367	1.749	1.909	2.225
-0.408	1.508	1.468	1.321	1.116	0.932	0.730	0.606	0.579	2.273	1.728	1.878	2.201
-0.392	1.517	1.462	1.339	1.128	0.917	0.727	0.600	0.558	2.231	1.743	1.857	2.147
-0.375	1.523	1.477	1.345	1.143	0.932	0.721	0.600	0.558	2.129	1.752	1.857	2.132
-0.358	1.532	1.477	1.357	1.146	0.935	0.733	0.621	0.570	2.023	1.779	1.851	2.123
-0.342	1.508	1.462	1.345	1.137	0.926	0.718	0.621	0.576	1.900	1.791	1.851	2.117
-0.325	1.541	1.483	1.354	1.134	0.920	0.715	0.603	0.564	1.803	1.806	1.836	2.135
-0.308	1.532	1.483	1.360	1.161	0.935	0.742	0.621	0.579	1.667	1.821	1.833	2.150
-0.292	1.526	1.489	1.357	1.182	0.944	0.721	0.615	0.588	1.646	1.857	1.866	2.150
-0.275	1.538	1.495	1.363	1.176	0.941	0.730	0.621	0.591	1.565	1.903	1.845	2.111
-0.258	1.541	1.499	1.357	1.164	0.938	0.727	0.621	0.591	1.495	1.930	1.821	2.171
-0.242	1.541	1.489	1.366	1.191	0.932	0.724	0.633	0.600	1.432	1.872	1.854	2.153
-0.225	1.535	1.486	1.357	1.155	0.962	0.721	0.633	0.600	1.399	1.960	1.845	2.123
-0.208	1.532	1.477	1.339	1.149	0.941	0.709	0.621	0.600	1.327	1.942	1.845	2.165
-0.192	1.508	1.450	1.321	1.122	0.920	0.690	0.624	0.585	1.342	2.002	1.866	2.162
-0.175	1.480	1.426	1.290	1.067	0.886	0.669	0.594	0.585	1.309	2.014	1.848	2.141
-0.158	1.450	1.399	1.245	1.061	0.844	0.627	0.588	0.564	1.278	2.050	1.887	2.123
-0.142	1.420	1.381	1.230	1.013	0.817	0.627	0.570	0.552	1.306	2.047	1.866	2.108
-0.125	1.405	1.378	1.206	1.001	0.811	0.621	0.546	0.555	1.269	1.999	1.866	2.102
-0.108	1.429	1.387	1.245	1.019	0.820	0.603	0.561	0.567	1.293	2.044	1.836	2.132
-0.092	1.438	1.396	1.242	1.052	0.847	0.621	0.570	0.567	1.287	2.056	1.903	2.102
-0.075	1.453	1.402	1.254	1.067	0.838	0.636	0.567	0.567	1.318	2.008	1.869	2.156
-0.058	1.495	1.435	1.287	1.058	0.847	0.651	0.558	0.567	1.290	1.951	1.900	2.153
-0.042	1.505	1.462	1.315	1.113	0.880	0.651	0.570	0.564	1.303	1.969	1.890	2.162
-0.025	1.535	1.456	1.348	1.098	0.883	0.651	0.588	0.579	1.336	2.008	1.869	2.168
-0.008	1.562	1.499	1.342	1.110	0.874	0.675	0.600	0.576	1.321	2.014	1.918	2.174
0.008	1.538	1.486	1.351	1.110	0.889	0.672	0.606	0.588	1.333	2.029	1.909	2.174
0.025	1.547	1.489	1.360	1.134	0.911	0.678	0.609	0.594	1.357	2.032	1.912	2.177
0.042	1.547	1.489	1.375	1.146	0.917	0.687	0.609	0.585	1.342	2.026	1.893	2.177
0.058	1.538	1.502	1.372	1.161	0.938	0.709	0.618	0.579	1.363	2.011	1.903	2.189
0.075	1.550	1.514	1.378	1.155	0.941	0.715	0.624	0.603	1.339	2.014	1.915	2.153
0.092	1.571	1.523	1.405	1.164	0.935	0.718	0.624	0.606	1.315	2.002	1.893	2.162
0.108	1.598	1.535	1.426	1.197	0.953	0.724	0.630	0.594	1.315	2.029	1.893	2.195
0.125	1.619	1.544	1.432	1.185	0.965	0.742	0.621	0.597	1.333	2.047	1.912	2.198
0.142	1.613	1.562	1.417	1.194	0.980	0.745	0.621	0.603	1.312	2.035	1.903	2.183
0.158	1.628	1.574	1.408	1.215	0.956	0.748	0.633	0.597	1.296	2.014	1.890	2.165
0.175	1.631	1.568	1.417	1.215	0.992	0.763	0.630	0.606	1.287	2.059	1.887	2.180
0.192	1.610	1.559	1.438	1.209	0.977	0.751	0.636	0.615	1.287	2.035	1.921	2.198
0.208	1.613	1.562	1.414	1.203	0.977	0.751	0.636	0.603	1.315	2.059	1.890	2.225
0.225	1.607	1.556	1.396	1.200	0.986	0.733	0.624	0.603	1.315	2.023	1.900	2.189
0.242	1.604	1.538	1.402	1.191	0.968	0.745	0.618	0.591	1.330	2.017	1.897	2.225
0.258	1.583	1.535	1.378	1.179	0.962	0.745	0.618	0.582	1.336	2.005	1.912	2.210
0.275	1.580	1.523	1.378	1.185	0.944	0.727	0.609	0.585	1.393	1.957	1.933	2.198
0.292	1.553	1.492	1.372	1.161	0.944	0.727	0.606	0.576	1.447	1.969	1.915	2.225
0.308	1.541	1.514	1.363	1.155	0.947	0.715	0.591	0.573	1.508	1.936	1.924	2.225

0.325	1.532	1.495	1.348	1.131	0.914	0.703	0.594	0.561	1.559	1.936	1.906	2.237
0.342	1.529	1.480	1.348	1.137	0.926	0.706	0.591	0.555	1.643	1.906	1.909	2.222
0.358	1.529	1.474	1.330	1.113	0.905	0.700	0.582	0.558	1.743	1.878	1.924	2.225
0.375	1.523	1.474	1.345	1.134	0.892	0.712	0.576	0.552	1.854	1.869	1.912	2.255
0.392	1.489	1.459	1.354	1.116	0.902	0.696	0.582	0.540	1.942	1.830	1.930	2.258

(FIG. 58)

RE=110000

M=0.621"

X/R=6.0

SPANWISE TRAVERSES WITH SCREEN

MULTIPLIER=0.27935 /MIL LOSS CORRECTION=0.108 MILS

Z/R	0	5	10	20	SH/√RE	35	50	65	75	80	85	90	95
-0.458	2.117	2.120	2.041	2.035	1.927	1.927	1.758	1.413	1.187	0.977	0.767	0.591	1.620
-0.442	2.144	2.144	2.065	2.068	1.939	1.939	1.782	1.489	1.202	0.964	0.739	0.573	1.616
-0.425	2.165	2.159	2.092	2.077	1.951	1.951	1.788	1.431	1.253	1.104	0.784	0.570	1.627
-0.408	2.192	2.201	2.126	2.111	2.002	2.002	1.857	1.580	1.311	1.158	0.864	0.588	1.580
-0.392	2.243	2.246	2.162	2.156	2.026	2.026	1.890	1.562	1.347	1.166	0.871	0.588	1.609
-0.375	2.373	2.249	2.150	2.108	2.005	2.005	1.884	1.576	1.333	1.173	0.871	0.591	1.562
-0.358	2.222	2.231	2.153	2.114	2.005	2.005	1.869	1.569	1.329	1.206	0.871	0.609	1.562
-0.342	2.183	2.210	2.159	2.117	1.984	1.984	1.839	1.569	1.329	1.206	0.871	0.609	1.562
-0.325	2.237	2.304	2.204	2.165	2.014	2.014	1.918	1.598	1.402	1.206	0.911	0.617	1.598
-0.308	2.222	2.285	2.189	2.150	2.032	2.032	1.912	1.613	1.405	1.220	0.868	0.609	1.584
-0.292	2.189	2.231	2.177	2.150	2.008	2.008	1.881	1.613	1.362	1.173	0.860	0.617	1.609
-0.275	2.171	2.210	2.150	2.114	1.981	1.981	1.839	1.591	1.325	1.187	0.846	0.620	1.667
-0.258	2.165	2.201	2.138	2.108	1.984	1.984	1.848	1.562	1.340	1.144	0.824	0.613	1.627
-0.242	2.117	2.165	2.135	2.074	1.966	1.966	1.824	1.565	1.300	1.140	0.795	0.620	1.725
-0.225	2.153	2.153	2.117	2.059	1.978	1.978	1.803	1.562	1.286	1.111	0.733	0.609	1.693
-0.208	2.114	2.108	2.080	2.038	1.948	1.948	1.797	1.489	1.242	1.053	0.708	0.617	1.729
-0.192	2.092	2.065	2.008	1.993	1.893	1.893	1.764	1.420	1.173	1.046	0.686	0.609	1.729
-0.175	2.038	2.041	1.981	1.957	1.845	1.845	1.688	1.387	1.115	0.995	0.653	0.606	1.773
-0.158	1.981	1.963	1.936	1.893	1.824	1.824	1.685	1.329	1.060	0.958	0.635	0.631	1.773
-0.142	1.999	1.957	1.924	1.897	1.797	1.797	1.622	1.336	1.060	0.926	0.609	0.624	1.783
-0.125	1.990	2.035	1.969	1.924	1.836	1.836	1.649	1.358	1.086	0.911	0.588	0.624	1.842
-0.108	1.999	2.041	1.987	1.909	1.806	1.806	1.649	1.344	1.057	0.875	0.588	0.609	1.849
-0.092	1.987	1.987	1.972	1.912	1.788	1.788	1.622	1.322	1.046	0.846	0.562	0.628	1.856
-0.075	2.005	1.972	1.924	1.912	1.773	1.773	1.613	1.293	1.038	0.831	0.566	0.617	1.871
-0.058	1.984	2.020	1.939	1.909	1.788	1.788	1.610	1.318	1.031	0.897	0.559	0.609	1.842
-0.042	1.999	2.020	1.963	1.933	1.785	1.785	1.604	1.304	1.024	0.835	0.551	0.620	1.907
-0.025	2.011	2.032	2.008	1.945	1.803	1.803	1.604	1.311	1.027	0.846	0.555	0.613	1.878
-0.008	2.014	2.053	1.990	1.945	1.809	1.809	1.589	1.296	1.046	0.860	0.570	0.613	1.867
0.008	2.023	2.017	1.975	1.945	1.797	1.797	1.589	1.296	1.009	0.824	0.595	0.617	1.845
0.025	2.065	2.023	2.008	1.972	1.815	1.815	1.613	1.275	1.013	0.820	0.580	0.613	1.871
0.042	2.056	2.096	2.041	1.990	1.848	1.848	1.661	1.307	1.049	0.842	0.606	0.599	1.849
0.058	2.059	2.096	2.086	2.017	1.930	1.930	1.685	1.336	1.057	0.860	0.595	0.617	1.860
0.075	2.080	2.150	2.105	2.029	1.924	1.924	1.707	1.369	1.097	0.871	0.606	0.606	1.849
0.092	2.114	2.165	2.096	2.065	1.966	1.966	1.743	1.398	1.093	0.889	0.606	0.606	1.852
0.108	2.129	2.198	2.129	2.105	1.969	1.969	1.767	1.409	1.111	0.922	0.617	0.595	1.798
0.125	2.138	2.195	2.150	2.105	1.975	1.975	1.758	1.405	1.100	0.911	0.642	0.599	1.838
0.142	2.144	2.219	2.177	2.099	1.969	1.969	1.770	1.438	1.144	0.937	0.649	0.606	1.842
0.158	2.141	2.207	2.171	2.099	1.978	1.978	1.752	1.431	1.147	0.955	0.639	0.606	1.845
0.175	2.117	2.186	2.171	2.083	1.981	1.981	1.761	1.409	1.129	0.955	0.635	0.595	1.831
0.192	2.132	2.198	2.135	2.065	1.960	1.960	1.770	1.405	1.133	0.933	0.620	0.584	1.813
0.208	2.168	2.177	2.123	2.083	1.948	1.948	1.734	1.405	1.100	0.926	0.617	0.588	1.813
0.225	2.114	2.150	2.111	2.038	1.921	1.921	1.740	1.395	1.111	0.933	0.620	0.591	1.809
0.242	2.114	2.150	2.126	2.047	1.912	1.912	1.731	1.391	1.111	0.929	0.628	0.570	1.769
0.258	2.129	2.126	2.138	2.059	1.939	1.939	1.743	1.395	1.093	0.962	0.617	0.570	1.791
0.275	2.053	2.141	2.150	2.074	1.942	1.942	1.758	1.409	1.107	0.929	0.613	0.580	1.794
0.292	2.099	2.156	2.141	2.089	1.936	1.936	1.761	1.409	1.126	0.940	0.628	0.573	1.783
0.308	2.150	2.135	2.153	2.108	1.942	1.942	1.749	1.413	1.122	0.947	0.617	0.566	1.809

0.325	2.174	2.153	2.105	2.086	1.960	1.743	1.416	1.144	0.944	0.624	0.584	1.783
0.342	2.186	2.162	2.168	2.074	1.966	1.773	1.442	1.155	0.973	0.628	0.588	1.783
0.358	2.165	2.171	2.147	2.102	1.975	1.779	1.449	1.162	0.995	0.639	0.595	1.816
0.375	2.162	2.144	2.144	2.083	1.969	1.782	1.453	1.155	0.987	0.635	0.599	1.820
0.392	2.180	2.162	2.129	2.092	1.984	1.788	1.456	1.169	0.969	0.631	0.595	1.838
0.408	2.135	2.162	2.123	2.089	1.942	1.734	1.445	1.147	0.962	0.631	0.595	1.809
0.425	2.135	2.156	2.126	2.105	1.975	1.767	1.445	1.162	0.980	0.635	0.602	1.900
0.442	2.123	2.132	2.120	2.071	1.972	1.755	1.435	1.147	0.962	0.620	0.613	1.903

(FIG. 57)

RE=110000

M=0.621" X/R=11.2

SPANWISE TRAVERSES WITH SCREEN

MULTIPLIER=0.21085 /MIL LOSS CORRECTION=0.117 MILS

Z/R	0	20	40	60	$\frac{SH}{\sqrt{RE}}$ 70	75	78	81	100	120	150	180
-0.458	2.008	1.891	1.708	1.458	1.173	0.942	0.743	0.631	2.742	2.346	2.337	2.837
-0.442	2.018	1.891	1.733	1.448	1.189	0.936	0.730	0.595	2.634	2.233	2.245	2.742
-0.425	2.014	1.935	1.749	1.467	1.199	0.936	0.730	0.595	2.530	2.157	2.195	2.615
-0.408	2.037	1.945	1.765	1.489	1.195	0.968	0.746	0.607	2.489	2.128	2.182	2.603
-0.392	2.065	1.954	1.796	1.505	1.217	0.983	0.759	0.607	2.463	2.103	2.160	2.615
-0.375	2.081	1.929	1.802	1.531	1.240	1.015	0.784	0.623	2.467	2.103	2.154	2.520
-0.358	2.090	1.992	1.809	1.565	1.259	1.028	0.791	0.620	2.441	2.040	2.131	2.568
-0.342	2.100	2.005	1.796	1.568	1.290	1.040	0.806	0.629	2.372	2.033	2.147	2.599
-0.325	2.100	1.989	1.863	1.562	1.309	1.072	0.822	0.651	2.327	2.037	2.112	2.590
-0.308	2.112	2.018	1.869	1.591	1.328	1.072	0.838	0.664	2.315	2.014	2.112	2.596
-0.292	2.135	2.043	1.888	1.584	1.366	1.100	0.829	0.655	2.365	2.021	2.112	2.634
-0.275	2.144	2.043	1.897	1.581	1.363	1.072	0.863	0.664	2.334	1.992	2.071	2.603
-0.258	2.150	2.049	1.875	1.616	1.382	1.107	0.854	0.661	2.334	1.995	2.059	2.603
-0.242	2.125	2.049	1.901	1.597	1.366	1.085	0.829	0.655	2.289	1.976	2.027	2.584
-0.225	2.141	2.055	1.904	1.606	1.379	1.078	0.854	0.658	2.337	1.967	2.043	2.590
-0.208	2.138	2.074	1.891	1.619	1.334	1.104	0.857	0.658	2.324	1.951	2.043	2.603
-0.192	2.125	2.062	1.875	1.648	1.363	1.066	0.816	0.664	2.277	1.907	2.084	2.615
-0.175	2.122	2.059	1.878	1.654	1.353	1.063	0.816	0.645	2.220	1.961	2.084	2.574
-0.158	2.109	2.049	1.891	1.594	1.350	1.034	0.791	0.642	2.305	1.926	2.081	2.590
-0.142	2.116	2.024	1.882	1.578	1.328	1.034	0.756	0.645	2.271	1.964	2.097	2.622
-0.125	2.087	2.030	1.875	1.597	1.293	1.015	0.759	0.639	2.280	1.967	2.128	2.612
-0.108	2.100	2.043	1.894	1.616	1.322	1.012	0.765	0.642	2.242	1.938	2.100	2.577
-0.092	2.084	2.014	1.834	1.568	1.284	0.987	0.746	0.629	2.252	1.916	2.081	2.612
-0.075	2.074	2.008	1.837	1.575	1.252	0.933	0.721	0.620	2.286	1.938	2.078	2.568
-0.058	2.074	2.008	0.0	0.0	0.0	0.0	0.724	0.629	2.286	1.980	2.154	2.612
-0.042	2.078	1.980	1.818	1.499	1.173	0.882	0.683	0.645	2.283	1.970	2.135	2.609
-0.025	2.065	1.964	1.793	1.499	1.151	0.866	0.667	0.629	2.283	1.970	2.135	2.609
-0.008	2.062	1.973	1.780	1.455	1.129	0.838	0.642	0.632	2.274	1.948	2.169	2.666
0.025	2.040	1.976	1.780	1.407	1.123	0.816	0.632	0.632	2.274	1.980	2.163	2.653
0.042	2.043	1.923	1.720	1.398	1.107	0.810	0.610	0.623	2.258	1.976	2.125	2.672
0.058	2.005	1.923	1.714	1.385	1.075	0.787	0.595	0.629	2.258	1.961	2.128	2.644
0.075	2.002	1.929	1.711	1.379	1.056	0.765	0.604	0.623	2.264	1.954	2.122	2.656
0.092	1.995	1.935	1.698	1.349	1.047	0.749	0.595	0.617	2.245	1.957	2.172	2.634
0.108	2.040	1.973	1.692	1.331	1.063	0.765	0.601	0.610	2.236	1.948	2.163	2.634
0.125	2.062	1.948	1.723	1.350	1.050	0.778	0.591	0.610	2.236	1.948	2.163	2.634
0.142	2.074	1.983	1.749	1.357	1.028	0.772	0.607	0.620	2.220	1.957	2.150	2.622
0.158	2.097	2.005	1.742	1.376	1.072	0.781	0.604	0.626	2.280	1.932	2.128	2.631
0.175	2.122	2.018	1.752	1.420	1.113	0.806	0.620	0.632	2.242	1.957	2.128	2.669
0.192	2.160	2.040	1.799	1.445	1.138	0.813	0.623	0.632	2.233	1.935	2.131	2.659
0.208	2.172	2.049	1.796	1.477	1.145	0.829	0.623	0.636	2.255	1.938	2.119	2.637
0.225	2.185	2.033	1.831	1.477	1.167	0.851	0.651	0.632	2.248	1.967	2.119	2.615
0.242	2.182	2.116	1.850	1.512	1.180	0.860	0.667	0.642	2.271	1.929	2.147	2.656
0.258	2.198	2.097	1.885	1.543	1.208	0.885	0.677	0.639	2.271	1.929	2.138	2.628
0.275	2.201	2.093	1.853	1.518	1.205	0.876	0.680	0.651	2.264	1.945	2.147	2.669
0.292	2.176	2.078	1.853	1.518	1.195	0.885	0.680	0.642	2.252	1.942	2.135	2.637
0.308	2.176	2.081	1.856	1.505	1.199	0.898	0.686	0.645	2.271	1.926	2.147	2.650

0.325	2.188	2.055	1.831	1.546	1.208	0.901	0.693	0.642	2.248	1.964	2.144	2.634
0.342	2.188	2.074	1.834	1.546	1.211	0.908	0.689	0.642	2.248	1.999	2.157	2.656
0.358	2.154	2.065	1.825	1.534	1.217	0.901	0.699	0.655	2.223	1.957	2.150	2.650
0.375	2.182	2.068	1.825	1.553	1.221	0.911	0.683	0.658	2.274	1.986	2.144	2.688
0.392	0.0	0.0	0.0	0.0	0.0	0.0	0.686	0.648	2.258	1.992	2.147	2.672

SPANWISE TRAVERSES WITH SCREEN										(FIG. 55)									
MULTIPLIER=0.19662 /MIL										RE=1100000									
LOSS CORRECTION=0.063 MILS										X/R=6.0									
SIL/√RE										M=0.875"									
Z/R	0	20	40	60	70	75	81	100	120	150	120	100	81	75	70	60	40	20	0
-0.458	2.198	2.077	1.897	1.562	1.399	1.293	1.076	2.487	2.671	1.423	2.671	2.487	1.076	1.173	1.173	1.562	1.897	2.077	2.198
-0.442	2.105	2.011	1.821	1.502	1.351	1.254	1.043	2.439	2.617	1.354	2.617	2.439	1.043	1.161	1.161	1.502	1.821	2.011	2.105
-0.425	2.038	1.951	1.770	1.492	1.327	1.221	0.992	2.361	2.569	1.300	2.569	2.361	0.992	1.098	1.098	1.492	1.770	1.951	2.038
-0.408	2.014	1.903	1.776	1.474	1.310	1.212	0.980	2.306	2.530	1.293	2.530	2.306	0.980	1.128	1.128	1.474	1.776	1.903	2.014
-0.392	2.014	1.927	1.731	1.489	1.318	1.203	0.965	2.406	2.503	1.287	2.503	2.406	0.965	1.104	1.104	1.489	1.731	1.927	2.014
-0.375	2.017	1.927	1.752	1.456	1.296	1.191	0.986	2.388	2.463	1.260	2.463	2.388	0.986	1.094	1.094	1.456	1.752	1.927	2.017
-0.358	2.014	1.906	1.722	1.474	1.309	1.164	0.986	2.357	2.457	1.254	2.457	2.357	0.986	1.082	1.082	1.474	1.722	1.906	2.014
-0.342	1.999	1.903	1.749	1.480	1.269	1.164	0.986	2.352	2.457	1.254	2.457	2.352	0.986	1.082	1.082	1.480	1.749	1.903	1.999
-0.325	2.014	1.921	1.743	1.459	1.269	1.173	0.986	2.352	2.457	1.254	2.457	2.352	0.986	1.082	1.082	1.459	1.743	1.921	2.014
-0.308	2.062	1.921	1.761	1.486	1.278	1.167	0.974	2.391	2.439	1.239	2.439	2.391	0.974	1.067	1.067	1.486	1.761	1.921	2.062
-0.292	2.050	1.918	1.791	1.459	1.281	1.167	0.974	2.391	2.424	1.245	2.424	2.391	0.974	1.076	1.076	1.459	1.791	1.918	2.050
-0.275	2.062	1.924	1.791	1.489	1.300	1.176	0.986	2.322	2.421	1.239	2.421	2.322	0.986	1.110	1.110	1.489	1.791	1.924	2.062
-0.258	2.023	1.960	1.812	1.505	1.287	1.179	0.986	2.400	2.469	1.254	2.469	2.400	0.986	1.085	1.085	1.505	1.812	1.960	2.023
-0.242	2.035	1.966	1.782	1.508	1.287	1.182	0.971	2.385	2.427	1.245	2.427	2.385	0.971	1.094	1.094	1.508	1.782	1.966	2.035
-0.225	2.014	1.945	1.800	1.483	1.312	1.191	0.974	2.421	2.451	1.266	2.451	2.421	0.974	1.079	1.079	1.483	1.800	1.945	2.014
-0.208	2.050	1.972	1.779	1.483	1.309	1.188	0.974	2.433	2.433	1.236	2.433	2.433	0.974	1.119	1.119	1.483	1.779	1.972	2.050
-0.192	2.032	1.975	1.794	1.483	1.315	1.188	0.980	2.457	2.433	1.248	2.433	2.457	0.980	1.101	1.101	1.483	1.794	1.975	2.032
-0.175	2.008	1.903	1.740	1.499	1.296	1.182	0.983	2.430	2.409	1.244	2.409	2.430	0.983	1.082	1.082	1.499	1.740	1.903	2.008
-0.158	1.996	1.942	1.773	1.529	1.303	1.179	0.962	2.448	2.400	1.251	2.400	2.448	0.962	1.098	1.098	1.529	1.773	1.942	1.996
-0.142	2.020	1.957	1.791	1.499	1.309	1.173	0.971	2.427	2.430	1.230	2.430	2.427	0.971	1.119	1.119	1.499	1.791	1.957	2.020
-0.125	1.984	1.954	1.746	1.468	1.333	1.167	0.986	2.454	2.466	1.248	2.466	2.454	0.986	1.116	1.116	1.468	1.746	1.954	1.984
-0.108	2.023	1.960	1.707	1.480	1.315	1.182	1.004	2.430	2.430	1.236	2.430	2.430	1.004	1.116	1.116	1.480	1.707	1.960	2.023
-0.092	2.062	1.945	1.758	1.492	1.342	1.212	0.992	2.430	2.472	1.275	2.472	2.430	0.992	1.122	1.122	1.492	1.758	1.945	2.062
-0.075	2.029	1.966	1.773	1.486	1.333	1.212	1.004	2.460	2.439	1.245	2.439	2.460	1.004	1.122	1.122	1.486	1.773	1.966	2.029
-0.058	2.017	1.957	1.764	1.502	1.318	1.185	0.995	2.460	2.439	1.245	2.439	2.460	0.995	1.116	1.116	1.502	1.764	1.957	2.017
-0.042	2.035	1.996	1.746	1.499	1.315	1.188	0.977	2.478	2.445	1.239	2.445	2.478	0.977	1.094	1.094	1.499	1.746	1.996	2.035
-0.025	2.065	1.996	1.743	1.544	1.306	1.197	0.974	2.469	2.442	1.251	2.442	2.469	0.974	1.098	1.098	1.544	1.743	1.996	2.065
-0.008	2.086	2.023	1.758	1.547	1.306	1.197	0.980	2.469	2.442	1.251	2.442	2.469	0.980	1.098	1.098	1.547	1.758	2.023	2.086
0.008	2.108	1.990	1.761	1.511	1.324	1.215	0.980	2.571	2.433	1.251	2.433	2.571	0.980	1.094	1.094	1.511	1.761	1.990	2.108
0.025	2.102	1.993	1.785	1.505	1.321	1.218	0.980	2.571	2.433	1.251	2.433	2.571	0.980	1.094	1.094	1.505	1.785	1.993	2.102
0.042	2.117	2.008	1.773	1.547	1.321	1.197	0.971	2.542	2.391	1.251	2.391	2.542	0.971	1.076	1.076	1.547	1.773	2.008	2.117
0.058	2.071	2.044	1.773	1.520	1.318	1.182	0.968	2.542	2.391	1.251	2.391	2.542	0.968	1.076	1.076	1.520	1.773	2.044	2.071
0.075	2.086	2.008	1.758	1.511	1.318	1.185	0.968	2.602	2.436	1.281	2.436	2.602	0.968	1.076	1.076	1.511	1.758	2.008	2.086
0.092	2.089	1.963	1.731	1.495	1.300	1.158	0.965	2.602	2.436	1.281	2.436	2.602	0.965	1.064	1.064	1.495	1.731	1.963	2.089
0.108	2.089	1.981	1.719	1.465	1.293	1.155	0.947	2.605	2.400	1.275	2.400	2.605	0.947	1.046	1.046	1.465	1.719	1.981	2.089
0.125	2.105	1.981	1.719	1.456	1.269	1.155	0.929	2.656	2.418	1.257	2.418	2.656	0.929	1.055	1.055	1.456	1.719	1.981	2.105
0.142	2.071	1.996	1.710	1.456	1.263	1.140	0.920	2.617	2.433	1.257	2.433	2.617	0.920	1.055	1.055	1.456	1.710	1.996	2.071
0.158	2.083	1.963	1.685	1.441	1.269	1.137	0.920	2.617	2.433	1.257	2.433	2.617	0.920	1.055	1.055	1.441	1.685	1.963	2.083
0.175	2.068	1.960	1.710	1.438	1.254	1.137	0.911	2.665	2.427	1.251	2.427	2.665	0.911	1.052	1.052	1.438	1.710	1.960	2.068
0.192	2.038	1.951	1.694	1.441	1.248	1.137	0.899	2.614	2.421	1.260	2.421	2.614	0.899	1.040	1.040	1.441	1.694	1.951	2.038
0.208	1.999	1.927	1.673	1.438	1.242	1.125	0.917	2.641	2.466	1.290	2.466	2.641	0.917	1.028	1.028	1.438	1.673	1.927	1.999
0.225	2.026	1.887	1.694	1.432	1.236	1.122	0.932	2.626	2.448	1.278	2.448	2.626	0.932	1.025	1.025	1.432	1.694	1.887	2.026
0.242	2.023	1.881	1.679	1.426	1.242	1.110	0.917	2.635	2.445	1.296	2.445	2.635	0.917	1.031	1.031	1.426	1.679	1.881	2.023
0.258	1.990	1.887	1.719	1.456	1.251	1.116	0.914	2.599	2.445	1.272	2.445	2.599	0.914	1.016	1.016	1.456	1.719	1.887	1.990
0.275	1.984	1.972	1.694	1.465	1.263	1.131	0.935	2.542	2.457	1.309	2.457	2.542	0.935	1.025	1.025	1.465	1.694	1.972	1.984
0.292	1.978	1.930	1.698	1.486	1.260	1.140	0.926	2.593	2.457	1.278	2.457	2.593	0.926	1.019	1.019	1.486	1.698	1.930	1.978
0.308	2.005	1.960	1.722	1.486	1.287	1.179	0.938	2.545	2.460	1.275	2.460	2.545	0.938	1.070	1.070	1.486	1.722	1.960	2.005

0.325	2.005	1.960	1.713	1.495	1.300	1.173	1.064	0.968	2.548	2.512	1.287
0.342	2.044	1.966	1.719	1.483	1.333	1.173	1.061	0.968	2.584	2.512	1.296
0.358	2.059	1.966	1.755	1.508	1.342	1.182	1.064	0.977	2.599	2.466	1.287
0.375	2.089	1.999	1.779	1.499	1.330	1.185	1.061	0.980	2.545	2.506	1.293
0.392	2.102	2.017	1.800	1.532	1.342	1.188	1.088	0.980	2.548	2.542	1.300

(FIG. 54)

RE=110000

M=0.875" X/R=18.7

SPANWISE TRAVERSES WITH SCREEN

MULTIPLIER=0.23174 /MIL LOSS CORRECTION=0.112 MILS

Z/R	0	5	10	20	SH/ \sqrt{RE}	35	50	65	75	80	85	90	95
-0.458	1.842	1.857	1.836	1.788	1.679	1.514	1.486	1.254	0.778	0.606	0.905	1.384	1.806
-0.442	1.824	1.836	1.872	1.806	1.664	1.514	1.514	1.254	0.760	0.582	0.911	1.360	1.758
-0.425	1.839	1.833	1.827	1.818	1.685	1.502	1.502	1.248	0.763	0.597	0.889	1.336	1.740
-0.408	1.800	1.860	1.806	1.833	1.676	1.489	1.489	1.224	0.742	0.591	0.892	1.342	1.716
-0.392	1.806	1.863	1.830	1.818	1.670	1.489	1.489	1.224	0.727	0.588	0.868	1.312	1.694
-0.375	1.827	1.872	1.830	1.824	1.673	1.502	1.502	1.227	0.712	0.603	0.757	1.275	1.664
-0.358	1.827	1.845	1.833	1.788	1.685	1.505	1.505	1.236	0.739	0.597	0.847	1.278	1.595
-0.342	1.842	1.860	1.848	1.839	1.704	1.517	1.517	1.251	0.751	0.609	0.868	1.284	1.577
-0.325	1.845	1.845	1.863	1.821	1.710	1.526	1.526	1.227	0.742	0.603	0.877	1.257	1.619
-0.308	1.887	1.839	1.845	1.818	1.682	1.538	1.538	1.254	0.733	0.603	0.877	1.263	1.601
-0.292	1.897	1.839	1.845	1.818	1.691	1.556	1.556	1.224	0.742	0.603	0.859	1.266	1.598
-0.275	1.872	1.851	1.875	1.833	1.710	1.529	1.529	1.236	0.742	0.597	0.868	1.257	1.577
-0.258	1.863	1.872	1.848	1.788	1.722	1.574	1.574	1.242	0.721	0.600	0.850	1.257	1.595
-0.242	1.884	1.872	1.878	1.860	1.728	1.556	1.556	1.248	0.745	0.594	0.868	1.284	1.577
-0.225	1.866	1.869	1.854	1.836	1.725	1.553	1.553	1.227	0.730	0.594	0.856	1.263	1.544
-0.208	1.884	1.881	1.869	1.836	1.722	1.556	1.556	1.221	0.721	0.582	0.838	1.254	1.574
-0.192	1.903	1.912	1.890	1.845	1.719	1.532	1.532	1.227	0.706	0.582	0.844	1.257	1.544
-0.175	1.906	1.866	1.857	1.818	1.673	1.544	1.544	1.227	0.693	0.591	0.841	1.248	1.559
-0.158	1.884	1.897	1.890	1.845	1.704	1.544	1.544	1.227	0.696	0.582	0.838	1.269	1.577
-0.142	1.909	1.909	1.893	1.863	1.691	1.541	1.541	1.227	0.700	0.591	0.856	1.263	1.583
-0.125	1.900	1.918	1.900	1.848	1.682	1.514	1.514	1.215	0.681	0.591	0.871	1.263	1.580
-0.108	1.903	1.900	1.915	1.851	1.710	1.505	1.505	1.188	0.675	0.585	0.868	1.272	1.595
-0.092	1.881	1.875	1.869	1.839	1.694	1.495	1.495	1.182	0.672	0.576	0.859	1.272	1.583
-0.075	1.875	1.906	1.881	1.824	1.685	1.489	1.489	1.158	0.660	0.570	0.859	1.272	1.583
-0.058	1.863	1.878	1.906	1.803	1.655	1.480	1.480	1.158	0.669	0.573	0.862	1.278	1.571
-0.042	1.857	1.854	1.863	1.797	1.643	1.468	1.468	1.140	0.651	0.576	0.868	1.275	1.595
-0.025	1.857	1.863	1.839	1.791	1.634	1.450	1.450	1.122	0.636	0.570	0.871	1.284	1.595
-0.008	1.833	1.857	1.824	1.779	1.628	1.441	1.441	1.131	0.633	0.564	0.865	1.272	1.592
0.008	1.821	1.839	1.818	1.743	1.628	1.423	1.423	1.116	0.624	0.555	0.844	1.257	1.595
0.025	1.824	1.830	1.821	1.749	1.643	1.435	1.435	1.125	0.621	0.555	0.850	1.272	1.604
0.042	1.815	1.857	1.818	1.764	1.628	1.432	1.432	1.116	0.624	0.561	0.838	1.245	1.568
0.058	1.821	1.845	1.836	1.752	1.634	1.426	1.426	1.128	0.630	0.555	0.826	1.257	1.595
0.075	1.842	1.833	1.833	1.752	1.613	1.429	1.429	1.134	0.636	0.558	0.835	1.248	1.607
0.092	1.836	1.821	1.818	1.773	1.643	1.456	1.456	1.146	0.642	0.555	0.829	1.239	1.571
0.108	1.848	1.830	1.827	1.761	1.643	1.465	1.465	1.149	0.642	0.549	0.826	1.227	1.574
0.125	1.851	1.827	1.818	1.764	1.649	1.471	1.471	1.152	0.666	0.555	0.826	1.227	1.568
0.142	1.851	1.848	1.830	1.788	1.661	1.495	1.495	1.167	0.678	0.555	0.814	1.227	1.565
0.158	1.857	1.857	1.860	1.794	1.673	1.508	1.508	1.194	0.690	0.555	0.823	1.245	1.568
0.175	1.863	1.839	1.851	1.797	1.664	1.505	1.505	1.182	0.684	0.552	0.811	1.224	1.562
0.192	1.869	1.857	1.860	1.806	1.673	1.535	1.535	1.194	0.696	0.552	0.835	1.227	1.547
0.208	1.863	1.863	1.863	1.812	1.698	1.517	1.517	1.215	0.696	0.561	0.802	1.242	1.556
0.225	1.854	1.836	1.833	1.800	1.704	1.529	1.529	1.209	0.696	0.564	0.802	1.230	1.577
0.242	1.878	1.869	1.857	1.836	1.701	1.532	1.532	1.221	0.712	0.564	0.802	1.242	1.562
0.258	1.887	1.869	1.863	1.830	1.710	1.541	1.541	1.236	0.739	0.561	0.808	1.236	1.571
0.275	1.890	1.890	1.875	1.836	1.694	1.562	1.562	1.245	0.721	0.564	0.829	1.242	1.580
0.292	1.878	1.881	1.860	1.821	1.707	1.553	1.553	1.239	0.721	0.555	0.817	1.230	1.589
0.308	1.872	1.903	1.884	1.851	1.698	1.553	1.553	1.239	0.721	0.555	0.817	1.263	1.589

0.325	1.887	1.930	1.875	1.830	1.701	1.541	1.230	0.730	0.570	0.820	1.272	1.604
0.342	1.900	1.890	1.875	1.842	1.701	1.547	1.230	0.724	0.564	0.829	1.272	1.625
0.358	1.884	1.903	1.869	1.836	1.679	1.538	1.242	0.727	0.558	0.841	1.306	1.640
0.375	1.875	1.893	1.875	1.836	1.707	1.526	1.215	0.733	0.558	0.853	1.327	1.679
0.392	1.866	1.878	1.860	1.818	1.688	1.541	1.200	0.736	0.555	0.850	1.348	1.688
0.408	1.878	1.869	1.857	1.836	1.698	1.523	1.209	0.724	0.567	0.859	1.351	1.694
0.425	1.887	1.860	1.872	1.836	1.688	1.502	1.218	0.724	0.579	0.902	1.381	1.758
0.442	1.924	1.893	1.893	1.827	1.716	1.511	1.206	0.724	0.606	0.895	1.417	1.782

1. Report No. NASA CR-174759		2. Government Accession No.		3. Recipient's Catalog No.	
4. Title and Subtitle Mass Transfer From a Circular Cylinder - Effects of Flow Unsteadiness and "Slight Nonuniformities"				5. Report Date September 1984	
				6. Performing Organization Code	
7. Author(s) M. L. Marziale and R. E. Mayle				8. Performing Organization Report No. None	
				10. Work Unit No.	
9. Performing Organization Name and Address Rensselaer Polytechnic Institute Troy, New York				11. Contract or Grant No. NSG-3262	
				13. Type of Report and Period Covered Contractor Report	
12. Sponsoring Agency Name and Address National Aeronautics and Space Administration Washington, D.C. 20546				14. Sponsoring Agency Code 505-31-42	
15. Supplementary Notes Final report. Project Manager, G. James Van Fossen, Aerothermodynamics and Fuels Division, NASA Lewis Research Center, Cleveland, Ohio 44135.					
16. Abstract Experiments were performed to determine the effect of periodic variations in the angle of the flow incident to a turbine blade on its leading edge heat load. To model this situation, measurements were made on a circular cylinder oscillating rotationally in a uniform steady flow. A naphthalene mass transfer technique was developed and used in the experiments and heat transfer rates are inferred from the results. The investigation consisted of two parts. In the first, a stationary cylinder was used and the transfer rate was measured for $Re = 75\ 000$ to $110\ 000$ and turbulence levels from .34 percent to 4.9 percent. Comparisons with both theory and the results of others demonstrate that the accuracy and repeatability of the developed mass transfer technique is about ± 2 percent, a large improvement over similar methods. In the second part identical flow conditions were used but the cylinder was oscillated. A Strouhal number range from .0071 to .1406 was covered. Comparisons of the unsteady and steady results indicate that the magnitude of the effect of oscillation is small and dependent on the incident turbulence conditions. Also reported are a series of experiments where a small amplitude periodic perturbation was superimposed on the mean flow by a woven wire grid. Spanwise traverses of the mean velocity and turbulence quantities and spanwise and circumferential traverses of the mass transfer rate on the cylinder were made. Although the perturbation was measured to be only .25 percent of the mean velocity and was buried in the stream's turbulence, disproportionately larger 15 percent variations in the spanwise transfer rate were observed. To the author's knowledge the measurements of the mass transfer variations and their connection to the flow disturbance are the first of their kind.					
17. Key Words (Suggested by Author(s)) Mass transfer Heat transfer Cylinder			18. Distribution Statement Unclassified - unlimited STAR Category 34		
19. Security Classif. (of this report) Unclassified		20. Security Classif. (of this page) Unclassified		21. No. of pages 243	
				22. Price* A11	

National Aeronautics and
Space Administration

Washington, D.C.
20546

Official Business
Penalty for Private Use, \$300

SPECIAL FOURTH CLASS MAIL
BOOK

Postage and Fees Paid
National Aeronautics and
Space Administration
NASA-451



NASA

POSTMASTER: If Undeliverable (Section 158
Postal Manual) Do Not Return
